DEVELOPMENT AND CHARACTERIZATION OF NOVEL ALLOSTERIC MODULATORS ACTING ON METABOTROPIC GLUTAMATE RECEPTORS 2 AND 3

By

Cody James Wenthur

Dissertation

Submitted to the Faculty of the

Graduate School of Vanderbilt University

in partial fulfillment of the requirements

for the degree of

DOCTOR OF PHILOSOPHY

in

PHARMACOLOGY

August, 2015

Nashville, Tennessee

Approved:

Professor Craig W. Lindsley

Professor P. Jeffrey Conn

Professor Randy D. Blakely

Professor Aaron B. Bowman

Professor Joey V. Barnett

To my beloved wife, Brielle, the author of my happiness

and

To the untested truths, out beyond the ragged frontier

ACKNOWLEDGEMENTS

The following work was generously supported by financial assistance from the Howard Hughes Medical Institute / Vanderbilt University Medical Center Certificate Program in Molecular Medicine, the NIGMS Vanderbilt Pre-Doctoral Pharmacology Training Program, NCATS funds awarded through the Vanderbilt Institute for Clinical and Translational Research, the NIH Clinical Research Loan Repayment Program, and the NIH Molecular Libraries Program. These visionary awards enable scientific studies at the boundaries between disciplines, emphasize the importance of applied science, and champion the development of the next generation of translational researchers. It is no overstatement to say that without such incredible backing, this manuscript would never have come to fruition.

Likewise, the continuous guidance and assistance of my committee members was essential. The insights and suggestions of Drs. Randy Blakely, Aaron Bowman, and Joey Barnett, along with their unwavering commitment to helping me pursue my career and research goals, were integral to the success of the project. The current and former chairs of my committee, Drs. Jeff Conn and Scott Daniels, respectively, have both gone far beyond the simple requirements of their positions, providing me with access to their labs, equipment, and expertise – I will always be grateful for the opportunity to have learned from them.

I especially thank my mentor, Dr. Craig Lindsley, for always allowing me to branch out and explore new avenues for the project, for allowing me time to pursue

additional techniques, for letting me pursue dissertation-enriching opportunities and grants, and for providing a professional, friendly atmosphere where a diverse group of students, post-docs, staff scientists, and faculty could work together to improve each other and pursue common goals.

Those wonderful colleagues in the Lindsley lab, and throughout the Vanderbilt Center for Neuroscience Drug Discovery, are particularly worth thanking here. There are quite literally dozens of individuals in the VCNDD who have given me individual help over the years, including a number of undergraduate, rotation, and exchange students. No problem was ever too complex or too trivial for them to assist me with, and I am indebted to them all for their tireless support. While I do not have space to thank all of the VCNDD members individually, I must specifically thank Adam Walker, who was instrumental in the design and implementation of the electrophysiology experiments described within, along with Peter Martin, Lana Olson, Hyekyung Plumley, Douglas Sheffler, Ryan Morrison, Colleen Niswender, Jerri Rook, and Kyle Emmitte.

Finally, I thank my friends and family, both old and new, for their unwavering faith in my success and their unfathomable ability to improve my life with every passing day. While no mere acknowledgment can suffice for any of the contributions mentioned on this page, all of my attempts to quantify the specific ways in which these individuals have enriched my existence seem especially inadequate. So to my parents, grandparents, brothers, cousins, aunts, uncles, in-laws, brunch-eaters, band-players, cast-mates and soul-mate, I will simply thank you for everything and hope that it is enough.

PREFACE

Note Regarding the Numbering of Figures, Tables, Schemes and Compounds

All figures, tables and schemes listed in this document are given a unique ID following the convention **Object type [Chapter number].[object number]** (e.g. **Figure II.3** or **Scheme III.1**). All chemical structures listed in this document are given a unique ID upon their first appearance in this document, following the convention [**Chapter number].[compound number]** (e.g. **IV.22**). Compounds generated during the course of this work are referred to in the text by this convention; the corresponding identifier generated by Vanderbilt University will be referenced alongside this numbering system for key compounds where further clarification is required. Commercially available materials that were purchased for use in this work are referred to by the name they are sold under (e.g. LY341495).

Note Regarding Animal Care and Use

All animal studies described in this document were performed under protocols that had been reviewed and approved by the Vanderbilt University Institutional Animal Care and Use Committee (IACUC), and all experiments are performed in strict accordance with the NIH Guide for the Care and Use of Laboratory Animals. Such studies were conducted in the vivarium facility or the mouse neurobehavioral core of

Vanderbilt University Medical Center, which operates under guidelines set forth by the NIH and is fully accredited by the Association for Assessment and Accreditation of Laboratory Animal Care (AAALAC). Animals used were under the care of veterinary and vivarium staff with extensive experience in the care of rodents.

Note Regarding Human Subjects Protection

All studies described in this document that use human DNA and medical records were conducted under a protocol that had been reviewed and approved by the Vanderbilt University Human Research Protections Program / Institutional Review Board (HRPP / IRB). All records and samples were obtained with patient consent using the opt-out policy of the Vanderbilt BioVU database, and were fully de-identified in compliance with the Health Insurance Portability and Accountability Act (HIPAA).

Note Regarding Copyright Permissions

Some portions of this document are reproduced from works previously published by the author. All necessary copyright permissions have been obtained for the use of text and figures from these document. Where necessary, such permissions are noted at the conclusion of the chapter where they are presented.

TABLE OF CONTENTS

LIST OF TABLES

Chapter III

Chapter IV

Chapter V

Chapter VI

Table Page

LIST OF FIGURES

Chapter I

Chapter II

Chapter III

Chapter IV

Figure Page

Chapter V

Figure Page

LIST OF EQUATIONS AND SCHEMES

Chapter II

Equation Page

Chapter III

Scheme Page

Chapter IV

Scheme Page

LIST OF ABBREVIATIONS

7TM	Seven-transmembrane domain
°C	Degrees Celsius
µW	Microwave radiation
AC	Adenylyl cyclase
ACN	Acetonitrile
AMPA	α-amino-3-hydroxy-5-methyl-4-isoxazolepropionic acid
ANOVA	Analysis of Variance
ATCM	Allosteric ternary complex model
BBB	Blood-brain barrier
BHB	Brain-homogenate binding
cAMP	Cyclic adenosine monophosphate
CL_{Hep}	Hepatic clearance
CL_{Int}	Intrinsic clearance
CNS	Central nervous system
CRC	Concentration-response curve
CRD	cysteine rich domain
CS	Conditioned Stimulus
DCM	Dichloromethane
DMEM	Dulbecco's modified Eagle's medium
DMPK	Drug metabolism and pharmacokinetics
DMSO	Dimethylsulfoxide
EAAT	Excitatory amino acid transporter
EC_{80}	Concentration required for 80% of maximal receptor activation
ECT	Electroconvulsive therapy
EDC	1-Ethyl-3-(3-dimethylaminopropyl)carbodiimide
EPM	Elevated plus maze
EPSP	Excitatory postsynaptic potential
ESI	Electrospray ionization
EtOAc	Ethyl Acetate
FDA	United States Food and Drug Administration
FDSS	Functional Drug Screening System 7000
fEPSP	Field excitatory postsynaptic potential
FST	Porsolt forced swim test

F_u	Fraction unbound
$F_{u,b}$	Fraction unbound in brain
$F_{u,p}$	Fraction unbound in plasma
$GABA_B$	gamma-amino butyric acid receptor B
GAD	Generalized Anxiety Disorder
GIRK	G-protein coupled inward rectifying potassium channel
GPCR	G-protein coupled receptor
GRM1-8	Genes encoding for metabotropic glutamate receptors 1 through 8
HEK	Human embryonic kidney cell line 293
HIPAA	Health Insurance Portability and Accountability Act
HOBt	Hydroxybenzotriazole
HPLC	High-performance liquid chromatography
HRMS	High resolution mass spectrometry
HTS	High-throughput screening
HWE	Hardy-Weinberg Equilibrium
IC_{50}	Concentration required for 50% inhibition of maximal receptor response
ICD-9	International classification of diseases, 9th edition
iGlu	Ionotropic glutamate
IP	Intraperitoneal
IV	Intravenous
K_A/K_B	Equilibrium dissociation constant
K_i	Equilibrium dissociation constant from competition binding
K_p	Brain: plasma partition coefficient
$K_{p,uu}$	Unbound Brain: plasma partition coefficient
LC/MS	Liquid Chromatography/mass spectrometry
LTD	Long-term depression
LTP	Long-term potentiation
MDD	Major depressive disorder
mGlu	Metabotropic glutamate
$mGlu_{1-8}$	Metabotropic glutamate receptor subtypes 1 through 8
MLPCN	Molecular libraries probe center network
MPEP	2-methyl-6-(phenylethynyl)pyridine
mPFC	Median prefrontal cortex
MTEP	2-methyl-4-(pyridin-3-ylethynyl)thiazole
NAL	Neutral allosteric ligand
NAM	Negative allosteric modulator
NMDA	N-methyl-D-aspartate
NMR	Nuclear magnetic resonance

PAM	Positive allosteric modulator
PBL	Plasma: brain level
PBS	Phosphate buffered saline
PFC	Prefrontal cortex
P-gp	P-glycoprotein
pIC_{50}	Negative logarithm of the concentration needed to inhibit 50% of signaling
PL	Prelimbic
PLC	Phospholipase C
PPB	Plasma-protein binding
PPR	Paired-pulse ratio
RCF	Relative centrifugal force
RED	Rapid equilibrium dialysis
SAR	Structure-activity relationship
SEM	Standard error of the mean
SFC	supercritical fluid chromatograph
SKAT	SNP-set kernel association test
SNP	Single nucleotide polymorphism
SXC	System Xc
$t_{1/2}$	Half-life
TEA	Triethylamine
THF	Tetrahydrofuran
TLC	Thin-layer chromatography
TOF	Time of flight
TRD	Treatment-resistant depression
TST	Tail suspension test
TTX	Tetrodotoxin
US	Unconditioned Stimulus
VANGARD	Vanderbilt Technologies for Advanced Genomics Analysis and Research Design
VANTAGE	Vanderbilt Technologies for Advanced Genomics
VCNDD	Vanderbilt Center for Neuroscience Drug Discovery
VFT	Venus-flytrap domain
VUID	Vanderbilt University identification number

CHAPTER I

BACKGROUND AND INTRODUCTION

Metabotropic Glutamate Receptors 2 and 3

The glutamatergic nervous system and the neurotransmitter glutamate

Glutamic acid, also known as glutamate, is a non-essential amino acid that contributes significantly to critical processes in cellular function, including metabolism and protein synthesis (Berg, Tymoczko, & Streyer, 2002). In addition to these roles, glutamate also functions as the most abundant excitatory neurotransmitter in the mammalian central nervous system (CNS) (Niswender & Conn, 2010a). In the CNS, extracellular glutamate concentrations are tightly regulated, generally around 1 µM, though concentrations may transiently be much higher in synaptic clefts (Robert & Sontheimer, 2014). Liberation of glutamate from neurons occurs primarily through vesicular packaging and release; reuptake occurs through the action of membrane transporters, particularly members of the excitatory amino acid transporter (EAAT) family. The system Xc (SXC) cystine/glutamate transporter is also an important regulator of extracellular glutamate concentrations. Appropriate regulation of glutamate concentrations by these processes is critical to maintaining neuronal health (Robert & Sontheimer, 2014). Because the majority of neuronal activation occurs as a result of glutamate binding to ionotropic glutamate (iGlu) receptors, persistently elevated

glutamate concentrations can induce excitotoxicity, a condition marked by excessive neuronal activation that eventually results in the widespread death of neurons and associated glial cells (Kritis, Stamoula, Paniskaki, & Vavilis, 2015).

The iGlu receptors are ligand-gated ion channels, which are divided into three groups based on structural composition, signaling profile, and ligand binding – N-methyl-D-aspartate (NMDA) receptors, α-amino-3-hydroxy-5-methyl-4-isoxazolepropionic acid (AMPA) receptors, and kainite receptors (Purves, AuGustine, Fitzpatrick, et al., 2001). Mechanistically, activation of these iGlu receptors by glutamate results in increased permeability of neurons to positively charged ions (cations), inducing a rapid influx of sodium and/or calcium ions, and efflux of potassium ions. This activation depolarizes the cellular membrane and generates an excitatory post-synaptic potential (EPSP) that activates voltage-gated ion channels to further propagate neuronal signaling. Various patterns of neuronal activity can induce alterations in the expression and function of NMDA and AMPA receptors, leading to long-term changes the strength of excitatory signals generated by a given synapse, a phenomenon termed 'synaptic plasticity' (Hrabetova et al., 2000; Peng, Zhang, Zhang, Wang, & Ren, 2011). Such synaptic plasticity is thought to be an essential phenomenon for learning and memory formation, and dysregulation of these receptors has been shown to contribute to the pathophysiology of many neuropsychiatric disorders (Baudry, Bi, Gall, & Lynch, 2011).

In addition to its actions at iGlu receptors, glutamate also activates a family of G-protein coupled receptors (GPCRs). These GPCRs are called metabotropic glutamate (mGlu) receptors, and they generally provide a slower-acting modulation of excitatory

activity as compared to iGluRs (Purves et al., 2001). As with the iGlu receptors, the eight known members of the mGlu receptor family are divided into three groups based on their structural composition, signaling profile, and ligand binding – group I is composed of metabotropic glutamate receptors 1 and 5 ($mGlu_1$ and $mGlu_5$); group II is composed of $mGlu_2$ and $mGlu_3$; group III is composed of $mGlu_4$, $mGlu_6$, $mGlu_7$, and $mGlu_8$ (P J Conn & Pin, 1997). The group I receptors couple to G_q and induce phospholipase C (PLC) activity and intracellular calcium release, the group II and group III receptors couple to $G_{i/o}$ and inhibit adenylyl cyclase (AC) to reduce the formation of cyclic adenosine monophosphate (cAMP). While the group I mGlu receptors are primarily localized post-synaptically, the group II and group III receptors are found on both pre- and post-synaptic neurons (Nicoletti et al., 2011). The $mGlu_3$ and $mGlu_5$ receptors also have significant levels of expression on glial cells, particularly astrocytes (Aronica et al., 2003; D'Antoni et al., 2008). There is evidence that this glial $mGlu_3$ population is responsible for a form of glial-neuronal communication that also implicates beta-adrenergic receptors (Winder, Ritch, Gereau, & Conn, 1996). The mGlu receptors are also known to regulate synaptic plasticity, with demonstrated involvement in both long-term potentiation (LTP) and long-term depression (LTD) of glutamatergic synapses (Johnson, Niswender, Conn, & Xiang, 2011; Lodge et al., 2013; D. J. Sheffler, Gregory, Rook, & Conn, 2011). In light of the staggering array of CNS functions that are under the control of glutamate it is unsurprising that nearly every brain region contains cells that express glutamate receptors (Majo, Prabhakaran, Mann, & Kumar, 2013).

These glutamate synapses also contain a number of other proteins required to synthesize, package, release, uptake, and degrade this neurotransmitter (**Figure I.1**). The ubiquity of such glutamatergic synapses presents both a significant opportunity and a considerable challenge for the interested scientist; the opportunity arises from the potential impact that glutamate-modulating compounds could have in understanding a broad spectrum of CNS physiology and pathophysiology, the challenge comes from the difficulty in accessing tools and therapeutics that can alter specific facets of glutamatergic signaling without inducing unwanted perturbations and engendering significant adverse events (P J Conn & Pin, 1997; Niswender & Conn, 2010b). This difficulty is highlighted by the relative lack of medications approved by the United States Food and Drug Administration (FDA) that target glutamatergic signaling – to date, only ketamine and memantine have been explicitly designed to provide therapeutic benefit through such a mechanism, although other compounds also exhibit significant effects at such receptors (Amiel & Mathew, 2007). For many years iGluRs were the only known class of glutamate receptors, making the development of glutamate-modulating therapeutics a precarious proposition. Although seizure liability and excitotoxicity increase the risks for clinical development of iGluR agonists and hallucinatory and dissociative effects increase risks for the development of iGluR antagonists, there is still some progress being made via the implementation of more sophisticated pharmacologic strategies (Chen & Lipton, 2006).

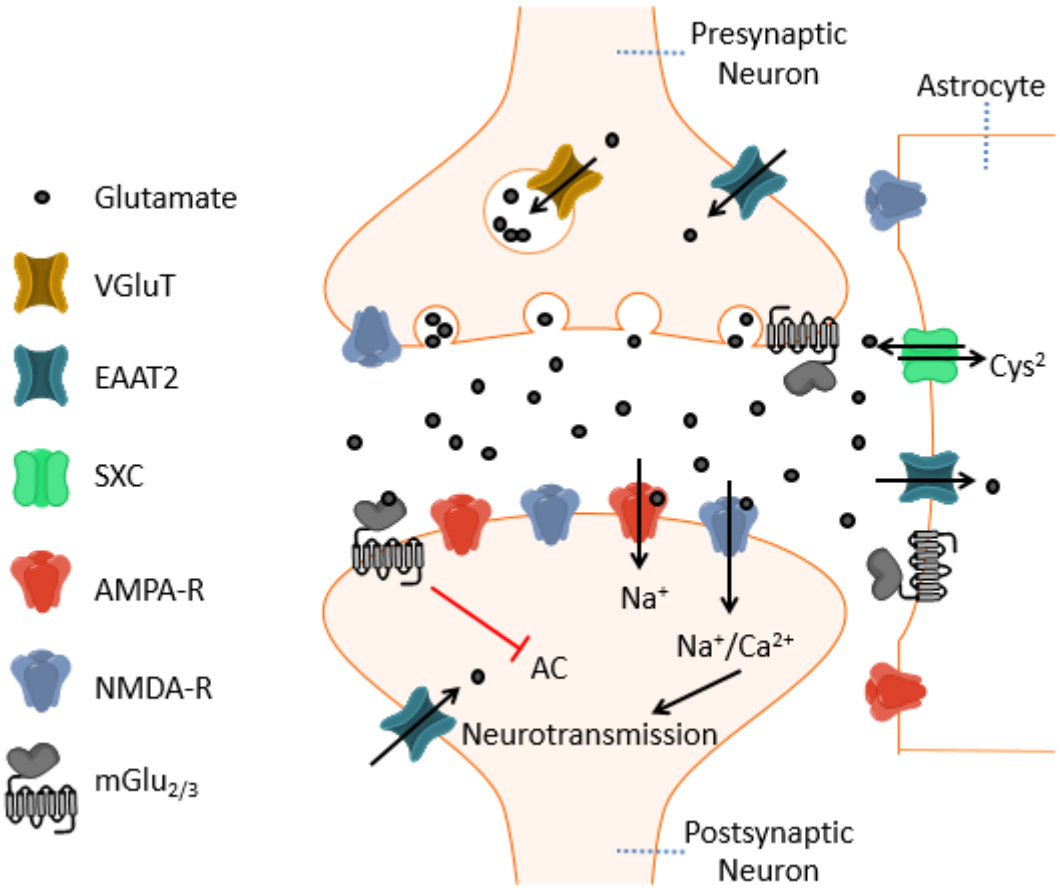

Figure I.1 A schematic model of a glutamatergic synapse expressing $mGlu_{2/3}$. Glutamate is packaged into vesicles by the vesicular glutamate transporter (VGluT) for subsequent release following membrane depolarization. Release of glutamate into the synaptic cleft allows it to act upon iGluRs and mGlu receptors. Activation of iGluRs causes cell membrane depolarization and furthering neurotransmission. Activation of the group II mGlu receptors, which are expressed on both pre- and post-synaptic receptors, as well as in astrocytes, decreases the activity of AC and generally acts to limit further glutamate release. Neuronal and astrocytic EAATs act to remove glutamate from the synaptic cleft and terminate signaling. SXC transporters can transport one molecule of glutamate to the extracellular environment for each cystine (the oxidation product of two cysteine residues joined by a disulfide bond) that is taken into the intracellular environment.

Fortunately, the discovery of mGlu receptors has opened up an alternative pathway to development of glutamate-modulating therapeutics; because these receptors primarily act to modulate the characteristics of glutamate response, rather than being responsible for the rapid, direct propagation of neuronal signals, they are thought to have lower intrinsic adverse effect liabilities than iGlu receptors (P J Conn & Pin, 1997). Since the time of their discovery there has been a steadily increasing interest in the elucidation of the physiological role of mGlu receptors, as well as in the development of mGlu receptor-targeting therapeutics for the treatment of a wide range of neuropsychiatric illnesses. Targeting of the group II mGlu receptors, $mGlu_2$ and $mGlu_3$, has been of particular interest in the context of schizoaffective, depressive, anxiety, and substance dependence disorder (Hovelsø et al., 2012; Nicoletti et al., 2011).

Structure and function of the group II metabotropic glutamate receptors

The group II mGlu receptors, like all of the members of the mGlu receptor family, are class C GPCRs. This class of proteins has four major structural elements: an N-terminal signal sequence, a large extracellular ligand-binding domain, a heptahelical transmembrane-spanning domain (7TM), and a C-terminal cytoplasmic tail. The extracellular domain is characteristic of the class C GPCRs, and is composed of the Venus-flytrap domain (VFT), so called due to its bilobate structure, and a cysteine rich domain (CRD) that is present in all family members aside from the gamma-amino butyric acid receptor B ($GABA_B$). In $mGlu_2$ and $mGlu_3$, the VFT contains the glutamate binding site, which is formed by the cleft between the two mobile lobes; glutamate binding stabilizes these lobes in a closed conformation, whereas antagonist binding stabilizes

the open conformation. A crystal structure of the $mGlu_3$ extracellular domain revealed that the CRD is a 68 amino acid region that contains nine fully-conserved cysteine residues among class C GPCRs and forms a structurally independent feature that separates the VFT and 7TM regions (Muto, Tsuchiya, Morikawa, & Jingami, 2007) (**Figure I.2**). *In vitro* mutagenesis studies have revealed that in mGlu receptor-like receptors the CRD contains a conserved disulfide bridge with the VFT that is required for agonist-induced activation of the receptors. Furthermore, class C GPCRs are distinguished from the other classes due to their formation of constitutive dimers that can undergo transactivation (Gregory, Noetzel, & Niswender, 2013). These dimer pairs can be either homo- or heteromeric – in the case of the Group II receptors, $mGlu_{2/3}$ heterodimers have been frequently observed, and the presence of $mGlu_2$ and serotonin 2A ($5HT_{2A}$) heterodimers has been experimentally confirmed to integrate serotonin (5HT) and glutamate signaling (González-maeso et al., 2008).

The human $mGlu_2$ and $mGlu_3$ receptors have a sequence homology of 66% overall, with a 70% homology in the glutamate binding site and 75% homology over the entirety of the 7TM domain. This high degree of homology has traditionally made it difficult to generate ligands that are selective for one of the receptor subtypes over the other (Lundström et al., 2011). However, mutagenesis studies have identified a ligand binding pocket in the 7TM domain of these receptors that is analogous to the endogenous ligand binding site in class A, rhodopsin-like, GPCRs (May, Leach, Sexton, & Christopoulos, 2007).

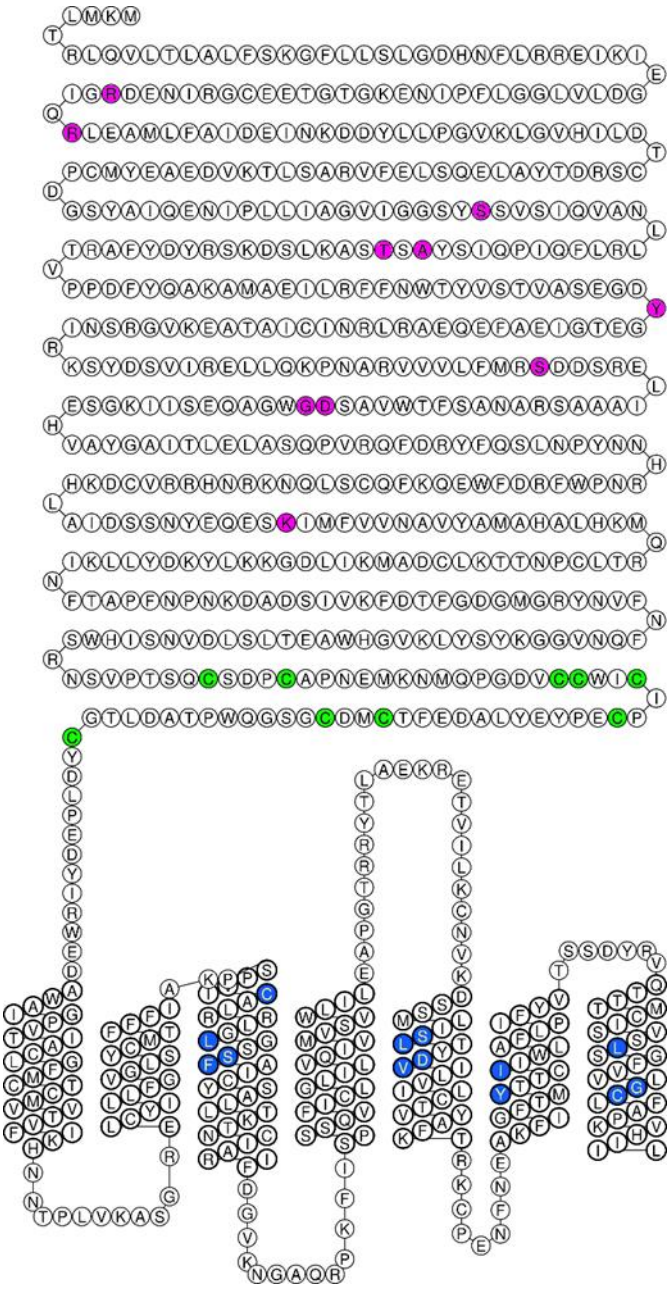

Figure I.2 A snake plot of the residues defining the major structural features of human $mGlu_3$ receptor, with the extracellular N-terminal VFT domain shown at the top, the CRD in the center, and the 7TM domain at the bottom. The final 52 residues comprising the C-terminal tail have been omitted. Residues that have been identified via crystal structures as either direct or indirect mediators of glutamate binding have been highlighted in magenta. The nine cysteine residues of the CRD have been highlighted in green. Residues that have been implicated in the binding of allosteric modulators by analogy to $mGlu_1$ and $mGlu_5$ are highlighted in blue.

Crystal structures of the 7TM regions of $mGlu_1$ and $mGlu_5$ with exogenous ligands bound at this site reveal that even with highly homologous receptors, subtle structural differences in this region can be exploited by small molecules, thus generating subtype-selectivity (Doré et al., 2014; H. Wu et al., 2014). Similar findings have been reported via mutagenesis studies (Gregory et al., 2013). This binding site is termed 'allosteric', and is a source of significant interest for the development of selective $mGlu_2$ and $mGlu_3$ ligands (Chun, Zhang, & Liu, 2012).

Ligands for Metabotropic Glutamate Receptors 2 and 3

Orthosteric versus allosteric regulation

Like the VFT described above for the mGlu receptors, each receptor possesses a distinctive binding site for its respective endogenous ligand(s). This location is defined as the orthosteric binding site, and both native and synthetic ligands that bind to this site are termed orthosteric ligands (Bridges & Lindsley, 2008). For GPCRs and ion channels, the orthosteric ligands may be small neurotransmitters or large peptides (Kenakin & Miller, 2010; Melancon et al., 2012) Classical synthetic orthosteric ligands, typically identified through radioligand binding assays, compete with these ligands for occupancy of the target and display a wide range of pharmacology – agonist, antagonist, partial agonist, and inverse agonist. Historically, almost all of the compounds that have been FDA-approved for therapeutic use bind at a receptor's orthosteric site; however, these ligands can suffer from a lack of efficacy, decreased efficacy upon chronic administration, limited or poor selectivity, and/or resistance (Keov, Sexton, &

Christopoulos, 2011). GPCRs, ion channels, caspases, kinases, and phospholipases have been found to possess, in addition to orthosteric binding sites, allosteric (from the Greek for "other site") binding sites that are topologically and often functionally distinct from their orthosteric counterparts, such as the 7TM site found in mGlu receptors (Christopoulos, 2002). The presence of such allosteric sites allows for numerous additional ligand-receptor interactions and signaling phenomena beyond those associated with the orthosteric sites. This new allosteric approach has been heralded by the evolution of high-throughput screening (HTS) and functional assays that enable the identification of molecules that affect target function irrespective of the site of binding. Although the pharmacology has many target-specific caveats, receptors and proteins that are conformationally dynamic can be modulated by small molecules that bind at allosteric sites, either alone or in the presence of the endogenous orthosteric ligand in order to stabilize an active or inactive conformation of the receptor. An active conformation elicits target activation and downstream signaling; an inactive one blocks signaling (Kenakin & Miller, 2010). As the allosteric ligand stabilizes a unique conformation of the protein, the protein-ligand complex is in essence a new receptor that has a propensity for unique pharmacology. This phenomenon has been termed 'ligand-biased signaling' (Digby, Conn, & Lindsley, 2010). Many efforts have failed to produce highly selective orthosteric compounds that would be suitable as drug leads for GPCRs, kinases, and ion channels owing to a highly conserved orthosteric site and/or to unfavorable physicochemical, metabolic, or pharmacokinetic properties of synthetic orthosteric ligands. In many cases, direct-acting agonists have proved either to be toxic

or to lead to receptor desensitization, internalization, or down-regulation due to prolonged periods of receptor activation. Allosteric ligands, by binding at sites that are under less evolutionary pressure for conservation across a receptor family, typically afford unprecedented levels of selectivity. Moreover, allosteric ligands have a ceiling effect in that once allosteric sites are occupied, no additional effects are observed. In addition, an allosteric modulator that lacks agonistic activity exerts its effects only when the endogenous agonist is present, preserving the temporal and spatial activity of the endogenous ligand.

For GPCRs and ion channels, allosteric ligands can possess a diversity of modes of pharmacology, including the following: positive allosteric modulators (PAMs), which potentiate agonist-mediated receptor response; negative allosteric modulators (NAMs), which noncompetitively decrease activity; and neutral allosteric ligands (NALs), which bind at allosteric sites and can block the activity of PAMs and NAMs, yet have no effect on orthosteric ligand responses by themselves (Kenakin & Miller, 2010). More elaborate modes of allosteric modulation have also been reported, although a formalized nomenclature for these modes of pharmacology has yet to emerge. Significant efforts have been directed at the development of allosteric agonists. These compounds are allosteric ligands that activate the receptor in the absence of the orthosteric ligand. However, many reported allosteric agonists may actually be bitopic ligands, that is, hybrid orthosteric/allosteric ligands that bind to both the orthosteric and allosteric sites. These bitopic ligands display receptor expression-dependent pharmacology, ligand-biased signaling, and confounding structure-activity relationships (SAR) (Digby et al.,

2012; Melancon et al., 2012). Other allosteric ligands are partial antagonists. These ligands fully occupy the NAM site but only partially block receptor signaling. Ago-PAMs, which are PAMs that have inherent allosteric agonist activity, have also been widely reported. However, SAR analysis has been challenging, as these modes of pharmacology are highly variable within a given chemical series.

Allosteric regulation in drug discovery

Although allosteric regulation of proteins by small molecules was first proposed in the mid-twentieth century, the concept took several decades to come to prominence. Many point to 1965 as the year that allosterism was formalized, as the Monod-Wyman-Changeux model proposed conformational selection mechanisms to describe the action of ligands with bacterial regulatory enzymes (Monod, Wyman, & Changeux, 1965). However, attention became more formally focused on allosteric drug discovery as a viable therapeutic strategy upon the clinical success of the benzodiazepines; these allosteric ligands potentiate the effect of the neurotransmitter GABA at the ionotropic $GABA_A$ receptor and overcome the potentially deadly effects of direct-acting $GABA_A$ agonists (Möhler, Fritschy, & Rudolph, 2002). Since this discovery, interest in the development of allosteric ligands as medications has been steadily increasing. In fact, the number of publications that reference allosteric receptor modulators has grown at a nearly exponential rate between 1985 and the present day, and this growth is paralleled in the patent literature. This increase in both publication and patent activity reflects a generalized spread of interest in the development of allosteric ligands across a broad range of targets, including ion channels, kinases, caspases, GPCRs, and phospholipases.

Each of these classes contains many therapeutically relevant targets, and a wide variety of academic and commercial groups have pursued allosteric drug discovery efforts. The development of this field reveals that a new small molecule design strategy, as well as more pharmacological and disposition scrutiny, is required to effectively develop safe and effective allosteric ligands as potential therapeutics (Kenakin & Miller, 2010; Melancon et al., 2012; Möhler et al., 2002).

Although many advantages over orthosteric modulation have been realized, allosteric modulation is not a panacea for drug discovery, and there are many pharmacological and chemical issues to consider when developing allosteric ligands. In terms of pharmacology, the sources of concern are the following: (*a*) The limited evolutionary pressure on allosteric sites can engender significant species differences; (*b*) the state dependence of allosteric modulators could be a liability in degenerative pathologies with progressive loss of endogenous orthosteric tone; (*c*) signal bias introduced by allosteric modulators could lead to unwanted or unpredicted physiological effects; and (*d*) allosteric modulators may be simultaneously activating homo- and heterodimers of the target receptor, which could unnecessarily complicate the physiological response (Fang, Grütter, & Rauh, 2012). Chemical complications are centered on very shallow allosteric ligand SAR, difficulty incorporating polar and solubilizing groups (lowering logP), and the propensity for these ligands to switch pharmacological mode or target with small structural modifications. Despite these challenges, two allosteric modulators of GPCRs have entered the market: a calcium-sensing receptor PAM named cinacalcet and a CCR5 NAM named maraviroc (Meanwell

& Kadow, 2007; Nemeth et al., 2004). Numerous allosteric kinase inhibitors are in various stages of human clinical trials, and the benzodiazepines have been highly successful therapeutics that allosterically regulate ion channels.

Orthosteric ligands for the group II metabotropic glutamate receptors

The first synthetic ligands that were designed to selectively modulate the signaling of the group II mGlu receptors were constrained glutamate analogues that bind at the orthosteric site of $mGlu_2$ and $mGlu_3$ (**Figure I.3**). Examples of compounds that contain a constrained version of glutamate (**I.1**) with a preference for activation of the group II receptors include (*1S,3R*)-ACPD) (**I.2**), (*2R,4R*)-APDC (**I.3**), L-CCG-1 (**I.4**), DCG-IV (**I.5**), (*S*)-3-carboxy-4-hydroxyphenylglycine (**I.6**), LY354740 (**I.7**), and LY379268 (**I.8**) (D. Sheffler & Pinkerton, 2011). Many of these constrained-glutamate orthosteric ligands for the group II receptors were developed by researchers at Eli Lilly and Co. as part of their program to advance an $mGlu_{2/3}$ agonist through clinical trials for the treatment of schizophrenia. *N*-acetyl-L-aspartyl-L-glutamic acid (NAAG) (**I.9**) is an intriguing orthosteric agonist that did not arise from any directed synthetic efforts; rather, it is an endogenous neuropeptide that arises from the conjugation of *N*-acetyl aspartic acid and glutamic acid by NAAG synthetase (Nicoletti et al., 2011). NAAG is the most abundant neuropeptide and the third most prevalent neurotransmitter in the mammalian CNS (Neale, Bzdega, & Wroblewska, 2000). NAAG is also noteworthy for being classified a selective $mGlu_3$ agonist, in contrast to the other non-selective group II agonists, which provided early evidence that $mGlu_2$ and $mGlu_3$ could be selectively targeted by appropriate compounds.

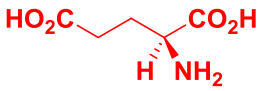

L-Glutamic Acid

I.1

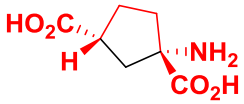

(1S,3R)-ACPD

I.2

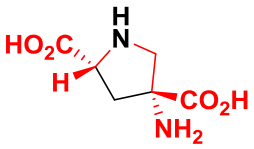

(2R,4R)-APDC

I.3

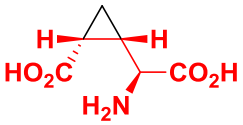

L-CCG-I

I.4

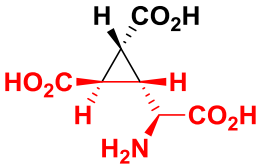

DCG IV

I.5

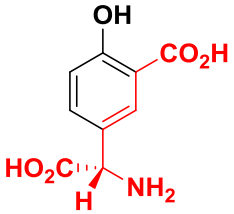

(S)-3-Carboxy-4-hydroxyphenylglycine

I.6

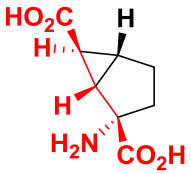

LY354740

I.7

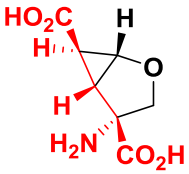

LY379268

I.8

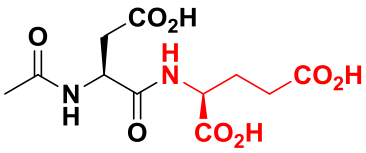

N-acetyl-L-aspartyl-L-glutamic acid

I.9

Figure I.3 The structure of the endogenous orthosteric ligand of $mGlu_2$ and $mGlu_3$, glutamate, along with examples of known orthosteric agonists that exhibit a preference for the group II mGlu receptors as compared to other mGlu receptor subtypes as of 2011. Portions of structures that resemble a constrained version of glutamate are shown in red. Compounds **I.1** and **I.9** are naturally occurring in the body, while compounds **I.2** – **I.8** are synthetically-derived.

In the case of orthosteric antagonists that have preference for blockade of the group II mGlu receptors, there is a bit more deviation from the constrained-glutamate approach, including compounds such as (*RS*)-APICA (**I.10**) and E4CPG (**I.11**); however, many of the most commonly used orthosteric antagonists, including EGLU (**I.12**) and LY341495 (**I.13**), still contain an obvious glutamate backbone (**Figure I.4**). The other available orthosteric antagonists suffer from significant inhibition of the other mGlu receptors, particularly the group III receptors, at similar concentrations needed to inhibit $mGlu_2$ and $mGlu_3$.

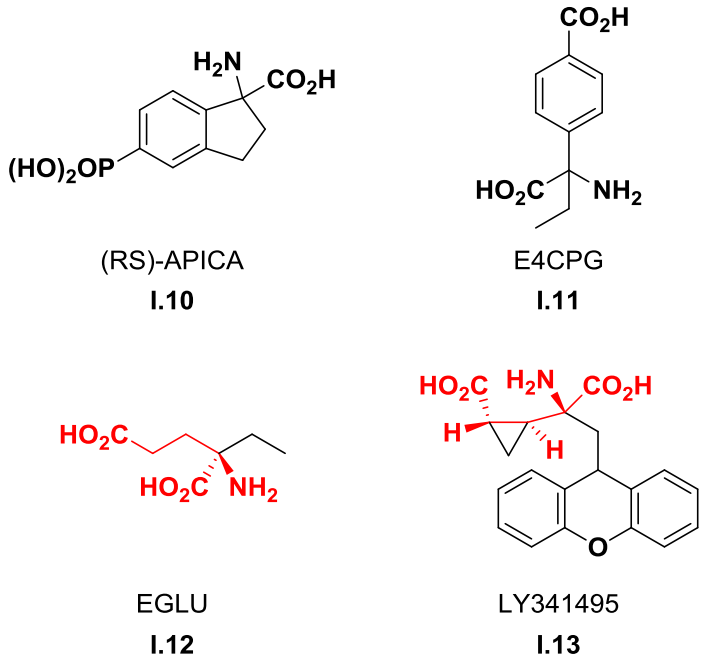

Figure I.4 Examples of known orthosteric antagonists as of August 2011 that exhibit a preference for the group II mGlu receptors as compared to other mGlu receptor subtypes. Portions of structures that resemble a constrained version of glutamate are shown in red. All compounds depicted are synthetically-derived.

Allosteric ligands for the group II metabotropic glutamate receptors

In contrast to the vast majority of the orthosteric ligands available for at the outset of the efforts detailed here, which could generally only distinguish between the three broad groups of mGlu receptors, allosteric ligands were already achieving high levels of specificity for individual mGlu receptor subtypes. Allosteric modulators of $mGlu_5$, both PAMs and NAMs, paved the way for an increasingly large number of mGlu receptor allosteric modulators (**Figure I.5**). Of the four possible categories of selective allosteric modulators for group II mGlu receptors ($mGlu_2$ PAMs, $mGlu_3$ PAMs, $mGlu_2$ NAMs, and $mGlu_3$ NAMs), only $mGlu_2$ PAMs had been described at the time this project was initiated. This category has traditionally been well represented across a broad range of chemical scaffolds, and highly-selective, well-characterized examples such as BINA (**I.14**), LY487379 (**I.15**), CBiPES (**I.16**), THIIC (**I.17**) and GSK1331268 (**I.18**) were relatively prevalent at the outset of this endeavor (D. J. Sheffler, Pinkerton, Dahl, Markou, & Cosford, 2011).

However, regarding compounds that diminished receptor activity, only dual $mGlu_{2/3}$ NAMs had been reported at the initiation of the work reported here, most notably MNI-137 (**I.19**), RO4491533 (**I.20**), and LY2389575 (**I.21**). Regardless of this dearth of NAM compounds, the documented success in generating selective $mGlu_2$ PAMs generated optimism that selective $mGlu_2$ and $mGlu_3$ NAMs, along with $mGlu_3$ PAMs, could eventually be discovered by pursuing additional chemical leads.

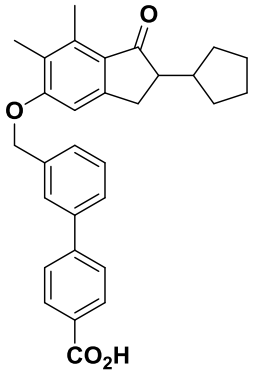

BINA
I.14

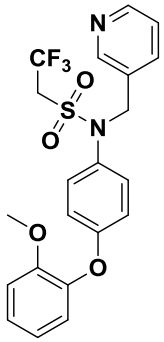

LY487379
I.15

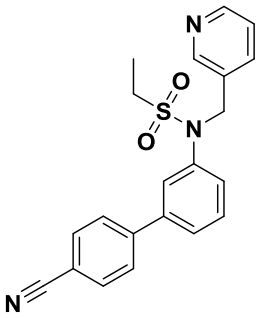

CBiPES
I.16

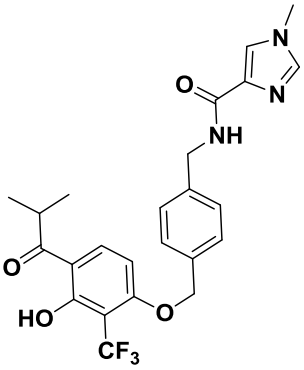

THIIC
I.17

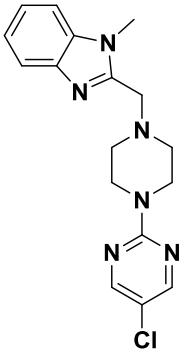

GSK1331268
I.18

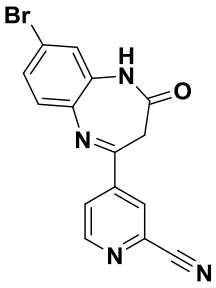

MNI 137
I.19

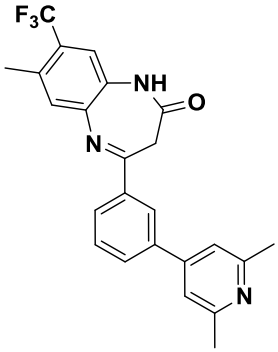

RO4491533
I.20

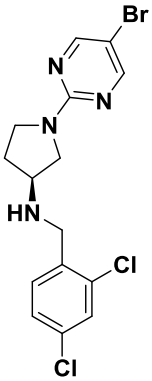

LY2389575
I.21

Figure I.5 Examples of known, well-characterized $mGlu_2$ PAMs and $mGlu_{2/3}$ NAMS as of August 2011. These allosteric ligands are thought to bind to the 7TM domain, inserting themselves between helices 3, 5, 6, and 7.

Role of the Metabotropic Glutamate Receptors 2 and 3 in Psychiatric Illnesses

The group II metabotropic glutamate receptors and schizophrenia

Schizophrenia is a psychiatric illness that affects around one out of every one-hundred individuals worldwide, and is characterized by three symptom clusters: positive, negative, and cognitive. The positive symptom cluster is largely defined as the presence of delusions and hallucinations; the negative symptom cluster includes social withdrawal, lack of motivation, and flattened affect; and the cognitive symptom cluster reflects dysfunction in memory, attention, and decision making (*Diagnostic and Statistical Manual of Mental Disorders*, 2013). Current antipsychotics are focused on antagonism of the dopamine receptor 2 (D_2) (Beaulieu & Gainetdinov, 2011). These therapeutics primarily treat the positive symptoms, with little to no efficacy for the amelioration of negative and cognitive symptoms. Additionally, these first- and second-generation antipsychotics have a substantial adverse effect burden, including the induction of metabolic dysfunction and a risk of developing severe motor disturbances, including tardive dyskinesia (Chien & Yip, 2013). These efficacy and side effect concerns demonstrate the need for the development of improved therapeutics for schizophrenia.

A large body of evidence now supports the involvement of dysfunctional glutamatergic signaling in the etiology of schizophrenia (Noetzel, Jones, & Conn, 2012). Initial indications that NMDA receptors could be involved came from observation of individuals taking NMDA receptor antagonists such as phencyclidine (PCP) or ketamine. These compounds appeared to mimic the positive, negative, and cognitive symptoms demonstrated by patients with schizophrenia, leading to the hypothesis that NMDA

receptor hypofunction was contributing to the etiology of schizophrenia (Moghaddam & Javitt, 2011). There has been a considerable amount of effort levied to investigate the mechanism by which NMDA receptor hypofunction could induce these effects. The current understanding invokes decreased downstream activation of GABAergic neurons to induce disinhibition and elevate excitatory signaling in key brain regions, including the hippocampus, amygdala, striatum, thalamus, and prefrontal cortex – regions that also happen to express high concentrations of the group II mGlu receptors. Because activation of presynaptic group II mGlu receptors is known to inhibit glutamate release, $mGlu_{2/3}$ agonism has been widely speculated to be a therapeutic mechanism to mitigate the effects induced by NMDA receptor hypofunction (Gregory et al., 2013; P. Harrison & Lyon, 2008).

Indeed, the interest in exploitation of this mechanism has led to a series of clinical trials sponsored by Eli Lilly and Co. to measure the safety and efficacy of an $mGlu_{2/3}$ agonist in patients with schizophrenia (Downing et al., 2014; Kinon et al., 2011). Through the course of these studies, no substantial safety concerns were seen with these compounds, but no consistent efficacy signals emerged either. Despite positive efficacy data in an early phase II trial, a second phase II study and a phase III study did not demonstrate superiority over placebo. These discrepancies have led some to venture that early efficacy signals seen in these trials were lost after chronic dosing due to receptor desensitization following constant activation of $mGlu_{2/3}$ (Hopkins, 2013). Others have suggested that there is a subset of individuals who are genetically-predisposed to respond more robustly (Kinon, Millen, Zhang, & McKinzie, 2015; Liu et

al., 2012). These conflicting viewpoints, along with the contradictory genetic and pharmacologic evidence implicating the involvement of only one or both of the group II mGlu receptors, highlight the importance of the development of selective allosteric modulators for $mGlu_2$ and $mGlu_3$ (P. Harrison & Lyon, 2008; Jia et al., 2014; Woolley, Pemberton, Bate, Corti, & Jones, 2008). Such compounds have significant potential as tools to help unravel the complex involvement of glutamatergic signaling in schizophrenia, and to help define the most appropriate pharmacologic mechanism to pursue when considering activation of the group II mGlu receptors for the treatment of schizophrenia.

The group II metabotropic glutamate receptors and depression

Major depressive disorder (MDD) is a highly-prevalent illness, with 350 million individuals estimated to be affected by MDD in 2012 (*Depression - WHO Fact Sheet*, 2012). The impact of this illness on society is correspondingly large, as depression is among the top three leading causes of lost disability-adjusted life-years (DALYs) as of 2010 (Ferrari et al., 2013). The enormous impacts of depression on workplace productivity and overall quality of life are derived from the debilitating nature of the symptoms that define the disorder, including loss of interest in formerly pleasurable activities, feelings of guilt of low self-worth, decreased energy, persistent sadness, and disturbances in sleep and appetite. Furthermore, depression is one of the most important risk factors for suicide, particularly in adolescents (*Diagnostic and Statistical Manual of Mental Disorders*, 2013). Worldwide, only about half of the individuals with depression are currently receiving treatment(*Depression - WHO Fact Sheet*, 2012). For

those patients who are receiving treatment, the primary classes of medications used are selective serotonin reuptake inhibitors (SSRIs), serotonin/norepinephrine reuptake inhibitors (SNRIs), tricyclic antidepressants (TCAs), and monoamine oxidase inhibitors (MAOIs). Unfortunately, these therapeutics often take 3-4 weeks before effects are seen. Although there is not currently a consensus definition for treatment-resistant depression (TRD), it is estimated that 30%-50% of patients are considered to have stage II TRD, meaning that they have failed to achieve adequate responses to at least two different classes of antidepressant medications (Trevino, McClintock, McDonald Fischer, Vora, & Husain, 2014). TRD patients will often be prescribed an augmenting drug, such as lithium or an antipsychotic; in the absence of efficacy with these options, some individuals will experience success with electroconvulsive therapy (ECT) (Bschor, Bauer, & Adli, 2014). Because of the stigma associated with these treatments, along with the significant treatment burden on patients to acquire these therapies, there is interest in developing rapid-acting antidepressants that work for TRD.

One of the agents that has been studied for the treatment of TRD is ketamine. In a double-blind crossover trial, ketamine has demonstrated a rapid and robust antidepressive effect in patients (Murrough, Iosifescu, Chang, & Al Jurdi, 2013). A separate study revealed that ketamine compares favorably to ECT for the treatment of TRD (Ghasemi et al., 2014). The efficacy of an NMDA antagonist in the treatment of depression has opened the door for the study of further mechanisms that will decrease glutamatergic signaling, including the use of $mGlu_{2/3}$ antagonists or NAMs. Thus far, several antagonists and dual $mGlu_{2/3}$ NAMs have shown efficacy in preclinical models of

antidepressant efficacy (Ago et al., 2013; Koike, Iijima, & Chaki, 2013; Pilc, Wierońska, & Skolnick, 2013). Paradoxically, $mGlu_{2/3}$ PAMs and agonists have also shown efficacy in these models (Chaki, Ago, Palucha-Paniewiera, Matrisciano, & Pilc, 2013). These seemingly conflicting results are suggestive of the possibility that different forms of depression are generated from distinct neurochemical changes, a possibility that is especially intriguing in the case of anxious depression. Another possibility is that $mGlu_2$ and $mGlu_3$ have differing effects on the pathways inducing the antidepressant effect, and individual compounds are exhibiting bias towards one or the other of the two receptor subtypes. Selective $mGlu_2$ and $mGlu_3$ NAMs have the potential to resolve some of these questions, and could open the door for a new class of antidepressant therapeutics.

The group II metabotropic glutamate receptors and anxiety disorders

As a group, anxiety disorders affect about 18% of American adults in any given year. These disorders feature an excessive or persistent period of fear and anxiety, typically lasting for six or more months, and panic attacks can feature prominently as a particular type of fear response (*Diagnostic and Statistical Manual of Mental Disorders*, 2013). Panic attacks are abrupt surges of fear or intense discomfort that peak within minutes and lead to a cluster of physical and mental symptoms, including palpitations, sweating, shaking, shortness of breath, chest pain, nausea, dizziness, chills, numbness, depersonalization, fear of losing control, or fear of dying. Within the overall anxiety disorder classification, the individual disorders differ from one another due to the object or situation that induces the fear and anxiety response. Individual disorders listed in the

5th edition of the Diagnostic and Statistical Manual of the American Psychiatry Association (DSM-5) are separation anxiety disorder, selective mutism, specific phobias, social anxiety disorder, panic disorder, agoraphobia, and generalized anxiety disorder (GAD). First-line therapeutics for the treatment of anxiety disorders are SSRIs or SNRIs, which can be problematic in terms of their time to onset, as described above. Other antidepressants are used as second-line therapies, and use of benzodiazepines is also common, although these $GABA_A$ receptor PAMs carry a substantial risk for the development of substance abuse problems. Dysregulation of several neurotransmitter systems, including glutamate, are thought to play a role in anxiety disorders (Amiel & Mathew, 2007). Both $mGlu_{2/3}$ antagonists and selective $mGlu_2$ PAMs have shown some efficacy in rodent behavioral models that predict anxiolytic activity (Bespalov et al., 2008; Linden et al., 2005). In clinical studies, one of Eli Lilly and Co.'s $mGlu_{2/3}$ agonists, LY354740, demonstrated efficacy in treating patients with either panic attacks or generalized anxiety disorder (Pitsikas, 2014). Unfortunately, the development of LY354740 was terminated due to seizure-liabilities seen in pre-clinical animal models, although no seizures were seen in human subjects. Given the frequent co-morbidity of depression and anxiety disorders, and the common neurochemical basis for treatment of both, it is not extraordinarily surprising that similar confusions regarding group II agonism versus antagonism have arisen in studies for both disorders. However, this discrepancy, where both agonists and antagonists of group II mGlu receptors appear to be efficacious in anxiety models, once again highlights the need for an improved

understanding of the individual roles that the group II mGlu receptors have in the etiology and treatment of psychiatric illnesses.

The group II metabotropic glutamate receptors and substance dependence

Substance dependence is a widespread problem with severe societal and economic impacts, but relatively few reliable treatment options. Approximately 8.5% of American adults will need treatment for alcohol or drug-related problems during their lifetime (Substance Abuse and Mental Health Services Administration, 2013). Although there has been a dramatic improvement in the understanding of how drugs of abuse interact with and perturb central reward pathways, these findings have not always fully translated into the successful development of new therapeutic strategies for the treatment of addiction (Nutt, Lingford-Hughes, Erritzoe, & Stokes, 2015). Indeed, there are still no currently-approved therapeutics for the treatment of cocaine, methamphetamine, or cannabis dependence; cognitive-behavioral therapy remains the primary treatment these forms of drug dependence. For other addictions, most notably nicotine and opioids, replacement therapies are the treatment modality of choice (Abuse, 1999).

However, several converging lines of evidence indicate that drugs of abuse can perpetuate their own use by inducing alterations in synaptic strength within key reward centers in the brain, including the nucleus accumbens (NAc) and the ventral tegmental area (VTA) (Shen, Moussawi, Zhou, Toda, & Kalivas, 2011; van Huijstee & Mansvelder, 2015). In addition to their widespread cortical distribution, the $mGlu_2$ and $mGlu_3$

receptors are also highly expressed in the NAc and VTA (Majo et al., 2013). Given the importance of glutamate-mediated dopamine release in these regions, along with the known role of mGlu receptors in the induction of synaptic plasticity, there has been tremendous interest in the development of $mGlu_{2/3}$ agonists and PAMs for the treatment of addictions. To date, the administration of these classes of compounds has resulted in decreased self-administration of cocaine, nicotine, and ethanol, suppression of cue- and stress-induced reinstatement, and reduced incubation of craving following withdrawal from cocaine or methamphetamine in animal models (Hovelsø et al., 2012; Moussawi & Kalivas, 2010). However, significant questions remain regarding the propensity of $mGlu_{2/3}$ agonists to suppress seeking of natural rewards, and the role of $mGlu_{2/3}$ dysfunction in the etiology of substance abuse. Further exploration of the individual roles of $mGlu_2$ and $mGlu_3$ in this context will help answer such questions.

The group II metabotropic glutamate receptors and other neuropsychiatric illnesses

Other disorders that have been postulated as potentially benefiting from application of compounds acting at $mGlu_2$ and $mGlu_3$ include Alzheimer's disease, Parkinson's disease, stroke, seizure, and certain brain tumors, particularly gliomas (Caraci et al., 2011; Ciceroni et al., 2013; Niswender & Conn, 2010b). The role of the group II receptors in these disorders is generally focused on the reduction of excitotoxicity in the presence of a noxious stimulus, and the importance of astrocytic $mGlu_3$ is often invoked in such discussions (Caraci et al., 2012; Durand, Carniglia, Caruso, & Lasaga, 2012). While the studies described within this document do not directly address any of these topics, the selective tools developed within certainly have the

potential to impact the future directions that researchers will be able to pursue while studying these conditions.

Conclusions

The group II mGlu receptors, $mGlu_2$ and $mGlu_3$, are broadly expressed glutamate receptors in the mammalian CNS. These receptors act to regulate synaptic glutamate release over both short and long-term time scales, thus impacting downstream neurotransmitter release and contributing to the broadly-described processes of learning and memory. Due to their similarity, previous generations of compounds have rarely been able to discriminate between the two receptors, leading to studies that could only make aggregate conclusions regarding the functions of these two receptors. A combination of medicinal chemistry, molecular biology, pharmacology, and structural biology studies have uncovered the existence of allosteric sites within these receptors. These sites can be exploited to generate chemical compounds that can selectively act at either $mGlu_2$ or $mGlu_3$ independently, and chemical tools of this type have the potential to impact the study and treatment of a number of highly-prevalent neuropsychiatric illnesses, including schizophrenia, depression, anxiety, and addiction.

CHAPTER II

MATERIALS AND METHODS

Chemical Synthesis, Analysis, and Purification Techniques

Iterative, parallel, multidimensional synthesis

The general strategy employed for the progression of the chemical efforts described herein was one of iterative, parallel, multidimensional synthesis. This strategy was directed towards the optimization of compound potency, efficacy, and pharmacokinetic parameters over repeated rounds of synthesis and analysis. At the outset of an optimization effort, the scaffold in question was retrosynthetically divided into regions that were synthetically accessible, and amenable to library synthesis. After this process, libraries containing 10-100 members would then be generated, each focused on installation of targeted chemical alterations at one of the identified retrosynthetic regions. Following purification, all final compounds were diluted in Dimethylsulfoxide (DMSO) to a 10 µM concentration in a 2D-barcoded vial. Each individual compound was then assigned a 7-digit VU number (VUID). This VUID was cross-correlated with the compounds' notebook number and structure during registration with the Chemcart™ or Dotmatics™ database maintained by the Vanderbilt Center for Neuroscience Drug Discovery (VCNDD).

These compounds were then screened in one or more of the molecular pharmacology assays described below in order to generate SAR data describing the relationship between structural changes and activity of the compounds at the assayed targets. Compounds with favorable potency and efficacy parameters in comparison to the other synthesized analogues would then undergo *in vitro* pharmacokinetic analysis using the techniques described in the pharmacokinetic analysis and metabolite identification section below. These data were then analyzed, and a new set of structural analogues were designed and generated with the benefit of the knowledge gained during the previous round of synthesis. In this way, several regions of the compound can be studied in parallel. Findings relevant to each region were then assessed in matrix libraries, where optimized structures from each region were combined to assess whether these alterations are compatible with one another in terms of potency, efficacy, and pharmacokinetics. This process would continue until an analogue was generated that fulfilled the goals of the optimization effort (**Figure II.1**).

General methods and instrumentation

NMR spectra were recorded on Bruker (300 - 600 MHz) spectrophotometers. ^{1}H chemical shifts are reported in ppm relative to the residual DMSO peak as an internal standard set to δ 2.50. ^{13}C chemical shifts are reported in ppm with the residual DMSO carbon peak set to 39.52 ppm. Data are reported as follows: chemical shift, multiplicity (s = singlet, d = doublet, t = triplet, q = quartet, br = broad, m = multiplet, dd = doublet of doublets), coupling constant (Hz), integration.

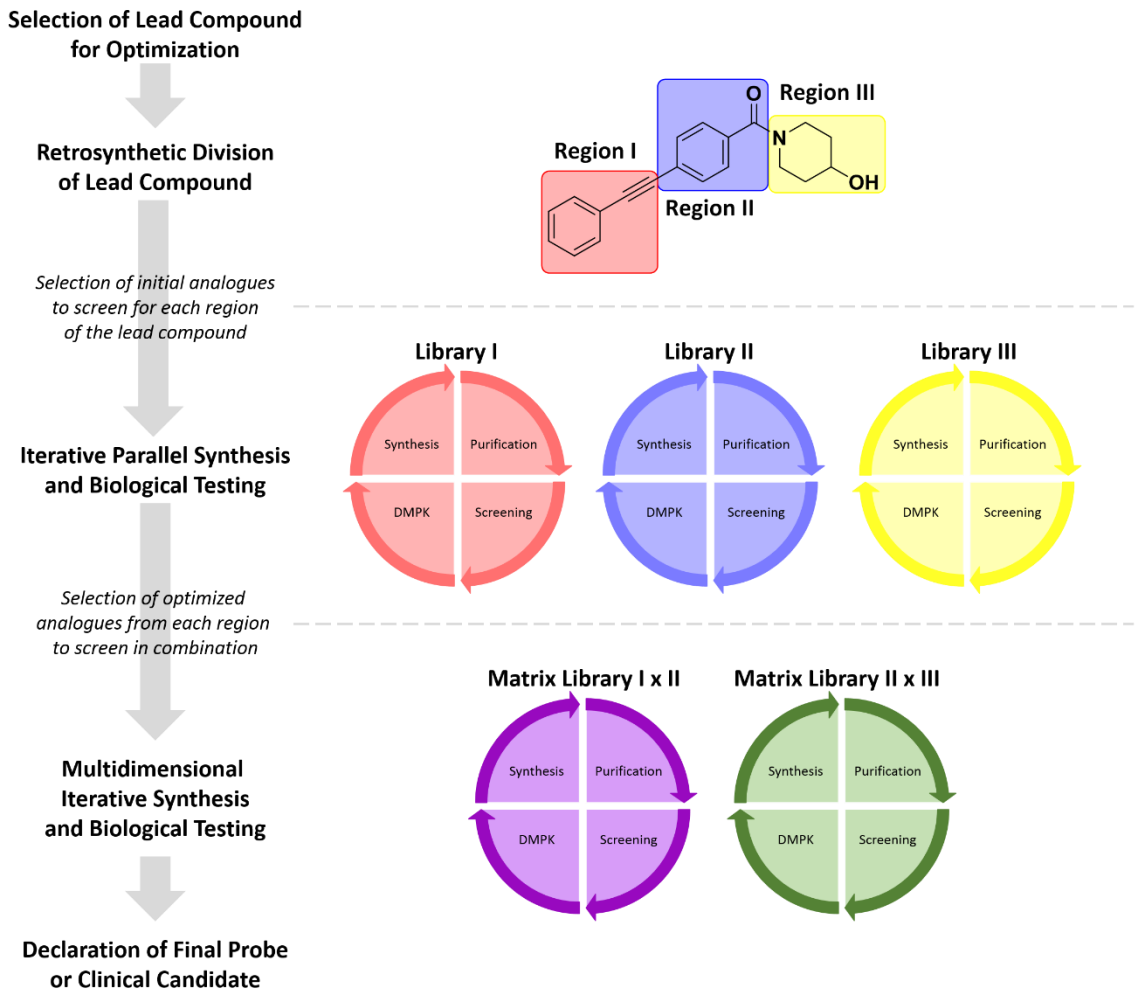

Figure II.1 A generalized diagram of the workflow associated with iterative, parallel, multidimensional synthesis in order to generate an optimized analogue within a chemical series. Starting with a lead compound, a retrosynthetic plan is devised to generate libraries with a high degree of diversity to explore chemical space around the lead compound. As new analogues are generated and tested, the data is used to devise new analogues with improved biological performance. The chemical properties of the best analogues can then be combined in an attempt to generate even better compounds. The process continues through several rounds until a compound is generated that has suitable achieved the target parameters defined by the goals of the program. This process may also be undertaken on several lead scaffolds at once.

Low resolution mass spectra were obtained on an Agilent 6130 Quadrupole LC/MS with electrospray ionization. High resolution mass spectra were recorded on a Waters Qtof-API-Us plus Acuity system with electrospray ionization. Analytical thin layer chromatography was performed on 0.25 mm silica plates from Sorbent Technologies, and visualized with UV light. Analytical HPLC was performed on an Agilent 1200 with UV detection at 214 and 254 nm along with ELSD detection. Preparative purification was performed on a Gilson chromatograph using a Luna 5u C_{18} (2) 100A AXIA column (30 x 50 mm) using a water/acetonitrile gradient. Purities of compounds were in all cases greater than 95%, as determined by reversed-phase HPLC analysis. Chiral separations were performed on a Thar Investigator II supercritical fluid chromatograph (SFC) using Lux Cellulose 4 (10x250 mm), Chiralpak IA (10 x 250 mm), and Chiralpak ID (10x250 mm) columns. Solvents for extraction, washing and chromatography were HPLC grade. Optical rotations were acquired on a Jasco P-2000 polarimiter at 23 ^{o}C and 589 nm. The specific rotations were calculated according to **Equation II.1**. Except where specifically noted, all reagents were purchased from Aldrich Chemical Co. and were used without purification.

$$[\alpha]\frac{23}{D} = \frac{100\alpha}{l} \text{ x } c \qquad \textbf{[II.1]}$$

Equation II.1 Calculation of specific rotations for enantiopure compounds. l is the path length in decimeters and c is the concentration in g/100 mL.

Molecular Pharmacology Techniques

Cell culture

Rat $mGlu_2$/HEK-293 cells stably transfected expressing the chimeric G protein $G_{\alpha15}$ were cultured in 90%Dulbecco's Modified Eagle Media (DMEM), 10% dialyzed fetal bovine serum (FBS), 100 units/mL penicillin/streptomycin, 20 mM HEPES (pH 7.3), 1 mM sodium pyruvate, 2 mM glutamine, 0.1 mM non-essential amino acids, 700 µg/mL G418 sulfate (Mediatech, Inc., Herndon, VA) and 600 ng/mL puromycin at 37 ^{o}C in the presence of 5% CO_2. Rat $mGlu_3$ ($mGlu_3$)/TReX cells transfected expressing the chimeric G protein $G_{\alpha15}$ under the control of a Tetracycline inducible promoter were cultured in 90% Dulbecco's Modified Eagle Media (DMEM), 10% dialyzed fetal bovine serum (FBS), 100 units/mL penicillin/streptomycin, 20 mM HEPES (pH 7.3), 1 mM sodium pyruvate, 2 mM glutamine, 0.1 mM non-essential amino acids, 700 µg/mL G418 sulfate (Mediatech, Inc., Herndon, VA), 100 µg/mL hygromycin, and 5 µg/mL Blasticidin S at 37 ^{o}C in the presence of 5% CO_2. All cell culture reagents were purchased from Invitrogen Corp. (Carlsbad, CA).

Calcium mobilization assays

Rat $mGlu_2$/$G_{\alpha15}$/HEK-293 or $mGlu_3$/$G_{\alpha15}$/TReX cells (15,000 cells/20 µL/well) were plated in black-walled, clear-bottomed, poly-d-lysine coated, 384 well plates (Greiner Bio-One, Monroe, North Carolina) in DMEM containing 10% dialyzed FBS, 20 mM HEPES, 100 units/mL penicillin/streptomycin, and 1 mM sodium pyruvate (Assay Media). The cells were grown overnight at 37 ^{o}C in the presence of 5% CO_2.

During the day of assay, the medium was replaced with 20 µL of 1 µM Fluo-4, AM (Invitrogen, Carlsbad, CA) prepared as a 2.3 mM stock in DMSO and mixed in a 1:1 ratio with 10% (w/v) pluronic acid F-127 and diluted in Assay Buffer (Hank's balanced salt solution, 20 mM HEPES and 2.5 mM Probenecid (Sigma-Aldrich, St. Louis, MO)) 1 hour at 37 °C. Dye was removed and replaced with 20 µL of Assay Buffer. Test compounds were transferred to daughter plates using an Echo acoustic plate reformatter (Labcyte, Sunnyvale, CA) and then diluted into Assay Buffer. Ca^{2+} flux was measured using the Functional Drug Screening System 7000 (FDSS, Hamamatsu, Japan). Baseline readings were taken (10 images at 1 Hz, excitation, 470±20 nm, emission, 540±30 nm) and then 20 µL/well test compounds were added using the FDSS's integrated pipettor. Cells were incubated with compounds for approximately 2.5 min and then an EC_{80} concentration of glutamate was applied.

For concentration-response curve experiments, compounds were serially diluted 1:3 into 10 point concentration response curves and were transferred to daughter plates using the Echo. Test compounds were again applied and followed by EC_{80} concentrations of glutamate.

For fold shift experiments, compounds were added at 2X their final concentration and then increasing concentrations of glutamate were added in the presence of vehicle or the appropriate concentration of test compound. Together, the CRC and fold-shift data were used to determine the potency and mechanism of action for each compound at $mGlu_2$ and $mGlu_3$ (**Figure II.2**).

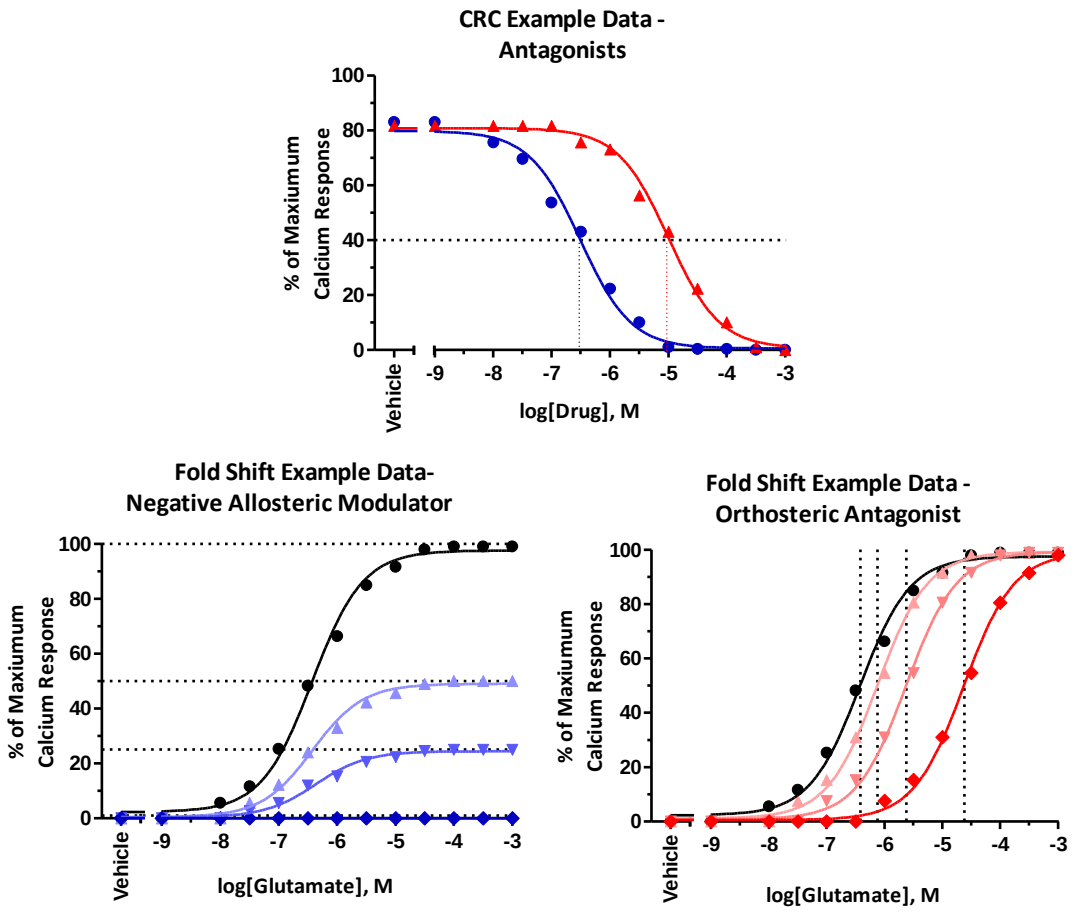

Figure II.2 Example data for CRC and fold shift experiments using antagonists. Potency for an antagonist can be determined by increasing the compound's concentration in the presence of a fixed concentration of an agonist (in this case, glutamate); finding the concentration of compound that inhibits 50% of the maximal cellular response will define that compound's IC_{50}. In the example above, the blue compound (IC_{50} = 300 nM) is more potent than the red compound (IC_{50} = 10 µM). The shape of the curve will not distinguish between orthosteric and allosteric inhibitors in a CRC assay. However, a fold-shift assay can distinguish between these two modes of action. In this assay, the response to a range of agonist concentrations (in this case, glutamate) is measured in the presence of several different fixed concentrations of an antagonist. Increasing concentrations of an allosteric modulator (blue) will proportionally decrease the maximal response of the agonist. In contrast, increasing concentrations of an orthosteric antagonist (red) will proportionally decrease the apparent potency of the agonist.

For selectivity experiments, full concentration-response curves of glutamate or L-AP4 (for $mGlu_7$) were performed in the presence of a 10 µM concentration of compound, and compounds that affected the concentration-response by less than 2 fold in terms of potency or efficacy were designated as inactive. All curves were fitted using a four point logistical equation using Microsoft XLfit (IDBS, Bridgewater, NJ). Subsequent confirmations of concentration response parameters were performed using independent serial dilutions of source compounds and data from multiple days experiments were integrated and fit using a four point logistical equation in GraphPad Prism (GraphPad Software, Inc., La Jolla, CA, version 5.01).

Thallium flux assays

Cells were plated into 384 well, black-walled, clear-bottom poly-D-lysine coated plates (Greiner) at a density of 15,000 cells/20 µL/well in DMEM containing 10% dialyzed FBS, 20 mM HEPES, and 100 units/ml penicillin/streptomycin (Assay Media). Plated cells were incubated overnight at 37 ˚C in the presence of 5% CO2. The following day, plated cells had their medium exchanged to Assay Buffer (Hanks Balanced Salt Solution (Invitrogen) containing 20 mM HEPES pH 7.3) using an ELX405 microplate washer (BioTek), leaving 20 µL/well, followed by addition of with 20 µL of 330 nM FluoZin-2 AM (Invitrogen, Carlsbad, CA) prepared as a 2.85 mM stock in DMSO and mixed in a 1:1 ratio with 10 percent (w/v) pluronic acid F-127 and diluted in Assay Buffer for 1 hour at room temperature. The dye was then exchanged to Assay Buffer using an ELX405, leaving 20 µL/well and the plates were incubated at room temperature for 10 min prior to assay. For concentration-response experiments, compounds were serially

diluted 1:3 into 10 point concentration response curves in DMSO, were transferred to daughter plates using an Echo acoustic plate reformatter (Labcyte, Sunnyvale, CA), and diluted into Assay Buffer to generate a 2X stock. Agonists were diluted in Thallium Buffer (125 mM sodium bicarbonate (added fresh the morning of the experiment), 1 mM magnesium sulfate, 1.8 mM calcium sulfate, 5 mM glucose, 12 mM thallium sulfate, 10 mM HEPES, pH 7.3) at 5X the final concentration to be assayed. Thallium flux was measured using the Functional Drug Screening System 6000 or 7000 (FDSS 6000 or FDSS 7000, Hamamatsu, Japan). Baseline readings were taken (10 images at 1 Hz, excitation, 470 ± 20 nm, emission, 540 ± 30 nm) and then 20 µL/well test compounds were added using the FDSS's integrated pipettor. Approximately 2.5 minutes later 10 µL of Thallium Buffer ± agonist was added. After the addition of agonist, data were collected for an approximately 3 additional min. Data were analyzed as described (Niswender et al., 2008). For fold shift experiments, compounds were added at 2X their final concentration and then increasing concentrations of glutamate were added in the presence of vehicle or the appropriate concentration of test compound. For selectivity experiments, full concentration-response curves of glutamate or L-AP4 (for $mGlu_7$) were performed in the presence of a 10 µM concentration of compound, and compounds that affected the concentration-response by less than 2 fold in terms of potency or efficacy were designated as inactive.

[^{3}H]-LY341495 competition binding

Membranes were prepared by harvesting confluent plates of stable HEK cell lines constitutively expressing rat $mGlu_2$ or $mGlu_3$ receptors. The media was aspirated from

these plates, followed by washing with 5 mL of ice-cold phosphate-buffered saline (PBS). The PBS was aspirated, then 5 mL of PBs was added, and cells were scraped off of the plate. The resulting cell-suspension was then transferred to a 50 mL conical tube, and centrifuged at 1,000 g for 5 minutes at 4 °C, using an Avanti JE Beckman Centrifuge mounted with a JS-5.3 rotor. The supernatant was aspirated following centrifugation, and 10 mL of assay buffer (10 mM KH_2PO_4, 100 mM KBr, pH 7.6) were added. The cells were homogenized three times in 10 second bursts, using a TR-10 Tekmar polytron, then centrifuged at 1,000 g for 10 min at 4 °C. The supernatants were removed and transferred into a 40 mL Nalgene centrifuge tube #3119-0050. The supernatants were then centrifuged at 20,000 g for 30 minutes at 4 °C after mounting a JA-20 Rotor on the centrifuge. The supernatant was then discarded, and the membrane pellet was suspended in assay buffer, to an approximate concentration of 1 mg/mL. This suspension was homogenized using a glass homogenizer, and absolute protein concentrations were determined by spectrophotometric analysis of the membrane suspension in the presence of serial dilutions of bicinchoninic acid (BCA) and cupric sulfate.

Binding reactions were carried out in 2 mL, clear, 96-well, deep well plates (Axygen Scientific) and contained 2 nM [^{3}H]-LY341495 (PerkinElmer), 20 µg of membrane protein, and an eleven-point concentration range of test compound or glutamate in a total volume of 500 µL assay buffer. Nonspecific binding was determined in the presence of 1 mM glutamate. The K_d of [^{3}H]-LY341495 was found to be 1.67 nM at $mGlu_2$ and 0.75 nM at $mGlu_3$. Binding reactions were performed at ambient

temperature and allowed to incubate for 3 hours on a Lab-Line Titer plate shaker at setting 7 (~750 rpm). Reactions were terminated by rapid filtration through GF/B glass microfiber filter plates (1 µm pore size) using a 96-well Brandel harvester and washed 3X with ice-cold harvesting buffer (50 mM Tris-HCl, 0.9% NaCl, pH 7.4). Filter plates were dried overnight and counted in a PerkinElmer TopCount scintillation counter (PerkinElmer Life and Analytical Sciences). Actual [^{3}H]-LY341495 concentration was back-calculated after counting aliquots of 10X [^{3}H]-LY341495 used in the reaction. For all assays, radioligand depletion was kept to approximately 30% or less. Plotting of data and calculation of *Ki* was performed using the curve-fitting software of GraphPad Prism.

[^{3}H]-LY341495 dissociation kinetics

Membranes were prepared from HEK cell lines constitutively expressing rat $mGlu_3$ receptors in the same manner as for the [^{3}H]-LY341495 competition binding experiments. Binding reactions were carried out in 2 mL, clear, 96-well, deep well plates (Axygen Scientific) and initially contained cell membranes (20 µg) and a saturating amount (1 nM) of [^{3}H]-LY341495 and test compound (10 µM). Binding was allowed to equilibrate at ambient temperature for 45 minutes on a Lab-Line Titer plate shaker at setting 7 (~750 rpm). LY341495 (100 nM) was then added at various time points over 3.5 hours in a final volume of 500 µL. Plate agitation was continued between additions. Nonspecific binding was determined in the presence of 100 nM LY341495. Reactions were terminated by rapid filtration through GF/B glass microfiber filter plates (1 µm pore size) using a 96-well Brandel harvester and washed 3X with ice-cold harvesting buffer (50 mM Tris-HCl, 0.9% NaCl, pH 7.4). Filter plates were dried overnight and

counted in a PerkinElmer TopCount scintillation counter (PerkinElmer Life and Analytical Sciences). Actual [^{3}H]-LY341495 concentration was back-calculated after counting aliquots of 10X [^{3}H]-LY341495 used in the reaction. For all assays, radioligand depletion was kept to approximately 10% or less. Plotting of data and calculation of $t_{1/2}$ was performed using the curve-fitting software of GraphPad Prism.

Ancillary/off-target screening assays

Prior to conducting *in vivo* experiments, compounds were submitted to Eurofins Panlabs Lead profiling screening panel of 68 GPCRs, ion channels, enzymes, transporters, and nuclear hormone receptors. Test compounds (10 µM) were evaluated in competition binding assays using standard orthosteric radioligands for each target (*n* = 2). Results were calculated as % inhibition of radioligand binding, with >50% inhibition representing significant activity at a given target.

Electrophysiological recordings

Coronal slices through the mPFC (300–400 µm) were prepared from ICR (CD1), $mGlu_2$, and $mGlu_3$ knockout mice with a vibrating microtome (VT1200s; Leica). After anesthesia with a mixture of ketamine and xylazine (100 mg/kg and 10 mg/kg IP), mice were perfused with a 4 °C sucrose-based cutting buffer containing 230 mM sucrose, 2.5 mM KCl, 10 mM $MgSO_4$, 0.5 mM $CaCl_2$, 1.25 mM NaH_2PO_4, 10 mM glucose, 26 mM $NaHCO_3$, and 0.5 mM sodium ascorbate. Brain slices were then incubated at 32 °C for 12–15 min in an N-methyl-D-glucamine (NMDG)-based recovery solution and then transferred to a holding chamber with artificial cerebrospinal fluid (aCSF) containing 126 mM NaCl, 2.5

mM KCl, 1 mM $MgSO_4$, 2 mM CaCl2, 1.25 mM NaH2PO4, 10 mM glucose, 26 mM $NaHCO_3$, 5 mM sodium ascorbate, and 12 mM N-acetylcysteine. Recording aCSF was identical aside from the exclusion of sodium ascorbate and N-acetylcysteine. fEPSPs were recorded from layer V of PL, using a pulled-glass pipette (3–5 MΩ), and evoked by electrical stimulation of layer II/III (0.05 Hz), using a concentric bipolar electrode. Three consecutive fEPSP slopes were averaged and then normalized to the mean baseline slope before drug application. LTD was measured as the average slope across the last 5 min of the recording session.

Intracellular calcium imaging experiments were conducted only on cells exhibiting stereotypical properties of pyramidal cells. Experiments commenced after at least a 15-min dialysis time and were conducted in the presence of tetrodotoxin (TTX; 1 µM) to isolate Ca^{2+} signals due to direct activation of postsynaptic receptors and to exclude modulation of presynaptic neurotransmitter release. Agonist application occurred for 10 min after fluorescence readings were stable for at least 5 min. Application of $mGlu_3$ NAMs began 5 min before the beginning of the baseline recording and co-terminated with the agonist application. Images were collected with a Cool Snap HQ camera (Photometrics) and MetaFluor software (Molecular Devices). An external shutter was mounted to a mercury light source (Olympus Instruments), connected to the microscope with a liquid light guide tube, and controlled with a Lambda 10-2 (Sutter Instruments) interfaced with the imaging software. Cellular fluorescence was measured from a region within the soma of the labeled neuron and was background subtracted using a fluorescence reading taken from a region near the cell, but not containing any

processes. Changes in fluorescence in the background-subtracted signal were calculated as ΔF/F.

Pharmacokinetic Analysis and Metabolite Identification Techniques

Plasma-protein and brain-homogenate binding

The protein binding of each compound was determined in plasma via equilibrium dialysis employing rapid equilibrium dialysis (RED) plates (ThermoFisher Scientific, Rochester, NY). Plasma was added to the 96 well plate containing test compound and mixed thoroughly for a final concentration of 5 µM. Subsequently, an aliquot of the plasma-compound mixture was transferred to the *cis* chamber (red) of the RED plate, with a phosphate buffer (25 mM, pH 7.4) in the *trans* chamber. The RED plate was sealed and incubated for 4 hours at 37°C with shaking. At completion, aliquots from each chamber were diluted 1:1 with either plasma (*cis*) or buffer (*trans*) and transferred to a new 96 well plate, at which time ice-cold acetonitrile containing internal standard (50 ng/mL carbamazepine) (2 volumes) was added to extract the matrices. The plate was centrifuged (3000 RCF, 10 min) and supernatants transferred and diluted 1:1 (supernatant: water) into a new 96 well plate, which was then sealed in preparation for LC/MS/MS analysis. Each compound was assayed in triplicate within the same 96-well plate.

A similar approach was used to determine the degree of brain homogenate binding, which employed the same methodology and procedure with the following modifications: 1) a final compound concentration of 1 µM was used, 2) naïve rat brains

were homogenized in DPBS (1:3 composition of brain: DPBS, w/w) using a Mini-Bead Beater™ machine in order to obtain brain homogenate, which was then treated in the same manner as the plasma samples in the previously described plasma protein binding assay. Fraction unbound for both plasma and brain samples was determined using **Equation II.2**.

$$F_u = \frac{Conc_{buffer}}{Conc_{plasma}} \qquad [\textbf{II.2}]$$

Equation II.2 Determination of fraction unbound in plasma. Fraction unbound in brain can be calculated in the same manner by using brain homogenate rather than plasma.

Hepatic microsomal intrinsic clearance

Human or rat hepatic microsomes (0.5 mg/mL) and 1 µM test compound were incubated in 100 mM potassium phosphate pH 7.4 buffer with 3 mM $MgCl_2$ at 37°C with constant shaking. After a 5 min preincubation, the reaction was initiated by addition of NADPH (1 mM). At selected time intervals (0, 3, 7, 15, 25, and 45 min), aliquots were taken and subsequently placed into a 96-well plate containing cold acetonitrile with internal standard (50 ng/mL carbamazepine). Plates were then centrifuged at 3000 RCF (4° C) for 10 min, and the supernatant was transferred to a separate 96-well plate and diluted 1:1 with water for LC/MS/MS analysis. The *in vitro* half-life ($t_{1/2}$, min), intrinsic clearance (CL_{int}, mL/min/kg) and subsequent predicted hepatic clearance (CL_{hep}, mL/min/kg) were determined using **Equations II.3 – II.5**

$$T_{1/2} = \frac{Ln(2)}{k} \qquad \textbf{[II.3]}$$

Equation II.3 Determination of half-life. *k* represents the slope from linear regression analysis of the natural log percent remaining of test compound as a function of incubation time.

$$CL_{\text{int}} = \frac{0.693}{in\,vitro\,T_{1/2}} x \frac{mL\ incubation}{mg\ microsomes} x \frac{45\,mg\,microsomes}{gram\ liver} x \frac{20^{a}\ gram\ liver}{kg\ body\ wt} \qquad \textbf{[II.4]}$$

Equation II.4 Determination of intrinsic clearance. [a]scale-up factors of 20 (human) or 45 (rat) were used in this calculation.

$$CL_{hep} = \frac{Q_h \cdot CL\,\text{int}}{Q_h + CL\,\text{int}} \qquad \textbf{[II.5]}$$

Equation II.5 Determination of predicted hepatic clearance. Q_h represents hepatic blood flow (ml/min/kg): 21 for human, 70 for rat.

LC/MS/MS bioanalysis of samples

Samples from plasma protein/brain homogenate binding and hepatic microsomal intrinsic clearance assays were analyzed on a Thermo Electron TSQ Quantum Ultra triple quad mass spectrometer (San Jose, CA) via electrospray ionization (ESI) with two Thermo Electron Accella pumps (San Jose, CA), and a Leap Technologies CTC PAL autosampler (Carrboro, NC). Analytes were separated by gradient elution on a dual column system with two Thermo Hypersil Gold (2.1 x 30 mm, 1.9 µm) columns (San

Jose, CA) thermostated at 40 °C. HPLC mobile phase A was 0.1% formic acid in water and mobile phase B was 0.1% formic acid in acetonitrile. The gradient started at 10% B after a 0.2 min hold and was linearly increased to 95% B over 0.8 min; hold at 95% B for 0.2 min; returned to 10% B in 0.1 min. The total run time was 1.3 min and the HPLC flow rate was 0.8 mL/min. While pump 1 ran the gradient method, pump 2 equilibrated the alternate column isocratically at 10% B. Compound optimization, data collection and processing was performed using Thermo Electron's QuickQuan software (v2.3) and Xcalibur (v2.0.7 SP1).

Inhibition of cytochrome P450 enzymes

A cocktail of substrates for cytochrome P450 enzymes (1A2: Phenacetin, 10 µM; 2C9: Diclofenac, 5 µM; 2D6: Dextromethorphan, 5 µM; 3A4: Midazolam, 2 µM) were mixed for cocktail analysis. For P450 2C19, the substrate stock (Mephenytoin, 40 µM) and substrate mix were prepared separately for discrete analysis. The positive control for pan-P450 inhibition (miconazole) was included alongside each test compound in analysis.

A reaction mixture of 100 mM Kpi, pH 7.4, 0.1 mg/mL human liver microsomes (HLM) and Substrate Mix is prepared and aliquoted into a 96-deepwell block. Test compound and positive control (in duplicate) were then added such that the final concentration of test compound ranged from 0.1 – 30 µM. The plate was vortexed briefly and then pre-incubated at 37 ^{o}C while shaking for 15 minutes. The reaction was initiated with the addition of NADPH (1 mM final concentration). The incubation

continued for 8 min and the reaction quenched by 2x volume of cold acetonitrile containing internal standard (50 nM carbamazepine). The plate was centrifuged for 10 min (4000 RCF, 4°C) and the resulting supernatant diluted 1:1 with water for LC/MS/MS analysis. A 12 point standard curve of substrate metabolites over the range of 0.98 nM to 2000 nM.

Samples were analyzed via electrospray ionization (ESI) on an AB Sciex API-4000 (Foster City, CA) triple-quadrupole instrument that was coupled with Shimadzu LC-10AD pumps (Columbia, MD) and a Leap Technologies CTC PAL auto-sampler (Carrboro, NC). Analytes were separated by gradient elution using a Fortis C18 3.0 x 50 mm, 3 µm column (Fortis Technologies Ltd, Cheshire, UK) thermostated at 40°C. HPLC mobile phase A was 0.1% formic acid in water (pH unadjusted), mobile phase B was 0.1% formic acid in acetonitrile (pH unadjusted). The gradient started at 10% B after a 0.2 min hold and was linearly increased to 90% B over 1.2 min; held at 90% B for 0.1 min and returned to 10% B in 0.1 min followed by a re-equilibration (0.9 min). The total run time was 2.5 min and the HPLC flow rate was 0.5 mL/min. The source temperature was set at 500°C and mass spectral analyses were performed using multiple reaction monitoring (MRM), with transitions specific for each compound utilizing a Turbo-Ionspray® source in positive ionization mode (5.0 kV spray voltage).

The IC_{50} values for each compound were obtained for the individual CYP enzymes by quantitating the inhibition of metabolite formation for each probe substrate. A 0 µM compound condition (or control) was set to 100% enzymatic activity and the effect of increasing test compound concentrations on enzymatic activity could then be calculated

from the % of control activity. Curves were fitted using XLfit 5.2.2 (four-parameter logistic model, equation 201) to determine the concentration that produces half-maximal inhibition (IC_{50}).

In vivo plasma and brain drug concentration measurements in rodents

Compounds were formulated as 10% tween 80 micro suspensions in sterile water at the concentration of 1 mg/mL and administered IP to male Sprague- Dawley rats weighing 225 to 250 g (Harlan, Inc., Indianapolis, IN) at the dose of 10 mg/kg. The rat blood and brain were collected at 0.25 h. Animals were euthanized and decapitated, and the brains were removed, thoroughly washed in cold phosphate buffered saline and immediately frozen on dry ice. Trunk blood was collected in EDTA Vacutainer tubes, and plasma was separated by centrifugation and stored at -80°C until analysis. Plasma was separated by centrifugation (4000 RCF, 4°C) and stored at 80°C until analysis. On the day of analysis, frozen whole-rat brains were weighed and diluted with 1:3 (w/w) parts of 70:30 isopropanol: water. The mixture was then subjected to mechanical homogenation employing a Mini-Beadbeater™ and 1.0 mm Zirconia/Silica Beads (BioSpec Products) followed by centrifugation. The sample extraction of plasma (20 µL) or brain homogenate (20 µL) was performed by a method based on protein precipitation using three volumes of ice-cold acetonitrile containing an internal standard (50 ng/mL carbamazepine). The samples were centrifuged (3000 RCF, 5 min) and supernatants transferred and diluted 1:1 (supernatant: water) into a new 96 well plate, which was then sealed in preparation for LC/MS/MS analysis.

In vivo samples were analyzed via electrospray ionization (ESI) on an AB Sciex API-5500 QTrap (Foster City, CA) instrument that was coupled with Shimadzu LC-20AD pumps (Columbia, MD) and a Leap Technologies CTC PAL auto-sampler (Carrboro, NC). Analytes were separated by gradient elution using a Fortis C18 3.0 x 50 mm, 3 µm column (Fortis Technologies Ltd, Cheshire, UK) thermostated at 40°C. HPLC mobile phase A was 0.1% formic acid in water (pH unadjusted), mobile phase B was 0.1% formic acid in acetonitrile (pH unadjusted). The gradient started at 30% B after a 0.2 min hold and was linearly increased to 90% B over 0.8 min; held at 90% B for 0.5 min and returned to 30% B in 0.1 min followed by a re-equilibration (0.9 min). The total run time was 2.5 min and the HPLC flow rate was 0.5 mL/min. The source temperature was set at 500°C and mass spectral analyses were performed using multiple reaction monitoring (MRM), with transitions specific for each compound utilizing a Turbo-Ionspray® source in positive ionization mode (5.0 kV spray voltage). The calibration curves were constructed in blank plasma. All data were analyzed using AB Sciex Analyst software v1.5.1.

Behavioral Pharmacology Techniques

All behavioral pharmacology experiments were carried out with male ICR (CD-1) mice between the ages of 5-7 weeks and weighing between 28-35 grams. All assays were conducted in a quiet room within the Vanderbilt Neurobehavioral Core; individual mice being assayed were isolated from all animals that had yet to undergo testing and all animals that had already completed the assay. Prior to initiation of any behavioral

study, the animals were allowed to habituate to their new cages for at least 3 days after arriving at the facility; following this time period, animals were habituated to handling for 2-3 additional days prior to beginning any assay procedures.

Extinction of conditioned-fear memory

Mice were fear conditioned with seven pairings of a tone conditioned stimulus (CS; 3.5 kHz, 80 dB, 30 s) with mild foot-shock unconditioned stimulus (US; 2 s, 0.6 mA).Mice were returned to their home cages. Twenty-four hours after fear conditioning, CS retrieval and extinction learning were assessed with 20 CS-alone trials (5-s intertribal interval). To limit the effects of contextual conditioning, mice were fear conditioned in a round-walled, metal bar-floored chamber that was scented with 10% (v/v) vanilla extract odor and housed in a room with white ceiling lights. Extinction training occurred in a square-walled, solid-floored chamber that was scented with 10% (v/v) peppermint and housed in a room with red ceiling lights. Mice were dosed with vehicle or $mGlu_3$ NAM VU0477950 (3–100 mg/kg) via intraperitoneal (IP) injection 30 min before extinction training. Freezing behavior defined as the absence of movement other than respiration was used to measure fear and was quantified by computer video analysis software (Video Freeze; Med Associates). Plotting of data and a two-way ANOVA calculation (dose x time) was performed using the curve-fitting software of GraphPad Prism (version 5.01). If significant differences were seen for the means of all groups, a Bonferroni comparison was performed for each group against all other groups.

Open-field locomotor activity

For locomotion experiments mice were injected with mice were injected IP with a dose of Elacridar (20 mg/kg) or vehicle 1.5 hours prior to initiation of the assay, then dosed with test compounds or vehicle 30 minutes prior to initiation of the assay. They were then placed in an open field chamber equipped with infrared beams (Med Associates) to monitor locomotor activity for 1 h. Analysis of total distance traveled, time spent in areas within 5 cm of the edge, and time spent in the center of the area were measured. Plotting of data and a two-way ANOVA calculation (drug x time) was performed using the curve-fitting software of GraphPad Prism (version 5.01). If significant differences were seen for the means of all groups, a Dunnett's comparison was performed for each group against the vehicle treated control.

Porsolt forced swim test

One day prior to the assay, mice were placed individually into 30 cm tall Plexiglas cylinders with a 20 cm diameter, which were filled with 22-25 cm of water at 21-23 ˚C. The animals were placed in the chamber for 15 minutes, then removed and dried with a towel, and placed into a heated cage for 15 minutes for recovery. The animals were then returned to their home cage. On the day of the assay, mice were injected IP with a dose of Elacridar (20 mg/kg) or vehicle 1.5 hours prior to initiation of the assay, then dosed with test compounds or vehicle 30 minutes prior to initiation of the assay. The animals were placed in the Plexiglas cylinders filled with 22-25 cm of water for 6 minutes. Their behavior was monitored by a video camera placed directly in front of the cylinder for the duration of the assay. After 6 minutes, the mice were removed and

dried with a towel, and placed into a heated cage for 15 minutes for recovery. The animals were then returned to their home cage. The videos of each mouse were analyzed for immobility behavior; during the final 4 minutes of each video, the immobility of the mouse was hand-scored by a blinded individual. Immobility was defined as a complete lack of movement by the mouse, other than the minimum necessary to keep the head above water. Plotting of data and a calculation of one-way ANOVA was performed using the curve-fitting software of GraphPad Prism (version 5.01). If significant differences were seen for the means of all groups, a Dunnett's comparison was performed for each group against the vehicle treated control.

Tail suspension test

For the tail suspension test, mice were injected IP with a dose of Elacridar (20 mg/kg) or vehicle 1.5 hours prior to initiation of the assay, then dosed with test compounds or vehicle 30 minutes prior to initiation of the assay. The animals then had a short plastic sheath (2.5 cm) placed around the base of their tail, and were then suspended with their tails in a straight line in an automated tail suspension test cubicle (MED Associates, St. Albans, VT) for a 6 minute observation period. Up to four animals were monitored simultaneously, but were shielded from view of each other. Afterwards, the mice were immediately returned to their home cages. Total time spent immobile was recorded during the 6 minute test, as measured by a force transducer. The threshold for immobility was set at 7 mA; this threshold reliably reproduced immobility scores generated by a blinded observer watching a video of the test. Plotting of data and a calculation of one-way ANOVA was performed using the curve-fitting

software of GraphPad Prism (version 5.01). If significant differences were seen for the means of all groups, a Dunnett's comparison was performed for each group against the vehicle treated control.

Elevated plus maze

For the elevated plus maze, mice were injected IP with a dose of Elacridar (20 mg/kg) or vehicle 1.5 hours prior to initiation of the assay, then dosed with test compounds or vehicle 30 minutes prior to initiation of the assay. The animals were then placed into the center of the elevated plus maze apparatus, which consists of four arms (each approximately 10 x 30 cm) connected in a plus configuration and elevated approximately 50 cm from the ground. Of the four arms, two arms are enclosed with walls approximately 20 cm high, and two arms are open without walls. All tests occurred in a room with a lighting intensity of 320-335 lux. The animals were then observed for a period of five minutes, then immediately returned to their home cage. The number of entries onto the open/walled arms, the amount of time spent in open/walled arms, and the distance traveled were measured. Plotting of data and a calculation of one-way ANOVA was performed using the curve-fitting software of GraphPad Prism (version 5.01). If significant differences were seen for the means of all groups, a Dunnett's comparison was performed for each group against the vehicle treated control.

Marble burying

Plexiglas cages (32 × 17 × 14 cm) were arranged on top of a large, round table. Mice were transported from the colony room to the testing room and were allowed to

habituate for 30 min. Mice were injected IP with a dose of Elacridar (20 mg/kg) or vehicle 1.5 hours prior to initiation of the assay, then dosed with test compounds or vehicle 30 minutes prior to initiation of the assay. Mice were individually placed in the cages in which 12 black glass marbles (14 mm diameter) had been evenly distributed on top of 2.5 cm Diamond Soft Bedding (Harlan Teklad, Madison, WI). Mice receiving the same drug were placed in cages on opposite sides of the table to control for effects of lighting and context. Clear, perforated plastic lids were set on top of each cage, and the amount of marble burying was recorded over a 30-min interval. The mice were then removed from the cages, and the number of buried marbles was counted using the criteria of greater than two-thirds covered by bedding. Plotting of data and a calculation of one-way ANOVA was performed using the curve-fitting software of GraphPad Prism (version 5.01). If significant differences were seen for the means of all groups, a Dunnett's comparison was performed for each group against the vehicle treated control.

Genetic Analysis Techniques

BioVU and the synthetic derivative

All human DNA samples were acquired from Vanderbilt's biorepository, BioVU. This resource consists of DNA samples that have been extracted from discarded blood collected during routine clinical testing. On average, BioVU accrues 500-1000 samples per week, currently housing a total of more than 192,000 DNA samples. While the program was initially designed with an opt-out enrollment process, it now uses an opt-in strategy, where Vanderbilt clinic patients will sign a BioVU research consent form to

signify willingness to participate. All newly-acquired samples are scanned via a program that includes automated exclusion criteria to eliminate samples that represent patients wishing to opt-out, samples not linked to a signed consent form, duplicate samples, and random exclusion to help ensure patient confidentiality. Manual exclusion is also possible for samples with an insufficient volume of blood and/or an unreadable label. Following acceptance of a sample, an encryption program then assigns a unique research ID number to the sample. This ID is generated by a Secure Hash Algorithm (SHA-512, National Security Administration). SHA-512 generates a 128 character, 512 bit code, and the original medical record number cannot be regenerated from the coded ID.

Once collected, DNA samples are then linked to the corresponding de-identified medical record in the Synthetic Derivative. The Synthetic Derivative is a replicate of the electronic medical records system in use at Vanderbilt, but with all personal identifiers removed, and dates shifted by a consistent, random value within a three month window. The removal of identifying information is very efficient – HIPAA identifiers are removed with an error rate of only 0.01%. Thus far, the Synthetic Derivative contains records for more than 2 million patients. These records maintain availability of all clinical information in a searchable form, with a history for each patient that can span for more than ten years. New clinical data are added to the database as they are created. The records in the Synthetic Derivative are labeled with the same 128-digit identifier as the DNA sample to maintain the link between the clinical data and DNA.

The database can be searched via a record counter tool available to all Vanderbilt investigators in order to estimate the number of cases and controls that are

potentially available for a given study. Searches can correspond to billing and/or procedure codes; free text values from clinical notes, such as histories and discharge summaries; and laboratory results.

These record counter searches can estimate values for the number of samples available in the entire Synthetic Derivative or only for records that have been associated with DNA. Once a researcher has determined whether or not the database will be likely to have patients that fit their inclusion and exclusion criteria, a study proposal can be submitted. Following approval by the BioVU Review Committee and the signing of a user agreement, a researcher can then request data access or genotyping for any of the DNA samples available.

Genotyping and data analysis

The Illumina Infinium HumanExome BeadChip includes >240,000 markers, mostly within exonic regions, as well as SNPs from the GWAS catalog (Welter et al., 2014). All samples used in the studies described herein had been previously genotyped on this chip in the Vanderbilt Technologies for Advanced Genomics (VANTAGE) Core, with genotype calling performed by GenomeStudio's GenCall algorithm. Genotyping quality was evaluated using SNP call rates – all SNPs with <95% call rate were excluded. Any SNP that was found to be monomorphic in the study population was also removed. For the control samples the Hardy-Weinberg Equilibrium (HWE) proportions were tested using a Chi-Square test. Any SNP that had a HWE p-value of < 0.0001 was removed.

The acquired genomic data were then processed by the Vanderbilt Technologies for Advanced Genomics Analysis and Research Design (VANGARD) Core using R (Lucent Technologies, version 3.1.2), PLINK (Shaun Purcell – Center for Human Genetics Research, Massachusetts General Hospital, version 1.07), and SNP-set Kernel Association Test (SKAT; TH Chan, Harvard School of Public Health, version 0.90).

CHAPTER III

DEVELOPMENT OF THE FIRST HIGHLY-SELECTIVE, CNS-PENETRANT MGLU$_3$ NEGATIVE ALLOSTERIC MODULATOR SUITABLE FOR *IN VIVO* USE

Prior Discovery of a Dual mGlu$_5$ PAM / mGlu$_3$ NAM on a Biarylacetylene Scaffold

Highly subtype-selective allosteric ligands (PAMs and/or NAMs) have been developed for mGlu$_1$, mGlu$_2$, mGlu$_4$, mGlu$_5$, and mGlu$_7$ (P Jeffrey Conn, Christopoulos, & Lindsley, 2009; Emmitte, 2011; Melancon et al., 2012; Owen, 2011; Robichaud & Engers, 2011; Stauffer, 2011; Gentaroh Suzuki, Tsukamoto, & Fushiki, 2007). However, aside from mGlu$_2$ PAMs, most Group II ligands do not discriminate between mGlu$_2$ and mGlu$_3$; a necessary requirement as these two receptors have highly divergent expression and function (P. J. Harrison, Lyon, Sartorius, Burnet, & Lane, 2008; Woltering et al., 2008). Thus, due to a lack of selective small molecule probes, it has been difficult to discern distinct pharmacological roles for mGlu$_3$. Numerous studies suggest that mGlu$_3$ is highly expressed in glial cells, is intimately involved in glial-neuronal communication, and is also involved in the dysregulation of glial cell precursors that can support growth of brain tumors. These roles indicate that mGlu$_3$ may have a unique therapeutic potential for the treatment of neurodegenerative and excitotoxic conditions including Parkinson's disease, Alzheimer's disease, glioma, stroke, or seizure, as compared to mGlu$_2$. Additionally, both mGlu$_2$ and mGlu$_3$ have been suggested as therapeutic targets for

treatment of schizophrenia, depression, anxiety, and substance dependence disorders (P Jeffrey Conn, Lindsley, & Jones, 2009; Matrisciano et al., 2007; Moghaddam & Javitt, 2011). At the outset of this effort, only two dual $mGlu_{2/3}$ NAMs had been reported (**Figure III.1**). The first, reported by Addex, is RO4491533 (**III.1**), which is based on a benzodiazepinone nucleus that was shown to be efficacious in preclinical cognition and depression models (Campo et al., 2011). At about the same time, Lilly disclosed LY2389575 (**III.2**) as a selective $mGlu_3$ NAM; however, when measuring native coupling of these receptors to G protein coupled inwardly-rectifying potassium (GIRK) channels via thallium flux, **III.2** is only modestly $mGlu_3$ preferring (Caraci et al., 2011).

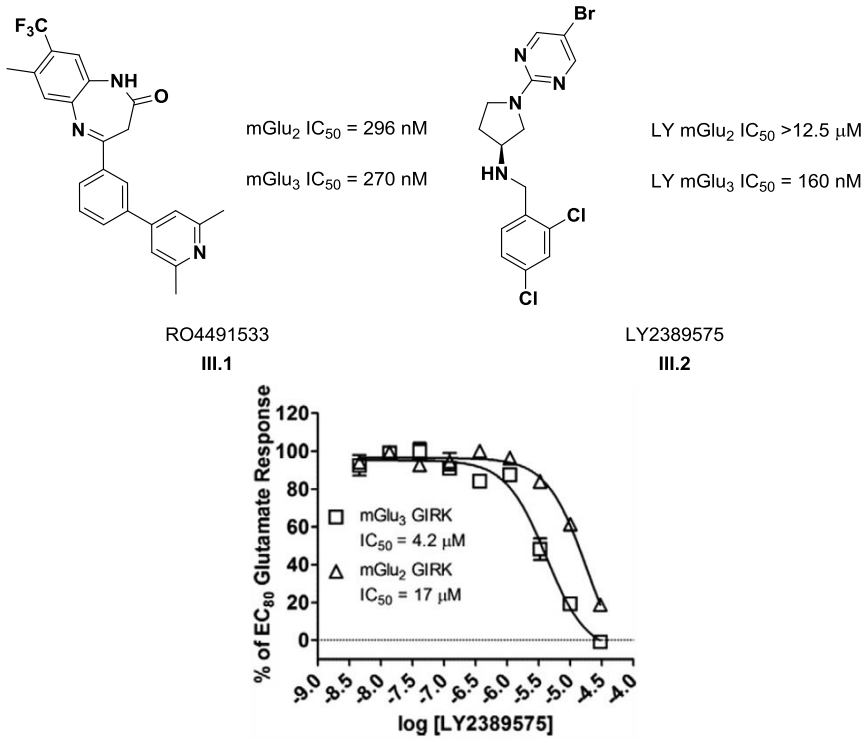

Figure III.1 Structures of previously reported dual $mGlu_{2/3}$ NAMs. The potencies listed alongside the structures represent values reported by the original investigators. In the case of LY2389575, the results of a thallium-flux assay against rat $mGlu_2$ and $mGlu_3$ receptors are presented, along with the calculated IC_{50}s from these results.

In the absence of an HTS campaign to identify novel $mGlu_3$ NAMs, we elected to take advantage of the propensity of certain $mGlu_5$ PAM chemotypes to easily modulate the mode of pharmacology or mGlu subtype selectivity with subtle structural alterations, that is 'molecular switches' (S Sharma & Kedrowski, 2009; Sameer Sharma, Rodriguez, Conn, & Lindsley, 2008; Wood, Hopkins, Brogan, Conn, & Lindsley, 2011).One such chemotype that has been reported to have a high propensity for displaying 'molecular switches' is represented by VU0092273 (**III.3**) (**Figure III.2**). This biarylacetylene scaffold had been previously explored as the basis for a series of $mGlu_5$ PAM compounds that were known to bind in the 7TM region of the mGlu receptors, rather than in the VFT, as is seen with orthosteric ligands. The prototypical biarylacetylene $mGlu_5$ PAM is 2-methyl-6-(phenylethynyl)pyridine (MPEP; **III.4**), although improved efficacy and selectivity were established with later ligands derived from this series, particularly 2-methyl-4-(pyridin-3-ylethynyl)thiazole (MTEP; **III.5**).

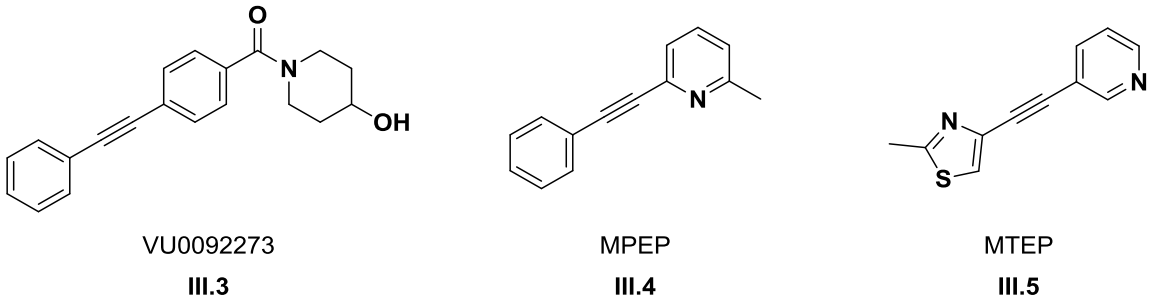

Figure III.2 Structure of VU0092273, the initial lead compound for development of a selective $mGlu_3$ NAM, along with the structures of MPEP and MTEP, two examples of biarylacetylene $mGlu_5$ PAMs.

When assayed using a calcium mobilization assay, this compound was found to possess potent PAM activity at rat $mGlu_5$ receptors, with an EC50 of 270 nM. Surprisingly, after assessing **III.3** with a thallium-flux assay at rat $mGlu_3$ receptors, it was also found to possess weak NAM activity (**Figure III.3**), with an IC_{50} of > 10 μM. Importantly, this compound otherwise showed no activity at the six other mGlu subtypes, including $mGlu_2$. To our knowledge, this represented the first synthetic ligand that had a substantial preference for $mGlu_3$ inactivation as compared to $mGlu_2$. Thus, even though it possessed significant residual activity at $mGlu_5$, **III.3** became the lead compound for our attempts to develop a potent and selective $mGlu_3$ NAM.

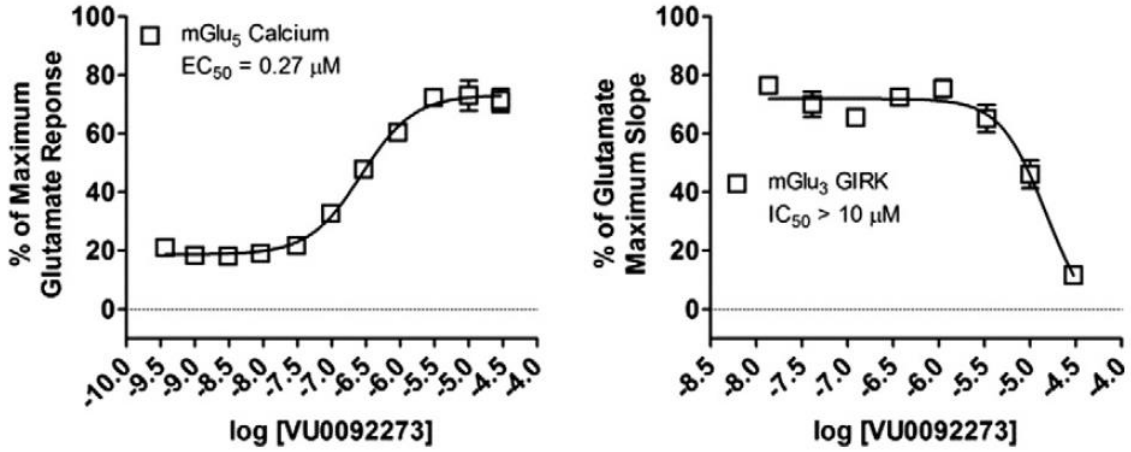

Figure III.3 Concentration-response curves for VU0092273, as determined by a calcium mobilization assay at rat $mGlu_5$ receptors and a thallium-flux assay at rat $mGlu_3$ receptors.

Development of a First-generation $mGlu_3$ NAM, VU0463597 from the Dual $mGlu_5$ PAM / $mGlu_3$ NAM VU0092273

Because it is relatively common to see significant alterations in compound potency following minor structural changes for allosteric modulators, especially in chemical series that are prone to undergo molecular switches, we decided to pursue an iterative parallel synthesis approach for the chemical optimization of **III.3**. This strategy would allow us to assess the impact of distinct chemical alterations at distinct sites across **III.3**, in order to rapidly assess its potential as an $mGlu_3$ NAM scaffold.

Introducing replacements for the distal phenyl group on VU0092273

Previous work on this scaffold indicated that $mGlu_5$ PAM activity could be greatly diminished with substitution other than fluorine on the distal phenyl ring, as well as with modifications to the amide moiety (Williams et al., 2011). Therefore, our first generation library initially held the 4-hydroxypiperidine amide constant, while surveying a diverse array of functionalized aryl and heteroaryl rings as well as other aliphatic groups. Once $mGlu_3$-preferring modifications were identified, these changes would be maintained while an amide scan would be performed in order to improve $mGlu_3$ NAM activity while eliminating $mGlu_5$ PAM activity (**Figure III.4**).

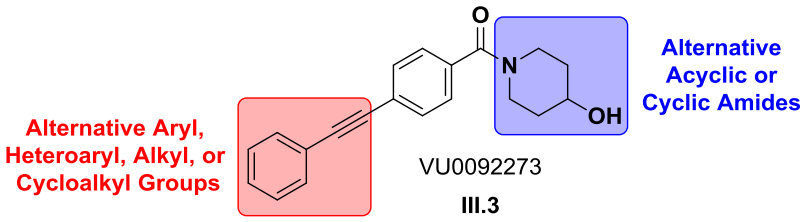

Figure III.4 Library optimization strategy for VU0092273 to eliminate $mGlu_5$ PAM activity while simultaneously improving $mGlu_3$ NAM activity.

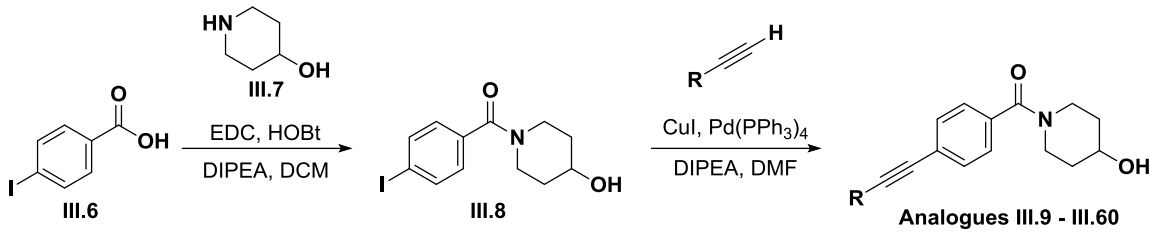

Scheme III.1 Amide coupling and Sonogashira coupling sequence for the synthesis of analogues exploring potential replacements for the distal phenyl moiety in VU0092273 (**III.3**).

Our first library was prepared as shown in **Scheme III.1** and purified, to >98% purity by reverse phase chromatography. Commercially-available 4-iodobenzoic acid (**III.6**) was coupled to commercially-available 4-hydroxypiperdine (**III.7**) under standard 1-Ethyl-3-(3-dimethylaminopropyl)carbodiimide (EDC) and Hydroxybenzotriazole (HOBt) conditions to provide amide **III.8** in 95% yield. Once synthesized, **III.8** then underwent Sonogashira coupling reactions with a diverse array of functionalized terminal acetylenes to provide analogs **III.9 – III.60**.

True to allosteric modulator SAR, nearly all of the analogs were either inactive on $mGlu_3$, with IC_{50}s >10 µM, or only afforded modest inhibition of the EC_{80} glutamate response, 5–50%. Only one compound, **III.31**, displayed an $mGlu_3$ NAM potency below 10 µM. This compound possessed a 4-methoxyphenyl moiety, and its calculated $mGlu_3$ IC_{50} was 3.8 µM, with an inhibited glutamate EC_{80} response (% Glu Min) that only allowed for 10% of the initial level of response. Interestingly, the regioisomeric 3-methoxyphenyl (**III.59**) and 2-methoxyphenyl (**III.60**) congeners were both found to be inactive. (**Table III.1**).

Table III.1 Structures and activities of compounds from library prepared as in **Scheme III.1** when assayed as CRCs in the thallium flux assay.

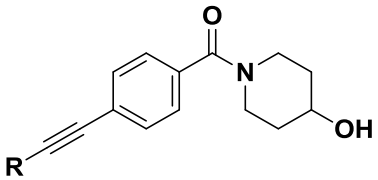

R =	Compound Number	VUID	$mGlu_3$ IC_{50} (μM)	$mGlu_3$ Glu Min %
	**III.9**	VU0092273	> 10	11.6
	**III.10**	VU0402211	> 10	75
	**III.11**	VU0402212	> 10	64.5
	**III.12**	VU0402214	> 10	37
	**III.13**	VU0402215	> 10	22.4
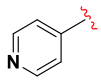	**III.14**	VU0402219	> 10	76.3

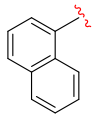	**III.15**	VU0402220	> 10	32.7
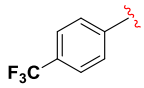	**III.16**	VU0402222	> 10	54.2
	**III.17**	VU0402226	> 10	77
	**III.18**	VU0457286	> 10	74.6
	**III.19**	VU0457287	> 10	76.5
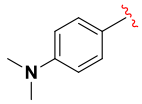	**III.20**	VU0457288	> 10	72.3
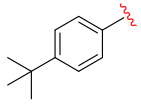	**III.21**	VU0457289	> 10	86.8
	**III.22**	VU0457290	> 10	59.4
	**III.23**	VU0457291	> 10	69.9

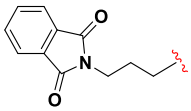	**III.24**	VU0457292	> 10	60.9
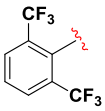	**III.25**	VU0457293	> 10	54.9
	**III.26**	VU0457294	> 10	65.6
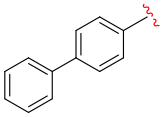	**III.27**	VU0457295	> 10	66.1
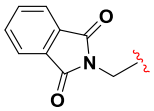	**III.28**	VU0457296	> 10	58.6
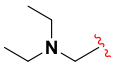	**III.29**	VU0457297	> 10	87.9
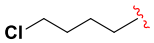	**III.30**	VU0457298	> 10	47.8
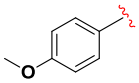	**III.31**	VU0457299	4.43	7.4
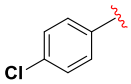	**III.32**	VU0457300	> 10	51.6

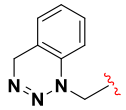	**III.33**	VU0457301	> 10	67.7
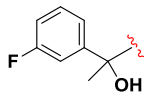	**III.34**	VU0457302	> 10	75.2
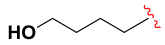	**III.35**	VU0457496	> 10	87
	**III.36**	VU0457497	> 10	46.1
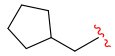	**III.37**	VU0457498	> 10	34
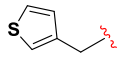	**III.38**	VU0457499	> 10	16.1
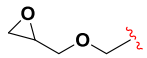	**III.39**	VU0457500	> 10	65.5
	**III.40**	VU0457501	> 10	64.4
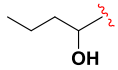	**III.41**	VU0457502	> 10	70.9
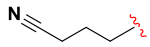	**III.42**	VU0457503	> 10	72
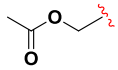	**III.43**	VU0457504	> 10	64.7

	**III.44**	VU0457505	> 10	64.5
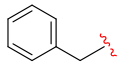	**III.45**	VU0457506	> 10	42.1
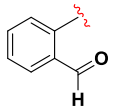	**III.46**	VU0457507	> 10	43.7
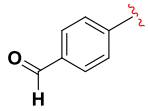	**III.47**	VU0457509	> 10	21.8
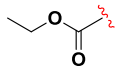	**III.48**	VU0457511	> 10	58.6
	**III.49**	VU0457513	> 10	10.8
	**III.50**	VU0457514	> 10	71
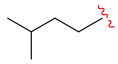	**III.51**	VU0457515	> 10	24.7
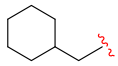	**III.52**	VU0457517	> 10	4.3
	**III.53**	VU0457518	> 10	83.1

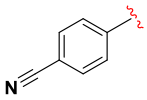	**III.54**	VU0457519	> 10	17.5
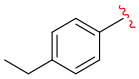	**III.55**	VU0458690	> 10	62
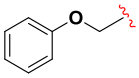	**III.56**	VU0458691	> 10	37.7
	**III.57**	VU0459804	> 10	92.8
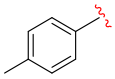	**III.58**	VU0459805	> 10	33.9
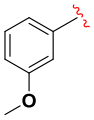	**III.59**	VU0459809	> 10	69
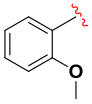	**III.60**	VU0459810	> 10	83.2

Introducing replacements for the piperidine head group on VU0092273

Based on these data, the next round of library synthesis held the 4-methoxyphenyl moiety in **III.31 (VU0457299)** constant, and a broad spectrum of amines were employed to survey alternative amides. This library was prepared according to **Scheme III.2**.

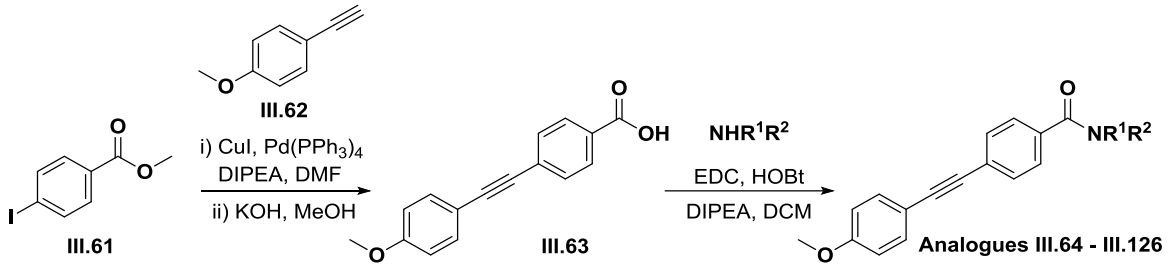

Scheme III.2 Sonogashira coupling, saponification, and amide coupling synthesis of analogues to explore alternative groups as replacements for the amide head group in VU0457299.

Overall, this library was far more productive than the initial one, providing several analogs with $mGlu_3$ NAM potencies below 10 µM. However, the SAR was still quite steep (**Table III.2**). In general, polar and basic substituents were the most efficacious. Of great interest was the enantioselective $mGlu_3$ inhibition displayed by the (R)-piperidine carboxylic acid **III.103** and the (S)-enantiomer **III.107**. While the (S) enantiomer had an IC_{50} of 5.7 µM, the (R)-enantiomer was essentially inactive, indicating an enantiospecific interaction of these compounds with the target receptor.

Table III.2 Structures and activities of compounds from library prepared as in **Scheme III.2** when assayed as CRCs in the thallium flux assay.

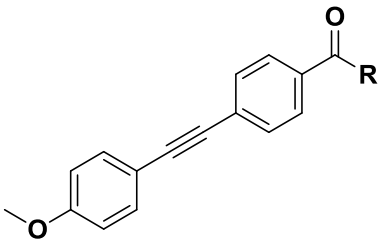

R =	Compound Number	VUID	$mGlu_3$ IC_{50} (μM)	$mGlu_3$ Glu Min %
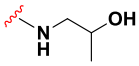	**III.64**	VU0459725	> 10	105.3
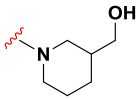	**III.65**	VU0459726	2.46	-2.3
	**III.66**	VU0459727	> 10	96.6
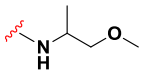	**III.67**	VU0459728	> 10	85.1
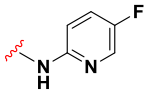	**III.68**	VU0459729	> 10	63.9
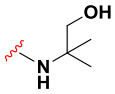	**III.69**	VU0459730	> 10	161.9
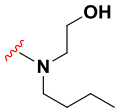	**III.70**	VU0459731	> 10	8.7

	**III.71**	VU0459732	> 10	35.3
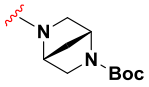	**III.72**	VU0459799	> 10	74.2
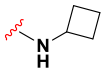	**III.73**	VU0459800	> 10	99.2
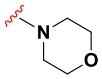	**III.74**	VU0459801	> 10	65.1
	**III.75**	VU0459802	> 10	31.5
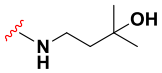	**III.76**	VU0459803	> 10	114.1
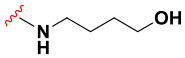	**III.77**	VU0459806	> 10	93
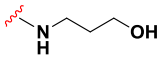	**III.78**	VU0459807	> 10	94
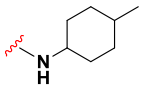	**III.79**	VU0459811	> 10	92.1
	**III.80**	VU0459812	> 10	92.1

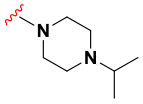	**III.81**	VU0459813	6.9	1.3
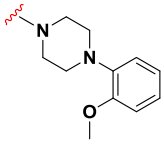	**III.82**	VU0459814	> 10	85.2
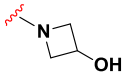	**III.83**	VU0459815	> 10	76
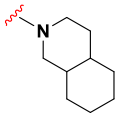	**III.84**	VU0459816	> 10	96.6
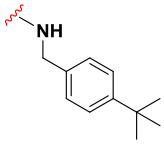	**III.85**	VU0459817	> 10	92.6
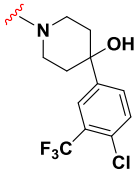	**III.86**	VU0459818	> 10	117.3
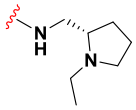	**III.87**	VU0459819	8.16	5.8
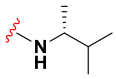	**III.88**	VU0459886	> 10	86.8

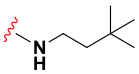	**III.89**	VU0459887	> 10	92.6
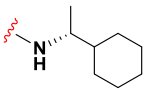	**III.90**	VU0461407	> 10	95.3
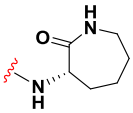	**III.91**	VU0461452	> 10	86.4
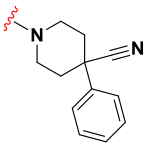	**III.92**	VU0461487	> 10	85.2
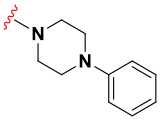	**III.93**	VU0461488	> 10	62.6
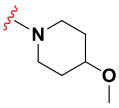	**III.94**	VU0461495	> 10	57.6
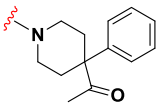	**III.95**	VU0461496	> 10	73.9
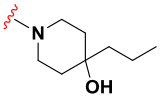	**III.96**	VU0462506	> 10	71.3
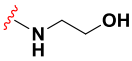	**III.97**	VU0462507	> 10	73.2

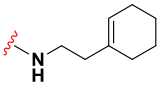	**III.98**	VU0462508	> 10	74.2
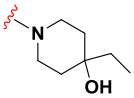	**III.99**	VU0462509	> 10	46.4
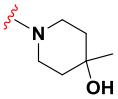	**III.100**	VU0462510	6.34	5.4
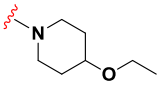	**III.101**	VU0462511	> 10	77.5
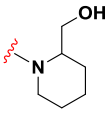	**III.102**	VU0463590	3.05	55.9
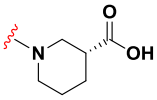	**III.103**	VU0463591	> 10	19.5
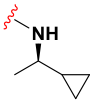	**III.104**	VU0463592	> 10	69.1
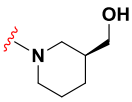	**III.105**	VU0463593	3.51	-4.1
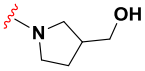	**III.106**	VU0463594	> 10	14.7

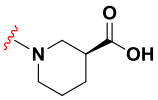	**III.107**	VU0463595	5.89	0.6
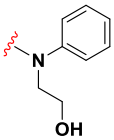	**III.108**	VU0463596	> 10	86.5
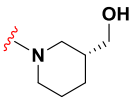	**III.109**	VU0463597	1.89	-0.5
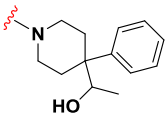	**III.110**	VU0463824	> 10	82.4
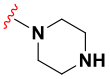	**III.111**	VU0463825	5.08	5.9
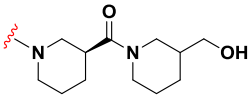	**III.112**	VU0464194	> 10	80
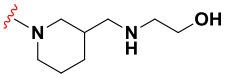	**III.113**	VU0464195	2.96	-10.4
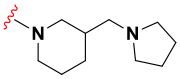	**III.114**	VU0464678	4.96	5.2
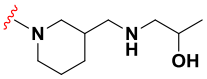	**III.115**	VU0464679	6.22	3

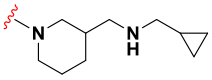	**III.116**	VU0464718	2.86	4.7
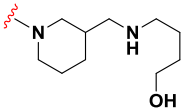	**III.117**	VU0464719	> 10	16.5
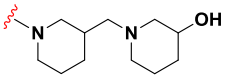	**III.118**	VU0464720	5.63	16.2
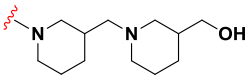	**III.119**	VU0464721	3.95	14.5
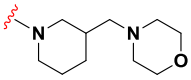	**III.120**	VU0464722	> 10	9.6
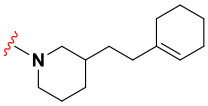	**III.121**	VU0464723	3.58	2.9
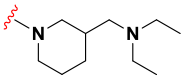	**III.122**	VU0464724	4.09	-3.7
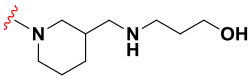	**III.123**	VU0464725	3.66	9.2
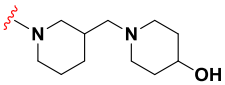	**III.124**	VU0464726	> 10	9

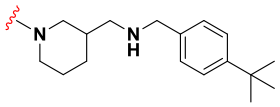	**III.125**	VU0464727	> 10	14.6
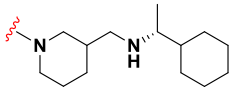	**III.126**	VU0464728	3.17	4.6

This result led us to resolve racemic 3-hydroxymethyl analog **III.65**, which had an IC_{50} of 2.1 μM and afforded a full block of the EC_{80}. Following the synthetic procedures outlined in **Scheme III.2**, both the (S)- and (R)-enantiomers of **III.65**, **III.105** (VU0463593) and **III.109** (VU0463597) were prepared and assayed in the $mGlu_3$ GIRK assay (**Figure III.5**). Here, **III.109**, with a pIC_{50} of 5.83 ± 0.05 and an IC_{50} of 1.5 μM was two-fold more potent than **III.109**, which had a pIC_{50} of 5.49 ± 0.02 and an IC_{50} of 3.3 μM., but both afforded full blockade of the $mGlu_3$ receptor at saturating concentrations. Efforts now shifted towards more fully characterizing **III.109** (VU0463597).

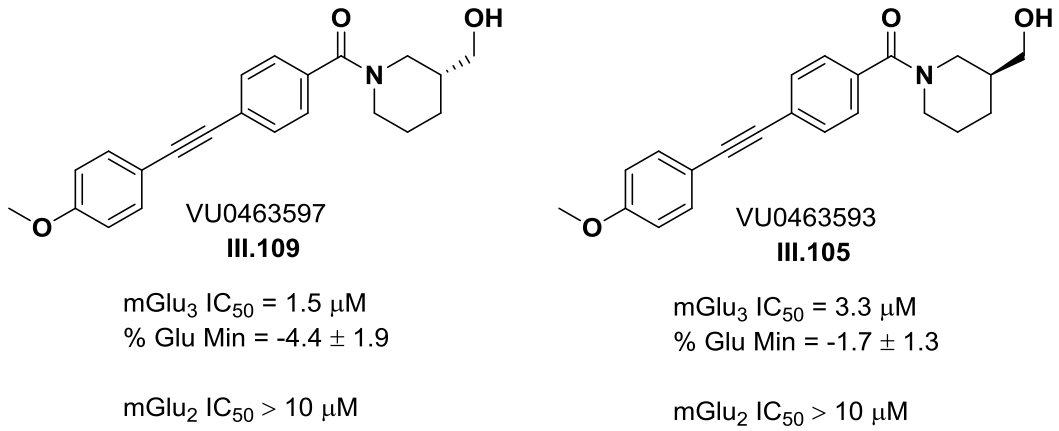

Figure III.5 Structure of first-generation $mGlu_3$ NAM VU0463597 and its enantiomer VU0463593, demonstrating a preference of the $mGlu_3$ receptor for the (S)-enantiomer of the compound in terms of inhibitory activity.

In vitro pharmacological characterization of VU0463597

We next evaluated the selectivity of **III.109** (VU0463597) between $mGlu_2$ and $mGlu_5$ (**Figure III.6**). Utilizing our $mGlu_2$ GIRK cell line, the IC_{50} was found to be greater than 10 μM, with the CRC not reaching baseline at the highest concentration tested.

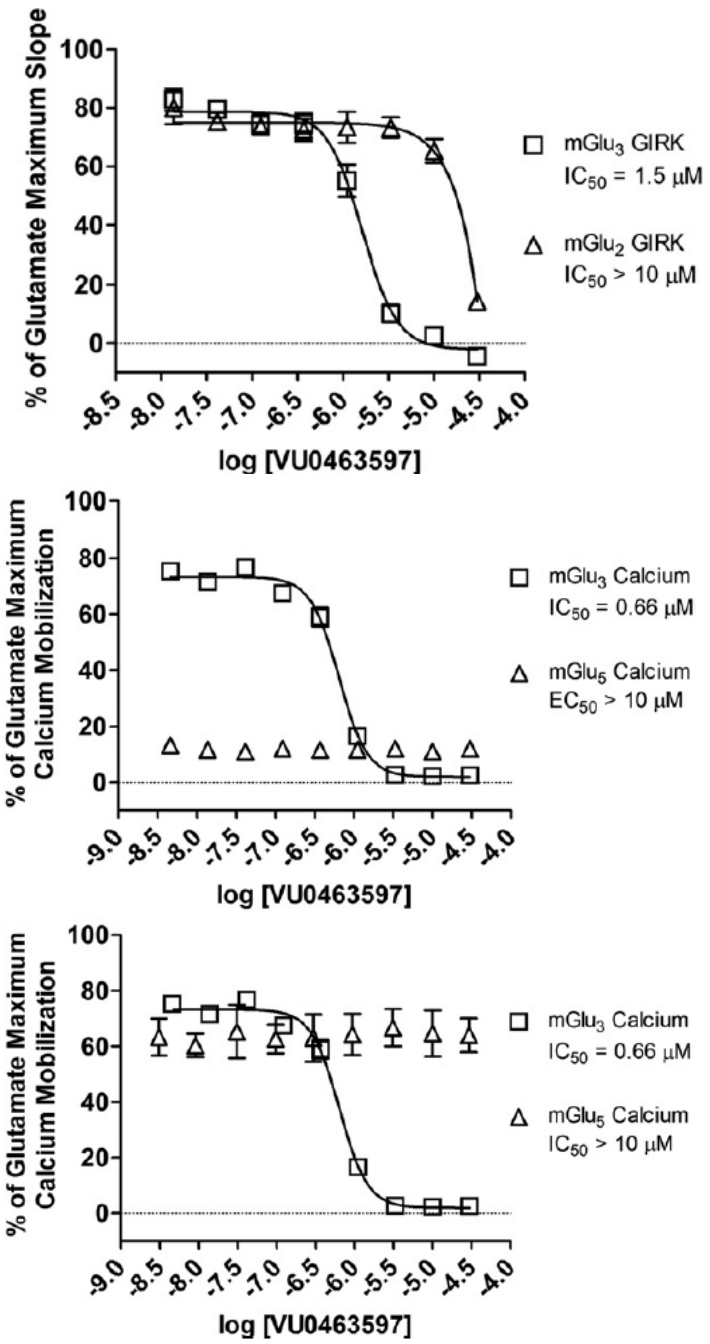

Figure III.6 Concentration-response curves for VU0463597 at $mGlu_2$ and $mGlu_3$, as measured by the thallium-flux assay; for $mGlu_3$ and $mGlu_5$ (in the presence of a glutamate EC_{20}) in the calcium-mobilization assay; and for $mGlu_3$ and $mGlu_5$ (in the presence of a glutamate EC_{80}) in the calcium mobilization assay.

Similarly, **III.109** was inactive for potentiating an EC_{20} concentration of glutamate or inhibiting an EC_{80} concentration of glutamate in our standard $mGlu_5$ calcium assay. As our calcium assays typically drive our mGlu drug discovery programs, we also evaluated **III.109** in an $mGlu_3$ calcium assay in which $mGlu_3$ is co-expressed with the promiscuous G protein $G_{\alpha 15}$. Here, we see slightly improved $mGlu_3$ NAM potency compared to the $mGlu_3$/GIRK line. In this assay, **III.109** had a pIC_{50} of 6.18 ± 0.03 and an IC_{50} of 0.66 µM, along with a % Glu Min of 2.1 ± 0.3 at $mGlu_3$.

To verify that **III.109** antagonizes $mGlu_3$ via a non-competitive (allosteric) mechanism of action, we next performed a progressive-fold shift assay. In these studies, **III.109** dose-dependently induced a rightward shift and decreased the maximal efficacy of the orthosteric agonist glutamate, consistent with a non-competitive (allosteric) mechanism of action (**Figure III.7**).

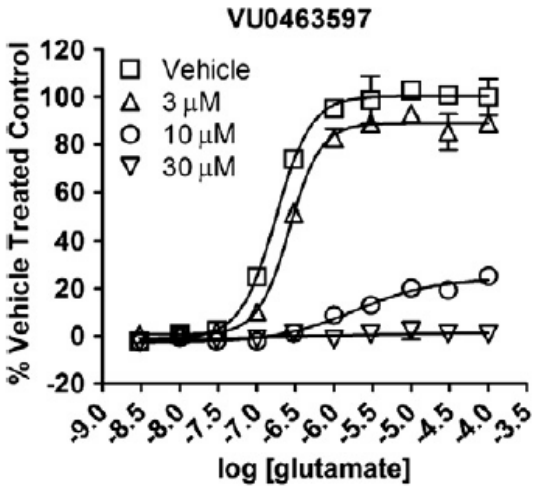

Figure III.7 Progressive-fold shift data for VU0463597 in the calcium-mobilization assay.

With this first-generation $mGlu_3$ NAM in hand, we began profiling **III.109** in a battery of ancillary pharmacology and DMPK assays to assess the quality of this probe for potential *in vivo* studies. A Lead Profiling Screen from Ricerca revealed that **III.109** had only limited off-target activity at 10 µM (**Table III.3**).

Table III.3 Binding activity of VU0463597 at a panel of relevant GPCRs, Ion channels, and transporters. Data are representative of inhibition of radioligands by 10 µM VU0463597. Entries in bold represent targets with > 50% inhibition of binding.

Binding Partner (Site)	% Inhibition (10 µM)
Melatonin MT_1	18
Muscarinic M_1	-16
Muscarinic M_2	3
Muscarinic M_3	-8
NeuropeptideY Y_1	14
NeuropeptideY Y_2	-5
Nicotinic Acetylcholine	-10
Nicotinic Acetylcholine (Bungarotoxin)	2
Delta Opiate	-9
Kappa Opiate	4
Mu Opiate	8
Phorbol Ester	1
Platelet Activating Factor PAF	5
K/ATP Potassium Channel	21
hERG Potassium Channel	13

Binding Partner (Site)	% Inhibition (10 µM)
Prostanoid EP_4	45
Purinergic P_{2XY}	5
Purinergic P_{2Y}	23
PDE_4 (Rolipram)	-17
Serotonin 5-HT_{1A}	-1
Serotonin 5-HT_{2B}	**71**
Serotonin 5-HT_3	-3
Sigma Rho_1	37
Tachykinin NK_1	5
Thyroid Hormone	7
Dopamine Transporter	**88**
GABA Transporter	6
Norepinephrine Transporter	28
Serotonin Transporter	**50**

Binding Partner (Site)	% Inhibition (10 µM)
Adenosine A_1	8
Adenosine A_{2a}	16
Adenosine A_3	44
Adrenergic α_{1A}	17
Adrenergic α_{1B}	-17
Adrenergic α_{1D}	-8
Adrenergic α_{2A}	-1
Adrenergic β_1	4
Adrenergic β_2	0
Androgen Receptor	12
Bradykinin B_1	11
Bradykinin B2	-1
L-type Calcium Channel (Benzothiazepine)	-3
L-type Calcium Channel (Dihydropyridine)	13
N-type Calcium Channel	5
Cannabinoid CB_1	13
Dopamine D_1	4
Dopamine D_{2S}	-5
Dopamine D_3	19

Binding Partner (Site)	% Inhibition (10 µM)
Dopamine D_4	4
Endothelin Et_a	4
Endothelin ET_b	2
Epidermal Growth Factor Receptor	11
Estrogen Receptor Alpha	17
$GABA_A$ (Flunitrazepam)	-14
$GABA_A$ (Muscimol)	21
$GABA_B$ (1A)	5
Glucocorticoid	6
Glutamate Kainate	0
Glutamate NMDA	4
Glutamate NMDA (Glycine)	-10
Glutamate NMDA Phencyclidine	5
Histamine H_1	-3
Histamine H_2	-4
Histamine H_3	7
Imidazoline I_2	35
Interleukin IL-1	5
Leukotriene LT_1 (Cysteinyl)	6

Pharmacokinetic characterization of VU0463597 and identification of metabolites

In our initial *in vitro* DMPK screen, **III.109** displayed no inhibition of CYP450 3A4, 2C9, 2D6, or 1A2 in human liver microsomes. In all cases the IC_{50} for inhibition was >30 µM. However, **III.109** had a low fraction unbound (F_u) in plasma, with only about 1- 2% free compound present in rat and human plasma. The F_u determined in rat brain homogenate was likewise low, only about 1%. Intrinsic clearance (CL_{int}) for **III.109** was determined in rat and human liver microsomes, and this assay indicated that **III.109** was rapidly cleared *in vitro*. In rat microsomes the CL_{int} was 240 mL/min/kg, and in human microsomes the CL_{int} was 571.8 mL/min/kg. These *in vitro* clearance rates lead to a predicted hepatic clearance around the limit of blood flow to the liver for both species, when using the well-stirred model. To test these predictions, an *in vitro* to *in vivo* clearance correlation was established. Intriguingly, **III.109** was found to be a moderately cleared compound in rat with a CL of 33 mL/min/kg following intravenous administration of 1 mg/kg of **III.109**. The more modest rate of clearance *in vivo* can likely be attributed to the low F_u of the parent compound, limiting the presentation of unbound **III.109** to microsomes. The volume of distribution at steady state (Vss) was found to be 0.6 L/kg. This low volume of distribution, combined with the moderate rate of clearance produced a $t_{1/2}$ *in vivo* of only 16.8 minutes. Metabolite identification studies in rat and human liver microsomes indicated that the principle biotransformation pathway was P450-mediated *O*-demethylation of **III.109** to generate the phenol **III.127**, a metabolite that was subsequently shown to be inactive at $mGlu_3$ and $mGlu_5$ (**Figure III.8**).

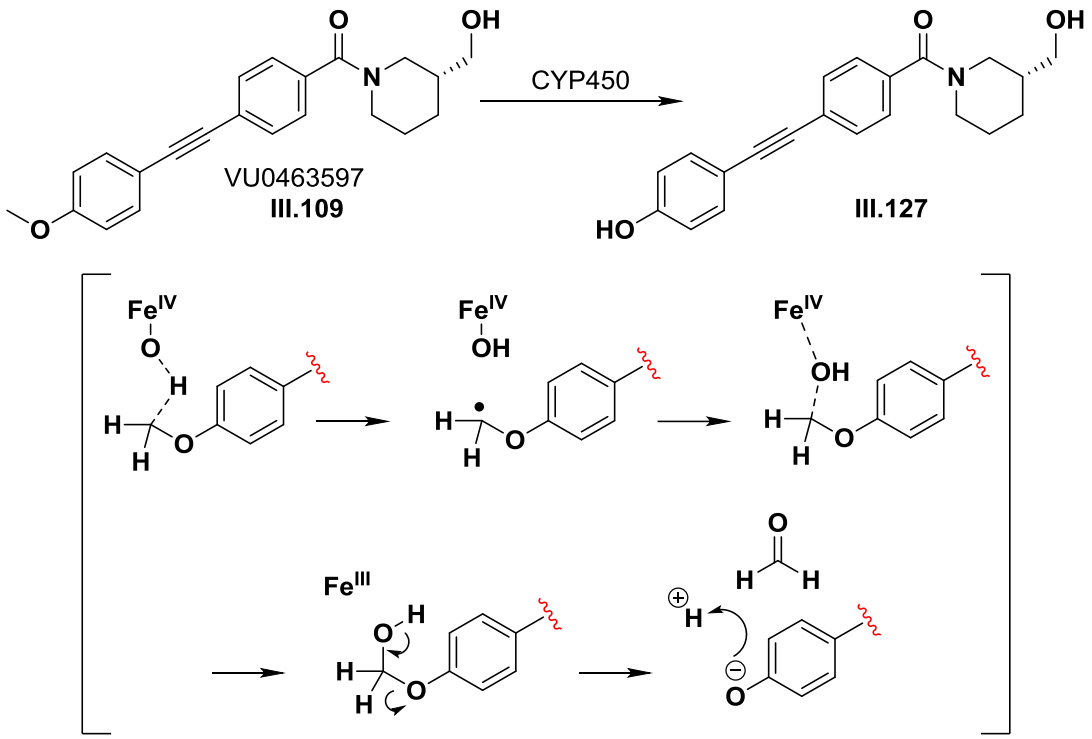

Figure III.8 CYP450-mediated O-dealkylation of VU0463597. A possible mechanism for formation of phenol **III.127** is presented in brackets. Dashed bonds represent hemolytic cleavage or formation of bonds; curved arrows represent heterolytic cleavage or formation of bonds. The iron atom represents the active site of the CYP450 enzyme.

As our earlier SAR work indicated that the methyl ether was critical for $mGlu_3$ NAM activity, we performed an IP plasma: brain level (PBL) study to determine if we could achieve meaningful CNS exposure if first-pass metabolism was bypassed. Significantly, in a 10 mg/kg (10% Tween80 in 0.5% methylcellulose) IP PBL study, we observed a brain to plasma ratio of 1.67, indicating that **III.109** was centrally penetrant. However, the data also revealed that this dose only generated a 163 nM concentration of free drug in the brain, indicating a need to further develop the compound in order to generate a compound with properties suitable for *in vivo* use.

Development of a Second-generation $mGlu_3$ NAM, VU0477950 from the First-generation $mGlu_3$ NAM VU0463597

In order to pursue further chemical optimization, **III.109** was divided into five sections for further SAR exploration and improvement of its properties to generate a tool compound that could be used *in vivo* (**Figure III.9**). First, we wanted to identify replacements for the metabolically labile *p*-methoxy moiety to improve disposition of the compound and increase its half-life. Second, we hoped to employ the wealth of acetylene replacements from previous $mGlu_5$ NAM discovery efforts to replace this less than optimal moiety, which has the potential to induce toxicity following chronic administration (Stauffer, 2011). Third, we desired to perform a broader amide scan to identify novel amide congeners that could completely eliminate the residual $mGlu_2$ activity of **III.109**. Finally, we wanted to see if alterations to either phenyl ring would offer advantages in terms of potency, solubility, selectivity, or DMPK properties.

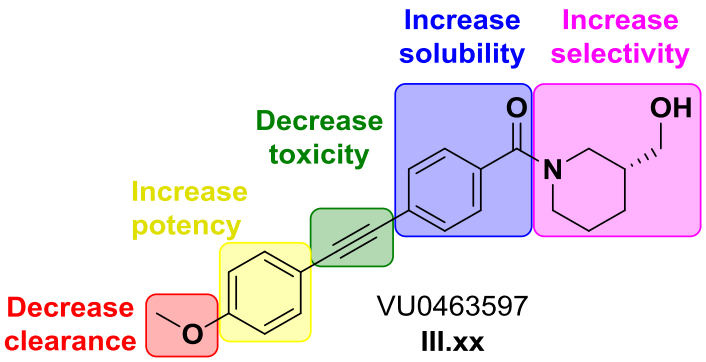

Figure III.9 Library optimization strategy for VU0463597 to improve its pharmacokinetic, pharmacodynamic, and physicochemical properties.

Introducing replacements for the methoxy group on VU0463597

The first libraries generated around **III.109** were aimed at identifying a replacement for the p-methoxy moiety or electronically perturbing the aryl ring, rendering P450-mediated *O*-dealkylation less facile. Following the synthetic route depicted in **Scheme III.3**, a library of analogs was readily prepared via standard amide and Sonogashira couplings, and screened against both $mGlu_3$ and $mGlu_2$ in the calcium-mobilization assay.

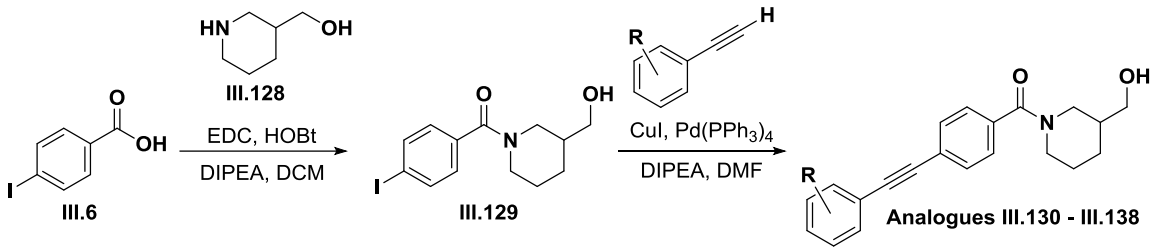

Scheme III.3 Amide coupling and Sonogashira coupling synthesis of analogues to explore alternative groups as replacements for the methoxy moiety in VU0463597 (**III.109**).

SAR in this region was found to be shallow, as all attempts to increase steric bulk on the ether or constrain its orientation relative to the phenyl ring led to a significant loss of $mGlu_3$ activity, resulting in compounds with an IC_{50} >10 μM. Even very conservative changes were poorly tolerated, indicating that the p-methoxy moiety is an essential component of the biarylacetylene pharmacophore with regards to activity at $mGlu_3$ (**Table III.4**).

Table III.4 Structures and activities of compounds from library prepared as in **Scheme III.3** when assayed as CRCs in the calcium mobilization assay.

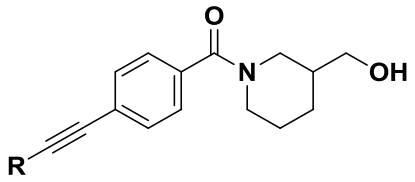

R =	Compound Number	VUID	$mGlu_3$ IC_{50} (µM)	$mGlu_3$ Glu Min %
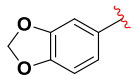	**III.130**	VU0468864	7.26	46.2
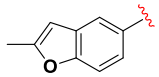	**III.131**	VU0468875	> 10	69.6
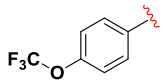	**III.132**	VU0465635	> 10	37.1
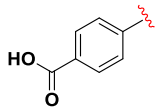	**III.133**	VU0467967	> 10	69.4
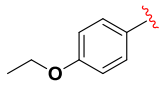	**III.134**	VU0468006	> 10	23.2
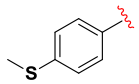	**III.135**	VU0468010	> 10	58.2

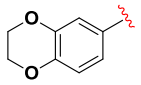	**III.136**	VU0468011	> 10	6.7
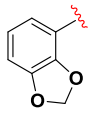	**III.137**	VU0468012	> 10	42.8
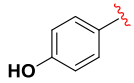	**III.138**	VU0468015	> 10	39.1

Introducing replacements for the piperidine head group on VU0463597

Based on these data, we elected to survey alternative amide moieties in an effort to improve $mGlu_3$ NAM activity and selectivity while holding the p-Methoxy phenyl acetylene pharmacophore constant. Amide analogues were prepared in high yield using the conditions shown in **Scheme III.4**.

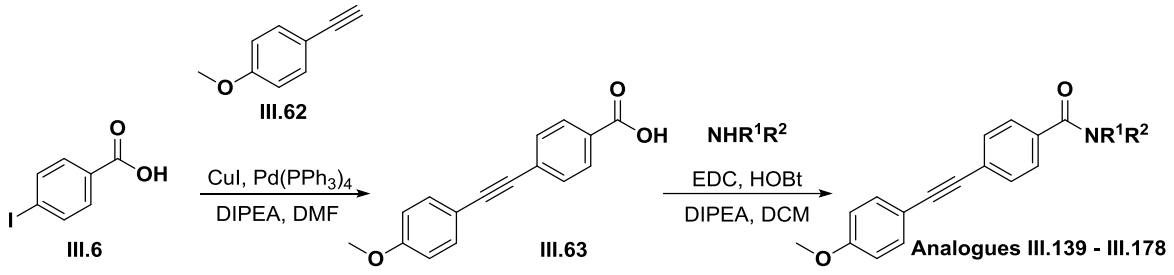

Scheme III.4 Sonogashira coupling, saponification, and amide coupling synthesis of analogues to explore replacements for the (*R*)-3-hydroxymethyl-piperidine of VU0463597.

The analogues selected for this second-generation piperidine replacement library were selected based on the results seen from the initial amide screen, where cyclic amides containing hydroxyl groups offered the best potencies at $mGlu_3$. Overall, this library proved far more productive than many of the previous libraries, yielding a number of active analogues, and for the first time, robust SAR and a general lack of activity at $mGlu_2$, as all compounds tested had an IC_{50} of at least 10 μM at $mGlu_2$, with most having an IC_{50} > 30 μM (**Table III.5**).

Table III.5 Structures and activities of compounds from library prepared as in **Scheme III.4** when assayed as CRCs in the calcium mobilization assay.

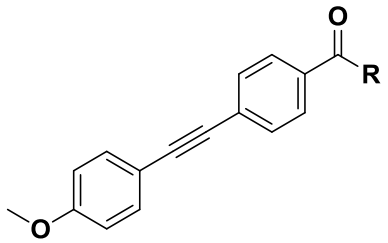

R =	Compound Number	VUID	$mGlu_3$ IC_{50} (µM)	$mGlu_3$ Glu Min %
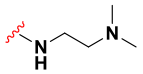	**III.139**	VU0465636	5.71	5.1
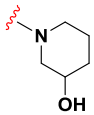	**III.140**	VU0459808	3.21	0
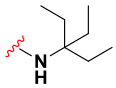	**III.141**	VU0468007	> 10	83.9
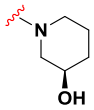	**III.142**	VU0468008	0.654	0.0
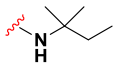	**III.143**	VU0468016	> 10	83.3

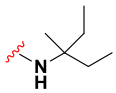	**III.144**	VU0468017	> 10	78.1
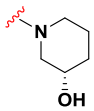	**III.145**	VU0468018	> 10	14.4
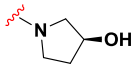	**III.146**	VU0468862	8.66	53.1
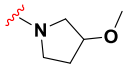	**III.147**	VU0468863	> 10	43.5
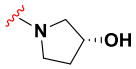	**III.148**	VU0468873	6.34	15.4
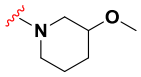	**III.149**	VU0468874	7.15	20.5
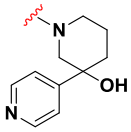	**III.150**	VU0469933	> 10	88.4
	**III.151**	VU0469934	1.65	20.3
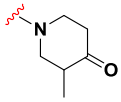	**III.152**	VU0469935	3.3	4.6

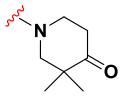	**III.153**	VU0469936	2.1	2.7
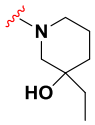	**III.154**	VU0469937	4.17	0.0
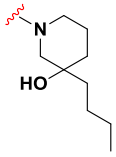	**III.155**	VU0469938	4.48	37.8
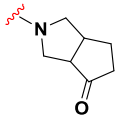	**III.156**	VU0469939	3.6	1.9
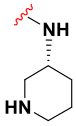	**III.157**	VU0469943	> 10	62.8
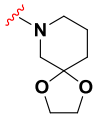	**III.158**	VU0469944	7.5	15.9
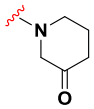	**III.159**	VU0469945	4.13	8.5
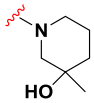	**III.160**	VU0469946	1.1	0.0

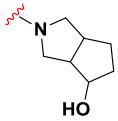	**III.161**	VU0469947	5.4	6.1
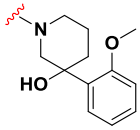	**III.162**	VU0475664	> 10	86.7
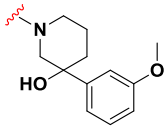	**III.163**	VU0475665	> 10	69
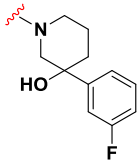	**III.164**	VU0475666	> 10	49.3
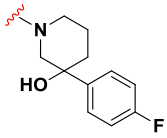	**III.165**	VU0475667	> 10	65.6
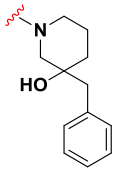	**III.166**	VU0475668	6.15	11.8

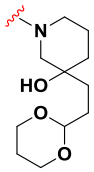	**III.167**	VU0475669	2.68	29.2
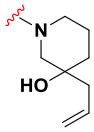	**III.168**	VU0475670	1.64	6
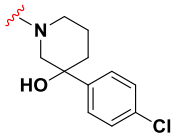	**III.169**	VU0475671	> 10	74.9
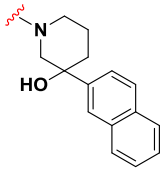	**III.170**	VU0475672	> 10	68.9
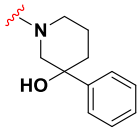	**III.171**	VU0475673	> 10	80.8
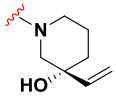	**III.172**	VU0477846	2.85	2.1
	**III.173**	VU0477847	1.42	2.5

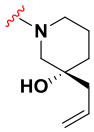	**III.174**	VU0477849	1.64	2.2
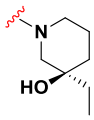	**III.175**	VU0477850	1.51	2.9
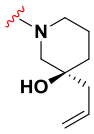	**III.176**	VU0477854	1.64	5.1
	**III.177**	VU0477855	1	5.1
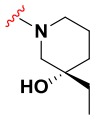	**III.178**	VU0477856	1.42	5.7

A racemic 3-hydroxy piperidine congener **III.140** showed significant activity, and upon synthesis of the pure enantiomers, enantioselective inhibition was noted. Here, the (*R*)-enantiomer **III.142** was more potent than the (*S*)-enantiomer **III.145**. When the hydroxyl group was capped as the methyl ether in **III.149**, $mGlu_3$ NAM activity was nearly lost. This result was confirmed upon repeated screening; the pIC_{50} for **III.140** was 5.87 ± 0.04, the pIC_{50} for **III.142** was 6.18 ± 0.02, and the pIC_{50} for **III.145** was 5.77 ± 0.04.

Interestingly, compounds containing [3.3.0] piperidine mimetics were active, including **III.156** and **III.161**, indicating that this moiety was a reasonably effective surrogate for the piperidine ring. The pIC_{50}s for **III.156** and **III.161** were 5.56 ±0.07 and 5.26 ± 0.11, respectively. Contraction to a pyrrolidine ring, as in **III.146** – **III.148**, led to a significant diminution in potency.

Based on the potency of the tertiary hydroxyl analogue **III.160**, which had a pIC_{50} of 5.96 ± 0.06, we prepared the ethyl and allyl congeners as well, and resolved the enantiomers via chiral SFC. Although in all cases the (+)-enantiomers were more potent, the difference in activity between the (+) and (-) analogues was only modest; approximately 2-fold increases in $mGlu_3$ NAM potency were noted for the (+)-enantiomers.

Introducing replacements for the acetylene linker on VU0463597

We next decided to move forward with exploring replacements for the acetylene linker. However, because the geometry of the resulting compounds could be significantly altered as compared to the parent compound, we did not select a single

head group for these compounds, electing to survey several potential amides in the presence of these acetylene replacements to better understand whether the SAR was additive across these regions of the molecule. From the literature regarding acetylene replacements in related $mGlu_5$ NAM biarylacetylene ligands, we synthesized and screened a diverse array of reported bioisosteres (**Figure III.10**). Unfortunately, only a few weak NAMs were identified, with most of the compounds screened being completely inactive, having an $mGlu_3$ IC_{50} > 30 µM (**Table III.6**). Due to this lack of active replacements, future libraries were synthesized with the acetylene linker in place. This also allowed for a more direct comparison of the newer generation of amide analogues with the acetylene-containing compounds previously synthesized during the generation of **III.109**.

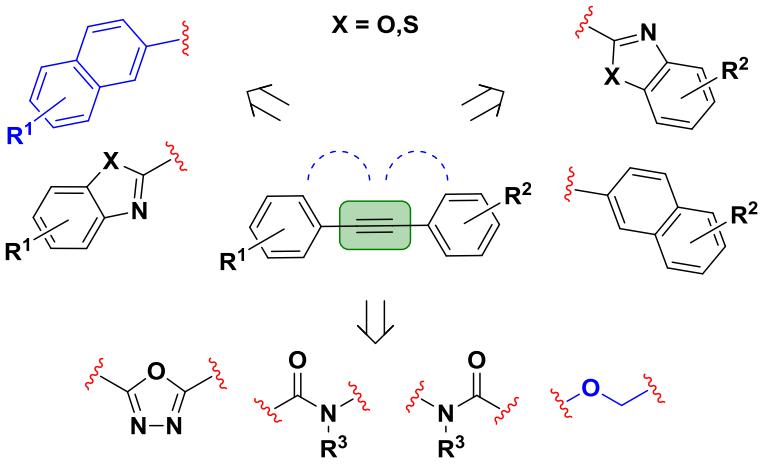

Figure III.10 Representative bioisosteres surveyed to replace the acetylene group in the biarylacetylene scaffold. Compounds containing replacements shown in blue are represented in the table below. Those shown in black were synthesized by colleagues in a parallel effort.

Table III.6 Structures of compounds that incorporated acetylene replacements, along with their activity at $mGlu_3$ when assayed as CRCs in the calcium mobilization assay.

Structure	Compound Number	VUID	$mGlu_3$ IC_{50} (μM)	$mGlu_3$ Glu Min %
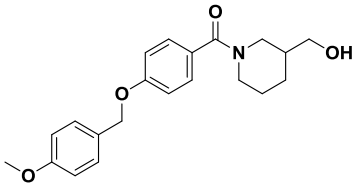	**III.180**	VU0468019	> 10	16.8
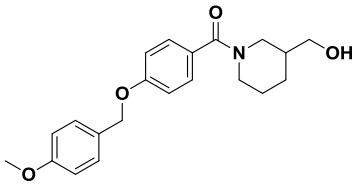	**III.181**	VU0468100	> 10	15.6
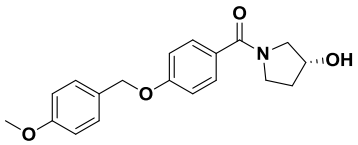	**III.182**	VU0468858	> 10	77.9
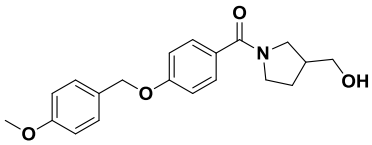	**III.183**	VU0468859	> 10	78.1

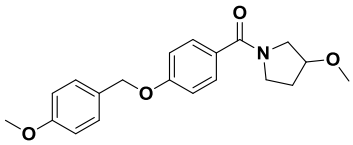	**III.184**	VU0468860	> 10	82.2
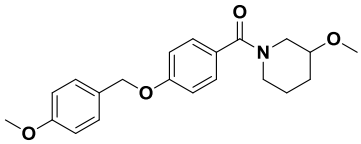	**III.185**	VU0468861	> 10	82.3
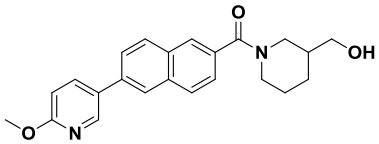	**III.186**	VU0468865	6.77	0.0
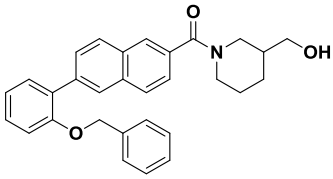	**III.187**	VU0468866	9.35	40.9
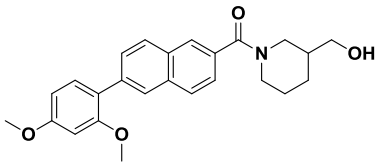	**III.188**	VU0468867	> 10	49.4
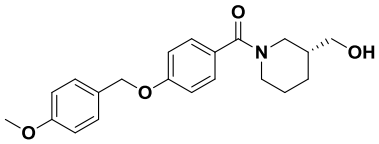	**III.189**	VU0468871	6.84	46.3
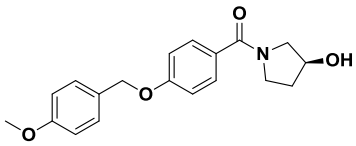	**III.190**	VU0468872	> 10	87.7

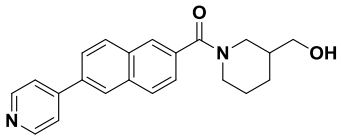	**III.191**	VU0468876	> 10	77.3
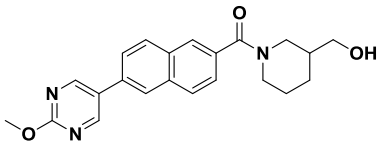	**III.192**	VU0468877	> 10	70.7
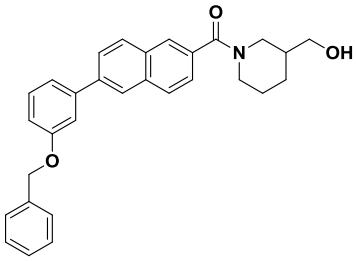	**III.193**	VU0468878	> 10	73.5
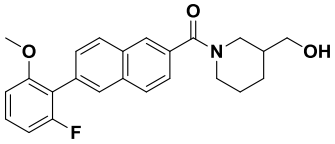	**III.194**	VU0468879	> 10	30.9
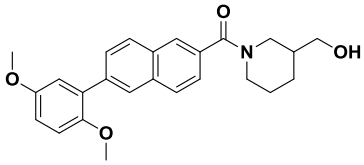	**III.195**	VU0468880	> 10	53.9
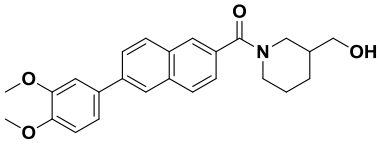	**III.196**	VU0468881	> 10	67.6

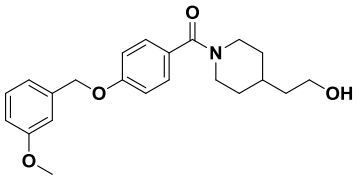	**III.197**	VU0469072	> 10	56.6
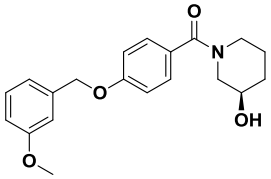	**III.198**	VU0469073	> 10	56.8
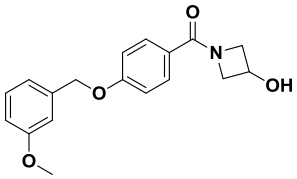	**III.199**	VU0469074	> 10	75.9
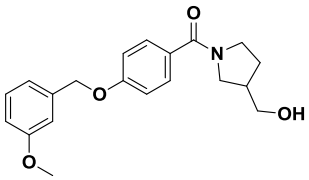	**III.200**	VU0469075	> 10	72.5
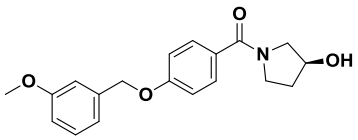	**III.201**	VU0469076	> 10	62.7
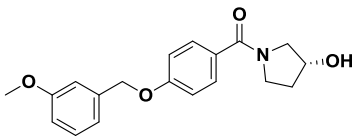	**III.202**	VU0469077	> 10	70.6

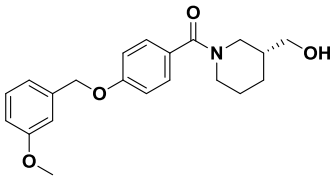	**III.203**	VU0469078	> 10	58.7
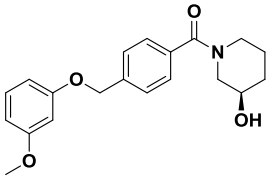	**III.204**	VU0469463	> 10	59.7
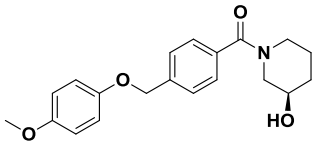	**III.205**	VU0469465	> 10	64.2
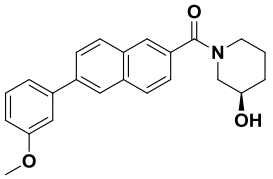	**III.206**	VU0469467	> 10	26.2
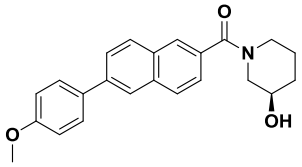	**III.207**	VU0469469	> 10	40.9
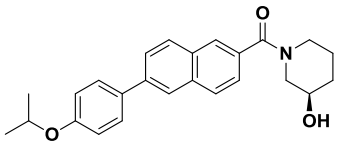	**III.208**	VU0469470	> 10	67.8

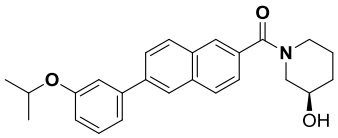	**III.209**	VU0469471	> 10	46.7
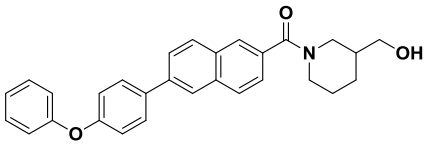	**III.210**	VU0469472	> 10	47
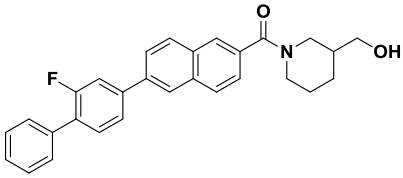	**III.211**	VU0469473	> 10	80.9
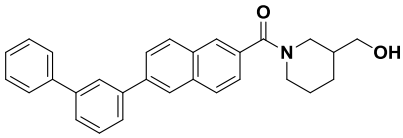	**III.212**	VU0469474	> 10	80
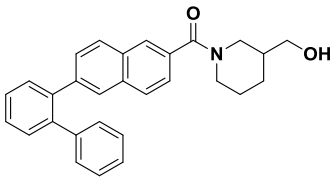	**III.213**	VU0469475	> 10	52.8
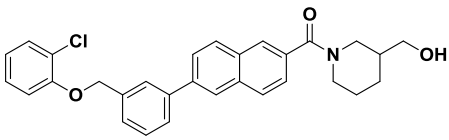	**III.214**	VU0469476	> 10	56

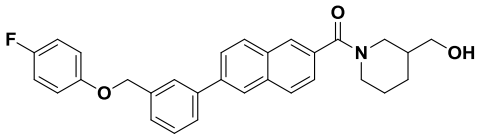	**III.215**	VU0469477	> 10	33.3
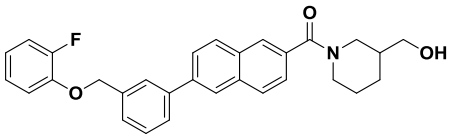	**III.216**	VU0469478	> 10	63
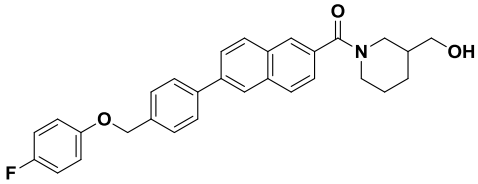	**III.217**	VU0469479	> 10	28.4

Introducing replacements for the phenyl groups on VU0463597

Finally, we incorporated alterations to each of the phenyl rings, including replacement of the amide linkage with either known bioisosteres or with constrained heterocyclic systems, including lactams, isoxazoles and pyrazoles. Additionally, we incorporated heteroatoms or fluorine substituents into various positions around both of the acetylene-flanking aryl rings as a method to alter the electronic properties of this highly conjugated system. While the amide replacements efforts were instituted in the presence of a variety of head groups and distal phenyl substitutions only a few of the resulting compounds showed activity at $mGlu_3$, with most having IC_{50}s above 10 μM (**Table III.7**).

Conversely, electronic perturbation of the aryl rings resulted in several compounds that retained activity at $mGlu_3$. Among these analogues, there were two additional sub-micromolar $mGlu_3$ NAMs worthy of further profiling: **III.238** and **III.239**. Upon repeated assessment, the robust activity of these compounds at $mGlu_3$ was confirmed; **III.238** has a pIC_{50} of 6.34 ± 0.03, and **III.239** has a pIC_{50} of 6.22 ± 0.03. These analogues incorporate fluorine substitutions on the phenyl ring that is proximal to the amide linkage, demonstrating that fluorine substitutions at the ortho- and para-positions to the amide were tolerated. Compounds incorporating fluorine substitutions on the distal phenyl ring had weaker activity at $mGlu_3$, with IC_{50}s above 4 μM.

Table III.7 Structures of compounds that incorporated changes to the aryl rings or the amide linkage along with their activity at $mGlu_3$ when assayed as CRCs in the calcium mobilization assay.

Structure	Compound Number	VUID	$mGlu_3$ IC_{50} (μM)	$mGlu_3$ Glu Min %
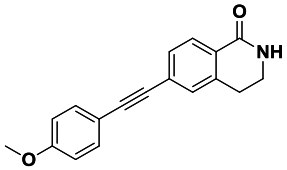	**III.218**	VU0402189	> 10	5
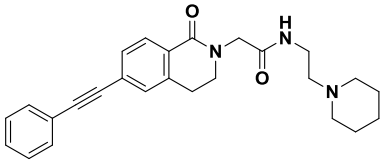	**III.219**	VU0402207	> 10	3.7
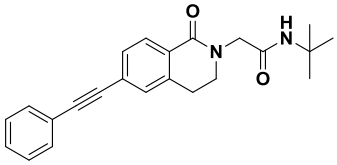	**III.220**	VU0457510	> 10	51.4
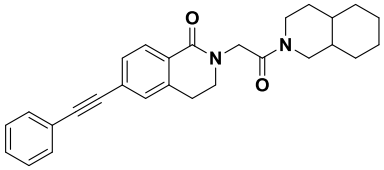	**III.221**	VU0457512	> 10	64.7

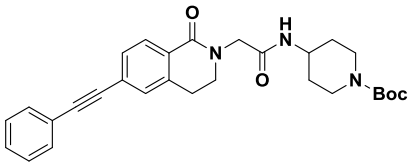	**III.222**	VU0457516	> 10	33.8
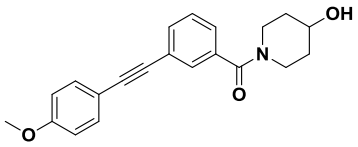	**III.223**	VU0461485	> 10	13.9
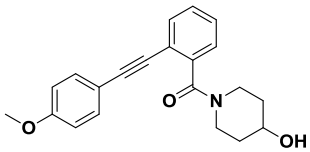	**III.224**	VU0461486	> 10	75.9
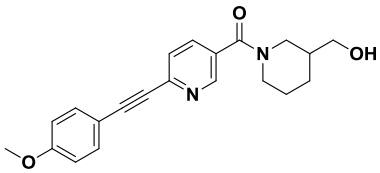	**III.225**	VU0464192	> 10	53.4
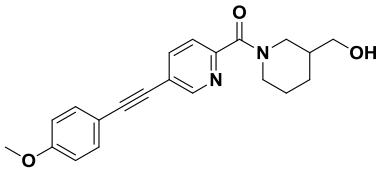	**III.226**	VU0464193	> 10	28.1
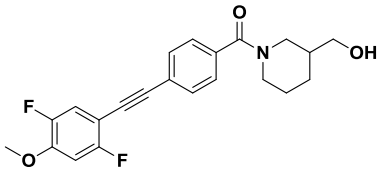	**III.227**	VU0467966	> 10	18.6

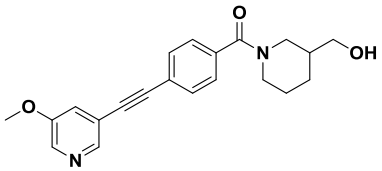	**III.228**	VU0467968	> 10	74
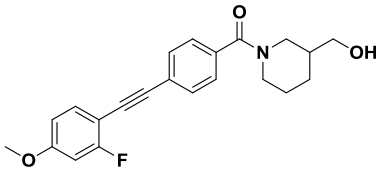	**III.229**	VU0468002	3.51	0.0
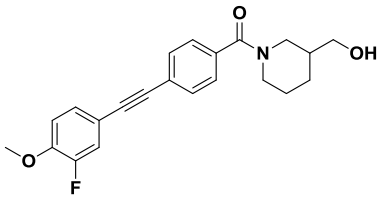	**III.230**	VU0468003	> 10	2.5
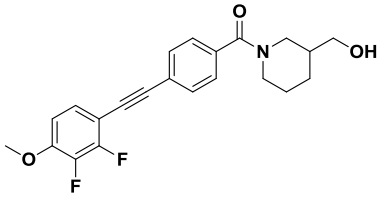	**III.231**	VU0468004	> 10	11.9
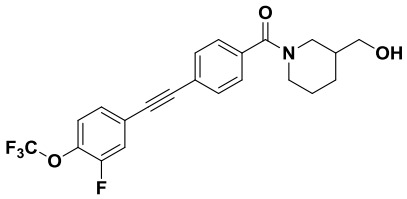	**III.232**	VU0468005	> 10	59.1
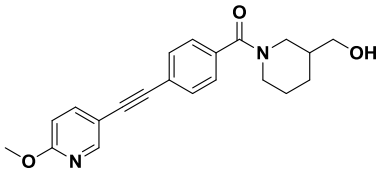	**III.233**	VU0468013	> 10	6

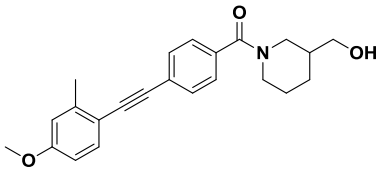	**III.234**	VU0468014	7.41	2.8
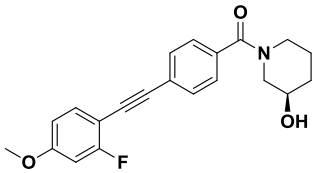	**III.235**	VU0468868	4.29	2.6
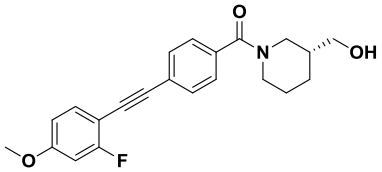	**III.236**	VU0468882	4.92	5.5
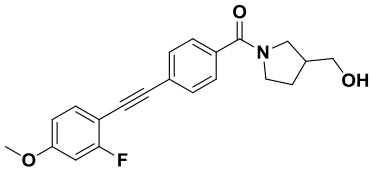	**III.237**	VU0468883	6.85	36.5
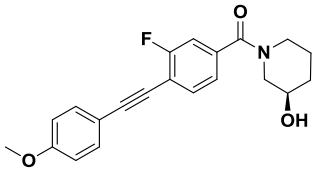	**III.238**	VU0469941	0.456	0.0
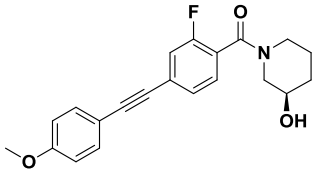	**III.239**	VU0469942	0.593	0.0

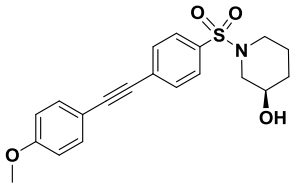	**III.240**	VU0476290	> 10	70
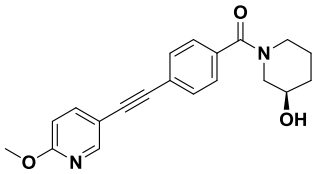	**III.241**	VU0476291	7.99	5.27
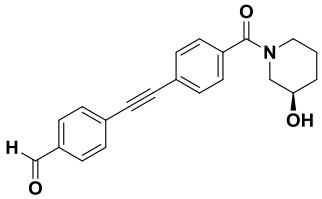	**III.242**	VU0476294	> 10	90
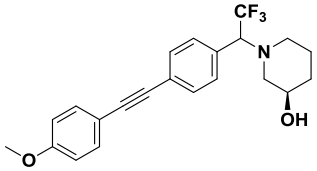	**III.243**	VU0476295	> 10	49.23
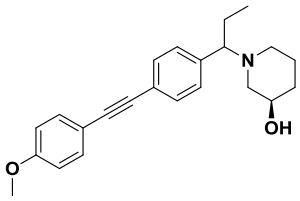	**III.244**	VU0476296	> 10	88
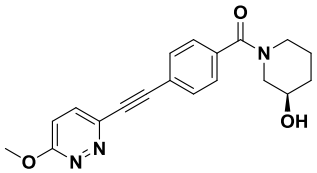	**III.245**	VU0476297	> 10	85

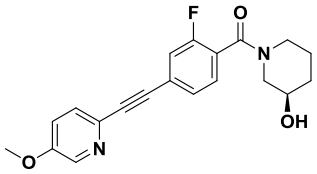	**III.246**	VU0476298	> 10	37.2
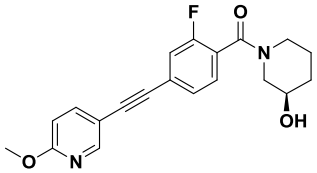	**III.247**	VU0476299	6.81	6.3
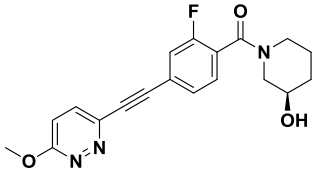	**III.248**	VU0476300	> 10	83
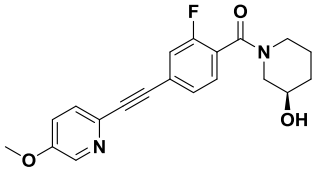	**III.249**	VU0476301	> 10	57.8
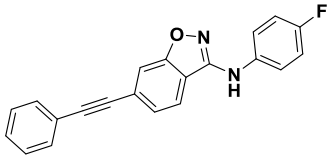	**III.250**	VU0476310	> 10	90
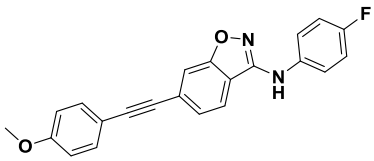	**III.251**	VU0476312	> 10	93

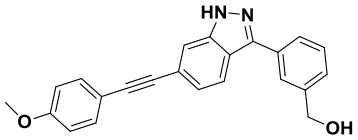	**III.252**	VU0477949	> 10	80
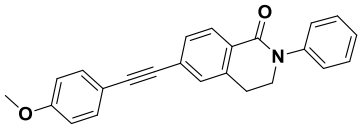	**III.253**	VU0477951	> 10	79.2
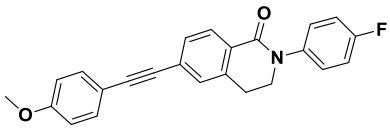	**III.254**	VU0477952	> 10	78.9
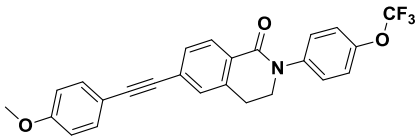	**III.255**	VU0477953	> 10	81.1
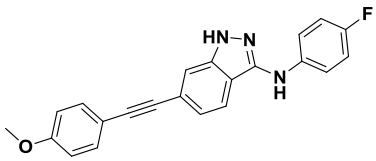	**III.256**	VU0477954	> 10	80.9
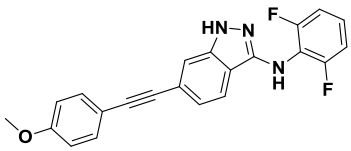	**III.257**	VU0477955	> 10	80.9
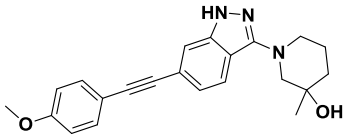	**III.258**	VU0477956	> 10	80.4

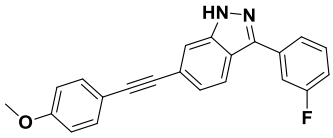	**III.259**	VU0477957	> 10	76.9
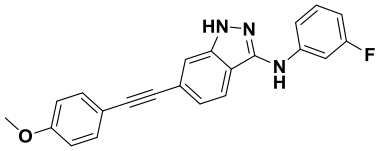	**III.260**	VU0477958	> 10	77.9
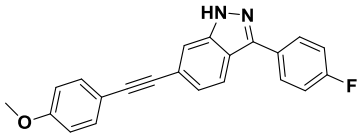	**III.261**	VU0477959	> 10	82.2
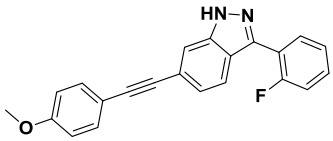	**III.262**	VU0477960	> 10	80.2
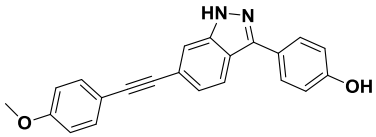	**III.263**	VU0477961	> 10	80.5
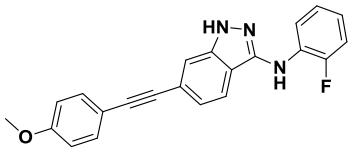	**III.264**	VU0477962	> 10	84.1
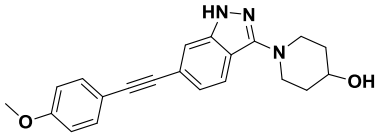	**III.265**	VU0477963	> 10	79.9

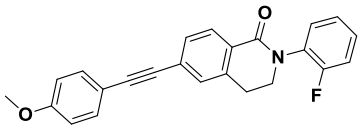	**III.266**	VU0477964	> 10	81.4
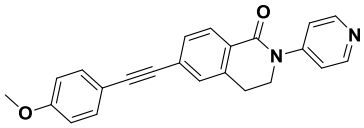	**III.267**	VU0477965	> 10	80.4
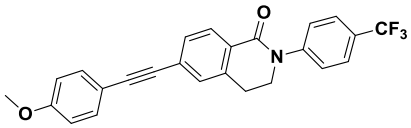	**III.268**	VU0477966	> 10	78.3

In vitro pharmacological characterization of VU0469942

At this point, the four leading $mGlu_3$ NAMs **III.142**, **III.160**, **III.238** and **III.239** proved to be selective versus $mGlu_2$, with no inhibitory activity at concentrations up to 30 µM. For further studies of the mechanism of action, **III.239** (VU0469942) was selected as an exemplar compound. The progressive-fold shift assay using **III.239** revealed that it inhibited glutamate-mediated signaling at $mGlu_3$ via an allosteric mechanism of action, as with the first generation compound **III.109**.

Furthermore, for studies looking at the physiological importance of the group II mGlu receptors, it can be necessary to apply an exogenous agonist in the place of glutamate. This will engender selective group II mGlu receptor activation, eliminating signaling due to other glutamate receptors that could otherwise confound the results. We therefore examined whether **III.239** would exhibit similar inhibition of $mGlu_3$ signaling due to glutamate and exogenous agonists. Using the calcium mobilization assay, we noted no differences in the inhibition of glutamate and the group II selective agonist LY379268 by **III.239** when it was tested at $mGlu_3$ (**Figure III.11**).

Importantly, **III.239** was found to be inactive against all of the other mGlu receptors at concentrations up to 30 µM when tested in the calcium mobilization assay. This selectivity against all other members of the mGlu receptor family was a critical milestone in the development of selective $mGlu_3$ NAM, as **III.239** represented the first example of a compound that could induce blockade of $mGlu_3$ *in vitro* with no confounding effects at other mGlu receptors, even at elevated concentrations.

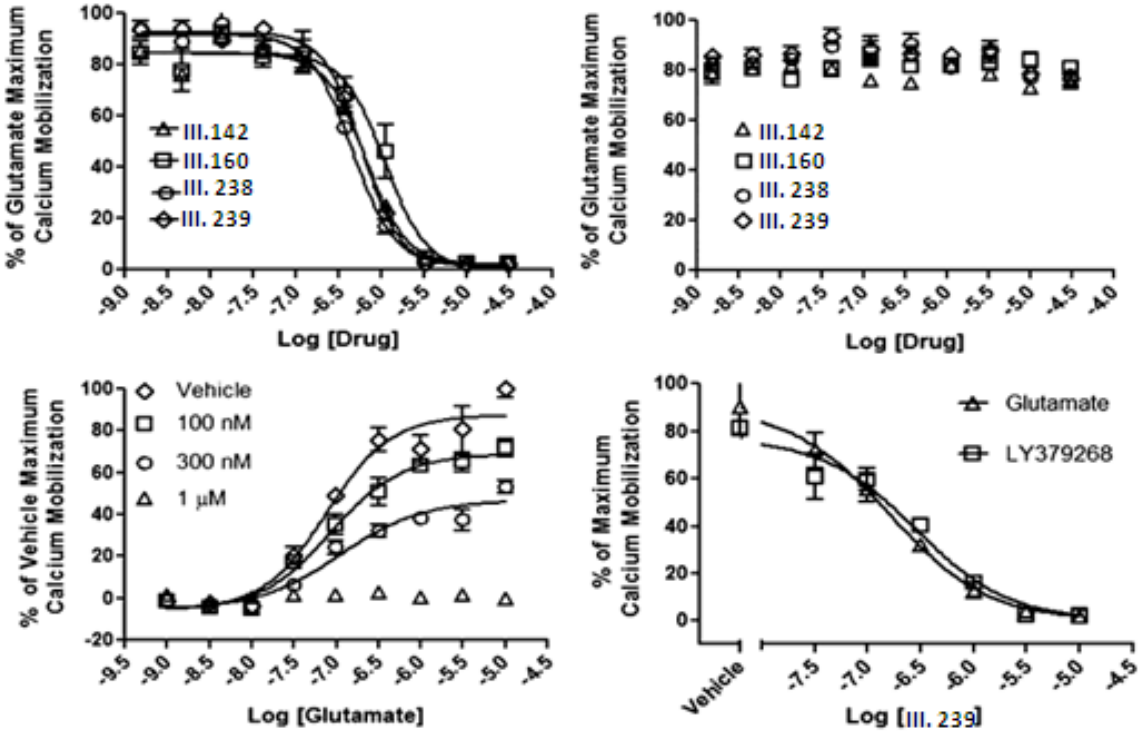

Figure III.11 Activities of lead compounds when assayed against $mGlu_3$ (upper left) and $mGlu_2$ (upper right) in a calcium-flux assay. Progressive fold-shift analysis of **III.239** revealed that it acts as a negative allosteric modulator of glutamate signaling (lower left). **III.239** inhibits the activity of synthetic agonist LY379268 and glutamate similarly at $mGlu_3$ (lower right).

In vitro and in vivo pharmacokinetic characterization of VU0469942

To rapidly assess the extent of CNS penetration, we performed a mouse tissue distribution study in which **III.142**, **III.160**, **III.238** and **III.239** were administered as a cassette via an IP route, followed by LC/MS/MS analysis of plasma and brain tissue. All four compounds afforded acceptable CNS exposure, producing brain-to-plasma ratios (B:P) ranging from 0.59 to 0.92 in mice, with brain concentrations up to 3.61 µM and plasma concentrations of up to 6.20 µM following a 10 mg/kg dose. In a microsomal clearance assay, **III.142**, **III.160**, **III.238** and **III.239** were found to have rapid clearance in rat and human microsomes. In PPB and BHB studies, these four compounds possessed free fractions in rat, mouse, and human plasma from 0.3 – 2.7%. They also displayed a generally favorable P450 inhibition profile (**Table III.8**). We also assessed the solubility characteristics of **III.239**, and found that it has an upper solubility limit of 7.8 µM in PBS.

Table III.8 Pharmacokinetic parameters of the lead $mGlu_3$ NAM compounds. For human P_{450} inhibition studies, the isoforms used were 3A4, 2C9, 2D6, and 1A2.

Compound	III.142	III.160	III.238	III.239
Mouse B:P	0.70	0.78	0.58	0.92
Human CL_{int} (ml/min/kg)	656	250	466	185
Rat CL_{int} (ml/min/kg)	214	254	219	239
Human $F_{u,p}$	0.019	0.018	0.017	0.027
Rat $F_{u,p}$	0.003	0.009	0.009	0.003
Rat $F_{u,b}$	0.004	0.006	0.004	0.005
Human P450 inhibition(µM)	All: > 30 µM	All: > 30 µM	1A2: 21.4 µM Other: > 30 µM	All: > 30 µM

In the Ricerca Lead Profiling Screen, **III.239** displayed significant activity at only two targets. Importantly, **III.239** did not have any functional activity at either of these two targets in follow-up studies, indicating that off-target effects are unlikely to manifest themselves upon administration of the compound *in vivo* (**Table III.9**).

Table III.9 Binding activity of VU0469942 at a panel of relevant GPCRs, Ion channels, and transporters. Data are representative of inhibition of radioligands by 10 µM VU0469942. Entries in bold represent targets with > 50% inhibition of binding.

Binding Partner (Site)	% Inhibition (10 µM)
Melatonin MT_1	21
Muscarinic M_1	11
Muscarinic M_2	-2
Muscarinic M_3	-11
NeuropeptideY Y_1	7
NeuropeptideY Y_2	-1
Nicotinic Acetylcholine	1
Nicotinic Acetylcholine (Bungarotoxin)	7
Delta Opiate	-4
Kappa Opiate	31
Mu Opiate	32
Phorbol Ester	1
Platelet Activating Factor PAF	11
K/ATP Potassium Channel	-1
hERG Potassium Channel	39

Binding Partner (Site)	% Inhibition (10 µM)
Prostanoid EP_4	-3
Purinergic P_{2XY}	9
Purinergic P_{2Y}	4
PDE4 (Rolipram)	3
Serotonin 5-HT_{1A}	36
Serotonin 5-HT_{2B}	**74**
Serotonin 5-HT_3	9
Sigma Rho_1	21
Tachykinin NK_1	19
Thyroid Hormone	0
Dopamine Transporter	**71**
GABA Transporter	7
Norepinephrine Transporter	29
Serotonin Transporter	2

Binding Partner (Site)	% Inhibition (10 μM)
Adenosine A_1	-10
Adenosine A_{2a}	-12
Adenosine A_3	8
Adrenergic α_{1A}	25
Adrenergic α_{1B}	11
Adrenergic α_{1D}	26
Adrenergic α_{2A}	22
Adrenergic β_1	32
Adrenergic β_2	9
Androgen Receptor	4
Bradykinin B_1	-1
Bradykinin B_2	-1
L-type Calcium Channel (Benzothiazepine)	22
L-type Calcium Channel (Dihydropyridine)	16
N-type Calcium Channel	4
Cannabinoid CB_1	11
Dopamine D_1	20
Dopamine D_{2S}	12
Dopamine D_3	18

Binding Partner (Site)	% Inhibition (10 μM)
Dopamine D_4	4
Endothelin Et_a	13
Endothelin ET_b	0
Epidermal Growth Factor Receptor	-9
Estrogen Receptor Alpha	11
$GABA_A$ (Flunitrazepam)	12
$GABA_A$ (Muscimol)	32
$GABA_B$ (1A)	3
Glucocorticoid	12
Glutamate Kainate	-1
Glutamate NMDA	6
Glutamate NMDA (Glycine)	-7
Glutamate NMDA Phencyclidine	8
Histamine H_1	23
Histamine H_2	4
Histamine H_3	8
Imidazoline I_2	-2
Interleukin IL-1	6
Leukotriene LT_1 (Cysteinyl)	-5

Exploiting an apparent kinetic-isotope effect on the methoxy group of VU0469942

The major metabolite of **III.239**, as with **III.109**, was P450-mediated O-demethylation. As mentioned above, all efforts to replace this group synthetically proved futile, resulting in inactive compounds. In an attempt to improve the PK in rodents, we elected to introduce deuterium atoms into the methoxy substituent (D_3) of both **III.160** and **III.239** in order to increase the metabolic stability of these $mGlu_3$ NAMs, providing **III.269** and **III.270** (VU0477950), respectively (Nelson & Trager, 2003). Because the rate-limiting step in the *O*-demethylation process was thought to be removal of a proton, the overall rate of metabolic transformation is subject to the strength of the carbon-proton bond being broken. Therefore, we thought that the kinetic isotope effect could potentially be exploited by introducing a stronger carbon-deuterium bond at the position of CYP450 action. As shown in **Table III.10**, introduction of the D_3CO moiety led to an analog with a substantially lower CL_{int} and predicted CL_{hep} *in vitro*, as compared to the non-deuterated analogues.

Indeed, the deuteration strategy resulted in a nearly 50% decrease in the plasma CL in rats while providing $mGlu_3$ NAMs of comparable potency and selectivity. Importantly, identification of the principal metabolites of the deuterated analogs revealed there to be no metabolic shunt from P_{450}-mediated *O*-demethylation. Thus, employing the apparent kinetic isotope effect as a means to combat the shallow SAR of these allosteric modulators led to improved disposition *in vivo*, and yielded analogues with a half-life of around 1 hour, making them suitable for acute *in vivo* rodent studies.

Table III.10 Comparison of the *in vitro* and *in vivo* clearance of deuterated analogues **III.269** and **III.270** with their parent compounds **III.160** and **III.239**.

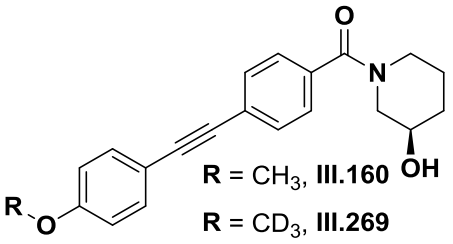

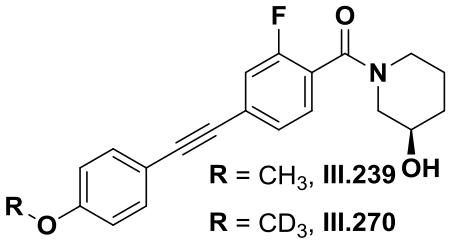

Compound	III.160	III.269	III.239	III.270
Rat CL_{int} (ml/min/kg)	214	97.3	239	73.7
Rat CL_{hep} (ml/min/kg)	52.7	40.7	54.1	35.9
Rat IV PK CL (ml/min/kg)	6.2	3.3	5.2	2.9
Rat IV PK V_{ss} (L/kg)	0.22	0.21	0.21	0.18
Rat $mGlu_3$ IC_{50} (nM)	650	310	590	450
% Decrease in Rat CL_{int}	54.53		69.16	
% Decrease in Rat IV CL	46.77		44.23	

Structural verification of VU0477950 and intermediates

After assessing the pharmacologic and pharmacokinetic profiles of the lead analogues, we decided to move forward with **III.270** (VU0477950) as our *in vivo* tool compound. During re-synthesis of **III.270** all intermediates were purified and submitted to analysis by high-resolution mass spectroscopy (HRMS), and both 1H and 13C Nuclear Magnetic Resonance (NMR) analysis. The synthesis of **III.270** proceeded with moderate-to-good chemical yields, and resulted in the generation of the expected compounds in >98% purity, as demonstrated by the concordance between the predicted and measured LC, MS, HRMS, 1H NMR and 13C NMR data gathered for each compound (**Table III.11**)

Table III.11 Experimental procedures and analytical data for all intermediates and final compounds generated during the scale-up of VU0477950.

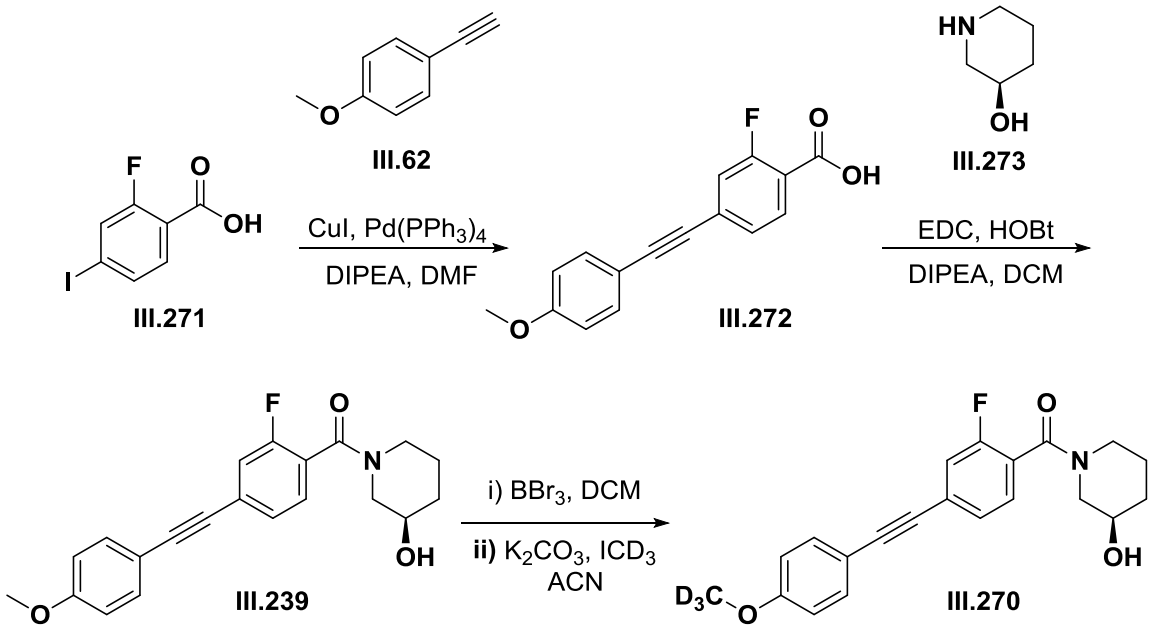

2-fluoro-4-((4-methoxyphenyl)ethynyl)benzoic acid **III.272**			
Procedure: To a solution of 2-Fluoro-4-iodobenzoic acid (798 mg, 3 mmol) in DMF (5 mL) was added CuI (23 mg, 0.12 mmol), $Pd(PPh_3)_4$ (70 mg, 0.06 mmol), diethylamine (241 mg, 3.3 mmol), and 1-ethynyl-4-methoxybenzene (475 mg, 3.6 mmol) under argon in a sealed microwave vial. The mixture was allowed to stir, was placed in a microwave reactor and heated to 100° C for 1 h. The reaction was allowed to cool to room temperature and was diluted with EtOAc (10mL), washed with water (10 mL), 5% LiCl (aqueous, 2 x 10 mL), and brine (10 mL). The organic layer was passed through a Celite pad, dried with $MgSO_4$, filtered, and solvent was removed under vacuum. Product was isolated following purification on reverse-phase HPLC.			
Yield	**LC (254 nm)**	**MS (ESI) *m/z***	**HRMS (TOF, ES+) *m/z***
92.5% (750 mg)	0.752 min	271.1	Calculated: 271.0770 Found : 271.0773
^{1}H NMR (400.1 MHz, *d*6-DMSO) δ (ppm)]: 7.87 (t, *J* = 7.9 Hz, 1H); 7.53 (m, 2H); 7.47 (dd, *J1* = 11.3 Hz, *J2* =1.2 Hz, 1H); 7.42 (dd, *J1* = 7.9 Hz, *J2* = 1.4 Hz, 1H); 6.99 (m, 2H); 3.80 (s, 3H)		**^{13}C NMR (100.6 MHz, *d*6-DMSO) δ (ppm):** 164.5, 162.2, 160.1, 159.6, 133.4, 132.3, 128.7 (d, *J* = 8.4 Hz), 127.2 (d, *J* = 5.6 Hz), 119.2 (d, *J* = 28.0 Hz), 114.6, 113.3, 93.2, 86.3, 55.4	

(R)-(2-Fluoro-4-((4-methoxyphenyl)ethynyl)phenyl) (3-hydroxypiperidin-1-yl)methanone **III.239**, (VU0469942)				
Procedure: To a solution of compound 2-fluoro-4-((4-methoxyphenyl)ethynyl)benzoic acid (675 mg, 2.5 mmol) in 20 mL DMF, was added diisopropylethylamine (1.07 g, 8.25 mmol) while stirring. 1-Ethyl-3-(3 dimethylaminopropyl)carbodiimide (560 mg, 3 mmol), hydroxybenzotriazole (337 mg, 2.5 mmol), and (R)-3-hydroxypiperidine hydrochloride (342 mg, 2.5 mmol) were then added. The reaction was allowed to stir for 4 h at room temperature, then quenched with a solution of saturated $NaHCO_3$ (20 mL), washed with 5% LiCl (aqueous, 2 x 20 mL), and brine (20 mL). The reaction was extracted into DCM (50 mL), and solvent was removed under vacuum. The residue was purified using HPLC. The product was obtained as an ivory solid.				
Yield	**LC (254 nm)**	**Optical Rotation ([α]D^{23})**	**MS (ESI) *m/z***	**HRMS (TOF, ES+) *m/z***
47.0% (420 mg)	0.704 min	-27.6˚	354.1	Calculated: 354.1505 Found : 354.1507
^{1}H NMR(400.1 MHz,*d*6-DMSO),75˚C, δ (ppm)]: 7.50 (m, 2H); 7.39 (m, 3H); 6.99 (m, 2H); 4.06 (s, 1H); 3.82 (s, 3H); 3.53 (s, 1H); 3.29 (m, 2H); 2.93 (m,1H); 1.87 (m, 1H); 1.74 (s, 1H); 1.44 (m, 2H)		**^{13}C NMR(100.6 MHz,*d*6-DMSO),75˚C, δ (ppm):** 163.3, 159.7, 158.0, 156.0, 132.7, 127.2, 125.2 (d, *J* = 9.3 Hz), 124.3 (d, *J* = 16.7 Hz), 117.7 (d, *J* = 22.7 Hz), 114.2, 113.4, 91.1, 85.9, 64.7, 55.0, 53.2, 48.2, 32.2, 28.9		

(R)-(2-fluoro-4-((4-(methoxy-d3)phenyl)ethynyl)phenyl)(3-hydroxypiperidin-1-yl)methanone **III.270**, (VU0477950)				
Procedure: To a stirred solution of (R)-(2-Fluoro-4-((4-methoxyphenyl)ethynyl)phenyl)(3-hydroxypiperidin-1-yl)methanone (50 mg, 0.14 mmol) in 1 mL of dichloromethane at 0° C was added 0.2 mL of boron tribromide (1 M solution in DCM) via dropwise addition. The reaction was allowed to warm to room temperature while stirring over a period of 3 h. The reaction was quenched with ice water (1 mL), extracted into ethyl acetate (2 mL), and the solvent was removed under vacuum. The resulting material was dissolved in 1.5 mL of acetonitrile, and K_2CO_3 was added while stirring. The reaction vessel was purged with argon 3 times, and deuterated iodomethane (99.5+% D) was added dropwise. Following addition, the reaction was heated to reflux and allowed to stir for 3 h. The reaction was then allowed to cool to room temperature, quenched with ice water, extracted into ethyl acetate, and solvent was removed under vacuum. The residue was purified using reverse phase HPLC, and the product was obtained as an ivory solid.				
Yield	**LC (254 nm)**	**Optical Rotation ([α]D^{23})**	**MS (ESI) *m/z***	**HRMS (TOF, ES+) *m/z***
64% (32 mg)	1.084 min	-19.7˚	356.9	Calculated: 357.1694 Found : 357.1693
^{1}H NMR(400.1 MHz,*d*6-DMSO),75˚C, δ (ppm)]: [* = Rotamers]: 7.50 (m, 2H); 7.40 (m, 3H); 7.00 (m, 2H); 4.75 (m, 1H); 3.92 (m, 2H); 3.51 (m, 1H);3.35 (m, 1H*); 3.03 (m, 1H*) 2.91 (m, 1H); 1.87 (m, 1H); 1.72 (m, 1H); 1.43 (m, 2H)		**^{13}C NMR(100.6 MHz,*d*6-DMSO),75˚C, δ (ppm):** 163.3, 159.8, 158.2, 156.2, 132.9, 129.0, 128.7, 127.4, 125.2, 124.4 (d, *J* = 21.5 Hz), 117.8 (d, *J* = 21.5 Hz), 114.3, 113.4, 91.3, 86.1, 64.9, 53.2, 48.2, 32.5		

Confirmation of an Allosteric Mode of Action for VU0477950

Because **III.239** (VU0469942) displayed classical non-competitive antagonism with respect to the orthosteric agonist glutamate in a progressive fold shift assay, we expected that **III.270** (VU0477950), its deuterated analogue, would also behave non-competitively.

In order to test this hypothesis, **III.270** binding was assayed in the presence of [^{3}H]-LY341495 to confirm that it was not binding to the orthosteric site. Since increasing concentrations of **III.270** did not alter the binding of [^{3}H]-LY341495, the binding of this compound to an allosteric site was further supported.

Additionally, the off-rate of [^{3}H]-LY341495 was assessed in the presence of **III.270**. This rate was not altered by **III.270**, indicating that the NAM activity of **III.270** was not due to alterations in the binding of orthosteric ligands (**Figure III.12**). Rather, the action of the NAM is potentially due to alterations in coupling of the $mGlu_3$ receptor to the G-protein.

This lack of evidence for interaction between the two binding sites is consistent with the known structural flexibility of the CRD that connects the orthosteric and allosteric sites. Because the VFD and CRD are not present in the Class A GPCRs, this indicates that there might be several different structural mechanisms underlying allosteric regulation, depending on the GPCR class; some may focus more on alterations in cooperativity between the orthosteric and allosteric binding sites, while others may focus on the efficacy of G-protein coupling.

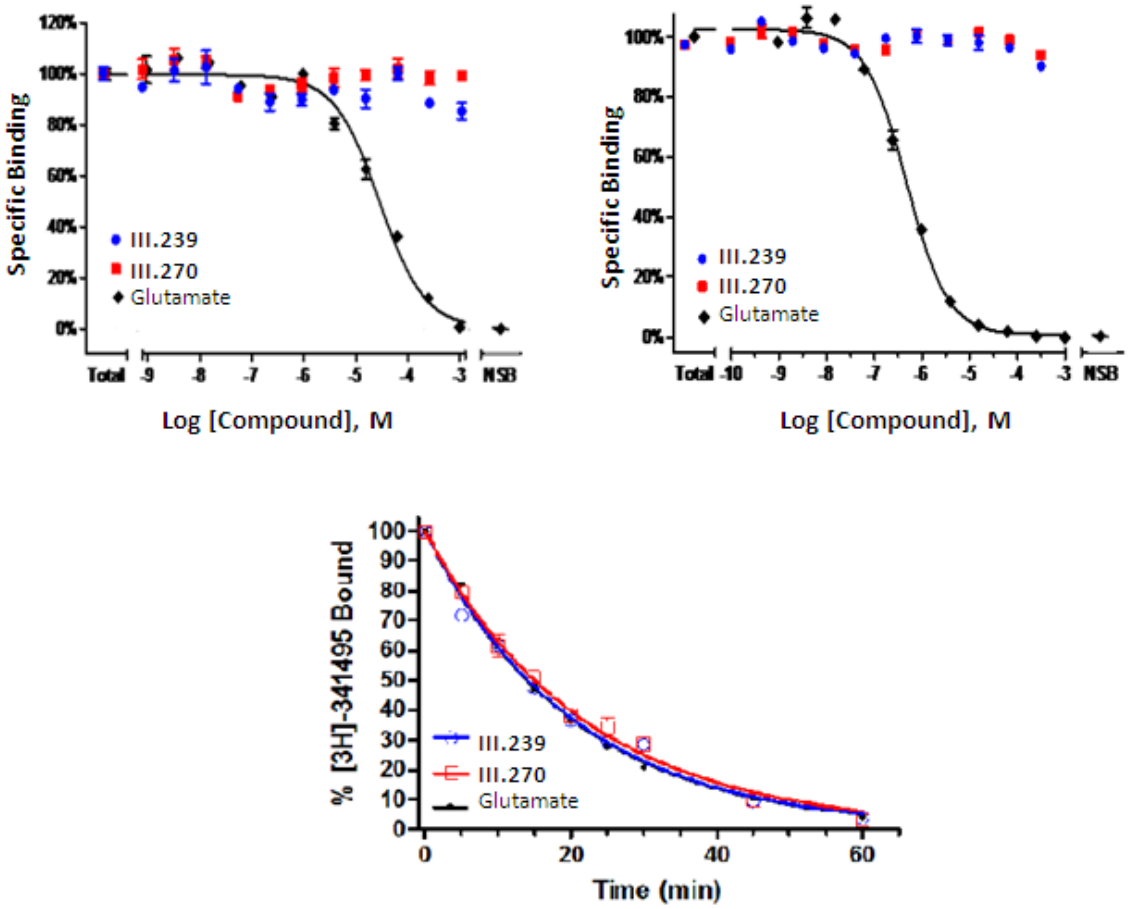

Figure III.12 Radioligand binding of [^{3}H]-LY341495 in the presence of VU0469942 and VU0477950 at $mGlu_2$ and $mGlu_3$ and off-rate of [^{3}H]-LY341495 in the presence of VU0469942 and VU0477950.

Conclusions and Future Directions

In summary, we have developed the first series of selective $mGlu_3$ NAM described to date, including **III.270** (VU0477950). This compound was developed using a multidimensional iterative parallel synthesis strategy, starting from an $mGlu_5$ PAM compound with weak NAM activity at $mGlu_3$. Initial SAR explorations revealed the importance of the para-methoxy group on the distal phenyl ring for eliminating activity at $mGlu_5$ and increasing potency at $mGlu_3$. Alterations to the piperidine head group resulted in compounds with improved selectivity versus $mGlu_2$.

The major metabolic soft spot for our initial lead compound was identified to be P450-mediated *O*-demethylation, a fate that could not be overcome through standard steric or electronic perturbations, due to extremely shallow allosteric ligand SAR. However, by exploiting apparent kinetic isotope effects, we were able to combat the shallow SAR within this allosteric modulator series and discover an $mGlu_3$ NAM with improved disposition. Overall, **III.270** possesses a favorable DMPK and ancillary pharmacology profile for use in mice. The compound is centrally-penetrant, with an *in vivo* half-life suitable for acute administration in rodent behavioral assays that are commonly used for estimation of psychiatric efficacy of compounds when administered to patients.

The highly hydrophobic nature of **III.270** remains a concern moving forward. This hydrophobicity can cause difficulty in formulation, and is likely a significant contributing factor to the high level of binding to plasma proteins and to the lipid and protein

constituents of brain-homogenate that were seen for **III.270**. This elevated non-specific binding increases the dose of compound required to reach efficacious concentrations in the brain. Because only a small fraction of the drug is free to interact with the target receptor, the total concentration of **III.270** that is needed in the brain also increases, and quickly approaches the solubility limit of the compound. Further exploration of this scaffold may uncover more potent analogues that will require lower dosing *in vivo*. Likewise, alternative scaffolds should be explored to look for a chemotype that exhibits improved physicochemical properties.

These concerns notwithstanding, **III.270** represents the most potent and selective $mGlu_3$ NAM yet described. Application of **III.270** to *in vitro* and *ex vivo* systems will allow for dissection of the molecular mechanisms underlying $mGlu_3$-mediated signaling and plasticity. Administration of **III.270** in rodent models of psychiatric illnesses will allow for observation of the impact of $mGlu_3$ blockade *in vivo*. Given the myriad hypotheses about the importance of $mGlu_3$ in schizophrenia, depression, anxiety, substance dependence, and excitotoxic conditions, the tools developed here have significant potential to improve our understanding of etiology and inform future treatment options for many neuropsychiatric disorders.

Sections of this chapter have been reprinted with permission from the following:

Development of a novel, CNS-penetrant, metabotropic glutamate receptor 3 ($mGlu_3$) NAM probe (ML289) derived from a closely related $mGlu_5$ PAM. Sheffler DJ, Wenthur CJ, Bruner JA, et al. Bioorg Med Chem Lett. 2012 Jun 15; 22(12):3921-5, Copyright 2012 American Chemical Society.

Discovery of (R)-(2-fluoro-4-((-4-methoxyphenyl)ethynyl)phenyl) (3-hydroxypiperidin-1-yl)methanone (ML337), an $mGlu_3$ selective and CNS penetrant negative allosteric modulator (NAM). Wenthur CJ et al. J Med Chem. 2013 Jun 27;56(12):5208-12. Copyright 2013 Journal of Medicinal Chemistry.

CHAPTER IV

EXPLORATION OF PYRAZOLO[1,5-A]QUINAZOLIN-5(4*H*)-ONE AND QUINOLINE CARBOXAMIDE SCAFFOLDS AS MGLU$_2$ NAMS

Prior Claims of Pyrazolo[1,5-a]quinazolin-5(4*H*)-ones as Group II mGlu receptor Allosteric Modulators

Recent disclosures have provided some evidence that compounds derived from a pyrazolo[1,5-a]quinazolin-5(4*H*)-one scaffold can act as dual inhibitors of mGlu$_2$ and mGlu$_3$ in a DtectAll^{TM} fluorescence resonance energy transfer (FRET) based binding assay system (Stephan Schann, 2013). Also, it has been reported that mGlu$_2$ NAMs, mGlu$_3$ NAMs, and mGlu$_3$ PAMs have been developed via directed alterations to this chemotype (**Figure IV.1**) (S. Schann, Manteau, Franchet, Frauli, & Mayer, 2013).

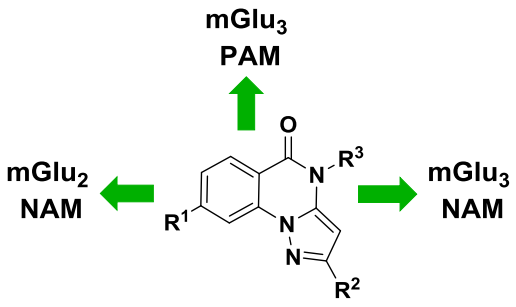

Figure IV.1 Depiction of mode-switching potential for the pyrazolo[1,5-a]quinazolin-5(4*H*)-one scaffold, as determined by Domain Therapeutics using their DtectAll^{TM} binding assay.

Such molecular switching has been previously reported for compounds targeting $mGlu_5$, a class I mGlu, and compounds targeting $mGlu_4$, a class III mGlu, but there has been limited information regarding the structural basis underlying the phenomenon amongst non-biarylacetylene compounds targeting class II mGlu receptors (Stephan Schann et al., 2010; S Sharma & Kedrowski, 2009). Given our interest in developing selective tools for the analysis of $mGlu_2$ and $mGlu_3$ function, this scaffold represented an attractive target from which to derive a selective $mGlu_2$ NAM. Since we had recently disclosed the first selective $mGlu_3$ NAM, the generation of a selective $mGlu_2$ NAM was our next aim, particularly because there were no disclosed structures of selective $mGlu_2$ NAMs at the time this study was initiated.

Rapid Development of a Potent Dual $mGlu_{2/3}$ NAM, VU0550418, Using a Convergent Matrix-library Strategy

Synthesis of multi-functionalized pyrazolo[1,5-a]quinazolin-5(4H)-ones

In order to improve understanding of the SAR underlying molecular switching amongst group II mGlu receptors, several chemical libraries were developed around a pyrazolo[1,5-*a*]quinazoline-5(4*H*)-one core (**Figure IV.2**).

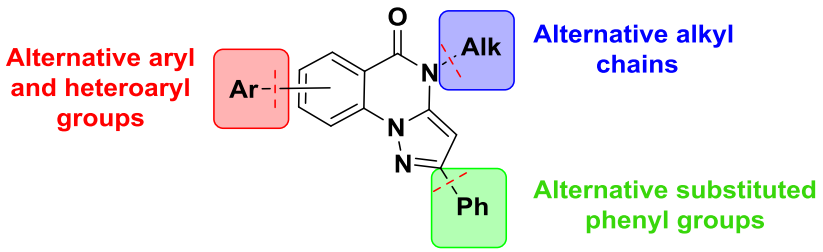

Figure IV.2 Matrix library strategy to rapidly assess the mode-switching capacity of the pyrazolo[1,5-*a*]quinazoline-5(4*H*)-one scaffold.

The initial compounds were synthesized using a matrix-library strategy, where alterations at R^1 and R_2 were combined in order to rapidly generate a large amount of structural diversity, as outlined in **Scheme IV.1**. Briefly, 2-amino-4-bromo-benzoic acid (**IV.1)** is converted to the hydrazine (**IV.2)**, which is condensed with an array of substituted benzoyl nitriles under microwave conditions in order to form a series of 8-bromo-pyrazolo[1,5-*a*]quinazolin-5(4*H*)-ones that are differentially substituted at the 2-position (**Intermediates IV.3**). These products are subjected to Suzuki coupling conditions with a diverse group of aryl and heteroaryl boronic acids to afford **Intermediates IV.4**, and then *N*-alkylated in order to generate the desired analogues **IV.5** - **IV.38**. All final products were purified using reverse-phase HPLC to >98% purity, as determined by analytical LC/MS (215, 254 and ELSD). Overall yields (5-57%) were moderate-to-good for the four step sequence.

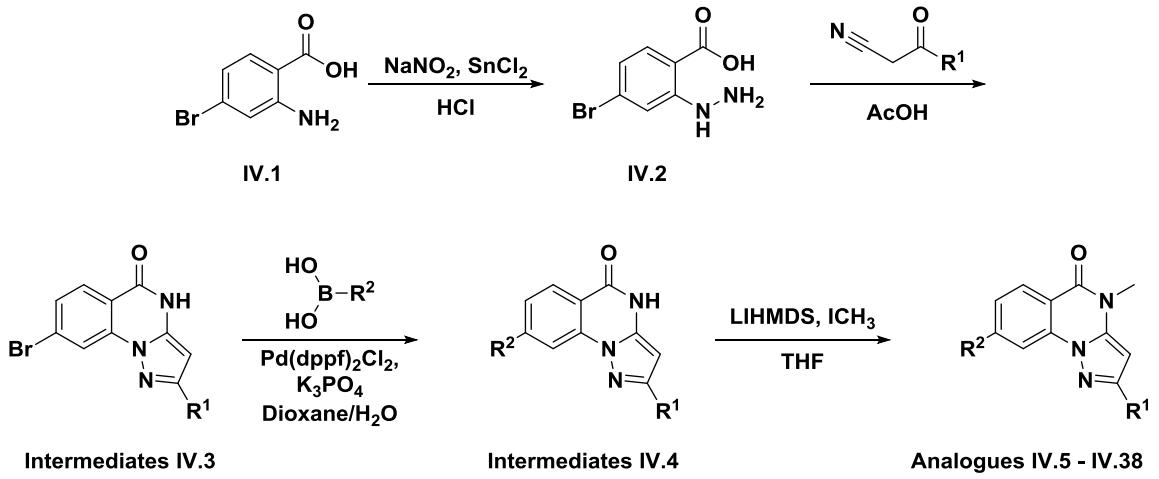

Scheme IV.1 Amination, condensation, Suzuki coupling, and methylation conditions to generate analogues exploring the structure-activity relationship of pyrazolo[1,5-*a*]quinazoline-5(4*H*)-ones at the group II mGlu receptors.

In vitro pharmacological screening of analogues

The compounds generated were initially screened at a single concentration of 3 µM for their ability to alter glutamate-dependent signaling, against cell lines stably expressing either rat $mGlu_2$ or rat $mGlu_3$ and mouse $G_{\alpha15}$ (**Figure IV.3**). During this effort all assays were carried out using a kinetic, plate-based, calcium-induced fluorescence reader.

From the initial group of compounds, none appeared to potentiate glutamate-dependent calcium signaling (EC_{20} of Glu) at either $mGlu_2$ or $mGlu_3$ when applied at 3 µM. Conversely, 6 analogs screened showed robust inhibition of $mGlu_2$, and 18 of the analogs showed robust inhibition of $mGlu_3$, meaning they inhibited an EC_{80} glutamate response by ≥ 50%. Thus, the initial library generated analogs biased towards inhibition of $mGlu_3$, based on the single point screen.

In order to follow up on these results, the most active compounds from this initial screen were selected, and a CRC was generated for each one. These curves were generated using the cell lines and agonist concentrations as in the single point assay, while using a broad range of test-compound concentrations (30 µM – 1 nM). This strategy allowed us to effectively determine the potencies of those compounds which exhibited significant activity, while eliminating inactive or weakly-active compounds from further analysis.

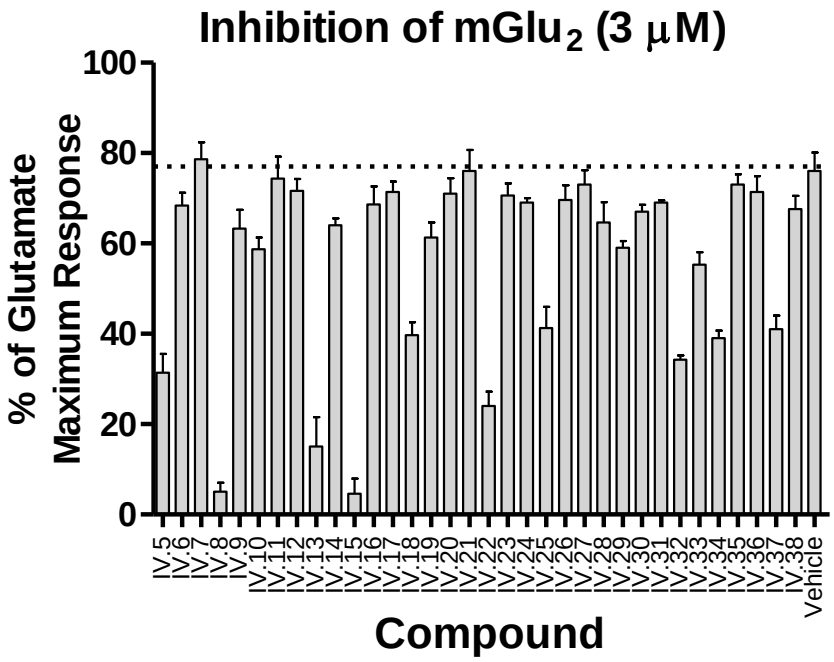

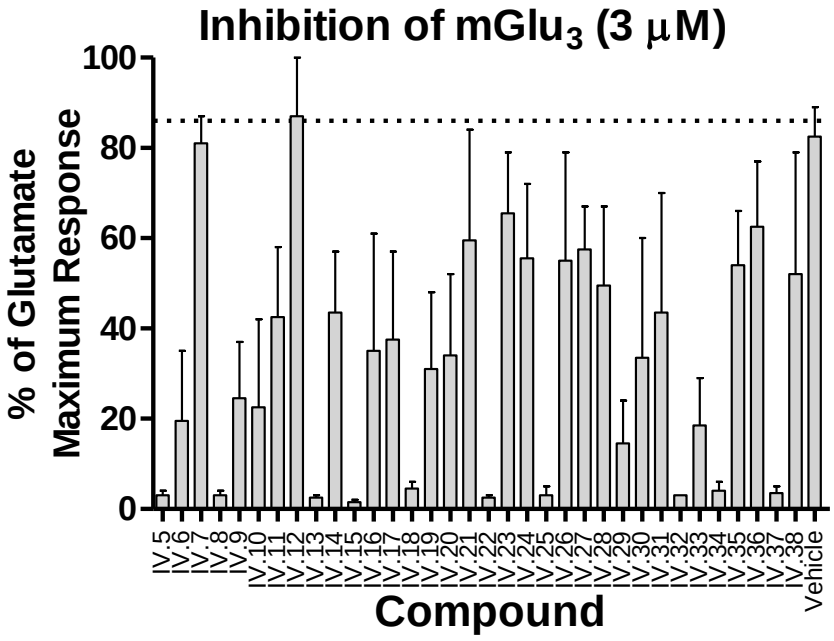

Figure IV.3 Inhibition of $mGlu_2$ response to an EC_{76} of glutamate and inhibition of $mGlu_3$ response to an EC_{87} of glutamate. Results are representative of three independent experiments and are presented as mean ± SEM.

Structure-activity relationship of analogues

As has been previously reported with allosteric modulators for mGlu receptors, the SAR profile of these compounds was fairly steep, with small structural changes leading to significant losses in efficacy (Sameer Sharma et al., 2008; Wenthur et al., 2013). When the R^1 position was held constant as a phenyl ring, and R^3 was held as a methyl, installation of a 3-sulfonylphenyl or 3-pyridyl group at R_2 yielded inhibitors with low-micromolar to high nanomolar IC_{50}s at both $mGlu_2$ and $mGlu_3$. In contrast, installation of a phenyl or 4-methoxyphenyl at this position yielded compounds with very little effect. Truncation of this position to a methyl group also resulted in much attenuated activity at both receptors. Results from installation of substituted phenyl groups at R^1 are summarized in **Table IV.1**.

In general, the presence of a 3-sulfonamidephenyl or 3-pyridyl at R_2 induces more robust inhibition than their phenyl, 4-methoxyphenyl, or methyl comparators. Some additional interesting trends can be seen by comparing similar compounds across alterations at R^1 exclusively. When replacing the phenyl at R^1 (**IV.5 – IV.9**) with a 3-fluoro phenyl (**IV.10** – **IV.14**), the analogous compounds generally exhibit a reduction in potency at $mGlu_2$ and $mGlu_3$. In the case where a 3-pyridyl is present at R_2, this reduction is approximately 2-fold. However, in the case where a 3-sulfonyl phenyl is at R_2, the potency reduction is even more pronounced: more than 5-fold at $mGlu_2$, and over 10-fold at $mGlu_3$. In contrast, when a 3-methoxyphenyl is present at R^1 (**IV.15 – IV.19**), there is an increase in potency, as compared to their phenyl analogues. An exception to this trend is when a 3-pyridyl group is present at R^2, as this compound has

notably diminished potency at the group II mGlu receptors in relation to its phenyl comparator. For the analogues screened here, having a 3-methylphenyl at R^1 (**IV.20 – IV.22**) results in an overall decrease in potency. This decrease has a similar magnitude as was observed with 3-fluorophenyl at this position.

Several 3-chlorophenyl (**IV.23 – IV.25**) and 3-bromophenyl (**IV.26 – IV.28**) analogues were screened at R^1 as well, allowing for analysis of increasing size of halogens at this position. The general trend seen is that potency decreases as halogen size increases, with **IV.25** providing one notable exception. This compound has an increased potency over its 3-fluoromethyl and phenyl comparators at $mGlu_2$, while its potency at $mGlu_3$ is decreased.

Those compounds with phenyl, 4-fluorophenyl, and methyl substitutions at R^2 are once again less active than their 3-sulfonamidephenyl and 3-pyridyl analogues. The presence of a 4-fluorophenyl group at R^1 (**IV.29 – IV.33**) most often yielded an approximately 2-fold increase in activity at $mGlu_2$ and $mGlu_3$, as compared to (**IV.5 – IV.9**). The exception to this is **IV.29**, which has an approximately 2-fold decrease. Notably, the presence of a 3-pyridyl group at R^2 resulted in the most potent compound generated from this initial screen, **IV.32**, with an IC_{50} of 427 nM at $mGlu_2$ and 67 nM at $mGlu_3$. In contrast, placing a 4-chlorophenyl group at R^1 (**IV.34 – IV.38**) did not increase the potency as compared to (**IV.5 – IV.9**). Rather, the major effect of this alteration appears to be a decrease in the maximal inhibition achieved. These compounds appear to possess partial antagonist properties, as their CRC's would plateau at a maximum of 60-70% inhibition, rather than continuing to depress the response toward the baseline.

Table IV.1 Structures of compounds generated as shown in **Scheme IV.1**, along with their activity at $mGlu_2$ and $mGlu_3$ receptors. Where an IC_{50} was not determined, the percent inhibition at 3 µM is shown in parentheses. The presence of " indicates that the sub-structure for that compound is the same as the sub-structure listed above.

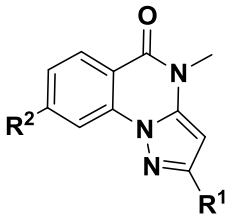

Compound	VUID	R^1	R^2	IC_{50} $mGlu_2$ (µM)	IC_{50} $mGlu_3$ (µM)
IV.5	VU0550432		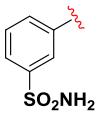	1.93	0.884
IV.6	VU0550428	"		> 10	> 10
IV.7	VU0550429	"	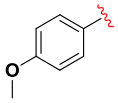	(4)	(0)
IV.8	VU0550405	"		0.852	0.165
IV.9	VU0550403	"		(17)	(59)
IV.10	VU0550393	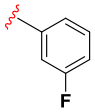	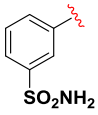	> 10	> 10

IV.11	VU0550435	"		(2)	(39)
IV.12	VU0550444	"	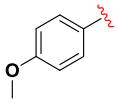	(6)	(2)
IV.13	VU0550407	"		1.56	0.247
IV.14	VU0550415	"		(16)	(38)
IV.15	VU0550391	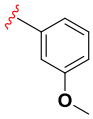	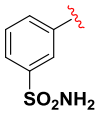	1.39	0.696
IV.16	VU0550404	"		> 10	>10
IV.17	VU0550441	"	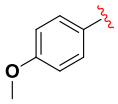	(6)	(48)
IV.18	VU0550411	"		3.12	1.18
IV.19	VU0550397	"		> 10	> 10
IV.20	VU0550409	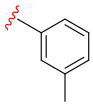		(7)	(49)

IV.21	VU0550443	"	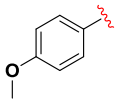	(0)	(34)
IV.22	VU0550396	"		1.79	0.53
IV.23	VU0550422	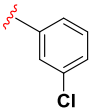		(-7)	(-19)
IV.24	VU0550424	"	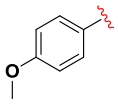	(-9)	(-31)
IV.25	VU0550439	"		0.564	0.293
IV.26	VU0550398	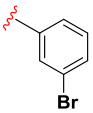		(-8)	(-28)
IV.27	VU0550425	"	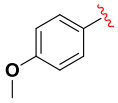	(-4)	(-23)
IV.28	VU0550440	"		> 10	> 10
IV.29	VU0550392	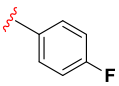	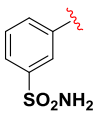	3.95	1.99

IV.30	VU0550434	"		(-12)	(-64)
IV.31	VU0550410	"	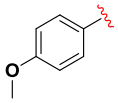	> 10	> 10
IV.32	VU0550406	"		0.427	0.067
IV.33	VU0550408	"		> 10	> 10
IV.34	VU0550394	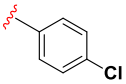	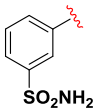	0.847	1.25
IV.35	VU0550436	"		(-4)	(-31)
IV.36	VU0550445	"	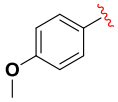	(-6)	(-21)
IV.37	VU0550414	"		1.11	0.645
IV.38	VU0550401	"		(-11)	(-33)

In a further attempt to expand the search for the molecular basis of mode switching that had been reported with this series, several analogues were made which examined alternative *N*-alkyl groups (**Table IV.2**) following the synthetic scheme depicted in **Scheme IV.1**. Starting from a compound of the type shown by **Intermediate IV.4** deprotonation with LiHMDS and trapping with either 2-iodoethanol or acetyl chloride afforded analogs **IV.39** - **IV.44**. These compounds retained a phenyl group at R^1, and either a 3-pyridinyl or phenyl group at R^2. The presence of a hydrogen (**IV.39**, **IV.42**) or acetyl group (**IV.40**, **IV.43**) at R^3 did not appear to be tolerated for these compounds, and installation of an ethanol group resulted in a significant decrease in potency at $mGlu_2$ and $mGlu_3$ (**IV.41**, **IV.44**).

Given the trend seen with **IV.5-IV.38**, wherein the presence of a 3-pyridyl group at R^2 resulted in compounds with elevated potency at $mGlu_2$ and $mGlu_3$, it was decided to explore the effects of additional heterocyclic replacements at R^2 while retaining R^1 as a phenyl group (**Table IV.3**). As compared to **IV.8**, the analogues with benzo-fused heterocycles at R^2 (**IV.45 – IV.51**) all had significantly diminished potency at $mGlu_2$ and $mGlu_3$. Installation of a 4-pyridyl group also caused a relative decrease in potency. In contrast, when a 3,5-pyrimidyl group is present at the R^2 position, it increased potency by nearly 3.5-fold at $mGlu_2$ and by over 2-fold at $mGlu_3$. The resulting compound, 4-methyl-2-phenyl-8-(pyrimidin-5-yl)pyrazolo[1,5-*a*]quinazolin-5(4*H*)-one (**IV.47**), was the most potent inhibitor of group II mGlu receptors discovered from this scaffold, with an IC_{50} of 245 nM (pIC_{50} = 6.611 $\pm$ 0.055) at $mGlu_2$, and 78 nM (pIC_{50} = 7.108 $\pm$ 0.073) at $mGlu_3$.

Table IV.2 Structures of compounds generated as shown in **Scheme IV.1**, along with their activity at $mGlu_2$ and $mGlu_3$ receptors. Where an IC_{50} was not determined, the percent inhibition at 3 µM is shown in parentheses. The presence of " indicates that the sub-structure for that compound is the same as the sub-structure listed above.

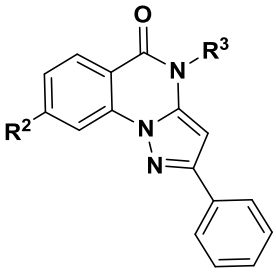

Compound	VUID	R^2	R^3	IC_{50} $mGlu_2$ (µM)	IC_{50} $mGlu_3$ (µM)
IV.39	VU0650648			(2)	(6)
IV.40	VU0650650	"		(3)	(8)
IV.41	VU0650642	"	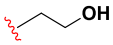	(0)	(3)
IV.42	VU0650641			(4)	(8)
IV.43	VU0650656	"		> 10	> 10
IV.44	VU0650649	"	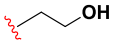	4.65	3.15

Table IV.3 Structures of compounds generated as shown in **Scheme IV.1**, along with their activity at $mGlu_2$ and $mGlu_3$ receptors. Where IC_{50}s were not determined, the percent inhibition at 3 µM is shown in parentheses. The presence of " indicates that the sub-structure for that compound is the same as the sub-structure listed above.

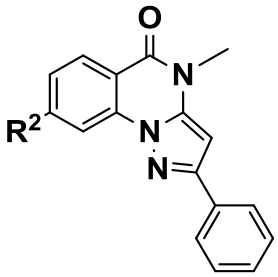

Compound	VUID	R^2	IC_{50} $mGlu_2$ (µM)	IC_{50} $mGlu_3$ (µM)
IV.45	VU0550402	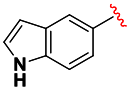	(9)	(34)
IV.46	VU0550417	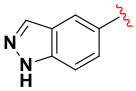	> 10	> 10
IV.47	VU0550418		0.245	0.078
IV.48	VU0550419	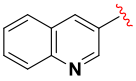	(4)	(33)
IV.49	VU0550426	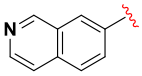	> 10	4.51

IV.50	VU0550427		1.77	0.509
IV.51	VU0550430	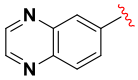	(0)	(16)

Pharmacological characterization of VU0550418

Due to its potency, **IV.47** (VU0550418) was selected as an exemplar compound from this series for further pharmacological characterization. In order to determine its mechanism of action (competitive orthosteric antagonism or negative allosteric modulation), **IV.47** was screened at several fixed concentrations against $mGlu_2$ and $mGlu_3$ against an increasing concentration of glutamate (1 nM – 30 μM). It diminished the response to glutamate in a dose-dependent manner at both $mGlu_2$ and $mGlu_3$, indicating that it is acting as a NAM, rather than a competitive antagonist (**Figure IV.4)**.

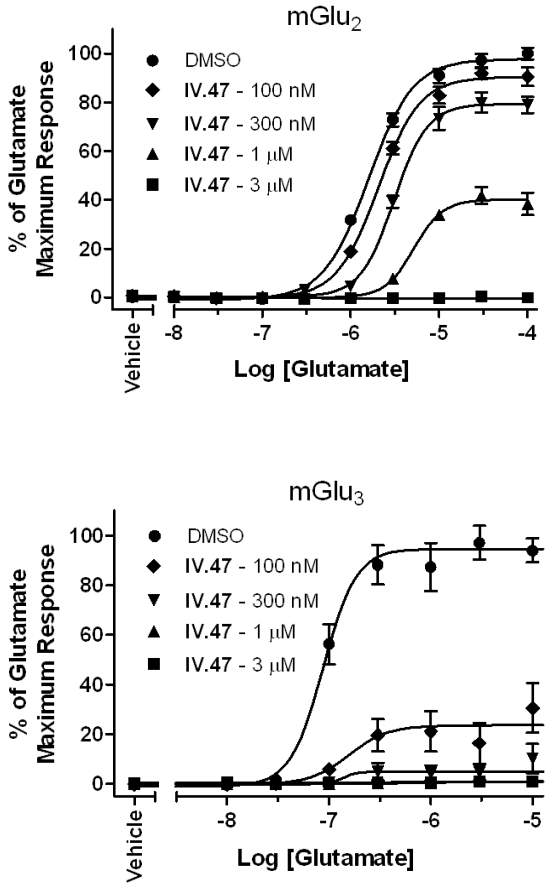

Figure IV.4 Progressive fold-shift experiments with VU0550418 at $mGlu_2$ and $mGlu_3$. Results are representative of three independent experiments.

Additionally, to measure the broader selectivity profile of this compound, it was screened against the entire family of mGlu receptors at a fixed concentration of 10 µM. At this concentration **IV.47** showed a 3-fold shift of $mGlu_1$, and had completely blocked the glutamate response at $mGlu_2$ and $mGlu_3$, but it did not alter the responses of the other mGlu receptors to glutamate (**Figure IV.5**). These data indicate that this scaffold can deliver compounds with highly preferential activity at group II mGlu receptors, in comparison to the group I and group III receptors. Overall, these results indicate that potent dual inhibitors of $mGlu_2$ and $mGlu_3$, such as **IV.47**, are rapidly accessible via alterations to a pyrazolo[1,5-*a*]quinazoline-5(4*H*)-one scaffold.

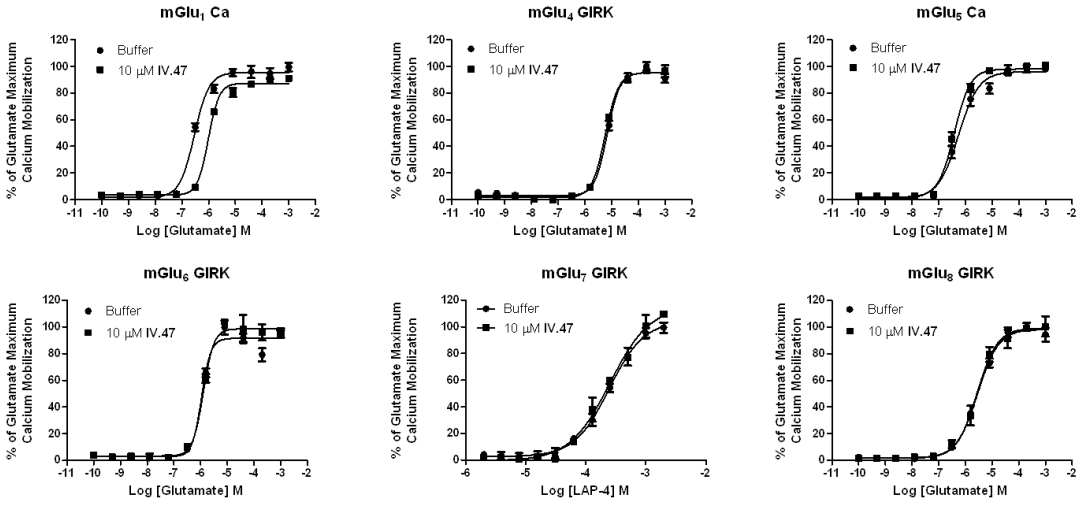

Figure IV.5. Fold-shifts of mGlu signaling for **IV.47** at 10 µM across the group I and group III receptors. Group I signaling measured using calcium response, group III measured using GIRK response. All responses measured at rat receptors, aside from $mGlu_1$ and $mGlu_6$, which used human receptors. Results are representative of three experiments.

Pharmacokinetic characterization of VU550418

Based on the attractive mGlu selectivity profile and favorable calculated properties (MW = 353, clogP = 2.72, tPSA = 60), we evaluated **IV.47** in a tier 1 DMPK panel to assess its disposition profile. Unfortunately, **IV.47** was very highly bound to protein in both rat (F_u 0.003) and human (**F_u** 0.008) plasma, and had a predicted clearance near hepatic blood flow in rat and human (CL_{hep} of 54.7 mL/ min/kg and 18.7 mL/min/kg, respectively). Compound **IV.32** exhibited similarly poor DMPK properties. Due to the flat, aromatic character of **IV.47** and **IV.32**, these results are understandable.

Although the lead compounds generated from this effort represent potent dual $mGlu_{2/3}$ NAMs, the SAR analysis did not reveal a significant propensity for mode switching with the alterations we made. Due to the poor pharmacokinetic properties of this series, and the absence of a robust signal that selective $mGlu_2$ NAMs could be generated from this pyrazolo[1,5-*a*]quinazoline-5(4*H*)-one scaffold, we elected to pursue an alternative scaffold in order to access selective $mGlu_2$ NAM compounds that would be suitable for *in vitro* and *in vivo* use.

Prior Claims of Quinoline Carboxamides as $mGlu_2$ NAMs

During our exploration of SAR around the pyrazolo[1,5-*a*]quinazoline-5(4*H*)-one scaffold, a Merck patent was disclosed that claimed a series of quinoline carboxamides as $mGlu_2$ NAMs ("International Patent Application PCT/US2012/06202," 2012). However, the patent did not disclose the activity of these compounds at any of the other mGlu receptors, and had no pharmacokinetic data, making it impossible to judge

the utility of these compounds as potential tools for the study of $mGlu_2$ receptor function. In order to evaluate the utility of these compounds as in vitro and in vivo tools, we elected to synthesize a small library of quinoline carboxamides and subject them to functional analysis across the entire mGlu family.

Synthesis of quinoline carboxamide containing compounds

These quinoline carboxamide compounds were synthesized from commercially available 4,7-dichloroquinoline as shown in **Scheme IV.2**, which is a modified version of the route reported in the patent filed by Merck.

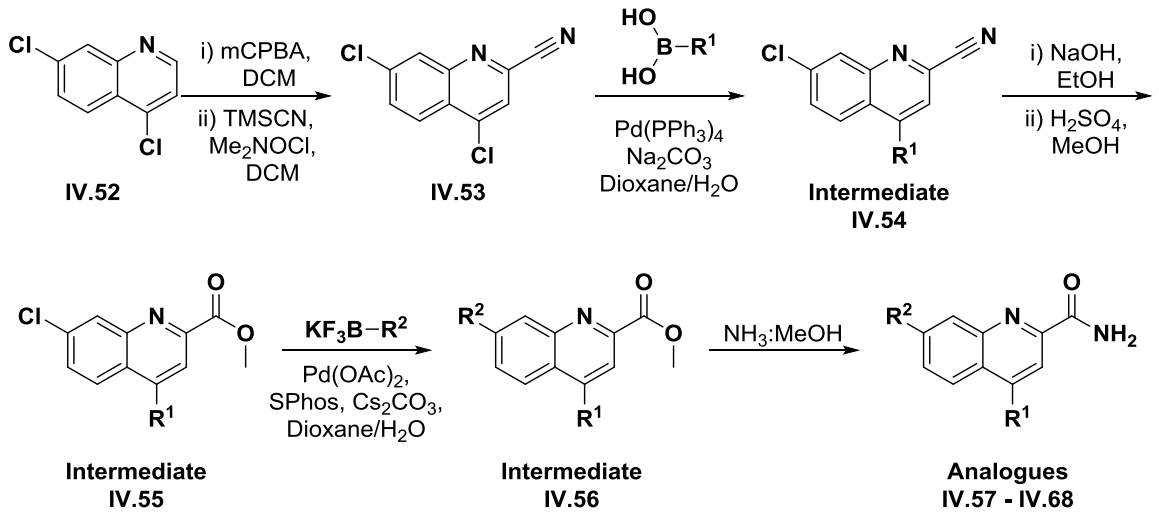

Scheme IV.2 Cyanation, Suzuki couplings, nitrile hydrolysis, and carboxamide formation to synthesize quinoline carboxamide compounds with the potential to generate selective $mGlu_2$ NAMs.

The N-oxide of the 4,7-dichloroquinoline was formed using 3-chloroperoxybenzoic acid, which was then transformed to 4,7-dichloroquinoline-2-carbonitrile in the presence of dimethylcarbamoylchloride and trimethylsilylcyanide. Analogues at R^1 were then prepared via a Suzuki coupling and varying the identity of the boronic acid used. These analogues were then subjected to base-mediated hydrolysis of the nitrile, followed by acidic esterification conditions in the presence of methanol to form the methyl ester at the 2-position. A second Suzuki coupling was then undertaken to prepare analogues at R^2. Those analogues which required an ethylene linker had a vinyl group installed in this position, which was subjected to Heck coupling conditions in the presence of an aryl halide, followed by hydrogenolysis. All analogues were then treated with 2 M ammonia in methanol in order to form the primary carboxamide from the methyl ester at the 2-position.

In vitro pharmacological characterization of quinoline carboxamide analogues

We then used a calcium-fluorescence assay to generate concentration response curves for each compound (**Table IV.4**). All compounds that retained the nitrile or methyl ether, as seen in **Intermediates IV.54** and **IV.55**, were inactive. Contrastingly, compounds with a carboxamide installed had efficacy at $mGlu_2$; this implicates the carboxamide moiety as a key mediator of inhibitory activity in this series. With this confirmation of the activity of quinoline carboxamides at $mGlu_2$, we then selected **IV.57** (VU6000446 / MRK-8-29), the most active analogue, for confirmatory screening, assessment of selectivity, and determination of the mode of inhibition.

Table IV.4 Structures of compounds generated as shown in **Scheme IV.2**, along with their activity at $mGlu_2$ receptors as determined by calcium mobilization.

Structure	Compound	VUID	IC_{50} $mGlu_2$ (μM)	$mGlu_2$ Glu Min %
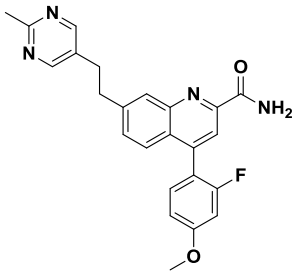	**IV.57**	VU6000446	0.149	1.1
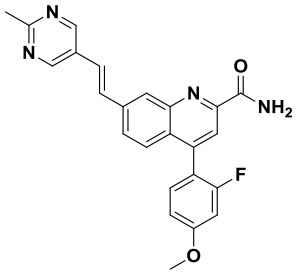	**IV.58**	VU6000447	0.675	0.5
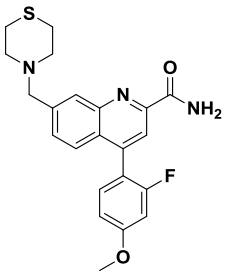	**IV.59**	VU6000468	0.745	0.7
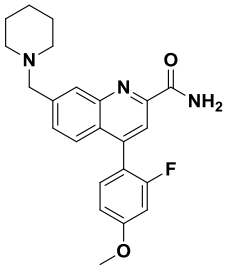	**IV.60**	VU6000469	2.38	1.9

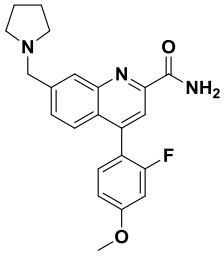	**IV.61**	VU6000470	2.78	-4.3
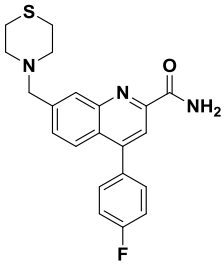	**IV.62**	VU6001134	0.987	4.9
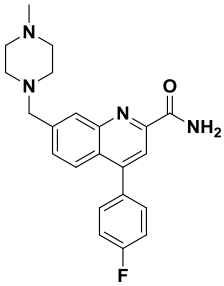	**IV.63**	VU6001139	1.71	3.7
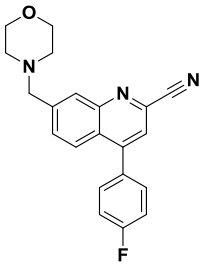	**IV.64**	VU6001126	>10	85.5

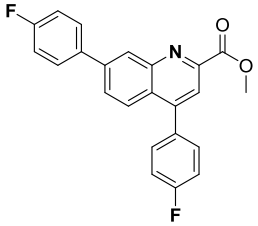	**IV.65**	VU6001130	> 10	86.2
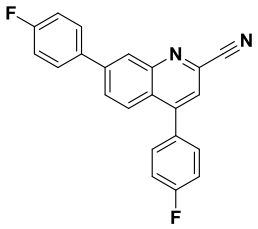	**IV.66**	VU6001131	> 10	86.7
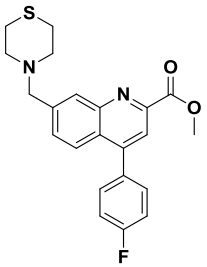	**IV.67**	VU6001135	> 10	88.3
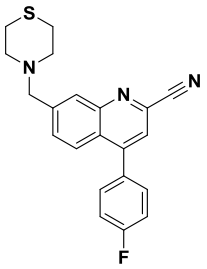	**IV.68**	VU6001136	> 10	86.9

Upon repeated screening, the IC_{50} of **IV.57** at $mGlu_2$ was found to be 146 nM. Critically, **IV.57** did not alter the response of rat $mGlu_3$ cells to an EC_{80} concentration of glutamate at all concentrations tested up to 30 µM. Furthermore, increasing concentrations of MRK-8-29 induced a progressive depression of the maximal efficacy of rat $mGlu_2$ in response to glutamate, indicating an allosteric mechanism of inhibition. Finally, a 10 µM concentration of **IV.57** did not alter the response of the remaining mGlu receptors to glutamate (**Figure IV.6**).

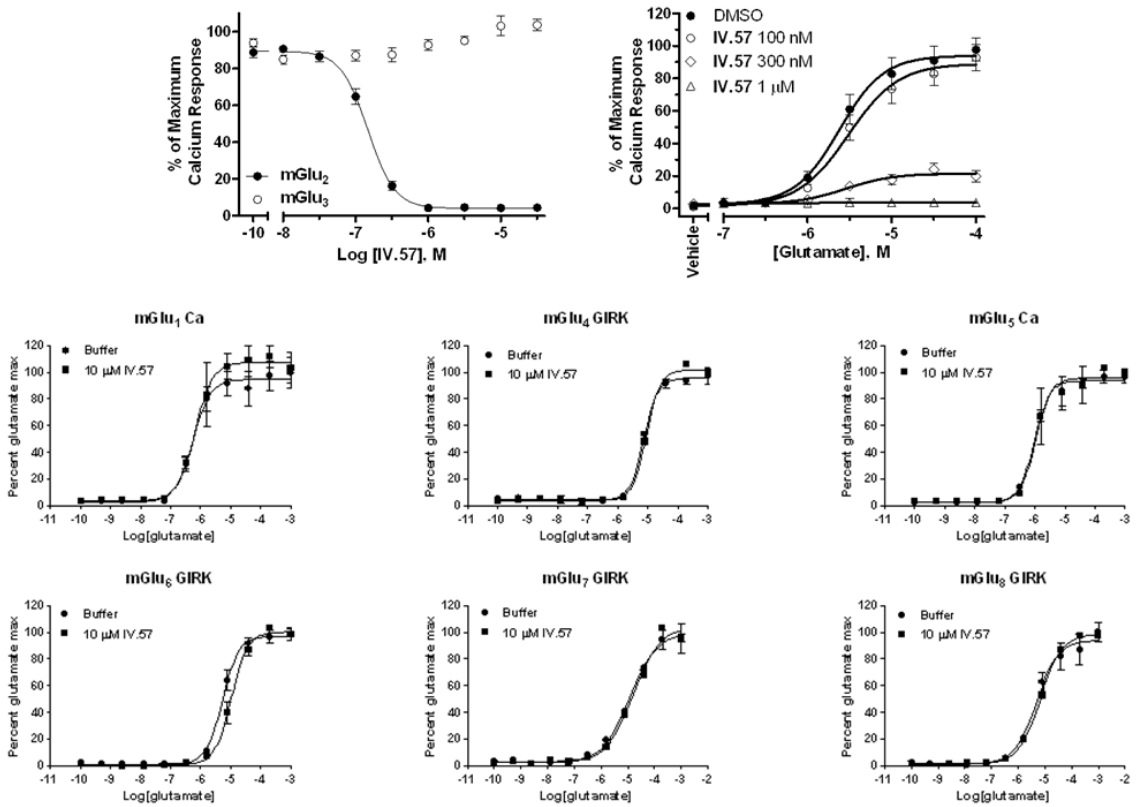

Figure IV.6 Activity of VU6000446 at $mGlu_2$ and $mGlu_3$ receptors as measured by calcium mobilization, progressive fold-shift data for VU6000446 at $mGlu_2$, and fold-shifts of mGlu signaling for VU6000446 at 10 µM across the group I and group III receptors. Group I signaling measured using calcium response, group III measured using GIRK response. All responses measured at rat receptors, aside from $mGlu_1$ and $mGlu_6$, which used human receptors. Results are representative of three experiments.

Pharmacokinetic assessment of VU6000446

Although the pharmacology results indicated that **IV.57** was a selective $mGlu_2$ NAM suitable for *in vitro* and *ex vivo* use, the utility of this compound as an *in vivo* tool was still unknown. Therefore, we subjected **IV.57** to a battery of DMPK analyses across several species; we first used *in vitro* methods to measure microsomal clearance, plasma protein binding, and brain homogenate binding, then proceeded to *in vivo* plasma: brain level studies to assess the disposition of the compound.

The results indicated that **IV.57** was rapidly cleared in all tested species, at a rate near the limit of blood flow to the liver for each tested species. It was found to have acceptable plasma free fractions, but was highly bound in brain tissue.

Furthermore, the *in vivo* studies revealed that the concentration of free drug was much lower in the brain than in the plasma at steady state when a low dose was given, but the concentrations were closer to unity when a much higher dose was administered. This disunity in the $K_{pu,u}$ indicates that **IV.57** is not distributed across the BBB via osmosis alone, but rather, that it is removed from the CNS via an active efflux process. The relative increase in free brain concentrations at a higher dose indicates that this process is saturable. However, even at the elevated dose we administered, the free concentration available in the brain was not able to reach the IC_{50} of **IV.57** at $mGlu_2$. The non-linear dose escalation seen with this compound is potentially due to solubility issues that may ultimately limit its ability to be used as an *in vivo* tool compound (**Table IV.5**).

Table IV.5 *in vitro* pharmacokinetic parameters of VU6000446 for humans, rats, and mice, along with *in vivo* pharmacokinetic parameters in mice.

In Vitro DMPK Assessment				
Species	**CL_{int} (ml/min/kg)**	**CL_{Hep} (ml/min/kg)**	**$F_{u,p}$**	**$F_{u,b}$**
Human	204	19.0	0.017	---
Rat	259.5 (n=2)	54.8 (n=2)	0.031 (n=2)	0.008
Mouse	433	74.5	0.029 (n=2)	0.005 (n=2)
In Vivo DMPK Assessment (Mouse)				
IP Dose (mg/kg)	**Time (min)**	**Free [Plasma], (nM)**	**Free [Brain], (nM)**	**$K_{p,uu}$**
1	30	7.97 (n=5)	1.15 (n=5)	0.14
56.6	30	58.0 (n=5)	27.31 (n=5)	0.47

Structural verification of VU6000446 and intermediates

After assessing the pharmacologic and pharmacokinetic profile of **IV.57** (VU6000446), we decided to move forward with it as our first-generation $mGlu_2$ NAM *in vitro* tool compound. During re-synthesis of **IV.57** all intermediates were purified and submitted to analysis by HRMS, and both 1H and 13C NM) analysis. The synthesis of **IV.57** proceeded with moderate-to-good chemical yields, and resulted in the generation of the expected compounds in >98% purity, as demonstrated by the concordance between the predicted and measured LC, MS, HRMS, 1H NMR and 13C NMR data gathered for each compound. (**Table IV.6**)

Table IV.6 Procedural details and analytical data for all intermediates and final products generated via the route employed for the preparation of VU6000446.

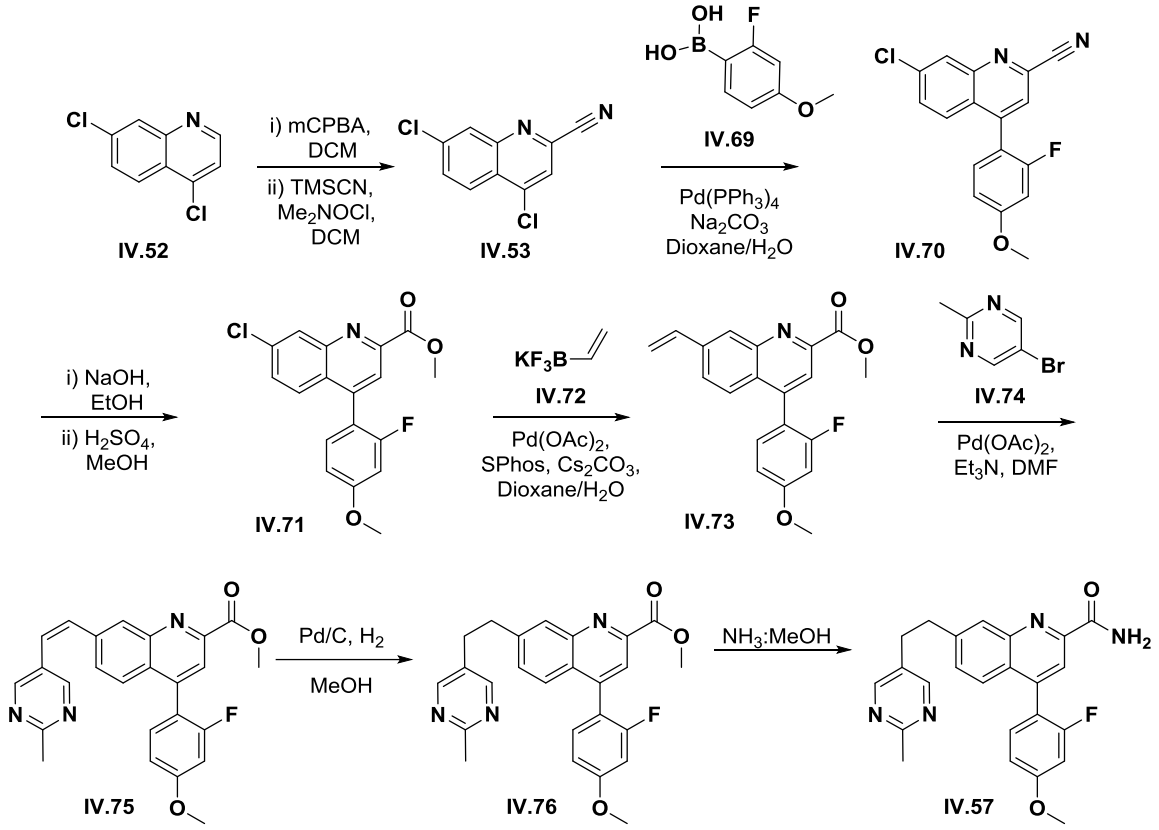

4,7-Dichloroquinoline-2-Carbonitrile IV.53		
Procedure: To a solution of 4,7-dichloroquinoline (9.90 g, 50 mmol) in dichloromethane (500 mL) was added 3-chloroperoxybenzoic acid (17.26 g, 100 mmol) in five portions, such that the temperature of the reaction did not rise above 34 °C. The resulting suspension was stirred for 1 h. The reaction was then quenched with an aqueous solution of NaOH (1 M, 500 mL) and extracted into dichloromethane (500 mL). The organic layer was separated, dried with $MgSO_4$, and filtered to yield a solution of 4,7-dichloro-1-oxido-quinolin-1-ium in dichloromethane, which was carried forward without purification. To this solution was added trimethylsilyl cyanide (13.00 mL, 100 mmol), followed by dimethylcarbamoyl chloride (9.50 mL, 100 mmol). The resulting solution was then heated to reflux for 48 h. The reaction was then quenched with a saturated aqueous solution of $NaHCO_3$ (500 mL), diluted with H_2O (500 mL), and extracted into dichloromethane (1 L). The organic layer was then separated, dried with $MgSO_4$, and filtered, and the solvent was removed under vacuum. The product was isolated following recrystallization in methanol.		
Yield	**LC (254 nm)**	**MS (ESI) *m/z***
58.0% (6.50 g)	1.167 min	222.9
^{1}H NMR (400.1 MHz, *CDCl$_3$*) δ (ppm)]: 8.22 (d, J = 9.0 Hz, 1H); 8.17 (d, J = 2.0 Hz, 1H); 7.77 (s, 1H); 7.74 (dd, J1 = 9.0 Hz, J2 = 2.0 Hz, 1H)	**^{13}C NMR (100.6 MHz, *CDCl$_3$*) δ (ppm):** 149.3; 144.6; 138.9; 134.7; 131.9; 129.5; 126.0; 125.9; 123.8;116.6	

7-Chloro-4-(2-Fluoro-4-Methoxyphenyl)Quinoline-2-Carbonitrile IV.70		
Procedure: To a stirred solution of 4,7-Dichloroquinoline-2-Carbonitrile (6.50 g, 29.14 mmol) in 1,4-dioxanes: H_2O (9:1, 60 mL) was added (2-fluoro-4- methoxyphenyl)boronic acid (4.95 g, 29.14 mmol), Cs_2CO_3 (18.95 g, 58.30 mmol), and $Pd(PPh_3)_4$ (0.842 g, 0.728 mmol, 2.5 mol%) under argon. The reaction was stirred at 75 °C for 18 h. The reaction was then diluted with ethyl acetate (300 mL), washed with brine (300 mL), and filtered through a Celite plug. The organic layer was separated, dried with $MgSO_4$, and filtered, and the solvent was removed under vacuum. The product was isolated following purification on reverse-phase HPLC.		
Yield	**LC (254 nm)**	**MS (ESI) *m/z***
80.0% (7.27 g)	1.250 min	312.9
^{1}H NMR (400.1 MHz,*CDCl$_3$*) δ (ppm)]: 8.20 (d, J = 2.0 Hz, 1H); 7.74(dd, J1 = 9.0 Hz, J2 = 2.5 Hz, 1H); 7.63 (s, 1H); 7.59 (dd, J1 = 9.0 Hz, J2 = 2.0 Hz, 1H); 7.29 (t, J = 8.5 Hz, 1H); 6.90 (dd, J1 = 8.5 Hz, J2 = 2.5 Hz, 1H); 6.82 (dd, J1 = 11.7 Hz, J2 = 2.5 Hz, 1H); 3.91 (s, 3H)	**^{13}C NMR (100.6 MHz, *CDCl$_3$*) δ (ppm):** 162.6 (d, 3JCF = 11.3 Hz); 160.5 (d, 1JCF = 249.8 Hz); 149.2; 145.1; 137.6; 134.6; 132.1(d, 3JCF = 4.8 Hz); 130.7; 129.4; 127.7; 126.5; 124.9; 117.5; 115.5 (d, 2JCF = 15.4 Hz); 111.2 (d, 4JCF = 3.1 Hz); 102.6 (d, 2JCF = 25.2 Hz); 56.2	

Methyl-7-Chloro-4-(2-Fluoro-4-Methoxyphenyl)Quinoline-2-Carboxylate IV.71		
Procedure: To a stirred solution of 7-Chloro-4-(2-Fluoro-4-Methoxyphenyl)Quinoline-2-Carbonitrile (7.27 g, 23.31 mmol) in ethanol (150 mL) was added an aqueous solution of NaOH (1 M, 225 mL). The reaction was heated to reflux for 14 h. After cooling to room temperature, the reaction was passed through a filter and the solid, 7-chloro-4-(2-fluoro-4-methoxyphenyl) quinoline-2-carboxylic acid, was retained. This solid was then suspended in methanol (180 mL), and concentrated H_2SO_4 (20 mL) was added dropwise with vigorous stirring. The reaction was heated to reflux for 2 h, then slowly neutralized to pH 7, using a saturated aqueous solution of $NaHCO_3$, and extracted into dichloromethane (250 mL). The organic layer was separated, dried with $MgSO_4$, and filtered, and the solvent was removed under vacuum. The product was isolated following purification on reverse-phase HPLC.		
Yield	**LC (254 nm)**	**MS (ESI) *m/z***
76.0% (6.16 g)	1.218 min	345.9
^{1}H NMR (400.1 MHz,*CDCl$_3$*) δ (ppm)]: 8.36 (d, J = 2.0 Hz, 1H); 8.31 (s, 1H); 7.73(dd, J1 = 9.0 Hz, J2 = 2.5 Hz, 1H); 7.54 (dd, J1 = 9.0 Hz, J2 = 2.0 Hz, 1H); 7.31 (t, J = 8.5 Hz, 1H); 6.88 (dd, J1 = 8.5 Hz, J2 = 2.5 Hz, 1H); 6.81 (dd, J1 = 11.7 Hz, J2 = 2.5 Hz, 1H); 4.08 (s, 3H); 3.89 (s, 3H)	**^{13}C NMR (100.6 MHz, *CDCl$_3$*) δ (ppm):** 165.9; 162.3 (d, 3JCF = 11.3 Hz); 160.5 (d, 1JCF = 249.8 Hz); 148.7 (d, 2JCF = 12.1 Hz); 144.7; 136.6; 132.1(d, 3JCF = 4.8 Hz); 130.0; 129.4; 127.5; 127.4; 127.0; 122.8; 116.7 (d, 2JCF = 15.2 Hz); 111.0 (d, 4JCF = 3.0 Hz); 104.6 (d, 2JCF = 24.3 Hz); 56.2; 53.6	

Methyl-4-(2-Fluoro-4-Methoxyphenyl)-7-Vinylquinoline-2-Carboxylate IV.73		
Procedure: To a stirred solution of Methyl-7-Chloro-4-(2-Fluoro-4-Methoxyphenyl)Quinoline-2-Carboxylate (6.16 g, 17.82 mmol) in 1,4-dioxanes: H_2O (9:1, 90 mL) was added potassium vinyltrifluoroborate (4.78 g, 35.64 mmol), Cs_2CO_3 (5.67 g, 53.46 mmol), 2-dicyclohexylphosphino-2′,6′-dimethoxybiphenyl (1.10 g, 2.67 mmol, 15 mol%), and $Pd(OAc)_2$(0.30 g, 1.34 mmol, 7.5 mol%) under argon. The reaction was stirred at 85 °C for 1 h, diluted with ethyl acetate (250mL), and then washed with brine (250mL). The organic layer was separated, dried with $MgSO_4$, and filtered, and the solvent was removed under vacuum. The product was isolated following purification on reverse-phase HPLC.		
Yield	**LC (254 nm)**	**MS (ESI) *m/z***
68.0% (4.10 g)	1.203 min	337.9
^{1}H NMR (400.1 MHz,*CDCl$_3$*) δ (ppm)]: 8.36 (d, J = 2.0 Hz, 1H); 8.30 (s, 1H); 7.71(dd, J1 = 9.0 Hz, J2 = 2.5 Hz, 1H); 7.54 (dd, J1 = 9.0 Hz, J2 = 2.0 Hz, 1H); 7.31 (t, J = 8.5 Hz, 1H); 7.03 (dd, J1 = 17.6 Hz, J2 = 11.0 Hz, 1H); 6.88 (dd, J1 = 8.5 Hz, J2 = 2.5 Hz, 1H); 6.81 (dd, J1 = 11.7 Hz, J2 = 2.5 Hz, 1H); 5.97 (d, J = 17.6 Hz, 1H); 5.45 (d, J = 11.0 Hz, 1H); 4.08 (s, 3H); 3.89 (s, 3H)	**^{13}C NMR (100.6 MHz, *CDCl$_3$*) δ (ppm):** 165.8; 161.7 (d, 3JCF = 12.0 Hz); 160.2 (d, 1JCF = 249.6 Hz); 148.1; 147.6; 144.0; 139.4; 135.9; 131.9 (d, 3JCF = 4.8 Hz); 129.7; 129.5; 128.4; 126.4; 125.8; 122.7; 116.7(d, 2JCF = 15.2 Hz); 110.4; 101.9 (d, 2JCF = 28.0 Hz); 55.7; 53.2	

Methyl-4-(2-Fluoro-4-Methoxyphenyl)-7-(2-(2-Methylpyrimidin-5-yl)vinyl)quinoline-2-Carboxylate IV.75		
Procedure: To a stirred solution of Methyl-4-(2-Fluoro-4-Methoxyphenyl)-7-Vinylquinoline-2-Carboxylate (3.76 g, 11.16 mmol) in N,N-dimethylformamide (100 mL) was added 5-bromo-2methylpyrimidine (1.93 g, 11.16 mmol), triethylamine (9.32 mL, 66.97 mmol), and $Pd(OAc)_2$(0.25 g, 1.12 mmol, 10 mol%). The reaction was heated to reflux for 2.5 h, quenched with H_2O (100 mL), and then extracted into dichloromethane (250 mL).The organic layer was separated, dried with $MgSO_4$, and filtered, and the solvent was removed under vacuum. The product was isolated following purification on reverse-phase HPLC.		
Yield	**LC (254 nm)**	**MS (ESI) *m/z***
28.0% (1.32 g)	1.074 min	429.9
^{1}H NMR (400.1 MHz,*CDCl$_3$*) δ (ppm)]: 8.82 (s, 2H); 8.42 (s, 1H); 8.13 (s, 1H); 7.79 (s, 2H); 7.36 (d, J = 16.2 Hz, 1H), 7.35 (t, J = 8.5 Hz, 1H); 7.18 d, J = 16.2 Hz, 1H); 6.89 (dd, J1 = 8.5 Hz, J2 = 2.5 Hz, 1H); 6.83 (dd, J1 = 11.7 Hz, J2 = 2.5 Hz, 1H); 4.10 (s, 3H); 3.91 (s, 3H); 2.78 (s, 3H)	**^{13}C NMR (100.6 MHz, *CDCl$_3$*) δ (ppm):** 167.2; 166.0; 162.1; 160.2 (d, 1JCF = 248.9 Hz); 157.1; 148.3 (d, 2JCF = 12.1 Hz); 144.2; 138.2; 132.3 (d, 3JCF = 5.3 Hz); 130.7; 129.5; 128.4; 127.6; 126.6; 124.2; 122.7; 117.0; 116.9(d, 2JCF = 15.8 Hz); 110.8 (d, 4JCF = 2.7 Hz); 102.3 (d, 2JCF = 25.3 Hz); 56.0; 53.4; 25.8	

Methyl-4-(2-Fluoro-4-Methoxyphenyl)-7-(2-(2-Methylpyrimidin-5-yl)ethyl)quinoline-2-Carboxylate IV.76		
Procedure: Methyl-4-(2-Fluoro-4-Methoxyphenyl)-7-(2-(2-Methylpyrimidin-5-yl)vinyl)quinoline-2-Carboxylate (1.25 g, 2.92 mmol) was placed in a flame-dried two-neck flask and dissolved in methanol (100 mL). Five percent Pd/C (636 mg, 0.3 mmol, 10 mol%) was added while stirring. The flask was purged and refilled with H_2 three times and then stirred at room temperature for 1 h. The reaction was then filtered through Celite, and the product (0.85 g, 68%) was isolated after the solvent was removed under vacuum.		
Yield	**LC (254 nm)**	**MS (ESI) *m/z***
68.0% (0.85 g)	1.068 min	431.9
^{1}H NMR (400.1 MHz,*CDCl$_3$*) δ (ppm)]: 8.39 (s, 2H); 8.11 (s,2H); 7.71(dd, J1 = 8.5 Hz, J2 = 2.5 Hz, 1H); 7.39 (dd, J1 = 8.5 Hz, J2 = 2.5 Hz, 1H); 7.32 (t, J = 8.5 Hz, 1H); 6.87 (dd, J1 = 8.5 Hz, J2 = 2.5 Hz, 1H); 6.80 (dd, J1 = 11.7 Hz, J2 = 2.5 Hz, 1H); 4.07 (s, 3H); 3.89 (s, 3H); 3.14 (t, J = 8 Hz, 2H); 3.00 (t, J = 8 Hz, 2H); 2.67 (s, 3H)	**^{13}C NMR (100.6 MHz, *CDCl$_3$*) δ (ppm):** 166.5; 166.2; 162.0 (d, 3JCF = 11.3 Hz); 160.4 (d, 1JCF = 248.9 Hz); 157.1; 148.1; 147.9 144.2; 142.7; 132.3 (d, 3JCF = 5.9 Hz); 130.5; 130.0 (d, 2JCF = 13.6 Hz) ; 129.3; 127.1; 126.3; 122.3; 120.0; 117.1(d, 2JCF = 16.1 Hz); 110.7 (d, 4JCF = 2.7 Hz); 102.3 (d, 2JCF = 25.3 Hz); 56.0; 53.4; 37.2; 31.4; 25.8	

4-(2-Fluoro-4-Methoxyphenyl)-7-(2-(2-Methylpyrimidin-5-yl)ethyl)quinoline-2-Carboxamide IV.57		
Procedure: Methyl-4-(2-Fluoro-4-Methoxyphenyl)-7-(2-(2-Methylpyrimidin-5-yl)ethyl)quinoline-2-Carboxylate (0.85 g, 1.98 mmol) was dissolved in methanol: ammonia (2 M, 5 mL) and stirred at 60 °C for 8 h. The solvent was removed under vacuum, and the product was isolated following purification on reverse-phase HPLC.		
Yield	**LC (254 nm)**	**MS (ESI) *m/z***
20.0% (0.15 g)	0.986 min	416.9
^{1}H NMR (400.1 MHz,*CDCl$_3$*) δ (ppm)]: 8.50 (s, 2H); 8.22 (s,1H); 8.12 (b, 1H); 7.94 (s, 1H) 7.73(dd, J1 = 8.5 Hz, J2 = 2.5 Hz, 1H); 7.39 (dd, J1 = 8.5 Hz, J2 = 2.5 Hz, 1H); 7.32 (t, J = 8.5 Hz, 1H); 6.87 (dd, J1 = 8.5 Hz, J2 = 2.5 Hz, 1H); 6.80 (dd, J1 = 11.7 Hz, J2 = 2.5 Hz, 1H); 5.72 (b, 1h); 3.90 (s, 3H); 3.17 (t, J = 8 Hz, 2H); 3.06 (t, J = 8 Hz, 2H); 2.73 (s, 3H)	**^{13}C NMR (100.6 MHz, *CDCl$_3$*) δ (ppm):** 166.9; 165.9; 162.0 (d, 3JCF = 11.3 Hz); 160.4 (d, 1JCF = 248.9 Hz); 157.1; 148.1; 147.9 144.2; 142.7; 132.3 (d, 3JCF = 5.9 Hz); 130.5; 130.0 (d, 2JCF = 13.6 Hz); 129.3; 127.1; 126.3; 122.3; 120.0; 117.1(d, 2JCF = 16.1 Hz); 110.7 (d, 4JCF = 2.7 Hz); 102.3 (d, 2JCF = 25.3 Hz); 56.0; 37.2; 31.4; 25.8	

Conclusions and Future Directions

Regarding the pyrazolo[1,5-a]quinazolin-5(4*H*)-one scaffold, our efforts focused on alterations of the identity of the phenyl, aryl, and alkyl substitutions off of this core. We uncovered a number of potent dual $mGlu_{2/3}$ NAMs by using a matrix library strategy to rapidly assess the SAR for these molecules, but did not uncover evidence of mode switching with the alterations that we attempted. When our findings are compared to previous reports of robust mode switching behavior from explorations of the scaffold, they apparently stand in direct contrast. However, there are several potential explanations for this apparent discrepancy.

Firstly, while we were able to screen a number of different substituents, the effort above was by no means an exhaustive search of the potential chemical space around the scaffold; it remains to be seen whether further exploration of substitutions off of the quinazoline or pyrazole rings will yield compounds with an increased preference for inhibition of $mGlu_3$, or whether the generation of selective $mGlu_2$ NAMs or $mGlu_3$ PAMs from this series can be achieved. Perhaps more extensive alterations to the core, including removal of the ketone, alteration of the positions for substitution on the quinazoline or pyrazole ring, or introduction of more extended linker species will reveal the nature of chemical species that can yield such pharmacologic behaviors. Because the previous reports did not disclose any structural information regarding their selective $mGlu_2$ or $mGlu_3$ NAMs and $mGlu_3$ PAMs, a direct comparison is impossible to make at this time.

Secondly, while our primary screen used a functional readout of $mGlu_2$ and $mGlu_3$ receptor activity, this screen was dependent on calcium mobilization in an engineered cell line via activation of a promiscuous $G_{\alpha15}$ subunit, rather than a using a direct measurement of $G_{i/o}$ activity, as would be necessary in mammalian systems expressing $mGlu_2$ and $mGlu_3$. However, when the lead compounds were assessed in our Thallium flux assay, which measures GIRK activity downstream of $G_{i/o}$ coupling, we did not see significant differences in activity, which limits our concerns that the alteration in G-protein coupling is the primary culprit. Nevertheless, both the calcium mobilization and thallium flux assays are functional readouts of receptor activity; previous studies of this scaffold's pharmacologic potential at $mGlu_2$ and $mGlu_3$ have employed an assay that measures binding of the compounds to a modified version of the TMD for these receptors in order to induce a conformational change that alters a FRET signal. The difference in what constitutes an active compound in a binding assay versus a functional assay could also be responsible for this discrepancy in results.

Finally, it is possible that we did not include high enough concentrations of compound in our screens to detect compounds that were $mGlu_2$-preferring, but had relatively elevated IC_{50}s. Because we ran our initial screen at 3 μM and generally did not rescreen compounds with weak inhibition at this concentration, there may be some compounds represented that have limited activity at $mGlu_3$, but have some activity at $mGlu_2$ at double digit-micromolar concentrations.

Even with these caveats in mind, our enthusiasm for the potential of the pyrazolo[1,5-a]quinazolin-5(4*H*)-one scaffold was significantly diminished due to the

poor DMPK properties exhibited by our lead compound **IV.47**. The flat, aromatic character of compounds generated from this scaffold appears to produce compounds that avidly bind to non-specific plasma proteins and are rapidly eliminated via hepatic metabolism. These concerns could potentially be overcome by incorporation of additional rotatable bonds and sp_3 hybridized carbons, or by increasing the number of heteroatoms and hydrogen bond donors / acceptors. Further explorations of this scaffold may uncover structures that exhibit improved DMPK properties and additional modes of pharmacology. Given the lack of known, useful $mGlu_2$ NAM and $mGlu_3$ PAM compounds, such disclosures would be of great value to the field.

In the absence of a straightforward route to generating a selective $mGlu_2$ NAM from the pyrazolo[1,5-a]quinazolin-5(4*H*)-one scaffold, we elected to explore a series of quinolone carboxamides that had structural information available, along with a facile route to their synthesis. A brief exploration of the SAR around this scaffold revealed the importance of the carboxamide moiety to retain activity at $mGlu_2$, and a tolerance for several substitutions at the 4- and 7-positions of the quinolone ring.

Pharmacologic analysis revealed the selectivity of these compounds for $mGlu_2$ over $mGlu_3$, along with their allosteric mode of activity. Further pharmacokinetic studies of lead compound **IV.57** indicated that while it had great potential as an *in vitro* or *ex vivo* tool to study the function of $mGlu_2$ receptors, its limited scalability and brain exposure would preclude its efficacy as an *in vivo* tool in rodents. Nevertheless, the pharmacologic and pharmacokinetic analysis of **IV.57** represented the first disclosure of a validated $mGlu_2$ NAM compound with exquisite selectivity against $mGlu_3$ and the

other members of the mGlu receptor family. Along with our development of the first selective $mGlu_3$ NAM, our synthesis and characterization of this $mGlu_2$ NAM paved the way for studies examining the individual functions of $mGlu_2$ and $mGlu_3$ receptors in wild type animals, including studies of the importance of these receptors in the etiology and treatment of neuropsychiatric disorders.

Sections of this chapter have been reprinted with permission from the following:

Synthesis and SAR or substituted pyrazolo[1,5-a]quinazolines as dual $mGlu_2$/$mGlu_3$ NAMs. Wenthur CJ, Morrison RD, Daniels JS, Conn PJ, Lindsley CW. Bioorg Med Chem Lett. 2014 Jun 15; 24(12):2693-8, Copyright 2014 American Chemical Society.

Metabotropic glutamate receptor 3 activation is required for LTD in medial prefrontal cortex and fear extinction. Walker AG, Wenthur CJ, Xiang Z, Rook JM, Emmitte KA, Niswender CM, Lindsley CW, Conn PJ. Proc Natl Acad Sci USA. 2015 Jan 27; 112(4):1196-201, Copyright 2015 National Academy of Sciences, USA.

CHAPTER V

ASSESSMENT OF $MGLU_2$- AND $MGLU_3$-SELECTIVE NAM EFFECTS IN RODENT MODELS RELEVANT TO PSYCHIATRIC ILLNESSES

The Effects of Group II mGlu receptors on Medial Prefrontal Cortical Function in Schizophrenia, Bipolar Disorder, and Addiction

Cognitive tasks dependent on the prefrontal cortex are disrupted in psychiatric illnesses

Several studies have identified single-nucleotide polymorphisms (SNPs) in GRM3, the human gene encoding $mGlu_3$, that are associated with poor performance on cognitive tests that are dependent on function of the prefrontal cortex (PFC) and hippocampus (Egan et al., 2004; P. J. Harrison et al., 2008). Additionally, these SNPs have also been associated with variations in functional magnetic resonance imaging (fMRI) indexes of prefrontal cortical activity during working memory tasks (Egan et al., 2004; Tan et al., 2007). Moreover, converging lines of evidence indicate that GRM3 represents a major locus associated with schizophrenia (Egan et al., 2004; P. J. Harrison et al., 2008; Working Group of the Psychiatric Genomics Consortium, 2015). GRM3 has also been associated with bipolar disorder and substance abuse disorders (Enoch et al., 2014; Kandaswamy et al., 2013; O'Brien et al., 2014; Xia et al., 2014). Because $mGlu_3$ is densely expressed in PFC, a brain region implicated as a site of pathology in these disorders, this genetic evidence has led to an increased interest in determining the role

of $mGlu_3$ in regulating PFC function and behavior (Ghose et al., 2008; Lewis, 2012; Noël, Brevers, & Bechara, 2013; Price & Drevets, 2012).

Group II mGlu receptors can influence synaptic plasticity in the mPFC

Previous studies have revealed that pharmacological activation of group II mGlu receptors results in LTD of excitatory transmission in layer V of the rat medial prefrontal cortex (mPFC) (Huang & Hsu, 2008; Huang, Yang, Lin, & Hsu, 2007). Although it is not known whether induction of LTD in the mPFC is mediated by $mGlu_2$ or $mGlu_3$, previous studies suggest that presynaptically localized $mGlu_2$ is typically responsible for inhibition of synaptic transmission by group II mGlu receptor agonists at many other synapses (Benneyworth et al., 2007; Galici, Jones, & Hemstapat, 2006; Hermes & Renaud, 2011; Johnson et al., 2011; Kew, Pflimlin, Kemp, & Mutel, 2002; Poisik, Smith, & Conn, 2007; Yokoi et al., 2012).

However, evidence suggests that induction of LTD in the mPFC is dependent upon activation of a postsynaptic group II mGlu receptor, suggesting that this response is mechanistically distinct from presynaptic effects of group II mGlu receptor agonists on transmission at other synapses (Otani, Auclair, Desce, Roisin, & Crépel, 1999; Otani, Daniel, Takita, & Crépel, 2002). Unfortunately, a lack of pharmacological agents that can selectively antagonize $mGlu_3$ or $mGlu_2$ has impaired progress in this area. Our studies employed the novel $mGlu_2$ NAM **IV.57** and the novel $mGlu_3$ NAM **III.270** in order to decipher the individual roles of these receptors and determine which group II mGlu, if either, is responsible for the postsynaptic signaling component.

Elucidation of $mGlu_2$ and $mGlu_3$ NAM Effects on mPFC Function

Effect of $mGlu_2$ and $mGlu_3$ NAMs on field EPSPs and postsynaptic calcium release

We recorded field excitatory postsynaptic potentials (fEPSPs) from layer V in response to stimulation of layer II/III in the prelimbic (PL) subregion of mPFC in ICR (CD1) mice. Application of the selective $mGlu_{2/3}$ agonist LY379268 (30–100 nM for 10 min) produced a concentration-dependent, transient inhibition of the fEPSP slope. Strong pharmacological activation of $mGlu_{2/3}$ with 100 nM LY379268 produced LTD of fEPSPs up to 60 min after drug washout. On average, these fEPSPs exhibited 40.3 ± 3.0% depression from baseline.

When similar experiments were performed in the presence of the NMDA receptor antagonist AP5 (50 µM), LTD was still observed, with an average decrease in signal size of 38.1 ± 6.3%. Conversely, when LY379268 was applied in the presence of group II antagonist LY341495 (500 nM), both the transient inhibition and induction of LTD were blocked, with an average reduction of fEPSPs by only 12.3 ± 4.6%, confirming this effect was solely due to actions at group II mGlu receptors.

Analysis of paired-pulse ratios (PPR) with a 25-ms interstimulus interval throughout the experiment showed a phasic PPR increase corresponding to the peak of the transient inhibition, which then returned to baseline levels 60 min later when LTD was observed. This suggests that although the initial fEPSP inhibition may have a presynaptic component, the observed LTD was not simply due to a long-term decrease in the neurotransmitter release probability.

Taken together, these findings from layer V of the mouse mPFC indicate that selective pharmacological activation of group II mGlu receptors produces an NMDA receptor-independent form of LTD that is expressed postsynaptically (**Figure V.1**). Such a postsynaptic mechanism is consistent with previous results from LTD studies in the mPFC when looking at group II mGlu receptor function.

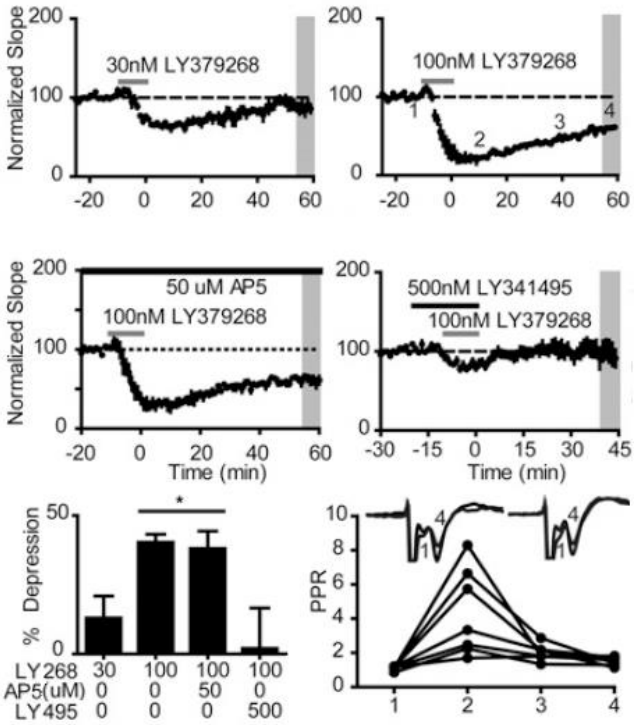

Figure V.1 Average time course of fEPSP slopes recorded from layer V mPFC. Application of LY379268 at 30 nM (n = 6) and 100 nM (n = 7). LY379268 LTD in the presence of AP5 (n = 5). LY379268 LTD in the presence of LY341495 (n = 6). Quantification of LTD measured 55–60 min after drug washout. * indicates P < 0.05 Tukey posttest vs. 30 nM and 500 nM LY341495. Data are expressed as mean ± SEM. Paired-pulse ratio analysis for fEPSPs. Insets show sample paired-pulse fEPSP traces from baseline (1) and 60 min after drug washout (4).

Next we sought to evaluate the contribution of the $mGlu_2$ and $mGlu_3$ subtypes to this form of LTD. We took advantage of our two lead $mGlu_3$-selective NAMs, **III.239** (VU0469942) and **III.270** (VU0477950) (Wenthur et al., 2013). When slices were pretreated with the $mGlu_3$-selective NAM **III.239** (10 µM), the agonist LY379268 caused a large transient depression, but the slope returned to near baseline levels during the 60-min drug washout, returning to only 12.3 ± 4.6% lower than original. Thus, the $mGlu_3$ NAM **III.239** blocked the ability of LY379268 to induce LTD, but did not inhibit the acute inhibition of synaptic transmission. When experiments were repeated in the presence of **III.270**, a similar profile emerged. LY379268 caused a transient depression of the fEPSP slope, which then returned to near baseline levels by the end of the experiment, only 16.9 ± 8.4% lower. Compared with LY379268 alone, both **III.239** and **III.270** significantly decreased the magnitude of LTD measured 55–60 min after washout (**Figure V.2**).

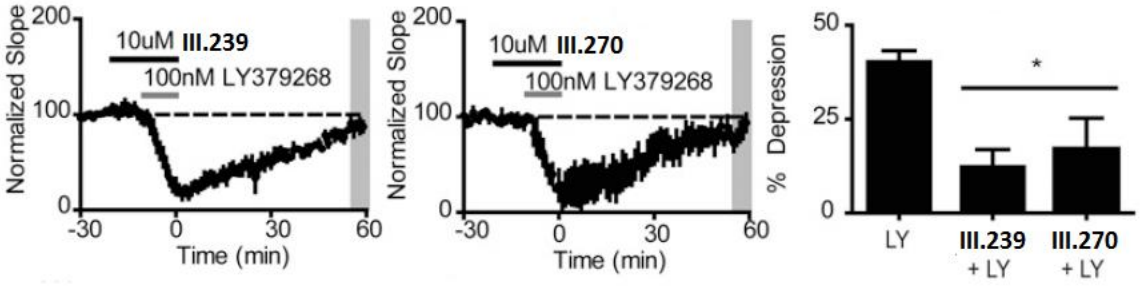

Figure V.2 Preincubating slices with the $mGlu_3$ NAMs VU0469942 (n = 6) and VU0477950 (n = 4) does not affect the transient inhibition of the fEPSP slope, but blocks LTD induced by LY379268. Quantification of the effects of $mGlu_3$ NAMs on LTD measured 55–60 min after drug washout (average of shaded region). * indicates $P < 0.05$ Tukey posttest vs. LY379268.

To further evaluate the role of the individual group II mGlu receptor subtypes, we compared LTD induced by LY379268 in $mGlu_2$ and $mGlu_3$ KO mice. In $mGlu_2$ KO mice agonist application induced a lasting depression of 31.6 ± 4.3% for fEPSPs, indicative of LTD measured 60 min after drug washout. In contrast, when LY379268 was applied to slices from $mGlu_3$ KO mice, a transient depression was observed, but LTD was absent when assessed 60 min after washout of the agonist, measuring a 4.0 ± 10.7% difference. Compared with LTD measured in the ICR (CD1) background strain and $mGlu_2$ KO mice, the magnitude of LTD was significantly smaller in $mGlu_3$ KO mice. Moreover, there was no difference between the magnitude of LTD observed in wild-type (WT) and $mGlu_2$ KO mice (**Figure V.3**).

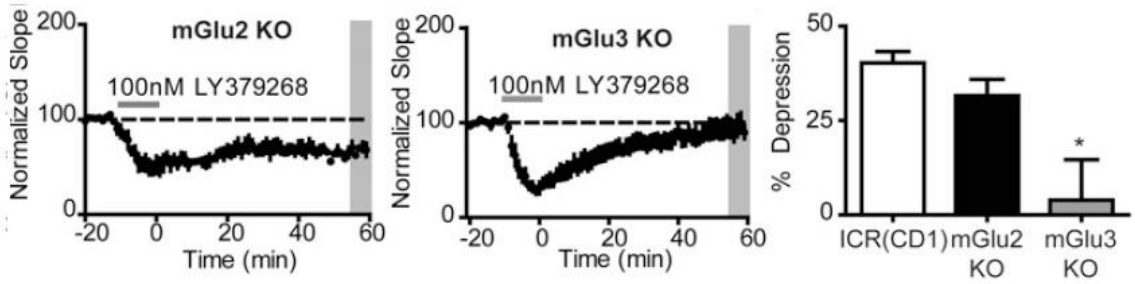

Figure V.3 LY379268 induces LTD in mPFC slices from $mGlu_2$ (n = 6) but not $mGlu_3$ KO mice (n = 9). Quantification of LTD in $mGlu_2$ KO, $mGlu_3$ KO, and the background strain ICR (CD1) (average of shaded region). * indicates $P < 0.05$ Tukey posttest vs. $mGlu_2$ and ICR (CD1) mice. Data are expressed as mean ± SEM.

In an additional test of the contribution of $mGlu_2$ activation to this LTD response, LY379268 (100 nM) was applied to slices in the presence of the selective $mGlu_2$ NAM **IV.57** (VU6000446 / MRK-8-29; 10 µM). Following application of these drugs, there was a rapid and lasting depression of the fEPSP slope that was still evidenced 60 min after agonist washout, indicative of induction of LTD at a level of 33.7 ± 9.8%. Compared with LY379268 alone, **IV.57** did not significantly affect the magnitude of LTD measured 60 min after agonist washout.

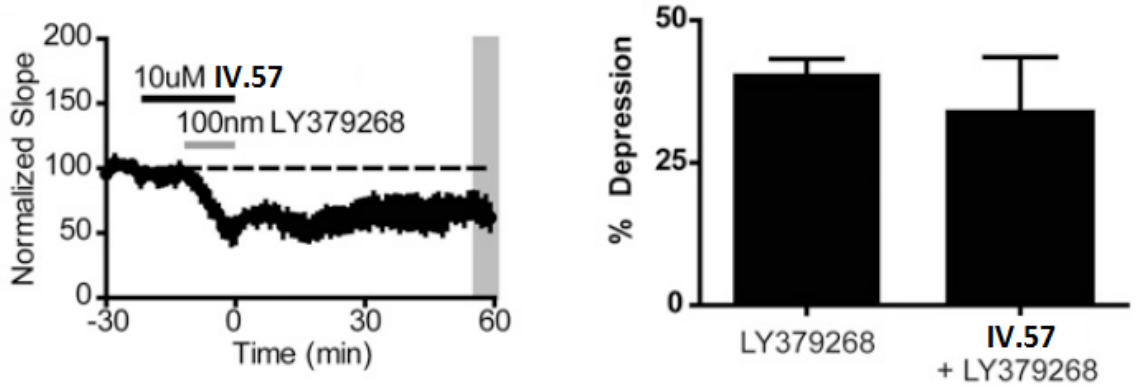

Figure V.4 Preincubation of slices with **IV.57** (n = 5) does not affect LTD induced by LY379268. Quantification of the effects of **IV.57** on LTD at 55–60 min after drug washout (average of shaded region). Data are expressed as mean ± SEM.

Although the transient inhibition induced by LY379268 appeared to be reduced by **IV.57** relative to control and **III.239**, this effect was not statistically significant. Likewise, the transient depression appeared to be attenuated in $mGlu_2$ KO mice relative to WT and $mGlu_3$ KO mice, but this effect also did not reach statistical significance (**Figure V.5**).

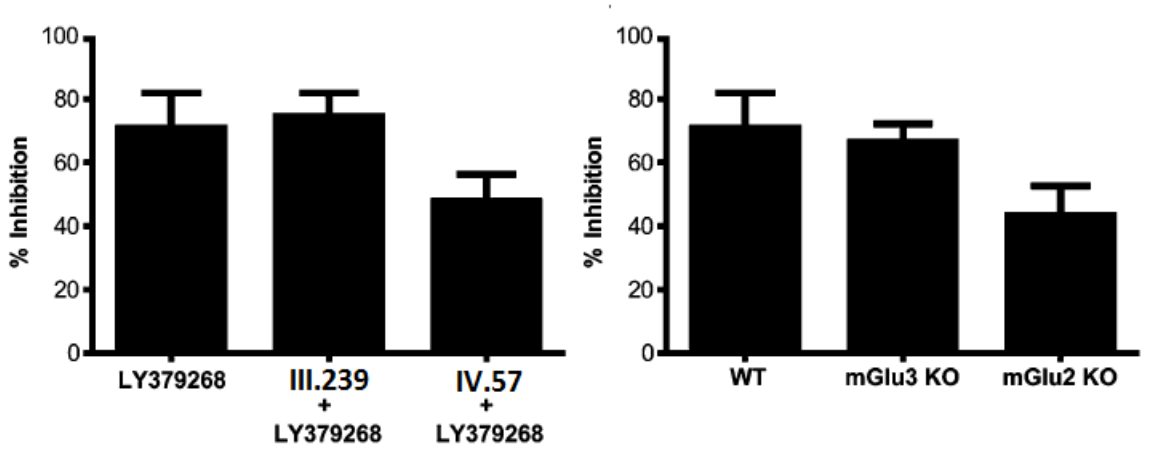

Figure V.5 Effects of group II mGlu subtype selective NAMs and receptor knockout on transient inhibition induced by LY379268 ($P > 0.05$, one-way ANOVA). Data are expressed as mean ± SEM.

Taken together, the loss of LTD induction by LY379268 in the presence of **III.239** and **III.270**, along with the lack of LTD by LY379268 in $mGlu_3$ KO mice indicate that $mGlu_3$ activation is required for the induction of group II mGlu LTD. Likewise, the lack of effect of **IV.57** on LY379268 induced LTD and the maintenance of LTD in $mGlu_2$ KO mice indicate that activation of $mGlu_2$ does is not required to induce LTD, although it may play an important role in the transient depression of synaptic transmission in layer V of the mouse mPFC.

To test these hypotheses and demonstrate that the actions of **III.239** require activity at $mGlu_3$, we evaluated the effects of this compound in slices prepared from $mGlu_2$ and $mGlu_3$ KO mice (**Figure V.6**). In control slices from both $mGlu_2$ and $mGlu_3$ KO mice, the agonist LY379268 induced a transient depression of fEPSPs of 43.5 ± 9.3% in $mGlu_2$ KO mice, and a depression of 66.4 ± 5.9% in $mGlu_3$ KO mice.

In contrast, when LY379268 was applied in the presence of **III.239**, inhibition was almost completely attenuated in $mGlu_2$ KO slices, down to only 11.3 ± 7.9%; in these slices LY379268 acts on only $mGlu_3$. In contrast, **III.239** did not antagonize the effect of LY379268 in slices from $mGlu_3$ KO mice, with a reduction of 67.2 ± 1.9%; in these slices the agonist would be acting only on the $mGlu_2$ subtype.

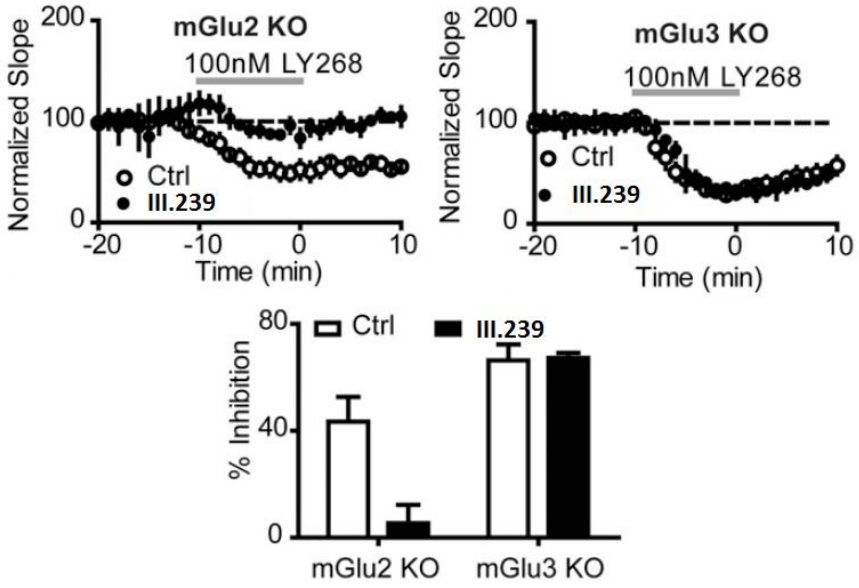

Figure V.6 Selectivity of the $mGlu_3$ NAM VU0469942 was confirmed by measuring the maximal inhibition of layer V fEPSPs induced by LY379268 in mPFC slices from $mGlu_2$ and $mGlu_3$ KO mice. Data are expressed as mean ± SEM.

These data confirm that the actions of **III.239** require the expression of $mGlu_3$ and are therefore mediated by selective inhibition of this receptor. Additionally, the lack of activity of **III.239** in the $mGlu_3$ KO mice helps to confirm the selectivity of this compound for $mGlu_3$ in an *in vivo* context with native G-protein coupling.

With this information in hand, we next wanted to probe the mechanism by which $mGlu_3$ was inducing LTP. Previous reports and our analysis of PPRs suggest that group II LTD in mPFC is expressed postsynaptically. Furthermore, LTD is dependent upon intracellular Ca^{2+} mobilization induced by activation of group II mGlu receptors in layer V pyramidal cells (Otani et al., 2002). Based on our findings that LTD is dependent upon $mGlu_3$ activation, we tested the hypothesis that Ca^{2+} signaling is downstream of $mGlu_3$ by monitoring Ca^{2+} in individual layer V pyramidal neurons (**Figure V.7**).

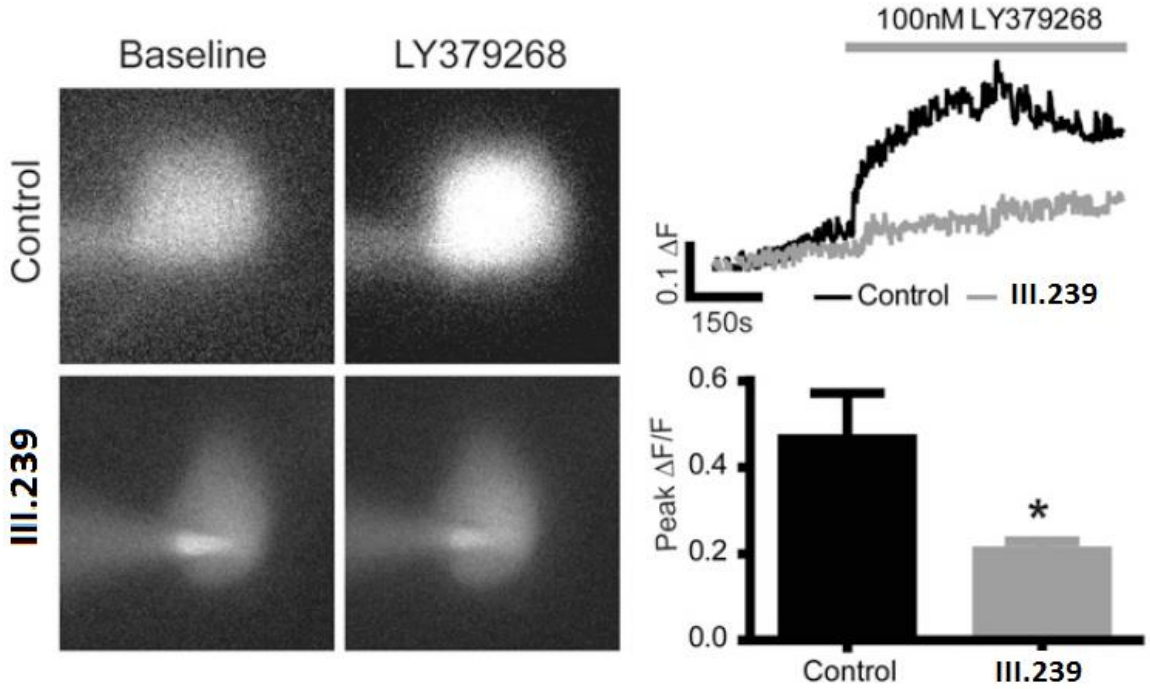

Figure V.7 Activation of postsynaptic $mGlu_3$ increases intracellular Ca^{2+} in layer V pyramidal neurons. Representative images demonstrating fluorescence levels during baseline (Left) and in the presence of LY379268 (Right). Top images are from a control experiment and Bottom images are from an experiment performed in the presence of **III.239**. Time course of fluorescence measurements for the experiments and quantification of Ca^{2+} imaging experiments (n = 7 per group). * indicates $P < 0.05$ unpaired t test vs. control. Data are expressed as mean ± SEM.

Cells were loaded with the Ca^{2+}-sensitive dye, Fluo-4, through a patch pipette; experiments were performed in the presence of TTX (1 μM) to isolate postsynaptic receptor actions. In control experiments, when group II mGlu receptors were activated with LY379268 (100 nM for 10 min) there was an increase in fluorescence intensity relative to baseline (0.47 ± 0.11 ΔF/F peak), indicating an elevation in intracellular Ca^{2+}. However, when these experiments were performed in the presence of **III.239** (10 μM), there was a significant reduction in the change in fluorescence (0.21 ± 0.024 ΔF/F peak; $P < 0.05$; unpaired t test). This is consistent with the hypothesis that group II agonists induce intracellular Ca^{2+} signals through activation of $mGlu_3$ in layer V pyramidal neurons. Furthermore, these data suggest that postsynaptic $mGlu_3$ is the critical site of action for induction of group II mGlu LTD.

Effect of $mGlu_3$ NAM VU0477950 on extinction of conditioned fear

We next sought to investigate how $mGlu_3$ is able to modulate fear extinction, a behavior that is dependent upon the integrity of the mPFC (Sotres-Bayon & Quirk, 2010). On day 1, drug naive mice were conditioned by pairing a tone CS with a mild foot-shock US. Twenty-four hours later, mice received an injection of vehicle or the $mGlu_3$ NAM **III.270** (VU0477950; 3–100 mg/kg IP). Thirty minutes after injection, mice were placed in a new context and received 20 CS-alone presentations to evaluate initial cue memory and subsequent extinction learning (**Figure V.8**).

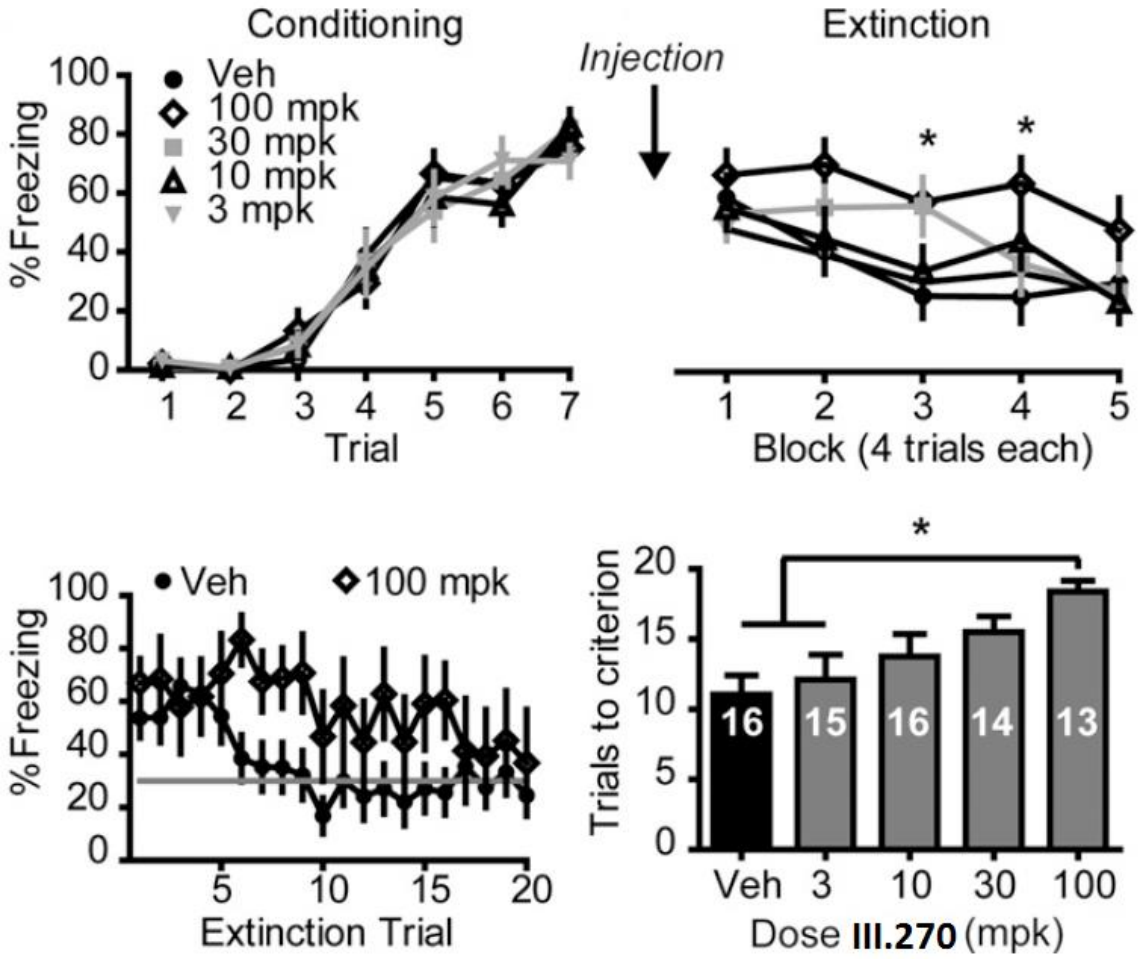

Figure V.8 An $mGlu_3$ NAM impairs fear extinction learning in mice. No drug was administered on the conditioning day. On day 2, mice received an IP injection of vehicle or the $mGlu_3$ NAM **III.270** (3–100 mg/kg) and then were trained on fear extinction with 20 CS-alone trials. Data are presented as mean freezing across 4 consecutive trials. * indicates $P < 0.05$, 100-mg/kg Bonferroni posttest vs. vehicle-treated mice. Extinction learning criterion was established by examining asymptotic learning (shaded horizontal line) across all 20 CS-alone trials in vehicle-treated animals. Freezing behavior of mice treated with 100 mg/kg is plotted for comparison. Quantification of the learning impairment induced by **III.270** as measured by trials to criterion. Numbers within the individual bars indicate number of mice within the respective group. * indicates $P < 0.05$ Tukey posttest vs. vehicle or 3-mg/kg–treated mice. Data are expressed as mean ± SEM.

During the training period, after seven CS–US presentations, there was a significant increase in the amount of time spent freezing during the CS presentation across trials for all subjects ($P < 0.0001$), indicating all mice were conditioned to associate the tone with the foot shock.

On the retrieval day, no effect of **III.270** on initial cue memory was observed as all mice had equivalent levels of freezing during the first block of CS-alone trials ($P > 0.05$). During subsequent CS presentations, vehicle-treated mice decreased freezing to an asymptotic level, a pattern of behavior consistent with extinction learning. However, in mice treated with **III.270**, there was a dose-dependent impairment in extinction learning. Specifically, mice treated with a 30-mg/kg or a 100-mg/kg dose of **III.270** maintained high levels of freezing through blocks 3 and 4, which reached significance in the 100-mg/kg group relative to vehicle-treated animals. Pharmacokinetic analysis indicated that mice treated with 100 mg/kg of **III.270** in 60% DMSO and 40% PEG 400 at a volume of 3 mL/kg were receiving an average of 86.41 µM of total compound in the brain (n=5). Given the $F_{u,b}$ of 0.005 in mice, this translates into approximately 450 nM free compound in the brain, a value near the IC_{50} of **III.270** at $mGlu_3$.

We quantified the impact of **III.270** on extinction learning by analyzing the number of trials required to reach criterion. The learning criterion was established by examining the performance of vehicle-treated animals across all extinction trials and determining asymptotic performance. On average, vehicle-treated mice achieved criterion learning of 30% freezing in approximately 11 trials. Consistent with analysis of freezing across blocks of trials, there was a dose-dependent increase in the number of

trials required to reach criterion in mice treated with **III.270**. Moreover, mice treated with the 100- mg/kg dose of the compound showed a significant increase in the number of trials to reach criterion compared with mice in the vehicle and 3-mg/kg groups.

Interestingly, there appeared to be no impairment in memory retrieval for extinction in animals treated with 30 mg/kg or 100 mg/kg of **III.270** relative to vehicle-treated animals when measured 24 h later in a second extinction session (**Figure V.9**). This indicates that the $mGlu_3$ NAM was not having a global effect on memory; once the treated mice eventually extinguished the conditioned fear memory, the extinction learning was retained at the same level seen with untreated mice. Thus, the selective $mGlu_3$ NAM **III.270** induces a dose-dependent increase in the number of trials to extinguish fear responses. This finding implicates $mGlu_3$ function as a mediator of PFC-dependent cognitive function and supports the concept that $mGlu_3$ could represent a therapeutic target in disorders where such cognitive functions are disturbed.

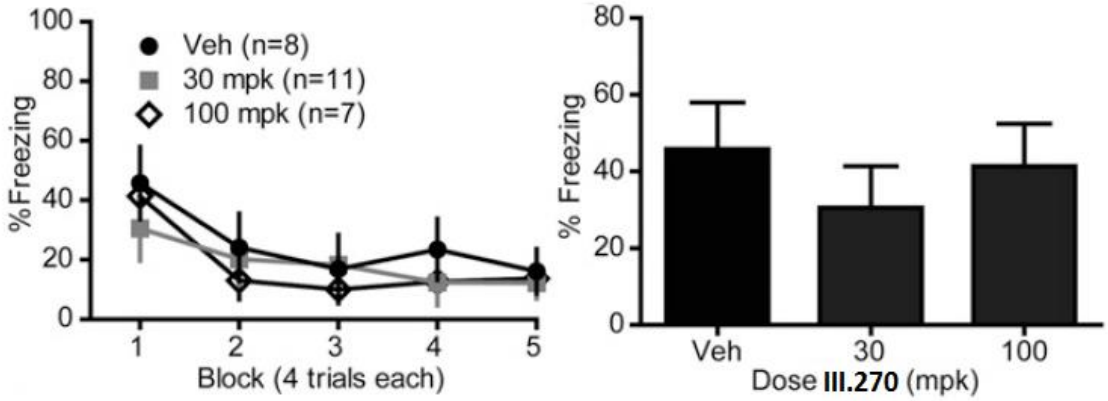

Figure V.9 The $mGlu_3$ NAM **III.270** does not affect extinction retrieval 24 hours after initial extinction. A subset of mice was tested on a second extinction session to evaluate extinction memory retrieval. Comparison of freezing during the first block of trials. There were no significant group differences.

The Effects of Group II mGlu Inhibition on Rodent Models of Depression and Anxiety

Pharmacologic modulation of glutamate signaling in depression and anxiety

Beginning with explorations using the NMDA receptor antagonist ketamine in the 1990's, there has been substantial interest in the use of glutamatergic targets to treat depression (Chaki et al., 2013; Goeldner et al., 2013; Matrisciano et al., 2007). In addition to NMDA receptor antagonists, other glutamate-modulating therapeutic strategies that have been attempted include AMPA receptor antagonists, $mGlu_5$ antagonists and NAMs, $mGlu_{2/3}$ agonists and PAMs, $mGlu_{2/3}$ antagonists and NAMs, $mGlu_7$ PAMs, EAAT2 inhibitors, and SXC inhibitors (Pilc et al., 2013). Many of these targets exhibit positive preclinical data, providing strong empirical support for the importance of glutamate regulation in depression. However, to date, only NMDA receptor antagonists have been clinically validated; these compounds unfortunately suffer from relatively severe side-effect liabilities, including dissociative/hypnotic properties and risk of coma and death on overdose. The increased therapeutic window exhibited thus far by mGlu receptor-targeting therapeutics makes them very attractive candidates for the next round of clinical study – careful selection of both mGlu receptor subtype and mechanism of action will be needed to maximize the potential for a successful proof of principle trial.

Such glutamatergic targets have likewise been of extreme interest in the context of anxiety disorders (Amiel & Mathew, 2007; Nicoletti et al., 2011; Pitsikas, 2014). There has been a long-standing hypothesis that anxiety symptoms arise due to an imbalance

between excitatory and inhibitory signaling, as regulated by glutamate and GABA, respectively (Pitsikas, 2014). While many current therapeutics for anxiety act by increasing GABAergic signaling, this strategy carries with it a significant risk of dependence. The converse approach, which is to decrease glutamatergic signaling, is not without its own risks, but has nevertheless become a generalized strategy in the development of new therapeutics and the repurposing of approved pharmaceuticals for the treatment of anxiety disorders (Amiel & Mathew, 2007). As with the search for glutamate-based antidepressants, a number of modes of pharmacologic activity are being pursued, including NMDA antagonism, glutamate transporter blockers, group I mGlu receptor antagonists, and $mGlu_{2/3}$ agonists. In fact, there is clinical data that demonstrates the efficacy of an $mGlu_{2/3}$ agonist in the treatment of GAD (Dunayevich et al., 2008). However, the preclinical literature on the desired mode of pharmacology for modulating the group II mGlu receptors in the context of anxiety remains mixed, with both agonists and antagonists variously exhibiting efficacy in animal models of anxiety (Bespalov et al., 2008; Linden et al., 2005; Pitsikas, 2014). In order to unravel the conflicting evidence to date, further elucidation of the specific effects induced by $mGlu_2$ and $mGlu_3$ signaling alterations in anxiety disorders is warranted.

Antidepressant effects seen with $mGlu_{2/3}$ antagonists

Several different pharmacological inhibitors of $mGlu_{2/3}$ signaling have demonstrated efficacy in pre-clinical models of antidepressant efficacy, including LY341495 and MGS0039, $mGlu_{2/3}$ antagonists, as well as RO4491533, an $mGlu_{2/3}$ NAM

(Chaki et al., 2013). In aggregate, these compounds have decreased immobility time in rat FST and mouse TST in wild type animals as well as socially-isolated animals, and in the Helpless strain of mice, which is a putative genetic model of depression (Campo et al., 2011). Furthermore, these compounds have reduced escape failures in a rodent learned-helplessness task and decreased hyperactivity and learning deficits in olfactory bulbectomized rats (Pilc et al., 2013). The efficacy of these compounds has been speculated to variously occur through potentiation of AMPA signaling and mTOR activation, increased pre-frontal release of 5-HT, and elevated DA in the NAc, although a full understanding of the mechanisms involved have yet to be determined (Ago et al., 2013; Chaki et al., 2013; Goeldner et al., 2013). This mechanistic confusion is only exacerbated by the apparently paradoxical efficacy shown by the $mGlu_2$ PAM THIIC in assays of antidepressant efficacy (Chaki et al., 2013). Explanations of these results have thus far invoked the concept of either brain-region specific alterations or effects on different subtypes of depressed patients. Such explanations are plausible, but they ignore the possibility that $mGlu_2$ and $mGlu_3$ signaling are independently, perhaps even antagonistically, modulating antidepressant responses.

The available data are consistent with a model where $mGlu_2$ activation and $mGlu_3$ blockade can independently induce antidepressant effects. Specifically, the addition of $mGlu_3$ activation in addition to $mGlu_2$ activation does not appear to improve antidepressant effects, and may even diminish them – $mGlu_2$ PAMs have shown efficacy alone, while $mGlu_{2/3}$ agonists have thus far only been efficacious when applied together with SSRIs or TCAs. The previous lack of selective $mGlu_2$ and $mGlu_3$ NAMs has precluded

assessment of the individual contributions of these receptors to the antidepressant-like effects of $mGlu_{2/3}$ antagonists. However, with **III.270** and **IV.57** in hand, such experiments became possible. Moreover, after the introduction and initial *ex vivo* and *in vivo* application of these first selective NAMs, the work of colleagues in the VCNDD led to the generation of additional selective $mGlu_2$ and $mGlu_3$ NAMs from chemically distinct scaffolds – **V.1** (VU6001192) and **V.2** (VU0650786), respectively (**Figure V.10**). Given the formulation difficulties and elevated doses needed to generate efficacy with **III.270**, along with the rapid clearance and poor scalability of **IV.57**, the second generation compounds **V.1** and **V.2** were selected for further evaluation as second- and third-generation tools for the *in vivo* study of $mGlu_2$ and $mGlu_3$ receptors as targets for antidepressant and anxiolytic activity.

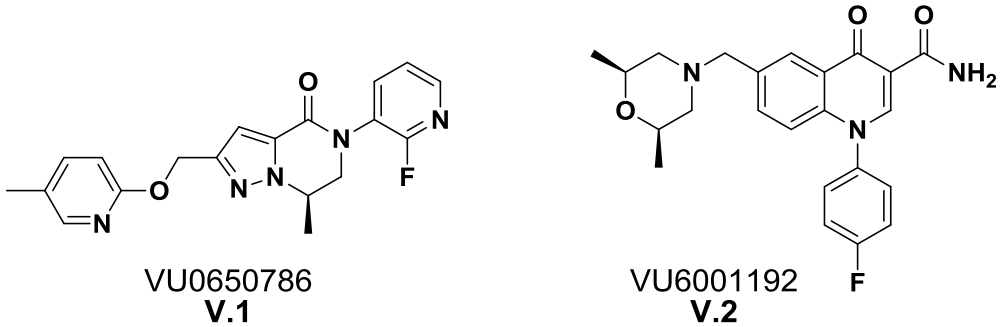

$mGlu_2$ IC_{50}: > 30 μM

$mGlu_3$ IC_{50}: 392 nM

$mGlu_2$ IC_{50}: 211 nM

$mGlu_3$ IC_{50}: > 30 μM

Figure V.10 Structures of the third-generation $mGlu_3$ NAM VU0650786 and the second-generation $mGlu_2$ NAM VU6001192, along with key pharmacologic parameters for each compound, as determined by the calcium mobilization assay.

Exposure of $mGlu_2$ and $mGlu_3$ NAMs after IP dosing

In order to select the appropriate compounds to assess the effects of the selective $mGlu_2$ and $mGlu_3$ NAMs on mouse behavior, it was first necessary to define a dose for each compound that could yield a free concentration in the brain sufficient to induce blockade of receptor activation. In the absence of radiolabeled versions of the compounds, the exact receptor occupancy at any given dose of each compound could not be directly determined. However, the IC_{50} for each compound, as determined by the *in vitro* calcium-mobilization assay, could be compared to the calculated free brain concentration, allowing for a qualitative determination of whether 50% or more of the receptors were likely to be inhibited following IP administration.

In order to calculate the free brain concentrations for each compound, a plasma/brain level study was run for **III.270**, **IV.57**, **V.1**, and **V.2**. This study began with the administration of each test compound via the IP route, using the same formulation and vehicle that would be used for the planned behavioral studies; the vehicle chosen for these studies was 10% Tween 80 in H_2O. Thirty minutes after administration the animals were euthanized using rapid replacement of their cage atmosphere with CO_2; this time period recapitulates the interval that the animals would experience before beginning the behavioral task, and thus reflects the expected brain concentration at the beginning of each behavioral experiment. Trunk blood was collected from each animal, along with the whole brain. The plasma was extracted from the blood samples, and the concentration of drug in each plasma and brain sample was analyzed to give a measurement of the total drug concentration in each tissue.

In order to determine the free drug concentration, the PPB and BHB of each drug was measured, yielding the fraction unbound; this was multiplied with the total concentration to determine free drug concentration. For compound **V.2**, a preliminary study had revealed that the compound had a low $K_{pu,u}$, indicating active clearance from the brain, so our exposure study with **V.2** was run in the presence of Elacridar, a P-gp inhibitor. The results of the study indicated that **V.1** and **V.2** (with 20 mg/kg Elacridar) could reach free brain concentrations in excess of the IC_{50}s for their primary targets when formulated in 10% Tween 80 in H_2O, while **III.270** and **IV.57** could not, even when given at high doses. (**Table V.1**).

Table V.1 Pharmacokinetic parameters of $mGlu_2$ and $mGlu_3$ NAMs as measured in ICR (CD1) mice 30 minutes after administration. **V.2** given with 20 mg/kg of Elacridar.

Compound	**III.270**	**IV.57**	**V.1**	**V.2 (+ Elac)**
Dose (mg/kg; IP)	100	56.6	56.6	30
CL_{INT} (ml/min/kg)	60	433	22.8	20.4
CL_{HEP} (ml/min/kg)	36	74.5	18.2	16.6
$f_{u,p}$	0.026	0.03	0.163	0.315
$f_{u,b}$	0.005	0.009	0.035	0.257
Total [Brain] (µM)	39.21	5.46	42.23	25.58
Total [Plasma] (µM)	2.23	2	15.03	6.88
Brain : Plasma	5.76	2.61	2.91	3.73
Free [Brain] (µM)	0.20	0.05	1.48	6.57
Free [Plasma] (µM)	0.16	0.06	2.45	2.17
$K_{pu,u}$	1.21	0.82	0.60	3.03
Free [Brain] : IC_{50}	0.44	0.34	3.78	31.14

Assessment of $mGlu_2$ and $mGlu_3$ NAM effects in the Porsolt forced swim test

With this information in hand, we decided to move forward with application of **V.1** and **V.2** in the Porsolt forced swim test, using **III.270** and **IV.57** to determine whether efficacy could be seen at concentrations that would be expected to have only low receptor occupancy. This behavioral task was chosen as a model of behavioral despair, a phenomenon that is characterized by a reduction in escape activity or mobility by a rodent when placed in a stressful environment. This behavior is interpreted to indicate despair on the part of the rodent; for humans, the condition of despair generally indicates a belief that a situation is hopeless and the outcome cannot be improved or changed by one's actions. While our current understanding of rodent motivation is insufficient to make a direct comparison across species, the interpretation of this study is nevertheless taken to indicate a change in the susceptibility of the animal to negative mood. Having a persistently depressed mood or a bias toward negative emotions is one of the diagnostic criteria for MDD, and is considered to be one of the psychopathological endophenotypes present in major depressive disorder (Hasler, Drevets, Manji, & Charney, 2004). As with the diagnosis of MDD overall, such an endophenotype can likely arise from several different biological causes, making mechanistic conclusions from the results from this study alone virtually impossible.

Despite the inherent difficulty in modeling depression and other complex neuropsychiatric phenomena in rodents, this test does present several advantages that make it useful in an introductory study of the antidepressant efficacy of a given pharmacologic strategy. The major utility of the Porsolt forced swim test lies in its

predictive validity – that is, the test can reliably identify compounds as active that have proven antidepressive efficacy in humans, while eliminating compounds that do not have antidepressive efficacy in humans. Although such predictive validity was necessarily validated with compounds exhibiting efficacy in humans, the predictive power of the test is thought to be strong enough that it is frequently used to screen compounds with novel mechanisms of action for potential antidepressant efficacy. In addition to its predictive usefulness, the Porsolt forced swim test also has several operational properties that make it a practical choice for incipient studies of antidepressant activity; it can be run rapidly, requiring only a one-day training session before implementing the task itself; it can be run using equipment that is not overly complex or expensive; it can be run with several animals in parallel, increasing the throughput of the assay; and finally, it can be run in both rats and mice, providing cross-species validation for any given compound (Overstreet, 2012).

Upon application of **III.270**, **IV.57**, **V.1**, and **V.2** (after 1 hour of treatment with 20mg/kg elacridar), along with our vehicle and LY341495 controls, we observed that LY341495 significantly decreased the immobility of male ICR(CD1) mice at a dose of 3 mg/kg, as had been reported previously (**Figure V.11**). It was intriguing to see, however, that **V.1**, a selective $mGlu_3$ NAM, could also significantly decrease immobility in this assay when dosed at 56.6 mg/kg IP. Contrastingly, neither **IV.57** nor **V.2**, selective $mGlu_2$ NAMs with low and high brain exposure, respectively, could alter the immobility time when compared to vehicle alone.

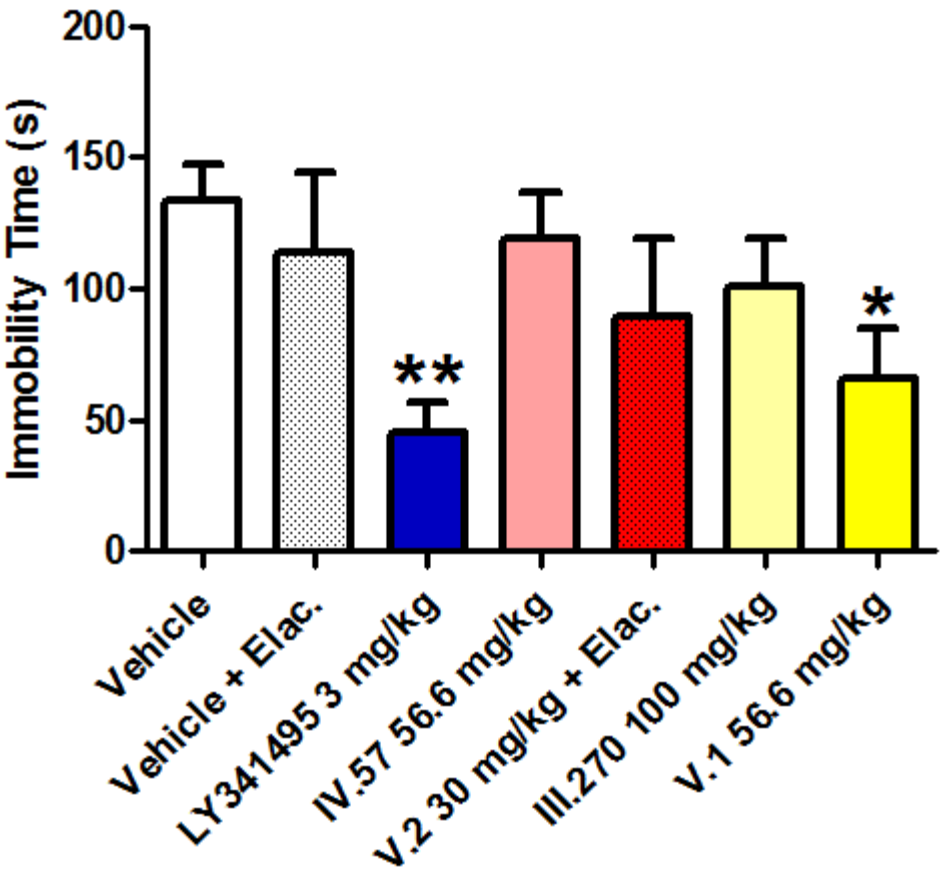

Figure V.11 Effects of an $mGlu_{2/3}$ antagonist, $mGlu_2$ NAMs, and $mGlu_3$ NAMs in the Porsolt forced swim test. Animals treated with elacridar receive 20 mg/kg IP one hour prior to administration of the test compound. (n; 8 - 12) * indicates $P < 0.05$, Bonferroni posttest vs. vehicle-treated mice. ** indicates $P < 0.01$, Dunnett's posttest vs. vehicle-treated mice.

Because **V.2** was dosed one hour after IP administration of 20 mg/kg elacridar, we also ran an elacridar plus vehicle control, and no significant difference was seen from vehicle alone, indicating that elacridar was not masking the $mGlu_2$ NAM efficacy. There was no significant effect for **III.270** when dosed at 100 mg/kg in the new 10% Tween 80 in H_2O vehicle. As this vehicle results in far lower exposure for **III.270** than the previous 60% DMSO, 40% PEG 400 vehicle used for the conditioned fear assay, the lack of effect

seen with this compound indicates that high receptor occupancy is likely needed to induce a response from an $mGlu_3$ NAM; this property has previously been reported for $mGlu_1$ and $mGlu_5$ NAMs (Michalon et al., 2012; Suzuki et al., 2009). In contrast, mGlu receptor PAMs have been shown to produce full efficacy with relatively low occupancy in the CNS because of the contributions of both affinity and cooperativity to PAM potency at a receptor (Rook et al., 2014). Overall, these data indicate that selective inhibition of $mGlu_3$ is sufficient to induce an antidepressant-like phenotype in the Porsolt forced swim test, while selective inhibition of $mGlu_2$ is not sufficient to induce such a phenotype.

Assessment of $mGlu_3$ NAM effects in the tail suspension test

In order to further explore the antidepressant potential of $mGlu_3$ selective NAMs, **III.270** and **V.1** were assayed in the tail suspension test. This test, like the Porsolt forced swim test, is used to measure behavioral despair; the results from this test are interpreted in the same way as those from the forced swim test. The tests differ primarily in the inescapable situations that they present. Additionally, the animal does not need to move at all while immobile in the tail suspension test, while the animals in the forced swim test may potentially initiate some minor motions to keep their head above water.

When assayed in this task, the dual $mGlu_{2/3}$ antagonist LY341495 again showed a significant decrease in immobility time as compared to vehicle, even when dosed at only 1 mg/kg (**Figure V.12**). The low exposure $mGlu_3$ NAM **III.270** once again did not show

any significant differences from vehicle. However, in contrast to the Porsolt forced swim test, the high exposure $mGlu_3$ NAM **V.1** did not significantly decrease immobility in this assay when dosed at 56.6 mg/kg. This discrepancy is potentially due to the overall smaller effect size seen with this test as compared to the forced swim test. Alternatively, the different mobility requirements for the tasks could be biasing the results, indicating a non-specific hyperlocomotive phenotype. Another potential explanation for the difference is that the relative amounts of stress induced by the two tasks could be interacting with the overall mobility of the mice; the different results may thus arise from an anxiolytic component of $mGlu_3$ NAM activity.

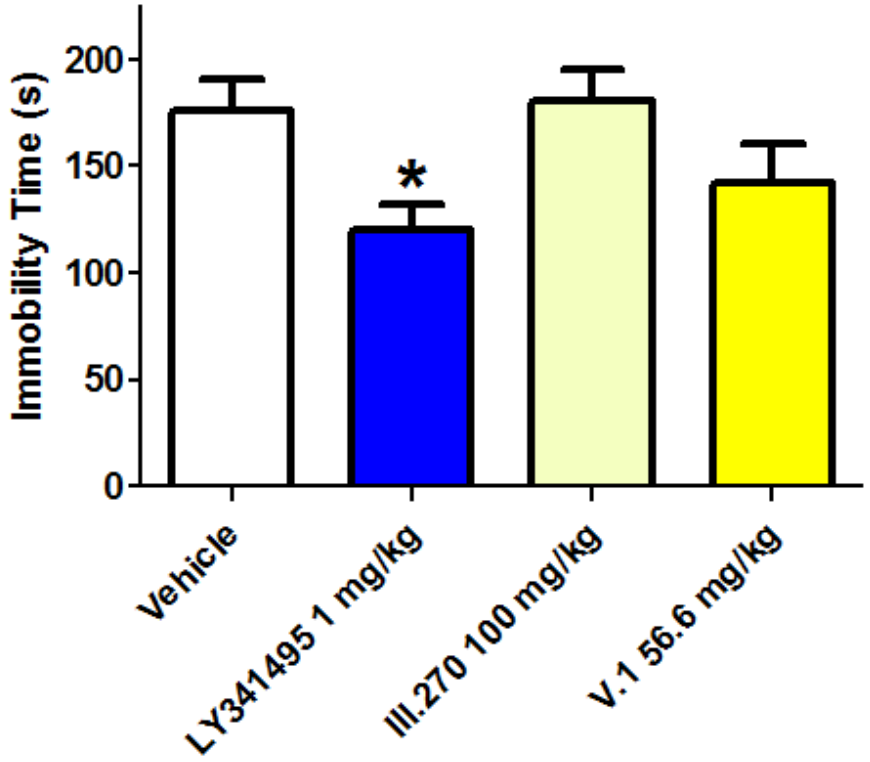

Figure V.12 Effects of an $mGlu_{2/3}$ antagonist and $mGlu_3$ NAMs in the tail suspension test. (n; 11 - 22) * indicates $P < 0.05$, Dunnett's posttest vs. vehicle-treated mice.

Effects of Group II antagonists on anxiety-related behaviors

In addition to the clinical and pre-clinical data indicating the anxiolytic activity of $mGlu_{2/3}$ agonists, there is a body of literature that indicates $mGlu_{2/3}$ antagonists may also exhibit anxiolytic properties (Linden et al., 2005; Pitsikas, 2014). Specifically, LY341495 has been shown to decrease marble burying behavior, attenuate stress-induced hyperthermia, and to modestly decrease the number of open arm entries in the elevated plus maze (Bespalov et al., 2008; Iijima, Shimazaki, Ito, & Chaki, 2007; Shimazaki, Iijima, & Chaki, 2004). Likewise, the $mGlu_{2/3}$ antagonist MGS0039 has been shown to be active in both the marble burying and stress-induced hyperthermia assays (Iijima et al., 2007; Shimazaki et al., 2004).

Assessment of $mGlu_2$ and $mGlu_3$ NAM effects in the elevated plus maze

To assess whether $mGlu_2$ or $mGlu_3$ signaling blockade alone could be responsible for the anxiolytic efficacy seen with dual $mGlu_{2/3}$ antagonists, we first assessed **V.1** and **V.2** (plus 20 mg/kg elacridar) in an elevated plus maze assay. These compounds were compared to vehicle, LY341495, and chlordiazepoxide, a benzodiazepine with known anxiolytic activity. We found that LY341495 had no effect on the percent of time spent in the open arms, and actually decreased the number of entries into these arms, as has previously been reported for this compound (Bespalov et al., 2008). Neither **V.1** nor **V.2** had any significant effect in this assay when tested at 56.6 mg/kg and 30 mg/kg, respectively (**Figure V.13**).

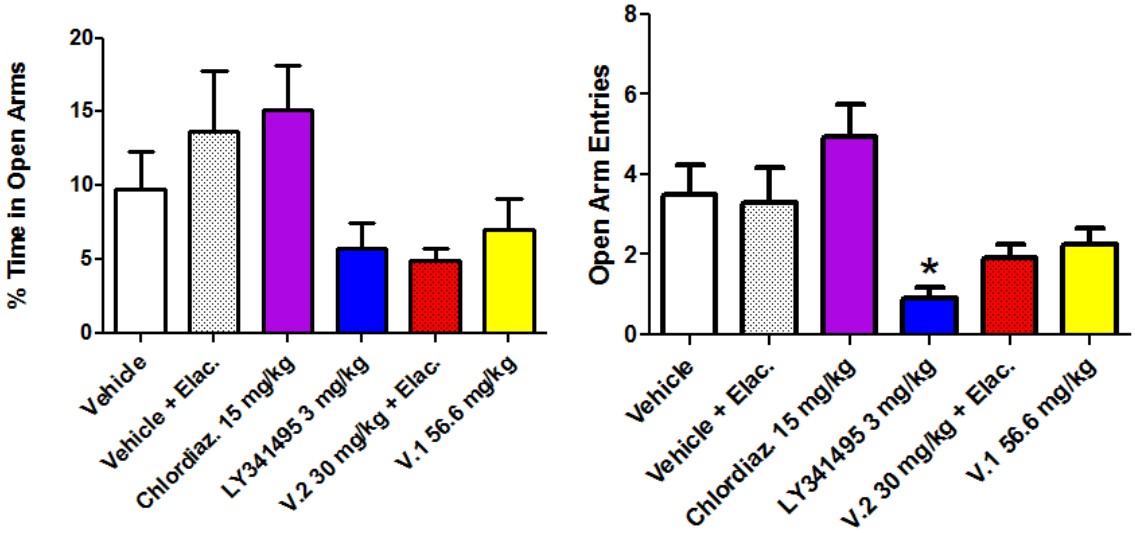

Figure V.13 Effects of a benzodiazepine, $mGlu_{2/3}$ antagonist, $mGlu_2$ NAM, and $mGlu_3$ NAM on the percent of time spent in the open arms and open arm entries in the elevated plus maze. Animals treated with elacridar receive 20 mg/kg IP one hour prior to administration of the test compound. (n; 10 - 15) * indicates $P < 0.05$, Dunnett's posttest vs. vehicle-treated mice.

Assessment of $mGlu_2$ and $mGlu_3$ NAM effects in a novel open field environment

It has been suggested that the previous anxiolytic and antidepressant-like results seen with dual $mGlu_{2/3}$ antagonists are the result of an impaired habituation to the test environment, which leads to a non-specific hyperlocomotor effect that causes a false positive for the forced swim and marble burying tasks, while not showing significant activity in tasks such as light-dark transition or differential reinforcement (Bespalov et al., 2008). In a follow up test, we confirmed a significant decrease in number of the marbles buried following treatment with 56.6 mg/kg of **V.1** versus vehicle (n = 13; $P < 0.05$, two-tailed t-test).

In order to test whether the positive results seen for **V.1** in the Porsolt forced swim test and the marble burying test are likely to be due to either an overt hyperlocomotive phenotype or due to impaired habituation to a novel environment, we assessed this compound in an open field locomotor activity assay and measured the total distance traveled over time as well as the time spent in the center of the chamber versus time spent near the edges, as an additional measure of anxiety behavior. In this assay, **V.1** did not reveal any differences from vehicle in either total distance traveled or in time spent near the edges of the box. There was also no indication of any difference in the time course for movement, indicating that the actions of the $mGlu_3$ NAM **V.1** were not likely to be due altered habituation to a novel environment. (**Figure V.14**).

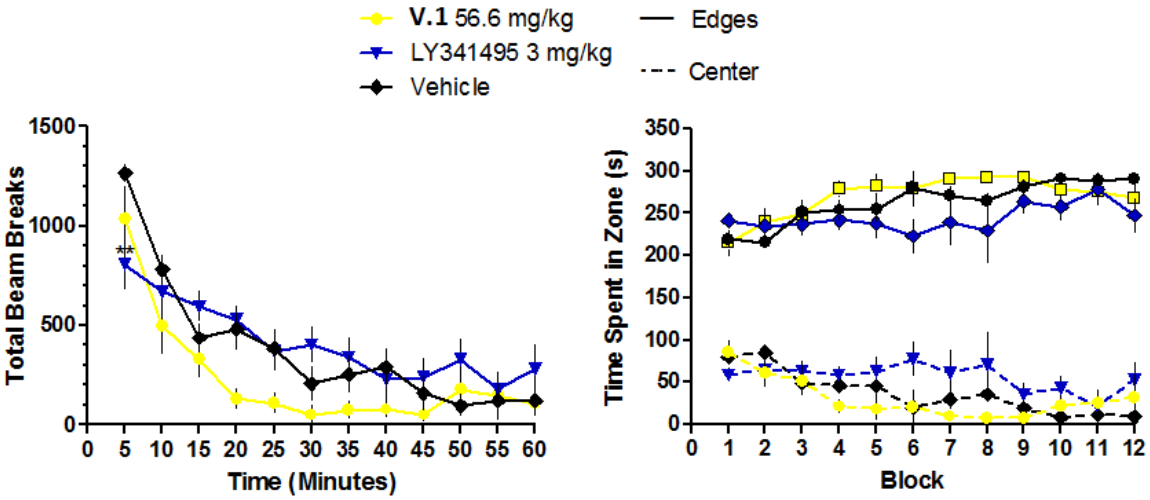

Figure V.14 Effects of an $mGlu_{2/3}$ antagonist and $mGlu_3$ NAM on the distance traveled and time spent in the center versus edge zones by block in the open field test. (n = 12) * indicates $P < 0.05$, Dunnett's posttest vs. vehicle-treated mice (two-way ANOVA; treatment x time).

Conclusions and Future Directions

Overall, the electrophysiological and behavioral studies presented here demonstrate the utility of **III.270**, **IV.57**, **V.1**, and **V.2** as tools to unravel the roles of $mGlu_2$ and $mGlu_3$ in the etiology and treatment of neuropsychiatric illnesses.

We have demonstrated that $mGlu_3$ plays a critical role in the regulation of mPFC neuroplasticity and is required for a specific learned behavior that is dependent upon the integrity of the mPFC. In agreement with reports from rat brain slices, we found that strong pharmacological activation of group II mGlu receptors results in LTD of fEPSPs recorded in layer V mPFC. The initial transient depression was found to be likely due to a presynaptic modulation of neurotransmitter release, while the LTD was likely mediated by a postsynaptic mechanism. This is consistent with previous studies showing postsynaptic actions of group II mGlu receptor agonists in mPFC pyramidal cells. Furthermore, under our experimental conditions this LTD does not require activation of NMDA receptors, as the magnitude was unaffected by an NMDA receptor antagonist.

Although the selective $mGlu_2$ NAM **IV.57** slightly reduced the magnitude of the transient depression, it did not prevent the induction of LTD. In contrast, $mGlu_3$ NAMs **III.239** and **III.270** completely blocked induction of LTD by the group II mGlu receptor agonist, but were without effect on the transient depression of fEPSPs. Similarly, LTD was observed in slices prepared from $mGlu_2$, but not $mGlu_3$, KO mice, whereas acute depression of synaptic transmission was intact in slices from $mGlu_3$ KO mice. Taken together, these results provide strong evidence that activation of $mGlu_2$ can induce

transient depression of synaptic transmission in mPFC neurons, while activation of postsynaptically localized $mGlu_3$ in induction of LTD in these neurons.

In agreement with previous studies, we found that a selective $mGlu_{2/3}$ agonist increases intracellular Ca^{2+} in layer V pyramidal cells and were able to determine that this response is mediated by $mGlu_3$. Although the exact mechanism by which $mGlu_3$, a $G_{i/o}$ coupled receptor, induces intracellular Ca^{2+} increases is unknown, similar effects of group II mGlu receptor agonists on intracellular Ca^{2+} are observed in hippocampal CA3 pyramidal cell and interneuron populations, and these responses are thought to be mediated by activation of $mGlu_3$ (Ster, 2011). In addition, there are examples of other $G_{i/o}$ coupled receptors inducing intracellular Ca^{2+} elevations (Murthy, Zhou, Huang, & Pentyala, 2004).

The finding that activation of $mGlu_3$ is required for induction of a form of synaptic plasticity in the mPFC is especially important in light of extensive studies demonstrating a central role of the mPFC in multiple domains of cognitive function and previous genetic studies implicating $mGlu_3$ in aspects of cognitive function that require integrity of this cortical region. Thus, our finding that the selective $mGlu_3$ NAM **III.270** induced a dose-dependent increase in the number of trials required to extinguish fear responses is consistent with a possible role of $mGlu_3$ in this specific form of prefrontal cortical-dependent cognitive function. The highest dose of **III.270** nearly doubled the number of trials needed to reach the extinction criterion and some animals even failed to reach criterion after the maximum number of cues given, suggesting a major role for

$mGlu_3$ in the process of acquisition of extinction learning, but we did not see effects on extinction retrieval.

When these data are considered together with recent reports of working memory deficits in $mGlu_3$ KO mice, the effects of GRM3 allelic variation on human cognitive performance, and the association of GRM3 mutations and psychiatric disorders, there is a convergent set of evidence indicating that $mGlu_3$ plays an important role in PFC-dependent cognitive behaviors, and that allosteric modulators of $mGlu_3$ may represent a novel therapeutic strategy for altering prefrontal function in patients.

We have also demonstrated that sufficient inhibition of $mGlu_3$ signaling can cause significant effects in the Porsolt forced swim test, which is indicative of antidepressant-like activity. The efficacy of this strategy appears to be dependent on a relatively high level of receptor occupancy, as demonstrated by the differential effects of **III.270** at 100 mg/kg and **V.1** at 56.6 mg/kg, although this hypothesis cannot be confirmed in the absence of a selective $mGlu_3$ radioligand. Furthermore, the selective inactivation of $mGlu_2$ receptors does not appear sufficient to induce antidepressant efficacy, as evidenced by the lack of effect of **V.2** in the Porsolt forced swim test, even when dosed to reach concentrations in > 40-fold excess of its IC_{50} at $mGlu_2$. Together, this data indicates that the majority of the $mGlu_{2/3}$ antagonist effect in this assay is due to inhibition of $mGlu_3$. This finding is at odds with reports from KO mice, where the $mGlu_2$ receptor appeared to be the key mediator of antidepressant efficacy (Gleason, Li, Smith, Ephlin, & Wang, 2013). However, the use of $mGlu_2$ and $mGlu_3$ KO mice for validation of mechanism, rather than as a confirmation of ligand specificity, is

complicated by the issue of compensation between these two receptors when one is missing during the developmental process (De Filippis et al., 2015; Lyon, Kew, Corti, Harrison, & Burnet, 2008). Such a developmental alteration could explain the differences seen with the genetic versus pharmacologic models, although additional studies with chemically distinct compounds should be undertaken to rule out the influence of off-target effects. Furthermore, future studies should look at combinations of $mGlu_2$ and $mGlu_3$ selective NAMs to determine whether there is an additive effect on receptor inhibition, or whether the antidepressant effects of group II mGlu receptor antagonists can be entirely attributed to a single receptor subtype. It is warranted to apply these compounds to more translatable models of antidepressant activity, including unpredictable chronic mild stress models and assessment of novelty suppressed feeding. Furthermore, assessment of the efficacy of a selective $mGlu_3$ NAM in a model of TRD, such as a corticosterone-induced model, will be important for comparing this class of compounds to currently available antidepressants (Ago et al., 2013; Koike et al., 2013).

Our assessment of the role of $mGlu_2$ and $mGlu_3$ in the anxiolytic effects previously seen with $mGlu_{2/3}$ antagonists indicates that these compounds do not exhibit a classical anxiolytic profile, as has been previously suggested (Bespalov et al., 2008). Neither a dual $mGlu_{2/3}$ antagonist, nor a selective $mGlu_2$ NAM, nor a selective $mGlu_3$ NAM were able to induce a robust anxiolytic response in the elevated plus maze. However, **V.1** was able to decrease marble burying behavior, which has sometimes been regarded as a measure of anxiety, though it has also been interpreted in the context of

obsessive compulsive disorder and autism spectrum disorders (Angoa-Pérez, Kane, Briggs, Francescutti, & Kuhn, 2013). Our results, along with those of other investigators, indicate that inhibition of group II mGlu receptors is unlikely to treat the same spectrum of anxiety-driven behaviors as classical anxiolytics, particularly SSRIs and benzodiazepines.

In contrast to previous suggestions regarding the cause for apparent efficacy of $mGlu_{2/3}$ antagonists in marble burying and forced swim tests, we do not find evidence that selective $mGlu_3$ NAMs are causing a false positive due to alterations in habituation to novel environments. Previous studies have indicated that $mGlu_2$ KO mice exhibit hyperlocomotor activity when exposed to novel environments, indicating that the locomotor and habituation abnormalities seen with LY341495 and other $mGlu_{2/3}$ antagonists may be driven by $mGlu_2$ inhibition (Morishima et al., 2005). Additional studies with selective $mGlu_2$ and $mGlu_3$ NAMs in the context of anxiety should potentially focus on repetitive or stereotyped behaviors in order to determine whether these compounds would be useful as adjunct therapies in disorders with anxiety-induced sequelae.

Sections of this chapter have been reprinted with permission from the following:

Metabotropic glutamate receptor 3 activation is required for LTD in medial prefrontal cortex and fear extinction. Walker AG, Wenthur CJ, Xiang Z, Rook JM, Emmitte KA, Niswender CM, Lindsley CW, Conn PJ. Proc Natl Acad Sci USA. 2015 Jan 27; 112(4):1196-201, Copyright 2015 National Academy of Sciences, USA.

CHAPTER VI

SINGLE NUCLEOTIDE POLYMORPHISMS IN EXONS OF GRM GENES AND RISK OF RECEIVING A SUBSTANCE DEPENDENCE DIAGNOSIS

Prior Evidence for a Role of Group II mGlu Receptors in the Etiology and Treatment of Addiction

Substance dependence continues to be a significant public health problem in the United States. A recent national survey reports that in 2010, an estimated 9.1 percent of Americans met criteria indicating they needed treatment for a problem related to drugs or alcohol, but only about 1 percent of Americans received treatment during that year (Substance Abuse and Mental Health Services Administration, 2013). Furthermore, the rate of relapse amongst patients with substance dependence disorders remains very high, even when treated with the current gold standard medications (Abuse, 1999). In fact, for many drugs of abuse, including cocaine, marijuana and inhalants, there are no therapeutics available. These issues potentially arise from an incomplete understanding of the factors leading to substance abuse and dependence issues (Nutt et al., 2015). The role of the mesolimbic dopamine circuitry as a target for many drugs of abuse has been established for some time now, but there is an increasing focus on understanding other signaling pathways which contribute to the development and progression of substance abuse. Glutamatergic signaling is now thought to be critically involved in substance dependence, with mGlu receptor signaling playing an important role in development

and maintenance of addiction (Bellone & Mameli, 2012; Morishima et al., 2005; Moussawi & Kalivas, 2010).

The novel $mGlu_2$ and $mGlu_3$ NAMs described in previous chapters represent a significant advance in our ability to understand the signaling events mediated by the group II mGlu receptors, both in healthy individuals and in a variety of neuropsychiatric conditions, and the availability of these selective tool compounds is important for the study of mGlu signaling in substance abuse. Use of such subtype-selective allosteric modulators will reveal critical information about the underlying molecular mechanisms which underlie these synaptic and behavioral responses. However, although these compounds will allow researchers to more exactly dissect the role of mGlu receptors in the progression and treatment of addiction, an important question remains that cannot be answered using pharmacologic methods alone: Do alterations in mGlu signaling competency contribute to the etiology of substance abuse?

Genetic evidence for GRM SNPs causing disruptions in PFC function

Previous research indicates that there is a large amount of variability present within the genes responsible for metabotropic glutamate receptor expression, and that individual single nucleotide polymorphisms (SNPs) can be associated with the development of psychiatric illnesses, including substance dependence disorders (Jia et al., 2014; Xia et al., 2012, 2014). There is also evidence to suggest that common polymorphisms of mGlu receptors can cause impairment in normal cognitive process, including those which help mediate goal-directed behaviors (Kawakubo et al., 2011).

However, the studies to date have looked at non-coding variants, causing difficulties in interpretation of the effects of these mutations on a biochemical level. Genetic studies focusing on SNPs in exons, the coding regions of genes, may be more amenable to mechanistic studies of how predisposition to addiction may manifest itself; SNPs in exonic regions can generate easily predictable and reproducible structural and functional alterations in their protein products.

In the case of the GRM genes, their products are the mGlu receptors. There are several lines of evidence indicating that exonic, functional variants GRMs could contribute to the development of substance dependence disorders. Firstly, drugs of abuse are known to have significant effects on mGlu receptor expression and function in the PFC, with downstream effects on memory and learning processes (Huang et al., 2007; Schwendt, Reichel, & See, 2012). Secondly, deletion of $mGlu_2$ receptors has been shown to yield increased sensitivity to cocaine (Morishima et al., 2005). Finally, early clinical evidence supports the efficacy of N-acetylcysteine, a therapeutic strategy designed to target glutamate homeostasis, in cannabis-smoking cessation, with additional large trials planned to further examine the findings thus far (Carpenter et al., 2012; McClure et al., 2014). If hypofunctional, exonic variants of GRMs are overrepresented in patients with substance dependence disorders, this would be consistent with the data gathered thus far, indicating that glutamatergic imbalances can initiate and propagate drug seeking behaviors.

Effects of group II mGlu receptor agonists and PAMs on behaviors relevant to addiction

To further implicate the involvement of mGlu receptors in substance dependence disorders, several pre-clinical studies have indicated that several mGlu targeting compounds, including group II mGlu agonists and PAMs, can prevent drug-seeking behavior in rodents (Cannella et al., 2013; Dhanya et al., 2014; Li, Xi, & Markou, 2012; Olive, 2010). *In vivo* evidence supports the paradigm that drug exposure alters mGlu-dependent synaptic plasticity, and equally strong evidence suggests that pharmacologically targeting mGlu receptors can lead to decreased drug seeking (Tessari, Pilla, Andreoli, Hutcheson, & Heidbreder, 2004; Xi et al., 2010). These compounds seem to derive efficacy from their ability to reverse drug-induced alterations in long term synaptic glutamate signaling, and it is thought that such drug-induced alterations in synaptic plasticity are an important part of the maintenance of addiction (Holmes, Spanagel, & Krystal, 2013; Olive, 2010).

Development of a Case-control Study to Assess the Effect of Exonic GRM SNPs on the Risk of Substance Dependence Diagnosis

While the exploration of mGlu ligands as potential therapeutics for substance dependence is well underway, the influence of deranged baseline glutamatergic signaling as a predisposing factor to drug-seeking behavior has received far less attention. Examining this genetic variability has the potential not only to uncover a risk factor for the development of substance dependence, but also to inform the ongoing development of mGlu-targeting compounds for the treatment of substance abuse.

Defining suitable case and control populations

In order to develop an improved understanding of the impact of genetic variation in mGlu receptors on the risk of developing substance abuse, we designed a pilot case-control genetic study to test the hypothesis that patients with substance dependence have an increased prevalence of SNPs in the exonic regions of their GRM genes as compared to non-dependent controls. This study was designed to look for preliminary signals of GRM involvement in substance dependence, in order to either support or rebuff future large-scale assessments of GRM function and addiction etiology.

For the genetic analysis, we used de-identified, pre-genotyped patient samples available through Vanderbilt's DNA databank, BioVU. This databank was designed as a resource for exploration of the relationships among genetic variation, disease susceptibility, and variable drug responses, and represents a key step in moving pharmacogenomics into clinical practice. Projects designed to find predictive genotype-phenotype associations within this program have been successfully completed across a wide array of disease states, including atrial fibrillation, Crohn's disease, multiple sclerosis, rheumatoid arthritis, and type 2 diabetes (Ritchie et al., 2010).

BioVU has over 122,000 samples from adult clinic patients and over 14,000 samples from pediatric patients currently in the repository. Of the currently collected samples, 43% are male and 57% female. The samples reflect the overall patient population at Vanderbilt; 86% are from Caucasians and 10% are from African Americans.

Asian and Hispanic populations comprise 1% each. There are more than 35,000 pre-genotyped samples available, with more than 16,000 that contain genome-wide SNP data. Each of the available samples is linked to a de-identified electronic medical record, which captures diagnostic and procedure codes (ICD-9 and CPT), demographics and text from clinical care.

In order to acquire genetic samples that represented appropriate individuals for our case and control populations, we first defined a set of inclusion and exclusion criteria that would be used to define our study population (**Table VI.1**).

Table VI.1 List of inclusion and exclusion criteria used in the algorithm that selected the case and control subjects using data available from the synthetic derivative.

Case Inclusion Criteria	Control Inclusion Criteria
Age ≥ 18 years **AND** Genotyped on Illumina Infinium Human Exome Bead Chip **AND** ICD-9 Codes 303.00-303.93 (2x)(Alcohol Dependence) **OR** ICD-9 Codes 304.00-304.93 (2x)(Drug Dependence) **OR** keywords "alcohol", "dependence", "cocaine", etc… in problem list (2x)	Age ≥ 50 years **AND** Genotyped on Illumina Infinium Human Exome Bead Chip **AND** ≥ 5 clinical notes **AND** ≥ 5 years of follow up between first and last note in patient history [Matched to cases by race and gender]
Case Exclusion Criteria	**Control Exclusion Criteria**
Lack of consent **OR** ICD-9 Codes 296.4-296.81 (Bipolar Disorder) **OR** ICD-9 Codes 295.00-295.93 (Schizophrenic Disorder)	Lack of consent **OR** ICD-9 Codes 303.00-303.93, 304.00-304.93, 296.4-296.81, 295.00-295.93 **OR** Problem list contains any of the key words for case inclusion **OR** Record of psychiatric treatment at Vanderbilt **OR** Presence of drug screening panel

Inclusion criteria for the case population required an individual from any race or gender who was ≥ 18 years old at the time of sample collection to have an electronic medical record that included at least two instances of an ICD-9 code from 303.00-303.93, or 304.00–304.93, indicating a diagnosis of alcohol or other drug dependence. We additionally included records with problem lists that had two or more mentions of the following terms "alcoholic, alcoholism, dependence, addiction, addict, addicted, cocaine, heroin, amphetamine, methamphetamine, opiate, opioid, cannabis, marijuana, withdrawal, delirium tremens" in the patient problem list. Only those samples which have already been genotyped on the Illumina Infinium Human Exome Bead Chip platform were included in the study.

Exclusion criteria from the case group included the absence of a signed consent-to-treatment form, a formal indication (on the consent-to-treatment form or elsewhere) that an individual wishes to opt out, duplicate samples, or the presence of an ICD-9 code from 295.00-295.93 or 296.45-296.89 indicating a diagnosis of bipolar disorder or a schizophrenic disorder, as variability in GRM3 had already been associated with these illnesses (O'Brien et al., 2014).

Control cases were comprised of those records for patients who were ≥ 50 years old that did not contain any of the above ICD-9 codes. The older age of the controls was designed to capture patients who have had sufficient time to develop a substance dependence disorder, but never did. The records of control subjects could also not contain any record of admission to an addiction clinic, either internal to Vanderbilt or otherwise. Control subjects could also never have received a drug screening panel,

regardless or result, in order to eliminate cases where intoxication was suspected. These controls must also have had at least five years of follow-up and at least five clinical notes in their records, in order to indicate that medical care was sought, but a substance dependence diagnosis was absent. Additionally, all samples associated with control records needed to have been previously genotyped on the Illumina Infinium Human Exome Bead Chip platform.

These inclusion and exclusion criteria initially generated 402 cases and 9,844 controls. In order to match the gender and race demographics of the two groups, 6,241 control samples were randomly removed, leaving 3,606 controls (**Table VI.2**). Power analysis indicated that a relative risk >1.58 above baseline to achieve 80% power at P < 0.005 could be detected for alleles with a minor allele frequency (MAF) of >10% with this number of samples, using a disease prevalence of 10%. Previous work suggests that significant differences in cognitive performance can be correlated with as few as 14 SNP's that have a MAF >15% (Baune et al., 2010).

Table VI.2 Demographics of original case and control populations, along with demographics of the control population after random culling to match demographics.

Identifier	Cases		Controls (Initial)		Controls (Matched)	
	(n =)	%	(n =)	%	(n =)	%
Total	402	100.00	9,844	100.00	3,603	100.00
Female	173	43.03	5,770	58.61	1,550	43.02
Male	229	56.97	4,074	41.39	2,053	56.98
African American	81	20.15	726	7.38	726	20.15
Caucasian	314	78.11	8,897	90.38	2,814	78.10
Other	7	1.74	221	2.25	63	1.75

SNP selection and quality control for genotyping data

Our SNP population of interest was defined by the 94 loci within the coding-regions of GRM1-8 that were covered on the Illumina Infinium Human Exome Bead Chip platform (**Table VI.3**). For all subjects, pre-genotyped data was gathered at each of these loci. The DNA from the study samples had been previously extracted in the DNA Resources Core, using the Gentra Systems AutoPure automated DNA extraction system. Genotyping occurred on the mid-throughput Sequenom platform via a single-base primer extension reaction coupled with mass spectrometry. Because all DNA samples were pre-genotyped for this pilot study they had previously had to pass internal quality control measures, which included a 95% sample and SNP call rate threshold, gender checking analysis, relatedness, concordance checking of sample and HapMap individuals, and Mendelian checking (Turner et al., 2011).

To further ensure the quality of our data, call rates for our SNPs of interest were confirmed on our subset of BioVU Exome Chip data. Any SNP or individual that had a call rate of < 95% in this subset will be removed from subsequent analysis, which eliminated 2 SNPs from consideration. An additional 29 SNPs that were found to be monomorphic in our study population were also removed, leaving 63 SNPs for study. For the control samples, we tested the Hardy-Weinberg Equilibrium (HWE) proportions using a Chi-Square test; no samples were found to deviate from HWE ($P < 0.0001$). We then checked 10% of the electronic medical records in order to ensure that the selection algorithms were identifying the correct patients, and the algorithm was found to be operating with a positive predictive value of > 98%.

Table VI.3 List of SNPs selected for analysis from the Illumina Infinium Human Exome Bead Chip, segregated by gene. All SNPs are present in coding regions of the gene. SNPs listed in orange were removed due to call rates < 95% and SNPs listed in red were not considered in the final analysis due to all samples being monomorphic for those loci.

GRM1	GRM2	GRM3	GRM4	GRM5	GRM7	GRM8
exm2266267	exm319100	exm2264265	exm2270464	exm16914280	exm2269601	exm654728
exm584534	exm319102	exm631177	exm539878	exm946691	exm2269397	exm654777
exm584536	exm319113	exm631194	exm539887	exm2267281	exm287016	exm654778
exm584551	exm2056741	exm631221	exm539902	exm946703	exm6768750	exm17691394
exm2270530	exm319128		exm539922	exm10831496	exm287068	exm11971186
exm584589	exm319140		exm539953	exm946617	exm2269398	exm654812
exm584602	exm319142		exm539862	exm946658	exm287108	exm2270685
exm584606	exm319147		exm2257775	exm946674	exm287115	exm2270686
exm584615	exm319150		exm2123157		exm287135	exm654844
exm584616	exm319179		exm539914		exm287161	exm654861
exm584617	exm2256077		exm539920		exm287075	exm654863
exm584628	exm319207				exm2060735	exm654859
exm584630	exm319157				exm287119	exm2138140
exm584634	exm2239880				exm287131	exm654734
exm584638	exm319169					exm654759
exm584648	exm319199					exm654768
exm584626						exm2138149
exm584650						exm654833
exm584608						exm654858
exm584566						exm654864
exm584583						

Analysis of Exonic GRM SNP Frequency and Risk of Substance Dependence Diagnosis

With our samples in hand, we then began to assess whether diagnosis of substance dependence varies with GRM phenotype via single-locus tests of association at each of the 63 SNPs remaining for study, and we calculated odds ratios and 95% confidence intervals for each SNP using an additive model (**Table VI.4**).

Table VI.4 Results of single locus association tests for each SNP with odds ratios, 95% confidence intervals and P-values (not corrected for multiple comparisons). MA represents minor allele, SEM represents standard error of the mean, L95 is the lower bound of the 95% confidence interval, and U95 is the upper bound of the 95% confidence interval. Where odds ratios had an SEM > 10, ND is entered; where 95% confidence intervals spanned from 0 to infinity, broad is entered.

GRM	SNP	Base Pair	MA	(n =)	Odds Ratio	SEM	L95	U95	P
1	exm584630	146755454	T	3939	2.72	0.44	1.14	6.45	0.024
1	exm584615	146755072	C	3937	4.77	0.87	0.87	26.15	0.072
1	exm2270530	146652354	C	3939	0.87	0.12	0.68	1.11	0.259
1	exm584534	146480637	A	3939	2.31	0.79	0.49	10.88	0.291
1	exm584617	146755132	A	3939	0.84	0.35	0.42	1.66	0.611
1	exm2266267	146394655	G	3939	1.04	0.08	0.89	1.21	0.624
1	exm584634	146755508	A	3939	1.28	1.07	0.16	10.39	0.816
1	exm584606	146720826	A	3938	0.99	0.32	0.53	1.85	0.970
1	exm584589	146720360	A	3939	1.00	0.34	0.51	1.96	0.995
1	exm584536	146480705	A	3939	ND		Broad		0.998
1	exm584551	146625869	A	3939	ND		Broad		0.999
1	exm584602	146720756	A	3939	ND		Broad		0.999
1	exm584616	146755073	C	3939	ND		Broad		0.999
1	exm584628	146755390	T	3939	ND		Broad		0.999
1	exm584638	146755553	T	3917	ND		Broad		0.999
1	exm584648	146755673	G	3939	ND		Broad		0.999
2	exm2256077	51750141	T	3939	5.18	1.23	0.46	57.77	0.182
2	exm319100	51743034	C	3938	0.78	0.34	0.40	1.51	0.453
2	exm319140	51747111	A	3933	1.59	0.77	0.35	7.13	0.545
2	exm319128	51746781	T	3937	1.45	0.76	0.33	6.46	0.625
2	exm319147	51747288	A	3939	0.96	0.34	0.49	1.89	0.914
2	exm319113	51743411	A	3934	ND		Broad		0.999
2	exm319142	51747125	A	3936	ND		Broad		0.999
2	exm2056741	51746780	A	3938	ND		Broad		0.999
2	exm319150	51749105	G	3932	ND		Broad		0.999
2	exm319207	51751813	T	3939	ND		Broad		0.999
2	exm319102	51743096	A	3939	ND		Broad		0.999
2	exm319179	51749863	T	3939	ND		Broad		0.999

3	exm2264265	86372884	C	3938	1.12	0.08	0.95	1.32	0.188
3	exm631177	86468254	A	3939	1.45	0.33	0.76	2.77	0.257
3	exm631194	86468787	A	3939	ND		Broad		0.999

4	exm539922	34029733	T	3939	6.29	0.92	1.05	37.82	0.044
4	exm2270464	33991368	C	3939	1.21	0.12	0.96	1.53	0.107
4	exm539878	34004293	C	3939	1.91	1.10	0.22	16.38	0.556
4	exm539887	34008014	A	3939	ND		Broad		0.999
4	exm539902	34008464	C	3939	ND		Broad		0.999
4	exm539953	34101143	T	3939	ND		Broad		0.999

5	exm10831496	88557991	G	3939	1.06	0.08	0.90	1.25	0.473
5	exm946691	88337922	A	3939	1.22	0.30	0.68	2.18	0.498
5	exm2267281	88353802	G	3938	1.04	0.11	0.84	1.29	0.738
5	exm16914280	88321724	T	3939	1.07	0.24	0.67	1.70	0.784
5	exm946703	88386336	C	3939	ND		Broad		0.999

7	exm6768750	7240675	A	3936	1.09	0.09	0.92	1.30	0.304
7	exm287068	7494419	T	3939	3.21	1.16	0.33	30.90	0.314
7	exm2269601	7080267	T	3939	0.90	0.16	0.66	1.24	0.526
7	exm2269398	7511375	C	3939	0.97	0.08	0.83	1.13	0.659
7	exm2269397	7142227	C	3939	0.99	0.08	0.85	1.15	0.899
7	exm287016	7188188	A	3939	ND		Broad		0.999
7	exm287115	7620433	T	3939	ND		Broad		0.999
7	exm287135	7620805	G	3939	ND		Broad		0.999
7	exm287108	7620302	G	3939	ND		Broad		0.999
7	exm287161	7721878	T	3939	ND		Broad		0.999

8	exm654777	126173898	A	3939	2.97	0.81	0.61	14.58	0.179
8	exm11971186	126437897	G	3938	0.94	0.08	0.80	1.10	0.431
8	exm2270686	126719170	C	3936	1.05	0.08	0.90	1.23	0.516
8	exm17691394	126324591	G	3939	1.07	0.11	0.86	1.34	0.517
8	exm654778	126173902	C	3939	0.79	0.40	0.36	1.75	0.566
8	exm2270685	126613163	T	3938	0.98	0.08	0.83	1.14	0.755
8	exm654728	126086242	C	3939	1.14	1.06	0.14	9.06	0.905
8	exm654812	126544139	C	3939	ND		Broad		0.999
8	exm654844	126882901	T	3938	ND		Broad		0.999
8	exm654861	126883197	C	3939	ND		Broad		0.999

This initial analysis of each of the individual SNPs detected only two SNPs that reached the predetermined cutoff of significance ($P < 0.05$), and neither of these were found to be significant when corrected for multiple comparisons using the false-discovery rate method (Benjamini & Hochberg, 1995). Likewise, when looking for SNP association with substance dependence diagnosis by race, there were no SNPs that were found to be significant once corrections for multiple comparisons were made.

However, because of the genetic heterogeneity known to underlie many psychiatric illnesses and because of the very low MAFs exhibited by our exonic, non-synonymous SNP selections, we recognized the high likelihood that no single mutant allele would be able reach statistical significance on its own. However, we also recognized the fact that glutamatergic dysfunction within substance dependence could plausibly be manifested through a large number of independent, rare SNPs at several loci within the same gene.

In order to look for such a difference in overall allele population between cases and controls, we decided *a priori* to use a SNP-set kernel association test (SKAT) for multi-locus association in the event that no individual SNP reached significance (M. C. Wu et al., 2010). We then carried out this analysis, grouping the SNPs into SNP-sets by gene. Again, when all races were studied as one population using SKAT, no gene was found to have higher variability in the SNP-set when comparing cases and controls.

In contrast, when each racial population was studied individually and the results were corrected for multiple comparisons, African Americans with substance

dependence were found to have higher variability in GRM1 than African American controls, with GRM2 at the threshold of significance. Additionally, in patients who self-reported race as neither African American nor Caucasian (predominantly Asian), there was a higher variability in GRM3 in cases than in controls. No differences were seen when comparing Caucasian cases and controls (**Table VI.5**).

Table VI.5 List of SNP-sets analyzed by race using SKAT methodology along with P-values corrected for multiple comparisons.

African American		Caucasian		Other	
SNP-Set	**P-value**	**SNP-Set**	**P-value**	**SNP-Set**	**P-value**
GRM1	0.049	GRM1	0.960	GRM1	0.860
GRM2	0.065	GRM2	0.990	GRM2	0.959
GRM3	0.654	GRM3	0.362	GRM3	0.032
GRM4	0.982	GRM4	0.314	GRM4	0.244
GRM5	0.513	GRM5	0.912	GRM5	0.913
GRM7	0.956	GRM7	0.262	GRM7	0.562
GRM8	0.178	GRM8	0.941	GRM8	0.719

Overall, these results indicate that the impact of mGlu receptor function on the development of substance dependence may differ depending on racial background. While such an idea is intriguing, and potentially highly impactful on the treatment of addiction, these results are nevertheless only preliminary; undertaking a larger study will be necessary to either confirm or refute these initial findings.

Conclusions and Future Directions

We found that GRM1 has a higher prevalence of SNPs in their coding regions for substance dependent individuals than controls amongst African American patients, and that GRM2 is also of potential interest. Likewise, amongst non-African American, non-Caucasian substance dependent individuals, there is a higher prevalence of non-synonymous exonic mutations in GRM3 than in controls. While such results are based on a relatively small sample size, and should be interpreted with caution, the specific genes that are indicated by this preliminary study, GRM1, GRM2, and GRM3, are interesting due to the proposed pharmacologic strategy that would be considered therapeutic. While the evidence for $mGlu_1$ activation and inactivation is mixed, only activation of the group II receptors has been submitted as potentially therapeutic mechanism (Loweth, Tseng, & Wolf, 2013; Olive, 2010). This observation leads to the prediction that the variant receptors identified here are more likely to be hypofunctional than hyperfunctional; considering the relative ease of inducing receptor dysfunction, as compared to improved function, such a prediction appears plausible.

In order to assess this prediction, it would be prudent to elucidate the effects that the identified differences in GRMs have on the binding and activity of glutamate as well as the effects on the binding and activity of compounds designed to act on the mGlu receptors. Those isoforms which are overrepresented in the case population could be used to develop homology models for each receptor subtype; selective ligands can be docked in these models in order to predict alterations in their binding. Directed mutagenesis can then be used to recreate the receptor isoforms most enriched in

substance dependent individuals, and measure the efficacy of selective compounds at these mutant receptors. Such screening results in these variant receptors could provide critical information as to whether patients with variant mGlu isoforms have similar alterations in their response to glutamate, and whether they have alterations in their response to allosteric modulators. Such results will contribute to the development of novel therapeutics for substance abuse by identifying whether variant isoforms of mGlu receptors will exhibit altered functionality in comparison to the population of mGlu isoforms present in healthy controls, and whether the dysfunctional signaling of these variants can be rescued by novel allosteric modulators for these receptors.

REFERENCES

Abuse, N. I. on D. (1999). Principles of Drug Addiction Treatment: A Research-Based Guide,1–43. Retrieved from http://www.ncjrs.gov/App/abstractdb

Ago, Y., Yano, K., Araki, R., Hiramatsu, N., Kita, Y., Kawasaki, T., Matsuda, T. (2013). Metabotropic glutamate 2/3 receptor antagonists improve behavioral and prefrontal dopaminergic alterations in the chronic corticosterone-induced depression model in mice. *Neuropharmacology*, *65*, 29–38.

Amiel, J. M., & Mathew, S. J. (2007). Glutamate and anxiety disorders. *Current Psychiatry Reports*, *9*(4), 278–283.

Angoa-Pérez, M., Kane, M., Briggs, D., Francescutti, D., & Kuhn, D. (2013). Marble burying and nestlet shredding as tests of repetitive, compulsive-like behaviors in mice. *Journal of Visual Experimentation*, *82*, 50978.

Aronica, E., Gorter, J. a., Ijlst-Keizers, H., Rozemuller, A. J., Yankaya, B., Leenstra, S., & Troost, D. (2003). Expression and functional role of mGluR3 and mGluR5 in human astrocytes and glioma cells: Opposite regulation of glutamate transporter proteins. *European Journal of Neuroscience*, *17*(10), 2106–2118.

Baudry, M., Bi, X., Gall, C., & Lynch, G. (2011). The biochemistry of memory: The 26year journey of a “new and specific hypothesis”. *Neurobiology of Learning and Memory*, *95*(2), 125–33.

Baune, B. T., Suslow, T., Beśte, C., Birosova, E., Domschke, K., Sehlmeyer, C., & Konrad, C. (2010). Association between genetic variants of the metabotropic glutamate receptor 3 (GRM3) and cognitive set shifting in healthy individuals. *Genes, Brain and Behavior*, *9*(5), 459–466.

Beaulieu, J. M., & Gainetdinov, R. R. (2011). The physiology, signaling, and pharmacology of dopamine receptors. *Pharmacological Reviews*, *63*(1), 182.

Bellone, C., & Mameli, M. (2012). MGluR-dependent synaptic plasticity in drug-seeking. *Frontiers in Pharmacology*, *3*, 1–6.

Benjamini, Y., & Hochberg, Y. (1995). Controlling the false discovery rate: a practical and powerful approach to multiple testing. *Journal of the Royal Statistical Society, 57*(1), 289-300.

Benneyworth, M. a, Xiang, Z., Smith, R. L., Garcia, E. E., Conn, P. J., & Sanders-Bush, E. (2007). A selective positive allosteric modulator of metabotropic glutamate receptor subtype 2 blocks a hallucinogenic drug model of psychosis. *Molecular Pharmacology*, *72*(2), 477–484.

Berg, J., Tymoczko, J., & Streyer, L. (2002). Biochemistry. In W. Freeman (Ed.), *Biochemistry* (5th ed.). New York: MacMillan Education.

Bespalov, A. Y., van Gaalen, M. M., Sukhotina, I. a, Wicke, K., Mezler, M., Schoemaker, H., & Gross, G. (2008). Behavioral characterization of the mGlu group II/III receptor antagonist, LY-341495, in animal models of anxiety and depression. *European Journal of Pharmacology*, *592*(1-3), 96–102.

Bridges, T., & Lindsley, C. (2008). G-protein-coupled receptors: from classical modes of modulation to allosteric mechanisms. *ACS Chemical Biology*, *3*, 530–542.

Bschor, T., Bauer, M., & Adli, M. (2014). Chronic and treatment resistant depression: diagnosis and stepwise therapy. *Deutsches Arzteblatt International*.

Campo, B., Kalinichev, M., Lambeng, N., El Yacoubi, M., Royer-Urios, I., Schneider, M., Celanire, S. (2011). Characterization of an mGluR2/3 negative allosteric modulator in rodent models of depression. *Journal of Neurogenetics*, *25*(4), 152–66.

Cannella, N., Halbout, B., Uhrig, S., Evrard, L., Corsi, M., Corti, C., Spanagel, R. (2013). The mGluR2/3 agonist LY379268 induced anti-reinstatement effects in rats exhibiting addiction-like behavior. *Neuropsychopharmacology : Official Publication of the American College of Neuropsychopharmacology*, 38(10), 2048-56.

Caraci, F., Battaglia, G., Sortino, M. A., Spampinato, S., Molinaro, G., Copani, A., Bruno, V. (2012). Metabotropic glutamate receptors in neurodegeneration/neuroprotection: Still a hot topic? *Neurochemistry International*, 61(4), 559-65.

Caraci, F., Molinaro, G., Battaglia, G., Giuffrida, M. L., Riozzi, B., Traficante, A., Copani, A. (2011). Targeting Group II Metabotropic Glutamate (mGlu) Receptors for the Treatment of Psychosis Associated with Alzheimer's Disease : Selective Activation of $mGlu_2$ Receptors Amplifies β-Amyloid Toxicity in Cultured Neurons , Whereas Dual Activation of $mGlu_2$ and $mGlu_3$ Is Neuroprotective, *Molecular Pharmacology, 79*(3), 618–626.

Carpenter, M. J., Ph, D., Baker, N. L., Desantis, S. M., Ph, D., Kryway, E., Hartwell, K.J. McRAe-Clark, A.L., Brady, K.T. (2012). A Double-Blind Randomized Controlled Trial of N-Acetylcysteine in Cannabis-Dependent Adolescents. *American Journal of Psychiatry*, *169*, 805–812.

Chaki, S., Ago, Y., Palucha-Paniewiera, A., Matrisciano, F., & Pilc, A. (2013). $mGlu_{2/3}$ and $mGlu_5$ receptors: potential targets for novel antidepressants. *Neuropharmacology*, *66*, 40–52.

Chen, H. S. V, & Lipton, S. A. (2006). The chemical biology of clinically tolerated NMDA receptor antagonists. *Journal of Neurochemistry*, *97*(6), 1611–1626.

Chien, W. T., & Yip, A. L. (2013). Current approaches to treatments for schizophrenia spectrum disorders, part I: an overview and medical treatments. *Neuropsychiatric Disease and Treatment*, *9*, 1311–1332.

Christopoulos, A. (2002). Allosteric binding sites on cell-surface receptors: novel targets for drug discovery. *Nature Reviews. Drug Discovery*, *1*(3), 198–210.

Chun, L., Zhang, W., & Liu, J. (2012). Structure and ligand recognition of class C GPCRs. *Acta Pharmacologica Sinica*, *33*(3), 312–323.

Ciceroni, C., Bonelli, M., Mastrantoni, E., Niccolini, C., Laurenza, M., Larocca, L. M., Melchiorri, D. (2013). Type-3 metabotropic glutamate receptors regulate chemoresistance in glioma stem cells, and their levels are inversely related to survival in patients with malignant gliomas. *Cell Death and Differentiation*, *20*(3), 396–407.

Conn, P. J., Christopoulos, A., & Lindsley, C. W. (2009). Allosteric modulators of GPCRs: a novel approach for the treatment of CNS disorders. *Nature Reviews. Drug Discovery*, *8*(1), 41–54.

Conn, P. J., Lindsley, C. W., & Jones, C. K. (2009). Activation of metabotropic glutamate receptors as a novel approach for the treatment of schizophrenia. *Trends in Pharmacological Sciences*, *30*(1), 25–31.

Conn, P. J., & Pin, J. P. (1997). Pharmacology and functions of metabotropic glutamate receptors. *Annual Review of Pharmacology and Toxicology*, *37*, 205–37. 5

D'Antoni, S., Berretta, A., Bonaccorso, C. M., Bruno, V., Aronica, E., Nicoletti, F., & Catania, M. V. (2008). Metabotropic glutamate receptors in glial cells. *Neurochemical Research*, *33*(12), 2436–43.

De Filippis, B., Lyon, L., Taylor, A., Lane, T., Burnet, P. W. J., Harrison, P. J., & Bannerman, D. M. (2015). The role of group II metabotropic glutamate receptors in cognition and anxiety: Comparative studies in GRM2−/−, GRM3−/− and GRM2/3−/− knockout mice. *Neuropharmacology*, *89*, 19–32.

Depression - WHO Fact Sheet. (2012). Retrieved from http://www.who.int/mediacentre/factsheets/fs369/en/

Dhanya, R. P., Sheffler, D. J., Dahl, R., Davis, M., Lee, P. S., Yang, L., Cosford, N. D. P. (2014). Design and synthesis of systemically active metabotropic glutamate subtype-2 and -3 ($mGlu_{2/3}$) receptor positive allosteric modulators (PAMs): Pharmacological characterization and assessment in a rat model of cocaine dependence. *Journal of Medicinal Chemistry*, *57*, 4154–4172.

Diagnostic and Statistical Manual of Mental Disorders. (2013) (5th ed.). Washington, DC: American Psychiatric Association.

Digby, G. J., Conn, P. J., & Lindsley, C. W. (2010). Orthosteric- and allosteric-induced ligand-directed trafficking at GPCRs. *Current Opinion in Drug Discovery & Development*, *13*(5), 587–594.

Digby, G. J., Utley, T. J., Lamsal, A., Sevel, C., Sheffler, D. J., Lebois, E. P., Conn, P. J. (2012). Chemical Modification of the M(1) Agonist VU0364572 Reveals Molecular Switches in Pharmacology and a Bitopic Binding Mode. *ACS Chemical Neuroscience*, *3*(12), 1025–36.

Doré, A. S., Okrasa, K., Patel, J. C., Serrano-Vega, M., Bennett, K., Cooke, R. M., Marshall, F. H. (2014). Structure of class C GPCR metabotropic glutamate receptor 5 transmembrane domain. *Nature*, *511*(7511), 557–62.

Downing, A. M., Kinon, B. J., Millen, B. a, Zhang, L., Liu, L., Morozova, M. A., Gomez, J. C. (2014). A double-blind, placebo-controlled comparator study of LY2140023 monohydrate in patients with schizophrenia. *BMC Psychiatry*, *14*(1), 1–12.

Dunayevich, E., Erickson, J., Levine, L., Landbloom, R., Schoepp, D. D., & Tollefson, G. D. (2008). Efficacy and tolerability of an $mGlu_{2/3}$ agonist in the treatment of generalized anxiety disorder. *Neuropsychopharmacology : Official Publication of the American College of Neuropsychopharmacology*, *33*(7), 1603–1610.

Durand, D., Carniglia, L., Caruso, C., & Lasaga, M. (2012). $mGlu_3$ receptor and astrocytes: Partners in neuroprotection. *Neuropharmacology*, (May), 1–11.

Egan, M. F., Straub, R. E., Goldberg, T. E., Yakub, I., Callicott, J. H., Hariri, A. R., Weinberger, D. R. (2004). Variation in GRM3 affects cognition, prefrontal glutamate, and risk for schizophrenia. *Proceedings of the National Academy of Sciences of the United States of America*, *101*(34), 12604–12609.

Emmitte, K. (2011). Recent advances in the design and development of novel negative allosteric modulators of $mGlu_5$. *ACS Chemical Neuroscience*, 411–432.

Enoch, M. -a., Rosser, a. a., Zhou, Z., Mash, D. C., Yuan, Q., & Goldman, D. (2014). Expression of glutamatergic genes in healthy humans across 16 brain regions; altered expression in the hippocampus after chronic exposure to alcohol or cocaine. *Genes, Brain and Behavior*, *13*(8), 758–768.

Fang, Z., Grütter, C., & Rauh, D. (2012). Strategies for the Selective Regulation of Kinases with Allosteric Modulators: Exploiting Exclusive Structural Features. *ACS Chemical Biology*.

Ferrari, A. J., Charlson, F. J., Norman, R. E., Patten, S. B., Freedman, G., Murray, C. J. L., Whiteford, H. a. (2013). Burden of Depressive Disorders by Country, Sex, Age, and Year: Findings from the Global Burden of Disease Study 2010. *PLoS Medicine*, *10*(11).

Galici, R., Jones, C., Hemstapat, K., Nong, Y., Echemendia, N.G., Williams, L.C., DePaulis, T., Conn. P.J. (2006). Biphenyl-indanone A, a positive allosteric modulator of the metabotropic glutamate receptor subtype 2, has antipsychotic-and anxiolytic-like effects in mice. *Journal of Pharmacology and Experimental Therapeutics*, *318*(1), 173–185.

Ghasemi, M., Kazemi, M. H., Yoosefi, A., Ghasemi, A., Paragomi, P., Amini, H., & Afzali, M. H. (2014). Rapid antidepressant effects of repeated doses of ketamine compared with electroconvulsive therapy in hospitalized patients with major depressive disorder. *Psychiatry Research*, *215*(2), 355–361.

Ghose, S., Crook, J. M., Bartus, C. L., Sherman, T. G., Herman, M. M., Hyde, T. M., Akil, M. (2008). Metabotropic glutamate receptor 2 and 3 gene expression in the human prefrontal cortex and mesencephalon in schizophrenia. *The International Journal of Neuroscience*, *118*(11), 1609–1627.

Gleason, S., Li, X., Smith, I., Ephlin, J., & Wang, X. (2013). $mGlu_{2/3}$ agonist-induced hyperthermia: an in vivo assay for detection of $mGlu_{2/3}$ receptor antagonism and its relation to antidepressant-like efficacy in mice. *CNS Neurological Disorders and Drug Targets*, *12*(5), 554–66.

Goeldner, C., Ballard, T. M., Knoflach, F., Wichmann, J., Gatti, S., & Umbricht, D. (2013). Cognitive impairment in major depression and the $mGlu_2$ receptor as a therapeutic target. *Neuropharmacology*, *64*, 337–46.

González-maeso, J., Ang, R., Yuen, T., Chan, P., Noelia, V., López-giménez, J. F., Sealfon, S. C. (2008). Identification of a Novel Serotonin/Glutamate Receptor Complex Implicated in Psychosis. *Nature*, *452*(7183), 93–97.

Gregory, K. J., Noetzel, M. J., & Niswender, C. M. (2013). *Pharmacology of metabotropic glutamate receptor allosteric modulators: Structural basis and therapeutic potential for*

CNS disorders. *Progress in Molecular Biology and Translational Science* (1st ed., Vol. 115). Elsevier Inc.

Harrison, P. J., Lyon, L., Sartorius, L. J., Burnet, P. W. J., & Lane, T. a. (2008). The group II metabotropic glutamate receptor 3 (mGluR3, $mGlu_3$, GRM3): expression, function and involvement in schizophrenia. *Journal of Psychopharmacology (Oxford, England)*, *22*(3), 308–22.

Hasler, G., Drevets, W. C., Manji, H. K., & Charney, D. S. (2004). Discovering endophenotypes for major depression. *Neuropsychopharmacology : Official Publication of the American College of Neuropsychopharmacology*, *29*(10), 1765–1781.

Hermes, M. L. H. J., & Renaud, L. P. (2011). Postsynaptic and presynaptic group II metabotropic glutamate receptor activation reduces neuronal excitability in rat midline paraventricular thalamic nucleus. *The Journal of Pharmacology and Experimental Therapeutics*, *336*(3), 840–849.

Holmes, A., Spanagel, R., & Krystal, J. H. (2013). Glutamatergic targets for new alcohol medications. *Psychopharmacology*, *229*(3), 539–554.

Hopkins, C. (2013). Is There a Path Forward for mGlu (2) Positive Allosteric Modulators for the Treatment of Schizophrenia? *ACS Chemical Neuroscience*, 211–213.

Hovelsø, N., Sotty, F., Montezinho, L. P., Pinheiro, P. S., Herrik, K. F., & Mørk, A. (2012). Therapeutic Potential of Metabotropic Glutamate Receptor Modulators. *Current Neuropharmacology*, 10, 12–48.

Hrabetova, S., Serrano, P., Blace, N., Tse, H. W., Skifter, D. a, Jane, D. E., Sacktor, T. C. (2000). Distinct NMDA receptor subpopulations contribute to long-term potentiation and long-term depression induction. *The Journal of Neuroscience : The Official Journal of the Society for Neuroscience*, *20*(12), RC81.

Huang, C.-C., & Hsu, K.-S. (2008). The role of NMDA receptors in regulating group II metabotropic glutamate receptor-mediated long-term depression in rat medial prefrontal cortex. *Neuropharmacology*, *54*(7), 1071–1078.

Huang, C.-C., Yang, P.-C., Lin, H.-J., & Hsu, K.-S. (2007). Repeated cocaine administration impairs group II metabotropic glutamate receptor-mediated long-term depression in rat medial prefrontal cortex. *The Journal of Neuroscience : The Official Journal of the Society for Neuroscience*, *27*(11), 2958–2968.

Iijima, M., Shimazaki, T., Ito, A., & Chaki, S. (2007). Effects of metabotropic glutamate 2/3 receptor antagonists in the stress-induced hyperthermia test in singly housed mice. *Psychopharmacology*, *190*(2), 233–9.

Merck, Sharp, and Dohme Corp. International Patent Application PCT/US2012/06202. (2012).

Jia, W., Zhang, R., Wu, B., Dai, Z.-X., Zhu, Y.-S., Li, P.-P., & Zhu, F. (2014). Metabotropic glutamate receptor 3 is associated with heroin dependence but not depression or schizophrenia in a chinese population. *PloS One*, *9*(1), e87247.

Johnson, K. A, Niswender, C. M., Conn, P. J., & Xiang, Z. (2011). Activation of group II metabotropic glutamate receptors induces long-term depression of excitatory synaptic transmission in the substantia nigra pars reticulata. *Neuroscience Letters*, *504*(2), 102–6.

Kandaswamy, R., McQuillin, A., Sharp, S. I., Fiorentino, A., Anjorin, A., Blizard, R. a, … Gurling, H. M. D. (2013). Genetic Association, Mutation Screening, and Functional Analysis of a Kozak Sequence Variant in the Metabotropic Glutamate Receptor 3 Gene in Bipolar Disorder. *JAMA Psychiatry (Chicago, Ill.)*, 1–8.

Kawakubo, Y., Suga, M., Tochigi, M., Yumoto, M., Itoh, K., Sasaki, T., Kasai, K. (2011). Effects of metabotropic glutamate receptor 3 genotype on phonetic mismatch negativity. *PloS One*, *6*(10), e24929.

Kenakin, T., & Miller, L. (2010). Seven transmembrane receptors as shapeshifting proteins: the impact of allosteric modulation and functional selectivity on new drug discovery. *Pharmacological Reviews*, *62*(2), 265–304.

Keov, P., Sexton, P. M., & Christopoulos, A. (2011). Allosteric modulation of G protein-coupled receptors: a pharmacological perspective. *Neuropharmacology*, *60*(1), 24–35.

Kew, J. N. C., Pflimlin, M. C., Kemp, J. a., & Mutel, V. (2002). Differential regulation of synaptic transmission by $mGlu_2$ and $mGlu_3$ at the perforant path inputs to the dentate gyrus and CA1 revealed in $mGlu_2$ -/- mice. *Neuropharmacology*, *43*(2), 215–221.

Kinon, B. J., Millen, B. a., Zhang, L., & McKinzie, D. L. (2015). Exploratory Analysis for a Targeted Patient Population Responsive to the Metabotropic Glutamate 2/3 Receptor Agonist Pomaglumetad Methionil in Schizophrenia. *Biological Psychiatry*, 1–9 [Epub ahead of print].

Kinon, B. J., Zhang, L., Millen, B. a, Osuntokun, O. O., Williams, J. E., Kollack-Walker, S., Jarkova, N. (2011). A multicenter, inpatient, phase 2, double-blind, placebo-controlled dose-ranging study of LY2140023 monohydrate in patients with DSM-IV schizophrenia. *Journal of Clinical Psychopharmacology*, *31*(3), 349–55.

Koike, H., Iijima, M., & Chaki, S. (2013). Effects of ketamine and LY341495 on the depressive-like behavior of repeated corticosterone-injected rats. *Pharmacology, Biochemistry, and Behavior*.

Kritis, A. a., Stamoula, E. G., Paniskaki, K. a., & Vavilis, T. D. (2015). Researching glutamate induced cytotoxicity in different cell lines: a comparative/collective analysis/study. *Frontiers in Cellular Neuroscience*, *9*(March), 1–18.

Lewis, D. a. (2012). Cortical circuit dysfunction and cognitive deficits in schizophrenia - implications for preemptive interventions. *European Journal of Neuroscience*, *35*(12), 1871–1878.

Li, X., Xi, Z.-X., & Markou, A. (2012). Metabotropic glutamate 7 ($mGlu_7$) receptor: A target for medication development for the treatment of cocaine dependence. *Neuropharmacology*, *7*.

Linden, a-M., Shannon, H., Baez, M., Yu, J. L., Koester, a, & Schoepp, D. D. (2005). Anxiolytic-like activity of the $mGlu_{2/3}$ receptor agonist LY354740 in the elevated plus maze test is disrupted in metabotropic glutamate receptor 2 and 3 knock-out mice. *Psychopharmacology*, *179*(1), 284–91.

Liu, W., Downing, a C. M., Munsie, L. M., Chen, P., Reed, M. R., Ruble, C. L., Nisenbaum, L. K. (2012). Pharmacogenetic analysis of the $mGlu_{2/3}$ agonist LY2140023 monohydrate in the treatment of schizophrenia. *The Pharmacogenomics Journal*, *12*(3), 246–54.

Lodge, D., Tidball, P., Mercier, M. S., Lucas, S., Hanna, L., Ceolin, L., Collingridge, G. L. (2013). Antagonists reversibly reverse chemical LTD induced by group I, group II and group III metabotropic glutamate receptors. *Neuropharmacology*, (April), 1–12.

Loweth, J., Tseng, K., & Wolf, M. (2013). Using metabotropic glutamate receptors to modulate Cocaine's synaptic and behavioral effects: mGluR1 finds a niche. *Current Opinion in Neurobiology*, *23*(4), 500–506.

Lundström, L., Bissantz, C., Beck, J., Wettstein, J. G., Woltering, T. J., Wichmann, J., & Gatti, S. (2011). Structural determinants of allosteric antagonism at metabotropic glutamate receptor 2: mechanistic studies with new potent negative allosteric modulators. *British Journal of Pharmacology*, 41–61.

Lyon, L., Kew, J. N. C., Corti, C., Harrison, P. J., & Burnet, P. W. J. (2008). Altered hippocampal expression of glutamate receptors and transporters in GRM2 and GRM3 knockout mice. *Synapse (New York, N.Y.)*, *62*(11), 842–50.

Majo, V. J., Prabhakaran, J., Mann, J. J., & Kumar, J. S. D. (2013). PET and SPECT tracers for glutamate receptors. *Drug Discovery Today*, *18*(3-4), 173–184.

Matrisciano, F., Panaccione, I., Zusso, M., Giusti, P., Tatarelli, R., Iacovelli, L., Girardi, P. (2007). Group-II metabotropic glutamate receptor ligands as adjunctive drugs in the

treatment of depression: a new strategy to shorten the latency of antidepressant medication? *Molecular Psychiatry*, *12*(8), 704–6.

May, L. T., Leach, K., Sexton, P. M., & Christopoulos, A. (2007). Allosteric modulation of G protein-coupled receptors. *Annual Review of Pharmacology and Toxicology*, *47*, 1–51.

McClure, E., Sonne, S., Winhusen, T., Carroll, K., Ghitza, U., & McRae-Clark, A. (2014). Achieving cannabis cessation -- evaluating N-acetylcysteine treatment (ACCENT): design and implementation of a multi-site, randomized controlled study in the National Institute on Drug Abuse Clinical Trials Network. *Contemporary Clinical Trials*, *39*(2), 211–223.

Meanwell, N. A., & Kadow, J. (2007). Maraviroc, a chemokine CCR5 receptor antagonist for the treatment of HIV infection and AIDS. *Current Opinion in Investigational Drugs*, *8*, 669–681.

Melancon, B. J., Hopkins, C. R., Wood, M. R., Emmitte, K. a, Niswender, C. M., Christopoulos, A., Lindsley, C. W. (2012). Allosteric modulation of seven transmembrane spanning receptors: theory, practice, and opportunities for central nervous system drug discovery. *Journal of Medicinal Chemistry*, *55*(4), 1445–64.

Michalon, A. (2012). Chronic pharmacological $mGlu_5$ inhibition corrects fragile X in adult mice. *Neuron*, *74*(1), 49–56.

Moghaddam, B., & Javitt, D. (2011). From Revolution to Evolution: The Glutamate Hypothesis of Schizophrenia and its Implication for Treatment. *Neuropsychopharmacology : Official Publication of the American College of Neuropsychopharmacology*, 1–12.

Möhler, H., Fritschy, J. M., & Rudolph, U. (2002). A new benzodiazepine pharmacology. *The Journal of Pharmacology and Experimental Therapeutics*, *300*(1), 2–8.

Monod, J., Wyman, J., & Changeux, J. P. (1965). on the Nature of Allosteric Transitions: a Plausible Model. *Journal of Molecular Biology*, *12*(1), 88–118.

Morishima, Y., Miyakawa, T., Furuyashiki, T., Tanaka, Y., Mizuma, H., & Nakanishi, S. (2005). Enhanced cocaine responsiveness and impaired motor coordination in metabotropic glutamate receptor subtype 2 knockout mice. *Proceedings of the National Academy of Sciences of the United States of America*, *102*(11), 4170–4175.

Moussawi, K., & Kalivas, P. W. (2010). Group II metabotropic glutamate receptors ($mGlu_{2/3}$) in drug addiction. *European Journal of Pharmacology*, *639*(1-3), 115–22.

Murrough, J. W., Iosifescu, D. V, Chang, L. C., & Al Jurdi, R. K. (2013). Antidepressant Efficacy of Ketamine in Treatment-Resistant Major Depression: A Two-Site Randomized Controlled Trial. *American Journal of Psychiatry*, *170*(10), 1143–1142.

Murthy, K., Zhou, H., Huang, J., & Pentyala, S. (2004). Activation of PLC-δ1 by $G_{i/o}$-coupled receptor agonists. *American Journal of Physiology and Cellular Physiology*, *287*(6), 1679–1687.

Muto, T., Tsuchiya, D., Morikawa, K., & Jingami, H. (2007). Structures of the extracellular regions of the group II/III metabotropic glutamate receptors. *Proceedings of the National Academy of Sciences of the United States of America*, *104*(10), 3759–3764.

Neale, J. H., Bzdega, T., & Wroblewska, B. (2000). N-acetylaspartylglutamate: The most abundant peptide neurotransmitter in the mammalian central nervous system. *Journal of Neurochemistry*, *75*(2), 443–452.

Nelson, S. D., & Trager, W. F. (2003). The use of deuterium isotope effects to probe the active site properties, mechanism of cytochrome P450-catalyzed reactions, and mechanisms of metabolically dependent toxicity. *Drug Metabolism and Disposition*, *31*(12), 1481–1498.

Nemeth, E. F., Heaton, W. H., Miller, M., Fox, J., Balandrin, M. F., Van Wagenen, B. C., Martin, D. (2004). Pharmacodynamics of the type II calcimimetic compound cinacalcet HCl. *The Journal of Pharmacology and Experimental Therapeutics*, *308*(2), 627–635.

Nicoletti, F., Bockaert, J., Collingridge, G. L., Conn, P. J., Ferraguti, F., Schoepp, D. D., Pin, J. P. (2011). Metabotropic glutamate receptors: from the workbench to the bedside. *Neuropharmacology*, *60*(7-8), 1017–41.

Niswender, C. M., & Conn, P. J. (2010). Metabotropic glutamate receptors: physiology, pharmacology, and disease. *Annual Review of Pharmacology and Toxicology*, *50*, 295–322.

Noël, X., Brevers, D., & Bechara, A. (2013). A neurocognitive approach to understanding the neurobiology of addiction. *Current Opinion in Neurobiology*, *23*(4), 632–638.

Noetzel, M. J., Jones, C. K., & Conn, P. J. (2012). Emerging approaches for treatment of schizophrenia: modulation of glutamatergic signaling. *Discovery Medicine*, *14*(78), 335–43.

Nutt, D. J., Lingford-Hughes, A., Erritzoe, D., & Stokes, P. R. a. (2015). The dopamine theory of addiction: 40 years of highs and lows. *Nature Reviews Neuroscience*, *16*(5), 305–312.

O'Brien, N. L., Way, M. J., Kandaswamy, R., Fiorentino, A., Sharp, S. I., Quadri, G., McQuillin, A. (2014). The functional GRM3 Kozak sequence variant rs148754219 affects the risk of schizophrenia and alcohol dependence as well as bipolar disorder. *Psychiatric Genetics*, *24*(6), 277–278.

Olive, M. (2010). Metabotropic glutamate receptor ligands as potential therapeutics for addiction. *Current Drug Abuse Reviews*, *2*(1), 1–29.

Otani, S., Auclair, N., Desce, J. M., Roisin, M. P., & Crépel, F. (1999). Dopamine receptors and groups I and II mGluRs cooperate for long-term depression induction in rat prefrontal cortex through converging postsynaptic activation of MAP kinases. *The Journal of Neuroscience : The Official Journal of the Society for Neuroscience*, *19*(22), 9788–9802.

Otani, S., Daniel, H., Takita, M., & Crépel, F. (2002). Long-term depression induced by postsynaptic group II metabotropic glutamate receptors linked to phospholipase C and intracellular calcium rises in rat prefrontal cortex. *The Journal of Neuroscience : The Official Journal of the Society for Neuroscience*, *22*(9), 3434–3444.

Overstreet, D. H. (2012). Psychiatric Disorders: Methods and Protocols. Chapter 7 - Modeling Depression in Animal Models. *Methods in Molecular Biology*, *829*.

Owen, D. (2011). Recent advances in the medicinal chemistry of the metabotropic glutamate receptor 1 ($mGlu_1$). *ACS Chemical Neuroscience*, *1*, 394–401.

Peng, S., Zhang, Y., Zhang, J., Wang, H., & Ren, B. (2011). Glutamate receptors and signal transduction in learning and memory. *Molecular Biology Reports*, *38*(1), 453–60.

Pilc, A., Wierońska, J. M., & Skolnick, P. (2013). Glutamate-based antidepressants: Preclinical psychopharmacology. *Biological Psychiatry*, *73*(12), 1125–1132.

Pitsikas, N. (2014). The metabotropic glutamate receptors: Potential drug targets for the treatment of anxiety disorders? *European Journal of Pharmacology*, *723*, 181–4.

Poisik, O. V, Smith, Y., & Conn, P. J. (2007). D1- and D2-like dopamine receptors regulate signaling properties of group I metabotropic glutamate receptors in the rat globus pallidus. *The European Journal of Neuroscience*, *26*(4), 852–862.

Price, J. L., & Drevets, W. C. (2012). Neural circuits underlying the pathophysiology of mood disorders. *Trends in Cognitive Sciences*, *16*(1), 61–71.

Purves, D., AuGustine, G., Fitzpatrick, D., & Al., E. (2001). Neuroscience. In *Neuroscience* (2nd ed.). Sunderland, MA: Sinaur Associates.

Ritchie, M. D., Denny, J. C., Crawford, D. C., Ramirez, A. H., Weiner, J. B., Pulley, J. M., Roden, D. M. (2010). Robust Replication of Genotype-Phenotype Associations across Multiple Diseases in an Electronic Medical Record. *American Journal of Human Genetics*, *86*(4), 560–572.

Robert, S. M., & Sontheimer, H. (2014). Glutamate transporters in the biology of malignant gliomas. *Cellular and Molecular Life Sciences*, *71*(10), 1839–1854.

Robichaud, A., & Engers, D. (2011). Recent progress on the identification of metabotropic glutamate 4 receptor ligands and their potential utility as CNS therapeutics. *ACS Chemical Neuroscience*, 2, 433–449.

Rook, J. M. (2014). Relationship between in vivo receptor occupancy and efficacy of metabotropic glutamate receptor subtype 5 allosteric modulators with different in vitro binding profiles. *Neuropsychopharmacology*, *40*(3), 755–765.

Schann, S. (2013). *GPCR/Membrane Protein Targets Brochure*. Boston, MA: 11th Annual Discovery on Target Meeting.

Schann, S., Manteau, B., Franchet, C., Frauli, M., & Mayer, S. (2013). *General Poster Session—EVE Session,*. Indianapolis, IN: 246th ACS National Meeting and Exposition.

Schann, S., Mayer, S., Franchet, C., Frauli, M., Steinberg, E., Thomas, M., Neuville, P. (2010). Chemical switch of a metabotropic glutamate receptor 2 silent allosteric modulator into dual metabotropic glutamate receptor 2/3 negative/positive allosteric modulators. *Journal of Medicinal Chemistry*, *53*(24), 8775–9.

Schwendt, M., Reichel, C. M., & See, R. E. (2012). Extinction-Dependent Alterations in Corticostriatal mGluR2/3 and mGluR7 Receptors following Chronic Methamphetamine Self-Administration in Rats. *PloS One*, *7*(3), e34299.

Sharma, S., & Kedrowski, J. (2009). Discovery of molecular switches that modulate modes of $mGlu_5$ pharmacology in vitro and in vivo within a series of functionalized, regioisomeric 2-and 5-(Phenylethynyl)Pyrimidines. *Journal of Medicinal Chemistry*, *52*(14), 4103–4106.

Sharma, S., Rodriguez, A. L., Conn, P. J., & Lindsley, C. W. (2008). Synthesis and SAR of a mGluR5 allosteric partial antagonist lead: unexpected modulation of pharmacology with slight structural modifications to a 5-(phenylethynyl)pyrimidine scaffold. *Bioorganic & Medicinal Chemistry Letters*, *18*(14), 4098–101.

Sheffler, D. J., Gregory, K. J., Rook, J. M., & Conn, P. J. (2011). *Allosteric modulation of metabotropic glutamate receptors. Advances in pharmacology (San Diego, Calif.)* (1st ed., Vol. 62). Elsevier Inc.

Sheffler, D. J., Pinkerton, A. B., Dahl, R., Markou, A., & Cosford, N. D. P. (2011). Recent progress in the synthesis and characterization of group II metabotropic glutamate receptor allosteric modulators. *ACS Chemical Neuroscience*, *2*(8), 382–93.

Sheffler, D., & Pinkerton, A. (2011). Recent progress in the synthesis and characterization of group II metabotropic glutamate receptor allosteric modulators. *ACS Chemical Neuroscience*, 2, 382–393.

Shen, H., Moussawi, K., Zhou, W., Toda, S., & Kalivas, P. W. (2011). Heroin relapse requires long-term potentiation-like plasticity mediated by NMDA2b-containing receptors. *Proceedings of the National Academy of Sciences of the United States of America*, *2011*, 1–6.

Shimazaki, T., Iijima, M., & Chaki, S. (2004). Anxiolytic-like activity of MGS0039, a potent group II metabotropic glutamate receptor antagonist, in a marble-burying behavior test. *European Journal of Pharmacology*, *501*(1-3), 121–125.

Sotres-Bayon, F., & Quirk, G. J. (2010). Prefrontal control of fear: More than just extinction. *Current Opinion in Neurobiology*, *20*(2), 231–235.

Stauffer, S. (2011). Progress toward positive allosteric modulators of the metabotropic glutamate receptor subtype 5 ($mGlu_5$). *ACS Chemical Neuroscience*, *5*, 450–470.

Ster, J. (2011). Enhancement of CA3 hippocampal network activity by activation of group II metabotropic glutamate receptors. *Proceedings of the National Academy of Sciences of the United States of America*, *108*(24), 9993–9997.

Substance Abuse and Mental Health Services Administration. (2013). Results from the 2012 National Survey on Drug Use and Health : Summary of National Findings. *NSDUH Series H-46, HHS*. Retrieved from http://store.samhsa.gov/home

Suzuki, G. (2009). Correlation of receptor occupancy of metabotropic glutamate receptor subtype 1 (mGluR1) in mouse brain with in vivo activity of allosteric mGluR1 antagonists. *Journal of Pharmacological Science*, *110*(3), 315–325.

Suzuki, G., Tsukamoto, N., & Fushiki, H. (2007). In vitro pharmacological characterization of novel isoxazolopyridone derivatives as allosteric metabotropic glutamate receptor 7 antagonists. *Journal of Pharmacology and Experimental Therapeutics*, 323(1), 147-156.

Tan, H.-Y., Chen, Q., Sust, S., Buckholtz, J. W., Meyers, J. D., Egan, M. F., Callicott, J. H. (2007). Epistasis between catechol-O-methyltransferase and type II metabotropic glutamate receptor 3 genes on working memory brain function. *Proceedings of the National Academy of Sciences of the United States of America*, *104*(30), 12536–12541.

Tessari, M., Pilla, M., Andreoli, M., Hutcheson, D., & Heidbreder, C. (2004). Antagonism at metabotropic glutamate 5 receptors inhibits nicotine- and cocaine-taking behaviours and prevents nicotine-triggered relapse to nicotine-seeking. *European Journal of Pharmacology*, *499*(1-2), 121–133.

Trevino, K., McClintock, S. M., McDonald Fischer, N., Vora, A., & Husain, M. M. (2014). Defining treatment-resistant depression : A comprehensive review of the literature. *Annals of Clinical Psychiatry*, *26*(3), 222–232.

Turner, S., Armstrong, L. L., Bradford, Y., Carlson, C. S., Dana, C., Crenshaw, A. T., Ritchie, M. D. (2011). Quality control procedures for genome wide association studies. *Current Proceedings in Human Genetics*, *68*(1), 1–24.

Van Huijstee, A. N., & Mansvelder, H. D. (2015). Glutamatergic synaptic plasticity in the mesocorticolimbic system in addiction. *Frontiers in Cellular Neuroscience*, *8*, 1–13.

Wenthur, C. J., Morrison, R., Felts, A. S., Smith, K. A., Engers, J. L., Byers, F. W., Je, P. (2013). Discovery of (R)-(2-fluoro-4-((-4-methoxyphenyl)ethynyl)phenyl) (3-hydroxypiperidin-1-yl)methanone (ML337), an $mGlu_3$ selective and CNS penetrant negative allosteric modulator (NAM). *Journal of Medicinal Chemistry*, 56(12) 5208–5212.

Williams, R., Manka, J., Rodriguez, A., Vinson, P., Niswender, C. M., Weaver, C. D., Stauffer, S. R. (2011). Synthesis and SAR of centrally active $mGlu_5$ positive allosteric modulators based on an aryl acetylenic bicyclic lactam scaffold. *Bioorganic & Medicinal Chemistry Letters*, *21*(56), 1350–1353.

Winder, D. G., Ritch, P. S., Gereau, R. W., & Conn, P. J. (1996). Novel glial-neuronal signalling by coactivation of metabotropic glutamate and beta-adrenergic receptors in rat hippocampus. *The Journal of Physiology*, *494(3)*, 743–755.

Woltering, T. J., Adam, G., Wichmann, J., Goetschi, E., Kew, J. N. C., Knoflach, F., Gatti, S. (2008). Synthesis and characterization of 8-ethynyl-1,3-dihydro-benzo[b][1,4]diazepin-2-one derivatives: part 2. New potent non-competitive metabotropic glutamate receptor 2/3 antagonists. *Bioorganic & Medicinal Chemistry Letters*, *18*(3), 1091–5.

Wood, M. R., Hopkins, C. R., Brogan, J. T., Conn, P. J., & Lindsley, C. W. (2011). “Molecular switches” on mGluR allosteric ligands that modulate modes of pharmacology. *Biochemistry*, *50*(13), 2403–10.

Woolley, M. L., Pemberton, D. J., Bate, S., Corti, C., & Jones, D. N. C. (2008). The $mGlu_2$ but not the $mGlu_3$ receptor mediates the actions of the mGluR2/3 agonist, LY379268, in mouse models predictive of antipsychotic activity. *Psychopharmacology*, *196*(3), 431–440.

Working Group of the Psychiatric Genomics Consortium, S. (2015). Biological Insights From 108 Schizophrenia-Associated Genetic Loci. *Nature*, *511*(7510), 421–427.

Wu, H., Wang, C., Gregory, K. J., Han, G. W., Cho, H. P., Xia, Y., Stevens, R. C. (2014). Structure of a class C GPCR metabotropic glutamate receptor 1 bound to an allosteric modulator. *Science (New York, N.Y.)*, *344*(6179), 58–64.

Wu, M. C., Kraft, P., Epstein, M. P., Taylor, D. M., Chanock, S. J., Hunter, D. J., & Lin, X. (2010). Powerful SNP-Set Analysis for Case-Control Genome-wide Association Studies. *American Journal of Human Genetics*, *86*(6), 929–942.

Xi, Z. X., Kiyatkin, M., Li, X., Peng, X. Q., Wiggins, A., Spiller, K., … Gardner, E. L. (2010). N-acetylaspartylglutamate (NAAG) inhibits intravenous cocaine self-administration and cocaine-enhanced brain-stimulation reward in rats. *Neuropharmacology*, *58*(1), 304–313.

Xia, Y., Ma, D., Hu, J., Tang, C., Wu, Z., Liu, L., & Xin, F. (2012). Effect of metabotropic glutamate receptor 3 genotype on N-acetylaspartate levels and neurocognition in non-smoking, active alcoholics. *Behavioral and Brain Functions : BBF*, *8*, 42.

Xia, Y., Wu, Z., Ma, D., Tang, C., Liu, L., Xin, F., Hu, J. (2014). Association of Single-Nucleotide Polymorphisms in a Metabotropic Glutamate Receptor GRM3 Gene Subunit to Alcohol-Dependent Male Subjects. *Alcohol and Alcoholism (Oxford, Oxfordshire)*, (20110301), 1–5.

Yokoi, M., Kobayashi, K., Manabe, T., Takahashi, T., Katsuura, G., Shigemoto, R., Nakanishi, S. (1996). Impairment of Hippocampal Mossy Fiber LTD in Mice Lacking mGIuR2. *Science (New York, N.Y.) 273*(5275), 645-647.